Hydrothermal systems in distal rifted margins and their role in the thermal evolution of sedimentary successions. Study of two fossil analogues in the Swiss Alps and Pyrenees

Nicolo Incerpi

Università degli Studi di Torino

Scuola di Dottorato in Scienze della Natura e Tecnologie Innovative

Universitè de Strasbourg

Ecole Doctorale en Sciences de la Terre et de l'Environnement

HYDROTHERMAL SYSTEMS IN DISTAL RIFTED MARGINS AND THEIR ROLE IN THE THERMAL EVOLUTION OF SEDIMENTARY SUCCESSIONS. STUDY OF TWO FOSSIL ANALOGUES IN THE SWISS ALPS AND PYRENEES

NICOLO' INCERPI

Tutor: Prof Luca Martire

Co-tutor: Prof. Gianreto Manatschal

XXIX Cycle

Date of finale examen: 12-04-2017

Author's address:

Nicolò Incerpi

nincerpi@unito.it - nincerpi@unistra.fr

Universitò degli Studi di Torino

Dipartimento di Scienze della Terra

Via Valperga Caluso, 35

10125 - Torino (Italy)

Universitè de Strasbourg

EOST-IPGS Institut de hysique du Globe

1 Rue du Blessig

67000 - Strasbourg (France)

Tutor and Co-tutor:

Prof. Luca Martire

luca.martire@unito.it

Università degli Studi di Torino

Dipartimento di Scienze della Terra

Prof. Gianreto Manatschal

manat@unistra.fr

Universitè de Strasbourg

Institut de Physique du Globe

Reviewers:

Prof. Stefano M. Bernasconi

ETH Zürich

Geologische Institut

Prof. Mikel López-Horgue

Universidad del País Vasco

Departamento de Estratigrafía y Paleontologia

Examining Committee:

Prof. Stefano M. Bernasconi

ETH Zürich

Geologische Institut

Prof. Mikel López-Horgue

Universidad del País Vasco

Departamento de Estratigrafía y Paleontologia

Prof. Giovanna Della Porta

Università degli Studi di Milano

Dipartimento di Scienze della Terra

Prof. Philippe Boulvais

Universitè de Rennes 1

Observatoire des Sciences de l'Univers

Aknowledgments

The first, huge, thanks is for my tutor Prof. Luca Martire who always supported me all along the PhD from the very first, “early-stage”, discussions to the last word written in this Thesis. If I can talk (properly?) about fluids & carbonates, it is because of your immense teachings. Thanks!

Another big thank goes to my co-tutor Prof. Gianreto Manatschal for all the time, discussions, suggestions and help he dedicated to me despite his super-busy life. Maybe I’m really learing how to jump from micro- to macro-scale observations.

Thanks to: Dott. Carlo Bertok who shared with me the holy Pyrenean jungle experience; Prof. Piergiorgio Rossetti and Prof. Simona Ferrando for helpful discussion on fluid inclusions; Prof. Axel Gerdes for U-Pb datings and Sr isotope analyses; Prof. Stefano M. Bernasconi for O-C isotope analyses and Dott. György Czuppon for He isotope measurements.

Prof. Mikel Lopez-Horgue and Prof. Stefano M. Bernasconi are thanked for the careful revision of the manuscript providing helpful suggestions which increased the quality of the Thesis.

Dott. Luca Barale…colleague, friend, honorary member of Alcatraz and poet. Thanks for all the discussions (serious and not), coffee-breaks, beer-breaks and for some of the funniest e-mails I have ever read. I will miss all of them!

To all the members of “Pausa pranzo-birra-cena-merenda” group and…yes…to Dio Garzena because we are the sum of something I still do not understand.

Massively giant thanks to my Friends…fundamental part of my madness.

Miro and Za! I know I should start to pay you the rent…

Last but not least, to my family and in particular to my parents, always the best!

The research was supported by the University of Turin (Doctoral School of Sciences and Innovative Technologies funds), Petrobras S.A. and MM4 Consortium.

Financial contribution to the mobility by the Università Italo-Francese (Bando Vinci 2014, Cap. II) is kindly acknowledged.

“Well, I got this guitar

and I learned how to make it talk…”

Bruce Springsteen

Table of contents

1. Introduction

1.1 GENERAL REMARKS

Despite many studies have been focused on magma-poor rifted margins in the last decades, some fundamental tiles in the frame of their evolution are still missing or, at least, they are incomplete. The study and the knowledge of the tectono-stratigraphic evolution of continental margins, nowadays at a very advanced stage, took advantage of different investigative methods (e.g. high resolution reflection/refraction seismic data and deep drill hole data), which allowed the definition of those steps that characterized the extensional evolution of rifted margins, their structures as well as their stratigraphic architecture (Iberia-Newfoundland, Péron-Pinvidic and Manatschal 2008; South, Central and North Atlantic, Contrucci et al. 2004, Moulin et al. 2005, Aslanian et al. 2009; NW and S-Australia, Karner and Driscoll 2000). These models show how a multiphase evolution of rift systems led to a complex architecture: a proximal 30 km-thick crust separated, by a necking zone, from a thinned continental crust (<10km), followed by a wide transition zone between the continental and oceanic crusts where mantle exhumation occurs. However, the thermal evolution of distal rifted margins is very poorly constrained, although the presence of hydrothermal systems seems to play a key role in determining the heat flow and thermal history. A deeper and more detailed study of such systems is thus fundamental to reconstruct the thermal and diagenetic evolution of the sedimentary successions lying above these margins. This Thesis aims to face exactly this problem highlighting the interplay between fluids and carbonate rocks involved in paleo-rifted margins development.

The evolution and formation of passive rifted margins is strictly linked to different geological processes (e.g. magmatic, tectonic and sedimentary) in which fluids play an essential role. Nonetheless, their physico-chemical

properties, their pathways and source areas are still less studied and understood expecially in the sedimentary environment. Due to the oceanographic surveys (e.g. IODP/ODP) and the discoveries of hydrothermal vents at present-day ocean ridges, as well as the occurrence of widespread serpentinization processes, the relevance and spatial abundance of fluid activity in response to the late stage of continental rifting and oceanization are relatively well understood (Pinto et al. 2015, Kelley et al., 2001; McCaig et al., 2007; Kelley and Shank, 2010; Edmonds, 2010). On the contrary, little attention has been paid to the study of such activity in the more internal part of the continental margins (proximal and distal domains) where the pre-mantle exhumation history is preserved. The difficulty in studying these sectors lies in the scarcity of available data from present-day rifted margins (most of which are proprietary) and the technical costs of drilling. Only few ODP (Ocean Drilling Program) drill holes are available, which, even if far to be considered exhaustive, shed light on the importance of fluid circulation and related mineralization (e.g. dolomitization at ODP Leg 103; Boillot et al., 1988). The only way to overcome these problems and to get enough valuable data is to study those fossil rifted margins actually preserved in collisional orogens.

1.2 THE STUDY AREAS: REMNANTS OF FOSSIL RIFTED MARGINS

The findings of fossil analogues in orogens (e.g. Alps and Pyrenees) have allowed to detect directly many aspects of the evolution of passive margins and their reactivation, otherwise impossible to investigate and understand. All the processes linked to the pre-, syn- and post-rift evolution, the related structures and final architecture have been considerably improved by these discoveries. The Alps, above all, represent probably the best natural laboratory where such studies can be addressed. This orogen clearly preserves rift-related evidence in both metamorphosed (e.g. Beltrando et al., 2010, 2012) and unmetamorphosed succesions (e.g. Mohn et al. 2010, Masini et al. 2011). To get an understanding as accurate as possible of the conditions in which the fluid circulation occurred, it is suggested to focus on those sectors of the chain that were not involved in

strong orogenic events (e.g. subduction). For this reason, two areas were chosen to be studied. The first is located in the Central Alps, at the Italian-Swiss border in SE Switzerland, where wide portions of the former Adriatic paleo-rifted margin are exposed. The second area, in the western French Pyrenees, comprises well-preserved features of the former Iberian continental margin. Both sites show the relationships among basement, sediments and rift-related structures during the Jurassic and early Cretaceous continental extension. Most importantly, no strong metamorphic overprint occurred during the compressional phases.

1.3 AIMS OF THE THESIS

The focus of this work is on the diagenetic, sedimentary and tectonic processes that were active during continental extension and to which fluid activity is intimately connected. Within this context, the main goal is then to propose a model of hydrothermalism and thermal evolution controlled primarly controlled by extensional tectonics by the investigation of different types of fluid-related products such as breccias, cements, veins, replacement and newly-formed minerals that could document any fluid-rock interaction.

The present Thesis has been carried out with the aim to answer to the following main questions:

- What are the fluid-related products and their characteristics?
- What is the geological context in which these products developed?
- Which are the relationships among these products, the stratigraphy and the main rift-related structures?
- Which is the physico-chemical signal recorded by these products? And what are the processes that lead to their formation?
- Where do the fluids come from and by which pathways?
- How long did the fluid activity last?
- Are the fluid systems shallow or deep? Do they involve only sediments or also crustal and mantle rocks?

In order to face these key points, a multi-disciplinary approach has been adopted (for detailed descriptions of each method see "Materials and Methods"): fieldwork, microscopic analyses, cathodoluminescence, SEM-EDS, O-C, Sr and He isotopes, fluid inclusions microthermometry, geochemistry of main, trace and rare earth elements, and U-Pb dating. This well supported scientific approach can represent a good "template" for future research, not only on fossil analogues but also on present-day continental margins (e.g. Newfoundland-Iberian, Angola, Red Sea) in order to further constrain their evolution.

1.4 THESIS STRUCTURE

The Thesis is divided in two main parts discussing the Alpine and Pyrenean study areas separately. The "Alpine chapter" represents the main part of the work for two main reasons: i) the deeper overall knowledge of the geological context, and ii) the much more spectacular exposure of the outcrops compared to the Pyrenean ones. The large scale structure of the former Adriatic margin will be illustrated, which will be followed by a detailed description of the architecture of its most distal domains: the hyper-extended distal margin preserved in the Err nappe and the exhumed-mantle domain belonging to the Platta nappe (SE Switzerland). To get a much more complete knowledge of the fluid activity along the entire margin and even to highlight similarities and differences among the different domains, the proximal margin (Ortler nappe, N Italy) and the inner distal margin (Bernina nappe, SE Switzerland) have also been considered.

Concerning the study area in the Pyrenees, it is located in the most distal part of the former Iberian continental margin actually preserved in the easternmost sector of the Mauléon Basin (the so-called Chaînons Béarnais). Unfortunately, in this area, because of the very low altitude as well as the rare outcrops and low quality of the exposed sections, it has not always been possible to properly reconstruct the relationships among stratigraphy, structures and fluid-related products. Nonetheless, it is clear that fluid circulation widely affected this portion of the margin during Cretaceous rifting phases. To overcome the

aforementioned problems and in order to properly interpret this area, some selected samples and key sites were chosen and compared with the Alpine ones.

2. Materials and methods

Fieldwork was performed in both the Alpine and Pyrenean areas. Pre, syn- and post-tectonic sedimentary sequences were sampled in the following sites:

- Il Motto (N Italy, Ortler nappe - former proximal Adriatic margin)
- Piz Alv (SE Switzerland, Err nappe - former inner distal Adriatic margin)
- Piz Val Lunga and Fuorcla Cotschna (SE Switzerland, Err nappe - former central distal Adriatic margin)
- Mal Pass (SE Switzerland, Err nappe - former outer Adriatic distal margin)
- Chaînons Béarnais (SW France, Mauléon Basin - former hyper-extended rift system)

Petrographic studies on uncovered thin sections (30 μm thick) were carried out by optical microscopy and cathodoluminescence (CL) with the aim of distinguishing different hydrothermal products that affected the sedimentary successions. CL observations were performed on polished thin sections using a CITL 8200 mk3 equipment (operating conditions of about 17 kV and 400 μA). In situ quantitative microprobe analyses were performed on carbon-coated thin sections with an energy dispersive x-ray spectroscopy (EDS) Energy 200 system and a Pentafet detector (Oxford Instruments) associated with a Cambridge Stereoscan S-360 scanning electron microscope (SEM). The operating conditions were 15 kV of accelerating voltage, 1 nA of probe current and 50 seconds counting time.

Carbon and oxygen isotopic compositions of the carbonates were measured at the Stable Isotope Laboratory of the ETH Geological Institute, ETH Zurich, Switzerland using a Thermo Fisher Scientific GasBench II coupled to a Delta V mass spectrometer as described in detail in Breitenbach and Bernasconi (2011).

The oxygen isotope composition of dolomite was calculated using the fractionation factor of Rosenbaum and Sheppard (1986). The isotopic ratios for carbon and oxygen are expressed as $\delta^{13}C$ and $\delta^{18}O$ per mil values relative to the VPDB (Vienna Pee Dee Belemnite) standard (precision ± 0.05%). The analyses have been performed on micro-drilled powder of an as pure as possible single mineral phase.

Fluid inclusion petrography has been performed at the University of Turin on bi-polished thin sections (100 μm). Micro-thermometry of primary fluid inclusions assemblages on dolomite, calcite and quartz was performed using a Linkam THMSG600 heating-freezing stage coupled with an Olympus polarizing microscope (100X objective), using the standard method described by Goldstein and Reynolds (1994). Primary fluid inclusions of useful size for micro-thermometry (i.e. more than 2 μm in diameter; Goldstein and Reynolds, 1994) have been considered. The distribution of these inclusions (along growth zones, as isolated inclusions, with negative crystal shape) and their constant vapor/bubble ratio have been adopted as evidence of their primary origin. Stretched crystals or inclusions have been observed but were not considered for micro-thermometry.

Sr isotope compositions were measured with a Finnigan MAT 262V multi-collector mass spectrometer at the CNR Istituto di Geoscienze e Georisorse in Pisa (Italy), running in dynamic mode. Conventional ion exchange methods were used for Sr separation from the matrix. Measured $^{87}Sr/^{86}Sr$ ratios were normalized to $^{86}Sr/^{88}Sr = 0.1194$. During the collection of isotopic data replicate measurements of NIST SRM 987 ($SrCO_3$) standard yielded values of 0.710242 ± 17 (2s, N=19). Measurements have been also performed at the Goethe University Frankfurt (Germany) on carbonate in thick sections, using a Thermo-Finnigan Neptune multicollector inductively coupled plasma – mass spectrometer (MC-ICP-MS) attached to a RESOlution 193 nm Ar–F Excimer laser ablation system (ComPexPro 102F, Coherent), equipped with a S-155 two-volume (Laurin Technic, Australia) ablation cell. Laser spots with diameters of

120-235 µm were drilled with repetition rate of 8 Hz, and energy density of about 6-7 J/cm^2, during 45 s of data acquisition. The depth penetration of the static spots was about 0.7 µm s^{-1}. Ablation and material transport occurred in a sample gas stream of Ar (0.8 l min^{-1}) mixed with He (0.6 l min^{-1}) and N_2 (0.005 l min^{-1}), and signal homogenization directly after ablation was carried out using a "Squid" (Laurin Technic, Australia). Wash out time for all important isotopes was less than 5 seconds, which allowed a relatively high sample troughput of ca. 20-30 measurements per hour. The raw data of $^{86}Sr/^{87}Sr$ were corrected for blank (mostly $^{84, 86}Kr$ in sample gas), and isobaric interferences arising from double charged rare earth elements (Er, Yb), as well as for Ca dimers, and Rb. Corrections for Kr, Er, Yb had only a negligible effect due to extremely low intensities for ^{167}Er, ^{173}Y (<0.0001 Volt), and ^{83}Kr (<0.0007 Volt). In contrast Rb interference correction was important. At the beginning of the analytical session, soda-lime glass SRM-NIST 610 was measured 2-3times for empirical determination of $^{87}Rb/^{85}Rb$ mass bias using the Sr mass bias ($^{86}Sr/^{88}Sr_m$ relative to $^{86}Sr/^{88}Sr_{true}$ = 0.1194) of each integration multiplied by an off-set factor. The procedure yielded after successful interference correction on ^{86}Sr, ^{88}Sr, and ^{85}Rb from doubly charged Yb and Er the $^{87}Rb/^{86}Sr$ ratio needed for accurate correction of the isobaric interference of ^{87}Rb on ^{87}Sr. Despite of the high $^{87}Rb/^{86}Sr$ of 2.82, with a ^{87}Rb 4 times the ^{87}Sr, we obtained a $^{87}Sr/^{86}Sr$ (0.7096 ±0.0010; n =12), which is within uncertainty of the reported value of Woodhead et al. (2001). Performance and accuracy was checked by multiple measurement of the feldspar in-house standard MIR-1, which is an isotopically homogeneous plagioclase megacryst from a lava of the Dutsin Miringa Hill volcano (Northern Cameroon Line; Rankenburg et al., 2004). The results of standard measurements yielded values of $^{87}Sr/^{86}Sr$, which were in agreement (within error) to conventional TIMS data of 0.703096 ± 0.000070 (2σ, Rankenburg et al., 2004).

The obtained values have been compared to those proposed by McArthur et al. (2012) for Triassic and Jurassic seawater.

U-Pb ages were acquired *in situ* in polished thin sections by laser ablation-inductively coupled plasma-mass spectrometry (LA-ICP-MS) at the Goethe University Frankfurt (GUF), using a modified method, as previously described in Gerdes & Zeh (2006, 2009). Recent studies have shown that this method yield precise and accurate ages on carbonate formed during different processes (Li et al., 2015; Ring and Gerdes, 2016). At GUF a ThermoScientific Element 2 sector field ICP-MS is coupled to a Resolution S-155 (Resonetics) 193 nm ArF Excimer laser (CompexPro 102, Coherent) equipped with a two-volume ablation cell (Laurin Technic, Australia). Samples were ablated in a helium atmosphere (0.6 l/min) and mixed in the ablation funnel with 0.7 l/min argon and 0.04 l/min nitrogen. Signal strength at the ICP-MS was tuned for maximum sensitivity while keeping oxide formation below 1% (UO/U). Static ablation used a spot size of 213µm and a fluence of < 1 J cm^{-2} at 6 Hz. This yielded for SRM-NIST 614 a depth penetration of about 0.5µm s^{-1} and an average sensitivity of 420000 cps/µg g^{-1} for ^{238}U. The detection limits for ^{206}Pb and ^{238}U were ~ 0.1 and 0.03 ppb, respectively. However, at a U signal of less 1000 cps (~ 2ppb) the data were generally discarded due to enhance scatter on the isotope ratios. Data were acquired in fully-automated mode overnight during two independent analytical sessions. Each analysis consists of 20s background acquisition followed by 20s of sample ablation and 25s washout. During 42s data acquisition, the signal of ^{206}Pb, ^{207}Pb. ^{208}Pb, ^{232}Th and ^{238}U were detected by peak jumping in pulse counting mode with a total integration time of 0.1s, resulting in 420 mass scans. Prior to analysis each spot was pre-ablated for 3s to remove surface contamination. Soda-lime glass SRM-NIST 614 was used as a reference glass together with 2 carbonate standards to bracket sample analysis. Raw data were corrected offline using an in-house MS Excel© spreadsheet program (Gerdes & Zeh, 2006, 2009). Following background correction, outliers (±2σ) were rejected based on the time-resolved $^{207}Pb/^{206}Pb$ and $^{206}Pb/^{238}U$ ratios. The $^{207}Pb/^{206}Pb$ ratio was corrected for mass bias (0.3%) and the $^{206}Pb/^{238}U$ ratio for inter-element fraction (ca. 5%), including drift over the 12 hours of sequence time, using SRM-NIST 614. Due to the carbonate matrix an additional correction of 9% has

been applied on the $^{206}Pb/^{238}U$, which was determined using WC-1 carbonate reference material dated by TIMS (252±2 Ma; E.T. Rasbury, pers. comm. 2014). The WC-1 (n= 36) common Pb corrected $^{206}Pb/^{238}U$ reproduce over the three consecutive days to 251.4±6.1 Ma (2SD = 2.4%; n = 36). The not common Pb corrected data yielded a lower intercept age of 252.9±3.1 Ma. Repeated analyses (n=56) of a Zechstein dolomite (Gypsum pit, Tettenborn, Germany) used as secondary (in-house) standard yielded a lower intercept age of 255.6 ± 3.0 Ma (MSWD: 1.4), implying an accuracy and repeatability of the method of around 2% or better. The analytical results are presented in ANNEX E. Data were plotted in the Tera-Wasserburg diagram and ages calculated as lower intercepts using Isoplot 3.71 (Ludwig, 2003). All uncertainties are reported at the 2sigma level.

For noble gas measurements, few grams of mineral separates (calcite, dolomite and quartz) were selected. After loading the samples into the crusher (Papp et al., 2012) the sample holders pumped out overnight at 50 °C. Samples were then crushed under high vacuum and measured using VG5400 noble gas mass spectrometer at Hertelendi Laboratory of Environmental Studies in Institute of Nuclear Research of the Hungarian Academy of Sciences, Hungary. The blank levels during the experiments were 1×10^{-10} cm^3 STP for He, 5×10^{-8} cm^3 STP for Ar. The blank correction was applied to all analyses (less than 1% for each noble gas). The sensitivity and the isotope discrimination of the mass spectrometer were calibrated by analysing known amounts of air aliquots of 2.5×10^{-5}-1.0×10^{-4} cm^3 for Ar and 0.12-0. 25 cm^3 for He (Varsányi et al., 2011; Papp et al., 2012). More details about the purifications and the mass spectrometer procedures can found in Papp et al. (2012). The CO_2 was extracted with noble gases during vacuum crushing, and then separated by freezing using a cold finger by liquid nitrogen. The cold fingers were then filled with pure helium and closed by high vacuum valves (VAT, series 541). The amount of CO_2 was determined by a stable isotope ratio mass spectrometer (DeltaPLUS XP) in scanning mode.

Main, trace elements and REE analysis were performed by ALS Global (ALS Minerals Division-Geochemistry, Sevilla, Spain) on about 100 gr of materials for each sample. Sample preparation procedures: fine crushing (70% < 2 mm), pulverize split to 85% < 75 μm, crushing QC Test, pulverizing QC Test. Analytical procedures: up to 34 elements by ICP-MS, loss on Ignition at 1000C, total calculatin for ICP06, base metals by 4-acid dig., whole rock package (ICP-AES), total carbon and sulphur (LECO), lithium borate fusion (ICP-MS).

3. The Adriatic continental margin

3.1 INTRODUCTION

The Alps are an orogenic chain formed in response of two main phases of deformation: one during Late Cretaceous and the other during Cenozoic time (e.g. Lemoine et al., 1986; Froitzheim et al., 1994; Schmid et al., 2004). In this mountain belt, remnants of former Adriatic and European rifted margins are widely preserved since they did not undergo most of the Alpine deformation and metamorphism (Froitzheim and Manatschal, 1996; Masini et al., 2013). The two paleo-rifted margins were separated one from each other by the Piemonte-Liguria domain, which represents an embryonic ocean developed during Middle to Late Jurassic time (Lemoine et al., 1987; Manatschal and Bernoulli, 1998). In the present-day nappe stack, the former Adriatic and European continental margins are preserved in the Southern Alps and Austroalpine units and in the Helvetic units respectively. Remnants of the Piemonte-Liguria ocean constitute the Penninic units (Fig. 3.1).

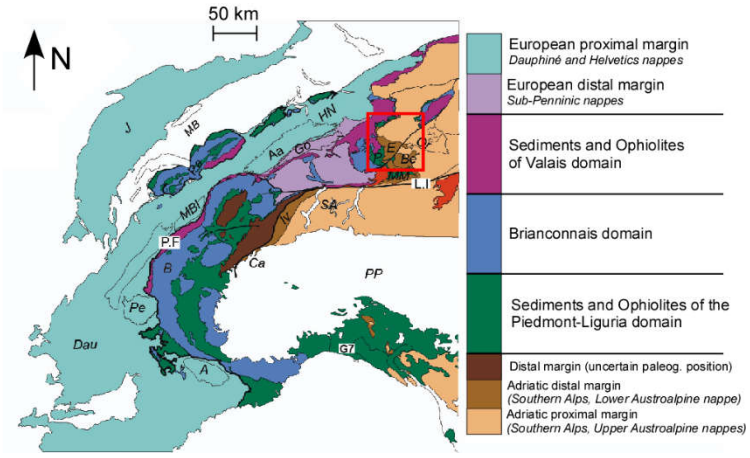

Fig. 3.1 - Tectonic map of the Alps modified after Schmid et al. (2004) and Mohn et al. (2010) with the location of study area (red square).

Since the focus of this Thesis is on the Triassic-Jurassic evolution of the former Adriatic continental margin and its transition to the oceanic domain, a general description of their former architecture will be given in the following sections.

3.2 GEOLOGICAL SETTING

The study area is located in the southeasternmost part of Switzerland and N-Italy. This sector belongs to the Austroalpine and Upper Penninic units, which preserve one of the most outstanding sections of a magma-poor rifted margin. Since they were not involved in the subduction during the Alpine orogeny, they reached metamorphic conditions that never exceeded prehnite-pumpellyite facies. This weak overprint led to the exceptional preservation of all the features related to the Adriatic continental margin during its Triassic-Jurassic evolution. The nappe stack is actually subdivided into Upper, Middle and Lower Austroalpine units that overlie the Upper Penninic units that consist of ophiolitic material (Fig. 3.2).

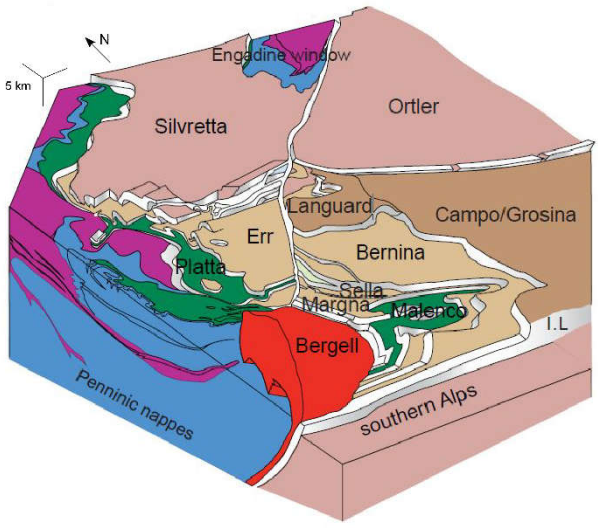

Fig. 3.2 - 3D block diagram of the present-day Alpine architecture of SE-Switzerland and N-Italy showing the Austroalpine and Penninic nappe stack (modified after Mohn et al., 2010; Froitzheim et al., 1994).

The thrust faults separating the nappes have a top-to-the-west sense of shear ("Trupchun phase or D1-phase" of Froitzheim et al. 1994, Mohn et al. 2010). Since the overall orientation of the Adriatic margin was SW-NE, the late

Cretaceous orogenic event resulted in the stacking of more proximal parts of the former margin onto more distal domains. The study of Mohn et al. (2010) on the Austroalpine units enabled to understand the former architecture of the margin by the definition of different paleogeographic domains (Mohn et al. 2010) tectonically stacked in the nappe pile. In this frame, the less thinned proximal margin represents the highest structural units lying above the units derived from the former necking zone (Campo-Grosina, not studied in this Thesis), the distal margin (Bernina/Err) and the exhumed mantle domain (Platta) (Mohn et al. 2010). Because of the altitude and the outstanding quality of the outcrops, this area became fundamental in the understanding of the architecture of hyper-extended rifted margins. The so-called "Grisons transect" has been widely studied allowing the definition of the four main domains in which usually a magma-poor rifted margin is divided: the proximal margin, the necking zone, the distal margin, the ocean-continent transition (Fig. 3.3).

Fig. 3.3 - Cartoon schematically showing the evolution of the Adriatic continental margin from the first rifting stages in Late Triassic-early Lower Jurassic to the exhumation of mantle-related rocks in Middle Jurassic time. The main stratigraphic record here represented varies in facies and thickness from the proximal margin to the distal margin and mantle exhumed areas. Location of key cross-sections from these areas, shown in figures 3.4, 3.5 and 3.6, are here highlighted as well as 10.3 and 10.4 which refer to fluid pathways within the proximal and distal margin. The section (d) shows also the distribution of the main paleogeographic domains of the margin (red terms) and refers to the major Alpine units (black terms). OCT: Ocean-Continent Transition; Err det.: Err detachment system; Bernina det.: Bernina detachment system. Modified after Mohn et al. (2012).

T_0 - INITIAL STAGE (Middle Triassic)

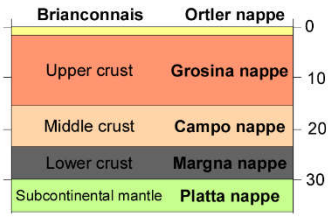

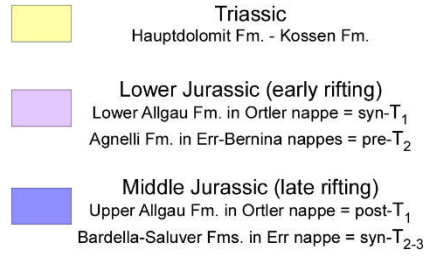

T_1 - STRETCHING STAGE (Late Triassic to late Sinemurian)

Creation of Proximal margin

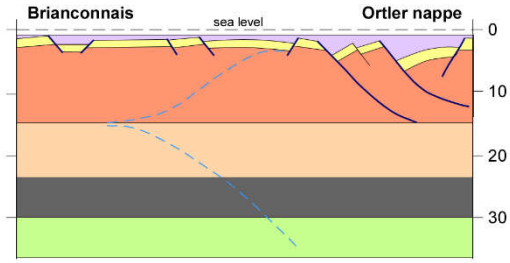

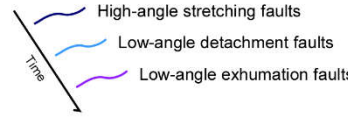

T_2 - THINNING STAGE (Pliensbachian to Toarcian)

Activation of Necking zone

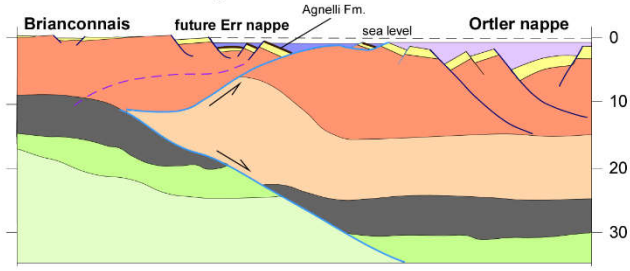

T_3 - EXHUMATION STAGE (Aalenian to Callovian)

Creation of Distal margin and OCT

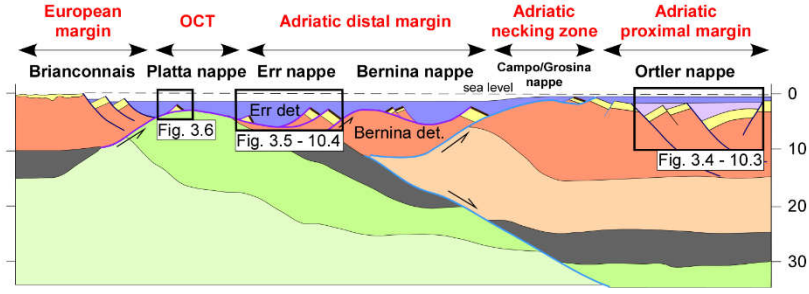

3.2.1 The proximal margin (Ortler and Ela nappes)

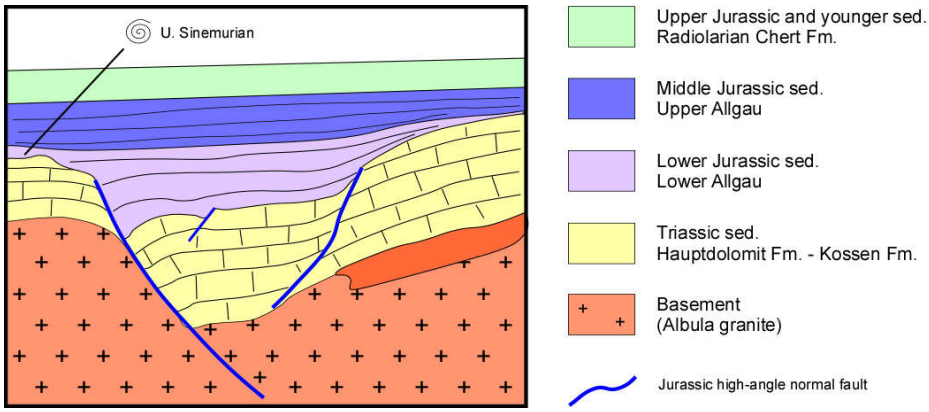

Fig. 3.4 - Schematic representation of the architecture of the proximal margin preserved in the Austroalpine nappe modified after Mohn et al. (2011).

The proximal margin is exposed in the Ortler and Ela nappes (Upper Austroalpine) and consists of classical fault-bounded tilted blocks with well-defined pre-rift sequences and thick Jurassic syn-rift sediments (Fig. 3.4). The pre-rift sequence overlies Paleozoic basement and consists mainly of continental deposits that grade upsection into shallow marine carbonates. Relics of Jurassic high-angle normal faults can be found associated with half-graben basins. These fault-bounded basins were active during initial rifting from late Triassic to Pliensbachian-Toarcian time and were mainly filled by mass flow breccias and calciturbidites interleavead with hemipelagic limestones (Allgäu Formation of Eberli 1988). All the reworked sediments derive exclusively from the pre-rift carbonate platform (Froitzheim 1988). The syn-rift sedimentary sequence is characterized by thinning- and fining-upward cycles as well as a thinning and fining away from the fault zone. Furthermore, an inversion of the clast stratigraphy is observed in the basin due to erosion of the footwall block and redeposition derived clasts (Eberli, 1988). In the present-day architecture, the Ortler nappe is under- and overlain, along Alpine tectonic contacts, by other upper Austroalpine units: the Quattervals nappe above and the Campo nappe below.

3.2.2 The necking zone

The necking zone, exposed in the Grosina-Campo nappe (Middle Austroalpine), is the domain where major crustal thinning occurred (Mohn et al., 2010, 2011). This zone juxtaposes crust that is little or not thinned (proximal margin) against strongly thinned, less than 10 km thick crust of the distal margin. Within this domain, the pre-rift sequence starts to be highly extended and can occur as extensional allochthons lying above top-basement detachment faults.

3.2.3 The distal margin (Err and Bernina nappes)

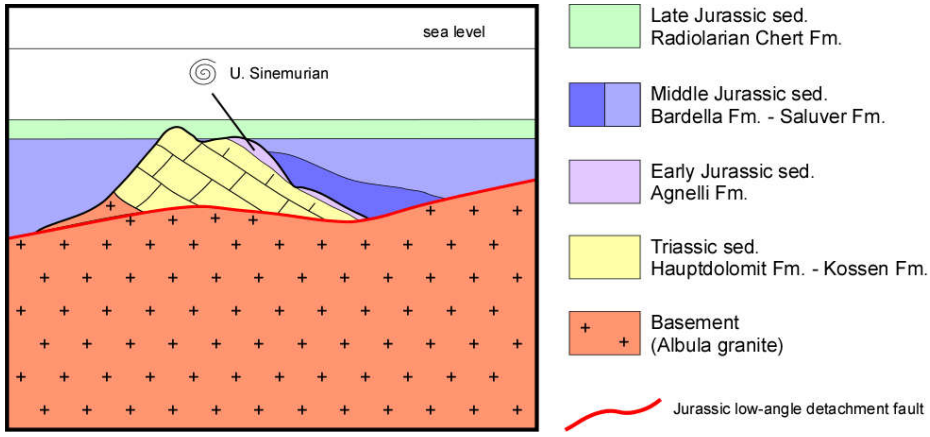

Fig. 3.5 - Schematic representation of the architecture of the distal margin preserved in the Austroalpine nappes (modified after Mohn et al. 2011).

Exposed in the Bernina nappe (inner distal) and the Err nappe (outer distal; Lower Austroalpine), it consists of hyper-extended continental crust. Rift-related low-angle detachment faults are the most characteristic rift structures. Two main detachment systems are described from this domain, the Bernina and the Err detachment systems. These faults separate continental crust and exhumed subcontinental mantle in the footwall from extensional allochthons made of basement and pre-rift sediments in the hangingwall (Fig. 3.5). Syn- to post-rift sediments overlie the detachment faults with an angle of even less than 20-30°,

which implies an almost flat geometry of these faults and their exhumation at the seafloor.

3.2.4 The ocean-continent transition (OCT, Platta nappe)

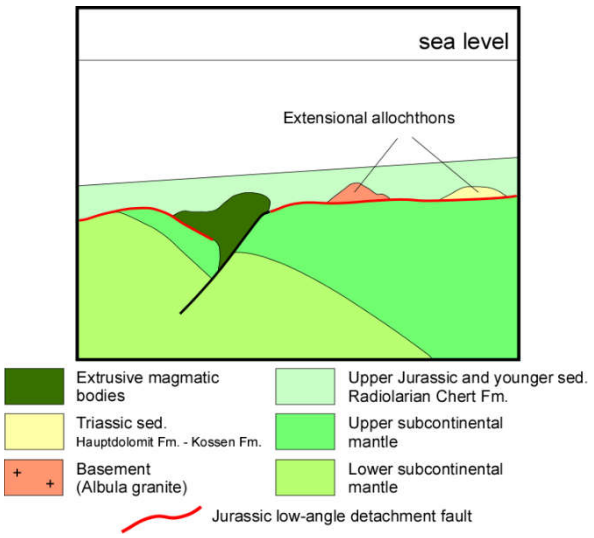

Fig. 3.6 - Schematic representation of the architecture of the ocean-continent transition preserved in the Penninic nappe modified after Mohn et al. (2011).

The ocean-continent transition is exposed in the Platta nappe (Upper Penninic). This domain is formed by exhumed mantle rocks intruded by gabbros and capped by detachment faults (Fig. 3.6). The Platta domain is interpreted to be associated with the same detachment system affecting also the hyper-extended domain. Such an interpretation is supported by the occurrence of extensional allochthons made of continental crust and pre-rift sediments over exhumed subcontinental mantle (Manatschal and Nievergelt, 1997). Further oceanward, the exhumed mantle rocks are overlain by MORB extrusives, indicating that this domain may have developed into an embryonic oceanic domain (Desmurs et al., 2002; Manatschal & Müntener, 2009).

3.3 THE ADRIATIC DISTAL MARGIN: THE ERR NAPPE

3.3.1 The present-day Alpine architecture

Like in the reminder of the Austroalpine units, the Err domain was overprinted by deformation phases, which are classically referred to as D1 to D5 phases (e.g. Froitzheim et al. 1994; Fig. 3.7). The major D1 structure in the study area is the thrust separating the Julier half-klippe, belonging to the Bernina nappe, from the underlying Err nappe. Second order D1 thrusts can also be found in the Err nappe subdividing it into an Upper, Middle and Lower Err unit. The Upper Err unit is only discontinuously preserved as klippen in post-thrust (D3) synclines (e.g. Padella-Schlattain and Piz Bleis Marscha; Manatschal and Nieverglet 1997). The middle Err unit represents the main body of the Err nappe. The Lower Err unit can be observed in the so-called Jenatsch tectonic window and also along the frontal contact of the Err nappe with the Platta nappe to the west. All three units preserve primary relationships between footwall and hangingwall rocks, including syn-tectonic sediments of the rift-related Err detachment system.

D2 structures reactivate, but also cut, D1 thrusts as extensional top-to-the-SE normal faults (Froitzheim et al. 1994, Handy et al. 1993, Handy 1996).

D3 structures consist of north to northwest vergent folds and steep S-dipping thrusts showing displacements in the order of hundreds of meters.

The latest Alpine deformation consists of high-angle faults limiting the northern border of the Zone of Samedan (ZoS, already described in Cornelius 1935). The total amount of normal displacement along this fault system can exceed half a kilometre in the center of ZoS and decreases eastwards. This phase is presumably linked to activity along the Engadine line (e.g. Schmid and Froitzheim 1993, Handy 1996).

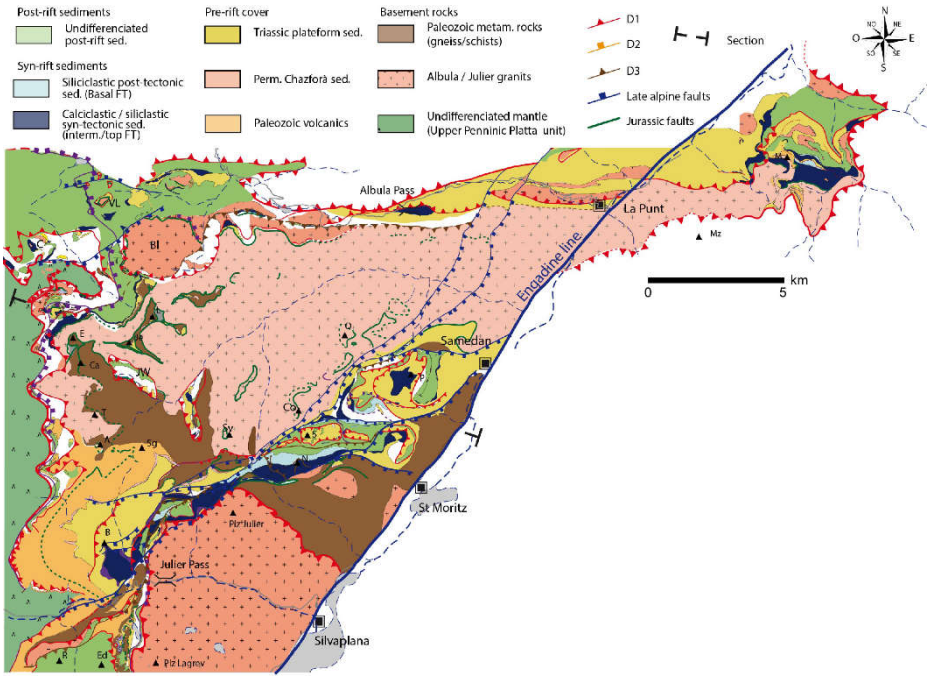

Fig. 3.7 - Geological map of the Err nappe (from Masini et al. 2012).

3.3.2 The Jurassic architecture: the Err detachment system

The weak Alpine overprint enables to map and describe a Jurassic detachment system that is exceptionally well exposed and preserved in the Err nappe. The detachment system consists of brittle fault zones that are made of cataclastic damage zones and a peculiar core zone that separates the footwall from a hangingwall in which the pre- and syn-rift sedimentary sequences are locally preserved.

3.3.2.1 The footwall

The footwall is constituted of Paleozoic rocks inherited from the late to post-Variscan history. They are made of calcalkaline Albula granitic bodies (Cornelius 1935, Staub 1948, Von Quadt et al. 1994) that intruded a Paleozoic polymetamorphic host-rock consisting of schists and gneisses. The Albula granite is by far the most common rock in the footwall. Since it preserves

primary stratigraphic contacts to Permo-Triassic sediments and volcanic rocks, these basement rocks had to be in the pre-rift upper crust before onset of rifting in Jurassic time.

3.3.2.2 The detachment faults

The detachment faults correspond, at least in the areas where the footwall is formed by the Albula granite, to well characterized brittle fault zones (Fig. 3.8). The faults are formed by tens of meter-thick damage zones constituted of characteristic green cataclasites and core zones made of black fault gouges (Manatschal, 1999). The green cataclasites result from the progressive cataclastic overprint of the host rock, which is related to fluid and reaction-assisted breakdown processes of feldspar (Manatschal, 1999). The textures show a progressive change from fractured host rock, to a clast-supported cataclasite to a matrix-rich green cataclasite. In the last uppermost meters, quartz veins are common. Since these veins occur only within the damage zone crosscutting cataclastic structures and are also observed to have a cataclastic overprint, they are interpreted to be coeval with detachment faulting (Manatschal and Nievergelt 1997). This is also confirmed by geochemical studies (Manatschal et al. 2010) as well as by their occurrence as clasts in the black gouges and reworked into the Jurassic syn-rift sediments. The black gouges occur along a centimeter- to some meter-thick core zone at the top of the green cataclasite corresponding to the main zone of displacement. Where the detachment is exhumed at the seafloor it can be either eroded or directly overlain by syn- to post-rift sediments. The occurrence of clasts of black gouge in the syn-rift sediments points to the erosion of the detachment fault. In the black gouge itself, hangingwall clasts made of Triassic dolomite (Fig. 3.9) exist, but are rare compared to more abundant footwall-derived material. The discovery of clasts of the black gouge in the Jurassic sediments enabled to demonstrate that these rocks were pre-Alpine.

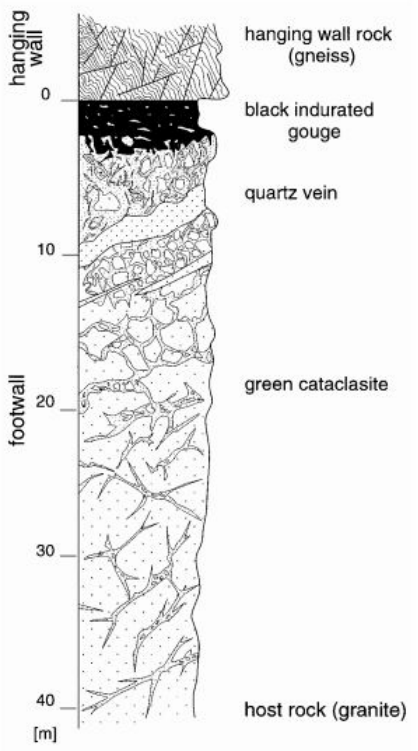

Fig. 3.8 - Schematic profile across a Jurassic detachment fault in the Err nappe showing the main lithologies accompanying the extensional detachment fault. The thickness of the lithologies in the profile are average values, since the real thickness changes considerably along strike (Manatschal, 1999).

Fig. 3.9 - Cm- to dm- large dolomite clasts within the black gouge, which marks the top of the detachment fault system at (a) Piz Val Lunga and (b) Fuorcla Cotschna areas (Err nappe).

Based on the observation that the detachment faults cut Triassic dolomites and are overlain by Jurassic sediments, Froitzheim and Eberli (1990) suggested a Jurassic age of these structures, which has been further supported by Manatschal and Nievergelt (1997). This detachment system was active in the upper crust as

documented by the break-down reactions of feldspars to phyllosilicates and by the crystal-plastic textures in quartz, suggesting that temperatures during faulting did not exceed 300 °C. Given the very characteristic nature of the fault rocks, but also their distinct chemical and mineralogical composition (Manatschal, 1999), the green cataclasite and the black gouge can be used as marker horizons to map the Jurassic detachment faults across the whole Err nappe.

3.3.2.3 The hangingwall

The hangingwall of the detachment system (Fig. 3.10) consists mainly of poly-metamorphic basement that shows primary contacts to either volcanic and volcano-sedimentary sequences or siliciclastic deposits. Ladinian to Norian platform carbonates (Hauptdolomit Formation) and Rhaetian limestones and shales (Kössen Formation) constitute the youngest parts of the pre-rift sediments. The Middle-Upper Triassic succession can be up to 500 m thick; however, it is important to note that throughout the margin, the Triassic dolomites are dismembered and never preserve the original thickness. As shown in Mohn et al. (2010) this is due to the onset of the major activity along the detachment faults. The Triassic to Lower Jurassic sedimentary units (Hauptdolomit-Kössen Fms. and Agnelli Fm. respectively) are very discontinuous in the Err nappe despite the fact that they were deposited as continuous carbonate platforms or hemipelagic sediments. In some areas, the syn- to post-rift sediments overlie directly the exhumed footwall of the detachment faults (e.g. Piz Nair, Pass Suvretta or Fuorcla Cotschna areas in Handy et al. 1993, Handy 1996, Manatschal and Nievergelt 1997) and the Triassic to Lower Jurassic cover is reworked in the syn-rift sediments. The pre-rift succession was disrupted as discontinuous blocks, with a very complex 3D shape over the detachment surface. These structures have been referred to as “extensional allochthon blocks” (Manatschal and Nievergelt 1997, Manatschal 2004).

The syn-rift sediments consist of complex gravitational to hemipelagic sedimentary deposits that occur either unconformably over extensional allochthons (e.g. Bardella block) or directly over the tectonically exhumed basement. Finger (1978) distinguished these syn-rift sediments in two formations, the Bardella and Saluver Fms. The subdivision was mainly based on their composition: the Bardella Fm. is made of reworked Triassic to Early Jurassic carbonates (pre-rift rocks > 185 Ma) whereas the Saluver Fm. includes mainly basement-derived material. The observation that the Bardella Fm. is interleaved with the Saluver Fm. shows that the two sedimentary systems co-existed. It implies that during the evolution of the basin, at least two clastic sedimentary sources where available, one resedimenting the pre-rift Mesozoic platform carbonates and the other reworking detachment fault rocks and tectonized basement (Fig. 3.10). Finger (1978) further subdivided the Saluver Fm. into a coarse-grained Saluver A sub-formation at the base, an intermediate Saluver B and a fine-grained Saluver C at the top. The author defined three different facies tracts, namely the basal, the intermediate and the top tracts corresponding approximately to the Bardella and Saluver A Fm. (basal), Saluver B (intermediate) and Saluver C and post-rift deposits (top).

3.3.3 The major time lines in the Adriatic distal margin

Because of the poly-phase nature of rifting along the whole margin, a new subdivision of the sediments filling the supra-detachment basins (*sensu* Masini et al. 2011) is required in order to avoid misunderstanding about the interpretation of the concept of pre-, syn- and post-rift sediments. Masini et al. (2011), therefore, tried to link sedimentation to tectonic activity of the detachment system. In this context, they highlighted the importance to define two major time horizons (Fig. 3.10): the Top of Agnelli Formation (TAF) and the base of the Radiolarian Cherts (RC) to better constraints the timing of the tectono-sedimentary history of the distal margin.

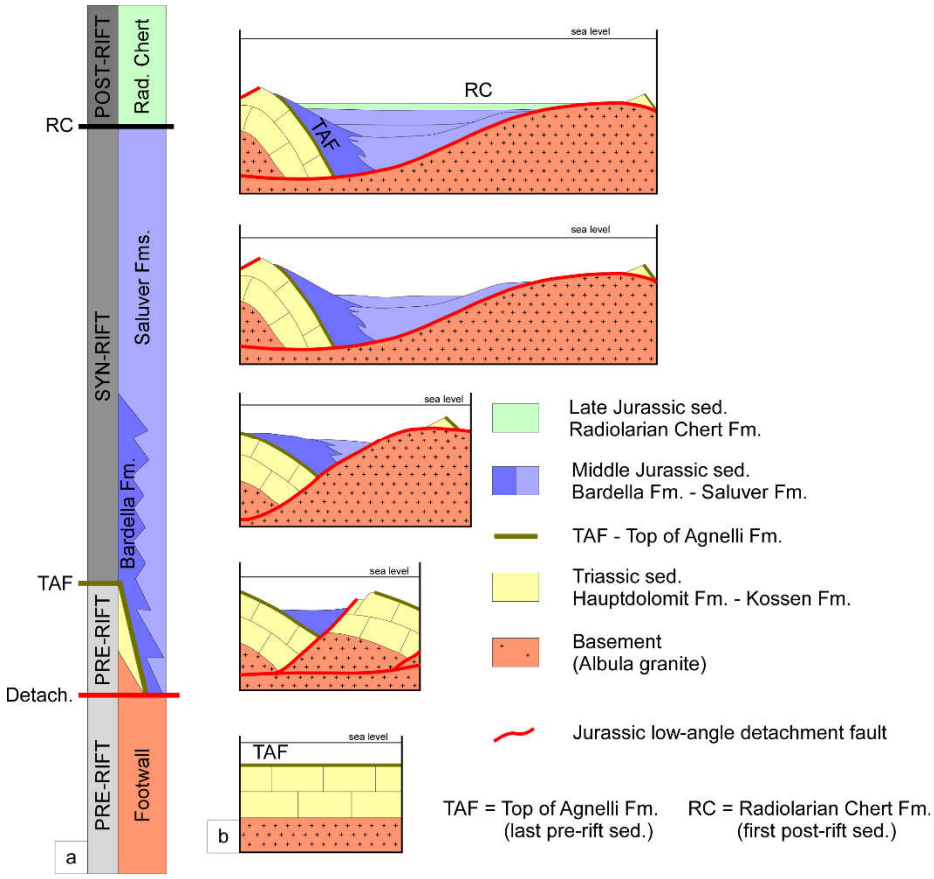

Fig. 3.10 - (a) Stratigraphic log through a supra-detachment basin in the Adriatic distal margin showing the general architecture of the pre-, syn- and post- rift sediments. (b) Evolution of the Samedan supra-detachment basin from the onset to the cessation of the tectonic activity within the Adriatic distal margin. Within this domain, the Agnelli Fm. is represented by a condensed horizon. (a) and (b) modified after Masini et al. (2011, 2012).

3.3.3.1 TAF - Top of Agnelli Formation

The TAF is well expressed in the distal margin where it is synchronous with the first sediments sealing deep fault-bounded basins filled by calciclastic sediments in the proximal margin (top of Lower Allgäu Formation of Eberli, 1988; Froitzheim and Eberli, 1990). Thus, in a classical rift stratigraphic terminology, it would correspond to the post-rift sequence in the proximal margin. As shown

by Froitzheim and Eberli (1990) and Manatschal and Nievergelt (1997), in the distal margin the TAF locally corresponds to a ferromanganese hardground representing a condensed horizon dated by ammonites as late Sinemurian to early Pliensbachian (Finger, 1978; Manatschal and Nievergelt, 1997; Dommergues et al., 2012). The occurrence of the TAF in extensional allochthons, truncated by the detachment system (e.g. Bardella allochthon) as well as the presence of hardground material as clasts in the sediments (Finger, 1978) covering the detachment clearly indicate that it predates the onset of detachment faulting. The best stratigraphic constraints are preserved in the area of Piz Bardella where the TAF caps an up to 500 m thick tilted pre-detachment succession. Elsewhere, the Agnelli Fm. can also be absent, either due to extension (tectonic omission) or erosion.

3.3.3.2 RC - Radiolarian Cherts

Radiolarian Cherts are widespread within the Alpine Tethys domain. They can be defined as the first "post-rift" sequence in the sense that they are the first sediments occurring over pillow basalts showing a MORB composition (Weissert and Bernoulli, 1985; Wilson et al., 2001; Fig. 3.6). In the central Alps, the RC are dated as Bathonian to Oxfordian (Baumgartner, 1987; Bill et al., 2001). In the "Grisons transect", the RC occur in the Platta and Err nappes and can be traced from there towards proximal domains. Thus, they represent an ideal time marker horizon to determine the onset of MORB activity. That is why Masini et al. (2011) used the RC as a time marker indicating the age of breakup within the continent, which then separates syn-rift from post-rift sequences.

The definition of these two time lines enabled the authors to define the sedimentary sequence from the onset of detachment faulting until the emplacement of MORB over exhumed mantle. This depositional interval corresponds to a time range between Pliensbachian (about 185 Ma) and Bathonian (about 165 Ma), giving the maximum duration during which

detachment systems may have been active in the distal margin and adjacent OCT.

3.4 THE ADRIATIC OCEAN-CONTINENT TRANSITION: THE PLATTA NAPPE

Together with the lower Austroalpine Err nappe, the Platta nappe preserves remnants of a segment of the southeastern margin of the Jurassic Piemonte-Liguria ocean. The Platta nappe, originally situated oceanwards of the Err nappe, represents the ocean-continent transition of the former Adriatic continental rifted margin (Fig. 3.11). Because of the lack of an Alpine-related high-pressure and temperature metamorphic overprint (T_{max} never exceeded approximately 250°C, Ferreiro-Mählmann, 2001), the pre-Alpine history related to the continental break-up is well documented. In the Platta nappe, relics of the Err detachment system are found and separate extensional allochthons consisting of continental crust, Permian to Late Triassic pre-rift sediments and syn-rift sediments (Saluver Formation) in the hangingwall from the exhumed mantle rocks constituting the footwall (Dietrich, 1969; Manatschal and Nievergelt, 1997). The latter are composed of serpentinized peridotites derived from spinel lherzolites and harzburgites in which minor gabbroic rocks and basaltic dykes are intruded. Palinspastic sections (Manatschal and Nievergelt, 1997; Desmurs et al., 2001) have shown that the Platta nappe consists of two units of ultramafic rocks, an upper and originally more internal (e.g. continentalward) one and a lower, external (e.g. oceanward) unit, separated by a thrust. The lower unit is covered by pillow lavas and basaltic flows and was locally intruded by Jurassic gabbros 161±1 my ago (Schaltegger et al., 2002), which crystallized at shallow depths within an already serpentinized mantle (Desmurs et al., 2001). Both gabbros and basalts are derived from a similar mantle source as demonstrated by Schaltegger et al. (2002). The upper serpentinite unit is almost free of magmatic rocks, except for a few dolerite dykes and a single basaltic flow. Major changes in the mantle composition and the volume and type of magma can be observed between the two units (Desmurs et al., 2001, 2002; Müntener et al., 2004). The serpentinites in the Platta nappe are overlain in some places by ophicalcites,

which are in turn covered by post-rift sediments (Dietrich, 1969) or by pillow lavas. These ophicalcites often show a red matrix made of carbonate containing only clasts of serpentinites (Manatschal and Nievergelt, 1997).

In both units forming the Platta nappe, exhumed mantle rocks, extensional allochthons and pillow basalts are stratigraphically overlain by Middle to Late Jurassic radiolarites and/or Early Cretaceous pelagic Calpionella Limestones.

Palinspastic reconstructions from the continental Err nappe to the ophiolitic Platta nappe show conspicuous analogies to present-day magma-poor continental rifted margins as the Iberian margin (W of Portugal), in terms of extensional detachment faulting, crustal thinning, sediment distribution, overall margin architecture, and tectonic evolution (Manatschal and Bernoulli, 1998; Whitmarsh et al., 2001).

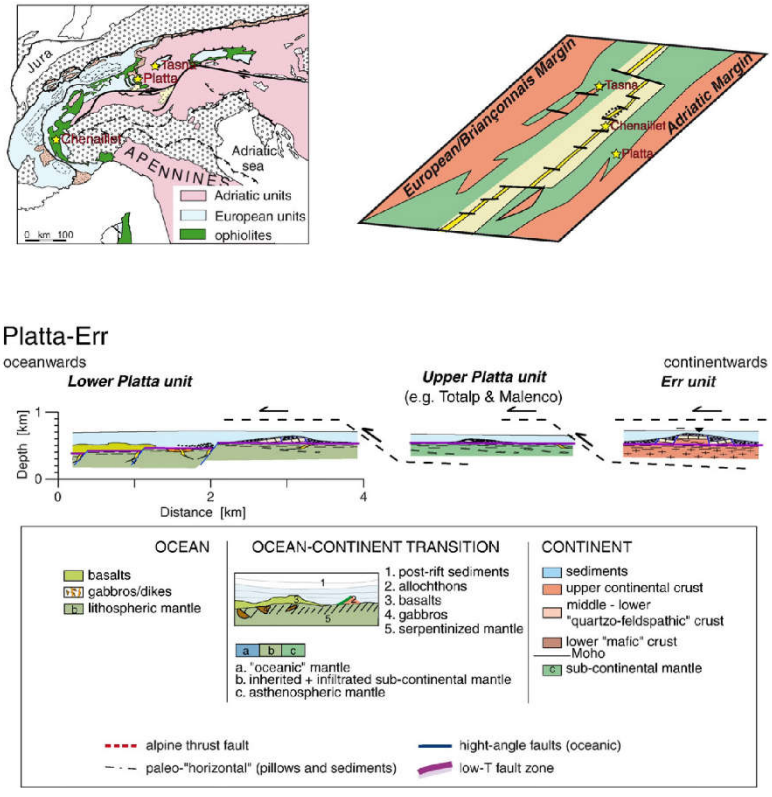

Fig. 3.11 - Section across the Platta-Err, Tasna and Chenaillet ophiolite units. The maps show the present-day position of these units in the Alps as well as their paleogeographic position in the northern Alpine Tethys basin. The Platta-Err section is modified after Manatschal et al. (2003) and the Tasna section after Manatschal et al. (2006).

THE RESULTS

4. The central distal margin

4.1 PIZ VAL LUNGA AREA

4.1.1 Stratigraphy and petrography

The Piz Val Lunga section belongs to the Upper Err unit and is interpreted as the overturned limb of a west to northwest-facing D1 fold (Manatschal and Nievergelt 1997). Its western ridge exposes one of the best-preserved sections across a Jurassic extensional detachment (Fig. 4.1). The footwall, now the summit of Piz Val Lunga, consists of Albula granite. The top of the basement (presently lying in an overturned position) is made of green cataclasites and black gouges (the latter containing mm- to dm-size clasts of Triassic dolostone, granitic basement and green cataclasites), which represent the fault rocks of the Jurassic detachment fault. Topographically below, but stratigraphically above the detachment, the former hanging wall is constituted by an extensional allochthon made of Triassic dolomites that are overlain by syn-tectonic sediments belonging to the Bardella formation (Fig. 4.2a). These rocks are separated from the underlying Lower Cretaceous Argille a Palombini by a D1 thrust that is localized in the post-rift sediments.

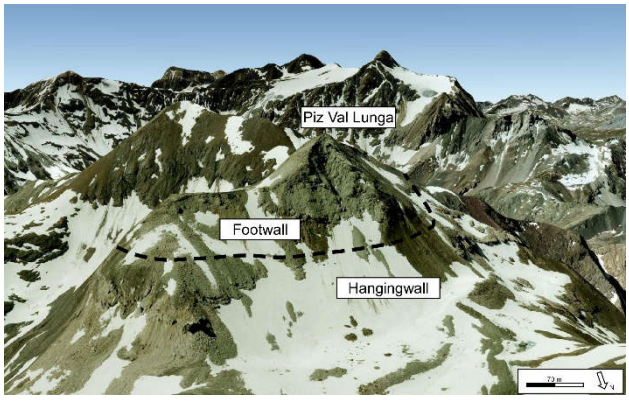

Fig. 4.1 - Panoramic view of Piz Val Lunga area. The dashed line marks the extensional detachment fault separating the extensional allochthon (hangingwall) and the Albula granite (footwall).

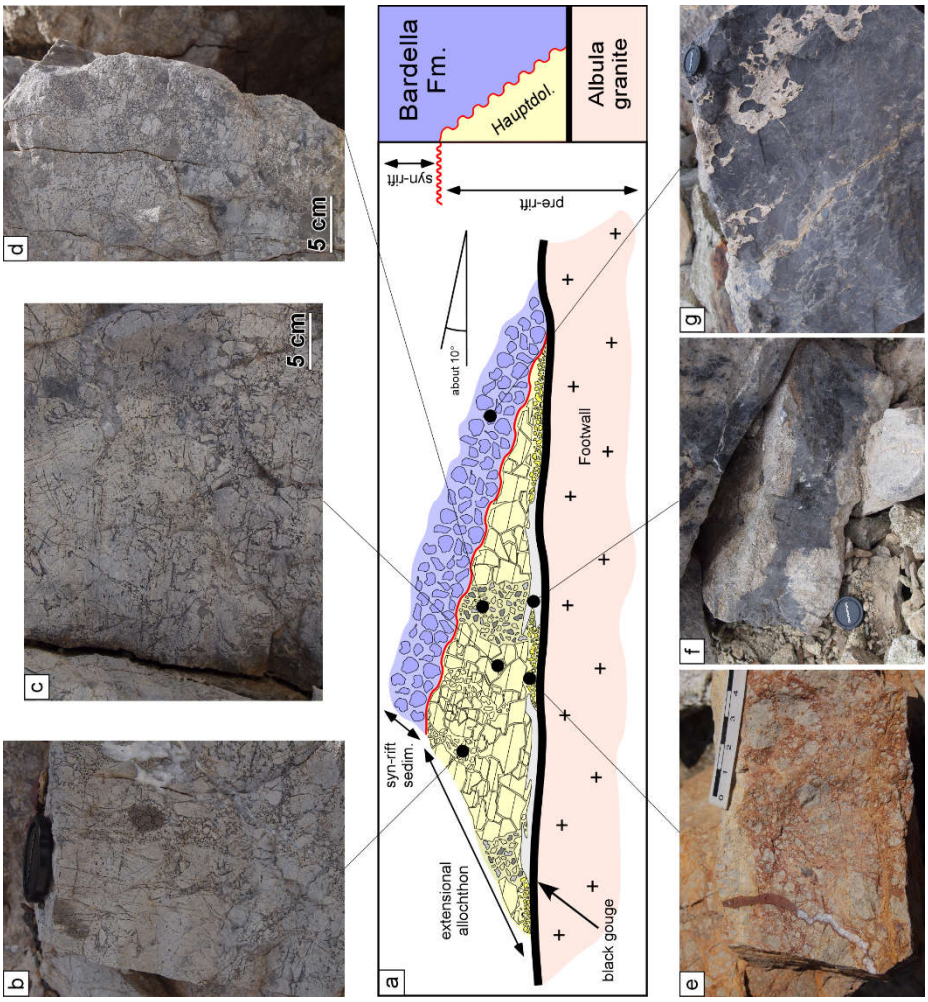

Fig. 4.2 - (a) Schematic sketch, not to scale, representing the main features observed in Piz Val Lunga area. The present-day stratigraphy is upside down due to Alpine tectonics. The extensional allochthon, made up of carbonates from the Hauptdolomit Fm., actually show different textures: monomict mosaic (b) and crackle (c) breccias, which are locally crossed by polymict rubble breccias (d). (e) The base of the allochthon is characterized by clast-supported, monomict, poorly sorted breccias with subangular to subrounded clasts. Note the fracture geopetally filled with red sediment and white quartz cement. (f) Irregular dedolomitization (bluish color) affects the greiysh dolomite breccias at the base of the allochthon. (g) Partial silicification (whitish color) of the matrix of the Bardella Fm. breccias. Scales: lens cap (about 6 cm in diameter).

The prevailing lithotype of the allochthon is represented by grey dolostones characterized by an alternation of homogeneous, finely crystalline and thinly laminated beds showing shrinkage pores filled with dolomite and calcite cement. These distinctive features allow to assign these rocks to the Upper Triassic peritidal dolomites of the Hauptdolomit Formation. Locally the allochthon is overlain by clast-supported breccias with angular to sub-rounded clasts of cm- to m-size. Clasts include: mudstones, grainstones with ooids whose cortices are partially dissolved and replaced by calcite spar; wackestones to packstones with peloids and benthic foraminifers (*Glomospira, Triasina*); wackestones with sponge spicules replaced by calcite spar; coarse crinoidal grainstones; packstones with peloids, crinoid and bivalve shell fragments, and sparse benthic foraminifers (*Involutina*). Clasts of cherts containing crinoids, ghosts of silicified peloids and patches of quartz and chalcedony, which represent void-filling silica cements, also occur. The matrix of the breccias consists of a packstone with peloids and bioclasts and sand-sized lithoclasts with the same composition and texture of the coarser clasts, and shows compactional features. The texture, composition and presence of biostratigraphically significant foraminifera allow to assign these clasts to the Upper Triassic Kössen and to the Lower Jurassic Agnelli Formations (Finger, 1978; Furrer, 1981). These breccias, by their composition and stratigraphic position, can be compared to the syn-rift Bardella Formation of Masini et al. (2011, 2012; Fig. 4.2 a). Among the largest clasts in the scree debris, one is particularly notable. It is more than 1 m in size and consists of grey, bedded limestones locally brecciated and is crossed by a neptunian dyke filled with yellow sediment. Grey limestones show a variety of textures, from mudstones to grainstones with crustaceans microcoprolites 0.3-1 mm in size (*Favreina*) and mudstones. The yellow infill ranges from mudstone to coarse packstone with bivalve shell fragments, mudstone intraclasts and angular quartz grains 50 to 100 μm in size. This block shows the typical facies of the Rhaetian Kössen Formation and, as no similar beds have been found in place, it is tentatively assigned to be the basal part of the Kössen Fm, which directly overlies the Hauptdolomit Formation in the stratigraphic succession.

Actually, the Hauptdolomit Formation appears almost completely brecciated with a variable degree of disruption of the rock and style of brecciation.

At one end, the rock is only crossed by a network of veins with minor displacement of fragments; these crackle breccias (Fig, 4.2 c; Morrow, 1982) pass transitionally to a breccia where clasts are significantly displaced but the fragments still fit one to another (mosaic breccias, Fig. 4.2 b). Bedding and/or lamination can still be recognized, although slightly offset. These rocks are locally crossed at high angles by irregular bodies of polymict rubble breccias i.e. breccias with lithologically different clasts, which do not match (Fig. 4.2 d, Fig. 4.3 a-b; Morrow, 1982). In addition to the fenestral laminated finely-crystalline dolomites, coarsely crystalline lithotypes also occur as clasts. All these breccias are matrix-free, clast-supported and the voids among clasts are filled with a coarse, equant calcite spar that in cathodoluminescence (CL) is characterized by a clear oscillatory zoning (Fig. 4.3 c). Cathodoluminescence and SEM-BSE images moreover show that the coarsely crystalline litho-types in the breccia mainly consist of sparry calcite, with a moderate to bright yellow luminescence, which selectively replaces discrete concentric zones within non-luminescent dolomite crystals (Fig. 4.3 d-e). The whole rock body is crosscut by a system of calcite-filled veins mainly perpendicular to the bedding. Another type of breccia occurs as dm-thick bodies close to and parallel to the detachment fault. It is a clast-supported, monomict, poorly sorted breccia with sub-angular to sub-rounded clasts, which do not exceed 5-10 cm and a yellowish to reddish matrix. Clasts are composed of dolostones with variable crystal sizes (Fig. 4.2 e). CL allows to distinguish clasts with very dull luminescence, from the brightly luminescing finely crystalline calcite matrix and thus to observe that clasts may be as small as a few tens of microns (Fig. 4.4 a-b). The breccias are crosscut by mm-wide fissures with complex fills that include fine-grained sediment, locally laminated, and quartz cement (Fig. 4.2 e; Fig. 4.4 c-d). The latter forms a thin rim of crystals on the edges of the fissure subsequently filled with sediment, and plugs the remaining voids with larger crystals. In larger veins, sediment and

quartz cement rims alternate with sediment geopetally lying on quartz crystal terminations (Fig. 4.4 e-f). Locally all these breccias show irregular, dm-sized portions where the brecciated structure is almost completely obliterated and the rock is fully made of calcite (Fig. 4.2 f). The latter, lastly, is affected by a patchy silicification, which gives rise to irregular, dm-large portions where the carbonate rock is replaced by a mosaic of fine-grained quartz. In some instances, the breccias are affected by a selective replacement of dolomite by calcite as described above, although on a lesser extent. Silicification also affects the breccias composed of clasts of the Upper Triassic Kössen and Lower Jurassic Agnelli Formations. The degree of silicification is variable on short distances (Fig. 4.2 g; Fig. 4.5 a-d), from nearly complete, to restricted to the matrix among clasts, or to mm- to cm-wide, irregular bands consisting of fine-grained quartz crystals or chalcedony.

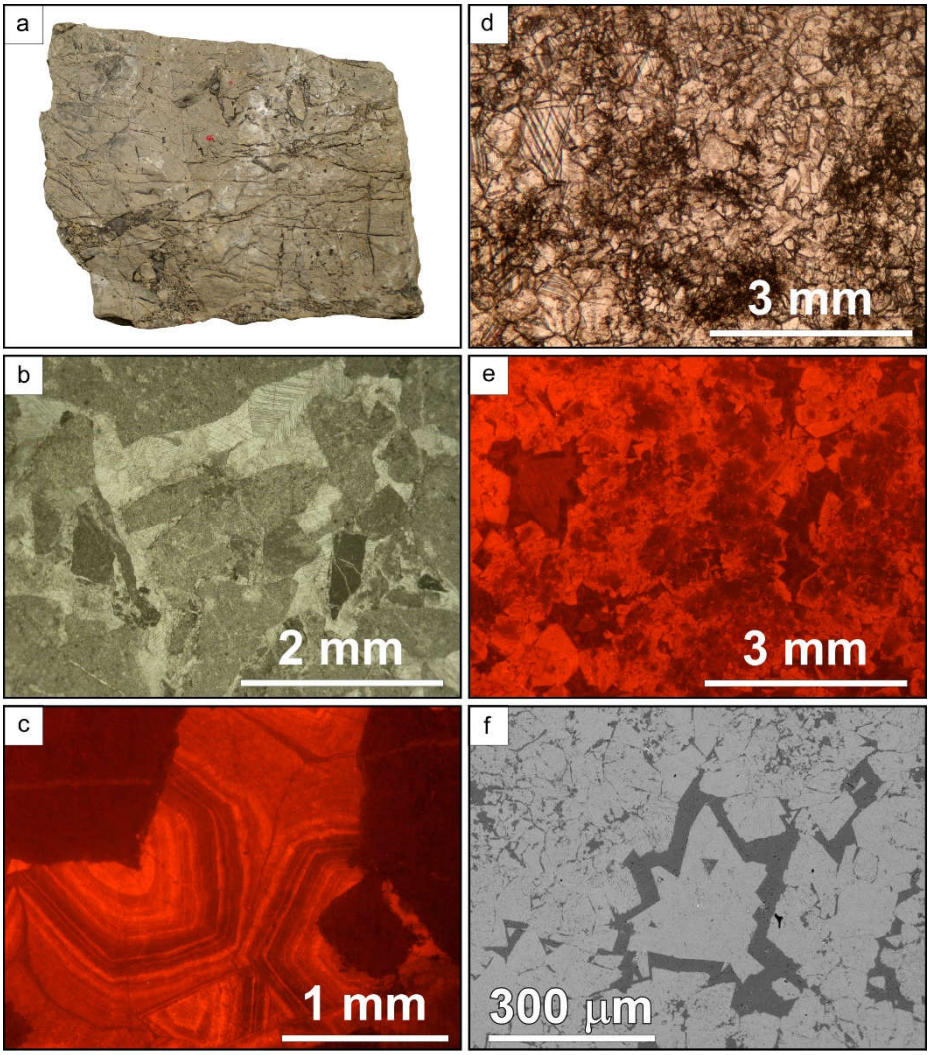

Fig. 4.3 - (a) Hand specimen of Hauptdolomit Fm. characterized by brecciated texture. (b) Transmitted light and (c) CL images of polymict rubble breccias cemented by coarse equant calcite spar, which shows oscillatory zoning. (d) TL, (e) CL and (f) SEM-BSE images of the former coarsely, crystalline, dull luminescent dolomite, dark grey in SEM-BSE, largely replaced by sparry calcite, which shows a moderate to bright yellow CL and is light grey in SEM-BSE.

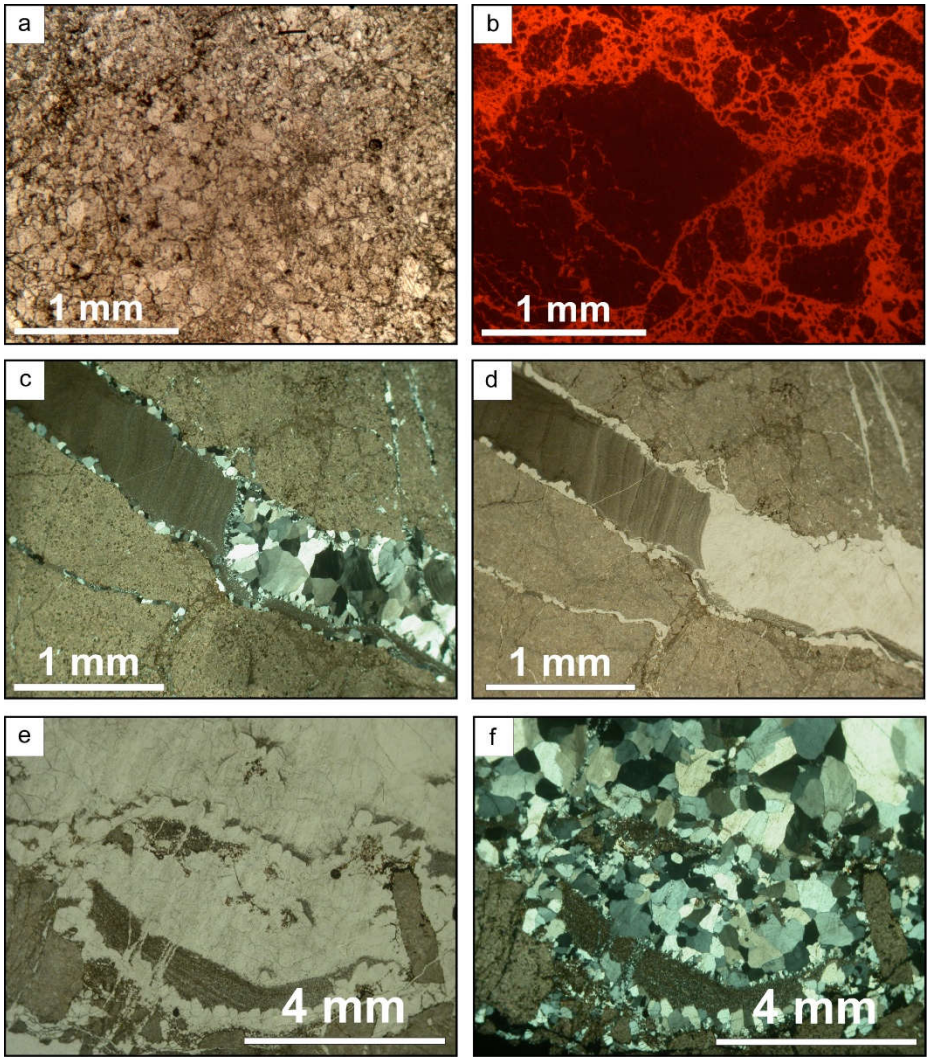

Fig. 4.4 - Hauptdolomit Fm. textures at the base of the allochthon: (a) TL and (b) CL images of clast-supported, monomict poorly sorted breccias with dull luminescent dolomite clasts in a finely crystalline calcite matrix. (c) TL and (d) crossed polarizers images of mm-large fissures within the clast-supported, monomict breccias with a complex fill including fine-grained sediment, locally laminated, and quartz cement. (e) TL and (f) crossed polarizer images of larger veins filled with quartz. Note thin sediment drapes geopetally overlying euhedral terminations of quartz crystals.

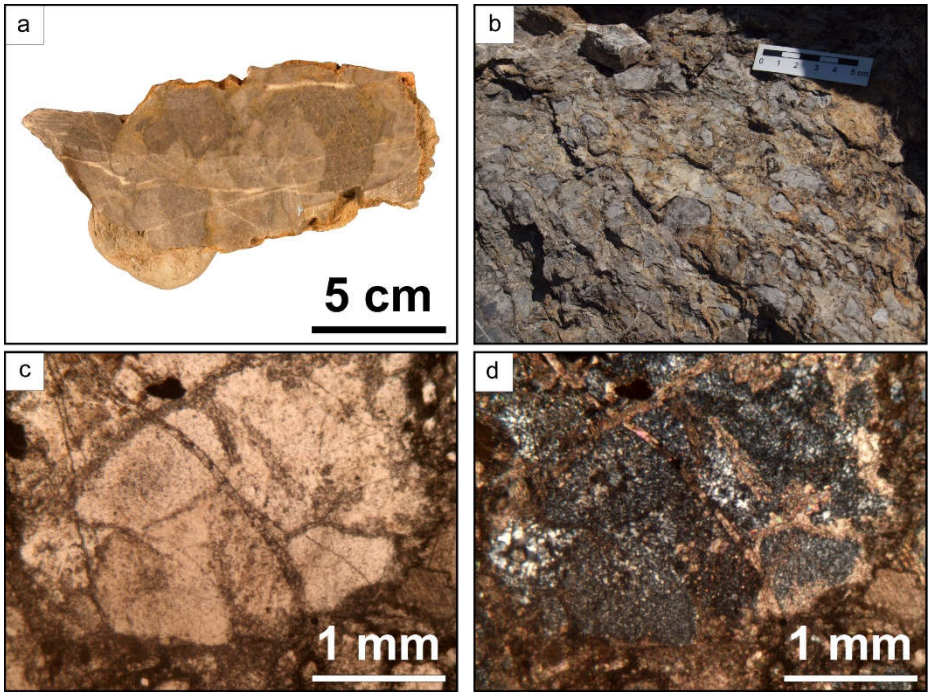

Fig. 4.5 - (a) Hand specimen and (b) outcrop scale images of partially to fully silicified syn-rift Bardella Fm. overlying the extensional allochthon. (c) TL and (d) crossed polarizer images highlighting the fine-grained silicification affecting the matrix of the Bardella Fm.

4.2 FUORCLA COTSCHNA AREA

4.2.1 Stratigraphy and petrography

The area of Fuorcla Cotschna, belonging to the Middle Err unit, preserves a quite complete section through a supra-detachment sedimentary basin (*sensu* Masini et al. 2011, 2012) filled with syn- to early post-rift sediments. The Fuorcla Cotschna section is under- and overlain by minor, Alpine shear zones, which may have overprinted some of the Jurassic structures. However, the observed field relations clearly indicate a pre-Alpine age for most of the structures both in the basement and in the sediments. Similar to the Piz Val Lunga area, a Jurassic detachment fault separates a granitic footwall, constituted by the Albula granite and poly-metamorphic basement rocks, from the hanging wall represented by the Bardella pre-rift extensional allochthon and syn-rift sediments onlapping the detachment with a very gentle angle (Fig. 4.6).

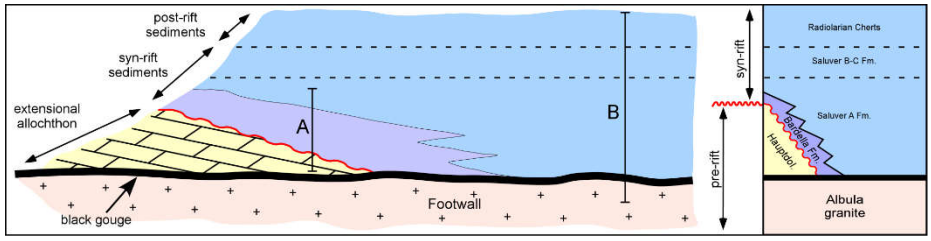

Fig. 4.6 - Schematic sketch, not to scale, of the Fuorcla Cotschna area and localization of the two transects (A and B) to which the stratigraphic description refers.

The footwall is highly tectonized at its top and is characterized by the presence of a black gouge in which clasts of basement and pre-rift dolomite are preserved. Due to the Alpine tectonic overprint, it has not been possible to observe a continuous stratigraphic section of the hanging wall. Nonetheless, two key areas have been considered to reconstruct the whole architecture of the Fuorcla Cotschna area. In the first one (transect A in Fig. 4.6), grey carbonate rocks occur, which texturally range from sucrosic, massive dolostones with crystals some 100's μm in size to laminated finely crystalline dolostones showing

shrinkage pores filled with a cement consisting of up to 1 mm-large dolomite crystals. The rock shows a dull to moderate reddish orange CL whereas the cement appears concentrically zoned with alternances of thin bright to dull reddish orange zones (Fig. 4.7 a-b; Fig. 4.8 a-d). The laminated dolostones are locally alternated with marly layers rich in bivalve shells. These carbonate rocks, by their lithofacies, can be referred to the upper part of the Upper Triassic peritidal Hauptdolomit Formation close to the boundary with the Rhaetian Kössen Formation and may be interpreted as the easternmost part of the Bardella extensional allochthon. They are crossed by a complex network of 100's micrometers- to few millimeter-thick, randomly oriented fractures mainly filled with saddle dolomite (Fig. 4.7 b, Fig. 4.8 d), whose crystals reach 2-3 mm in size and are generally very dull in CL. On weathered outcrop surfaces, these veins are clearly identifiable because of a yellow to orange color. Locally, up to 1 cm-thick veins occur with a more complex filling made of quartz and euhedral to subhedral albite crystals some 100's micrometres large associated with dolomite. Quartz crystals poikilotopically include carbonate grains, from minute particles less than 10 μm large to euhedral dolomite crystals 100's micrometres large. Stratigraphically above the pre-rift sequence, even if the contact is not clearly shown, a sedimentary clast-supported breccia made up of carbonate clasts occur (Fig. 4.7 c). The clasts, mostly rounded and ranging from few centimeters to some decimeters in size, consist of Triassic carbonates belonging to the pre-rift sequence and are commonly crossed by the same kind of veins described above, which stop at the edge of the clasts. The whole rock mass is characterized by several sets of veins, up to some millimeters large, cemented by coarsely crystalline saddle dolomite, quartz and calcite. Since no basement-related clasts have been observed, this sedimentary body can be assigned to the syn-rift Bardella Formation (Masini et al 2011, 2012, Finger 1978; Fig. 4.6; Fig. 4.7 a). Above, a different coarse-grained sedimentary sequence occurs. It consists of clast- to matrix-supported conglomerates with angular to rounded clasts. Carbonate clasts prevail but granitic basement-derived ones are also common. The matrix consists of a medium to very coarse sandstone rich in quartz and

feldspar grains. Due to the presence of footwall-related material and its stratigraphic position, this sequence has been interpreted as Saluver A Formation (Masini et al. 2011, 2012, Finger 1978; Fig. 4.6; 4.7 d; Fig. 4.9a-f). As in the Bardella Formation, carbonate clasts are commonly crossed by veins, which stop at the edge of the clasts (Fig. 4.9 c). In some instances, these veins show a first isopachous rim of dolomite cement, 200 μm thick, with a dull brown luminescence, followed by fibrous quartz, which documents a syn-kinematic growth (Fig. 4.9 e-f). Millimeter-thick veins cemented by quartz and subordinated saddle dolomite crosscut the whole conglomerate (Fig. 4.9d). Microprobe analyses of the dolostones occurring in the allochthon and in the clasts within the Bardella and Saluver Formations show that on the whole the replacement dolomite and the pore-filling dolomite cement are very poor in or completely free of Fe whereas vein dolomite contains up to 2.0 mole % $FeCO_3$.

The Fuorcla Cotschna area clearly shows the relationships between the granitic footwall, the detachment fault and the overlying basin-filling sediments (transect B in Fig. 4.6). The footwall displays the same features already described in the Piz Val Lunga area. The detachment surface is overlain by a stratigraphic succession that starts with medium to coarse sandstone beds made up of basement-derived quartz and feldspar grains alternated with cm-thick pelitic beds. This decimeter-thick interval passes upward into a plurimetric, clast-supported and roughly graded sedimentary breccia. In its basal part, the cm- to dm-sized clasts are almost completely constituted by allochthon-derived carbonate rocks whilst the matrix is composed of a medium to coarse grained quartz and feldspar sandstone.

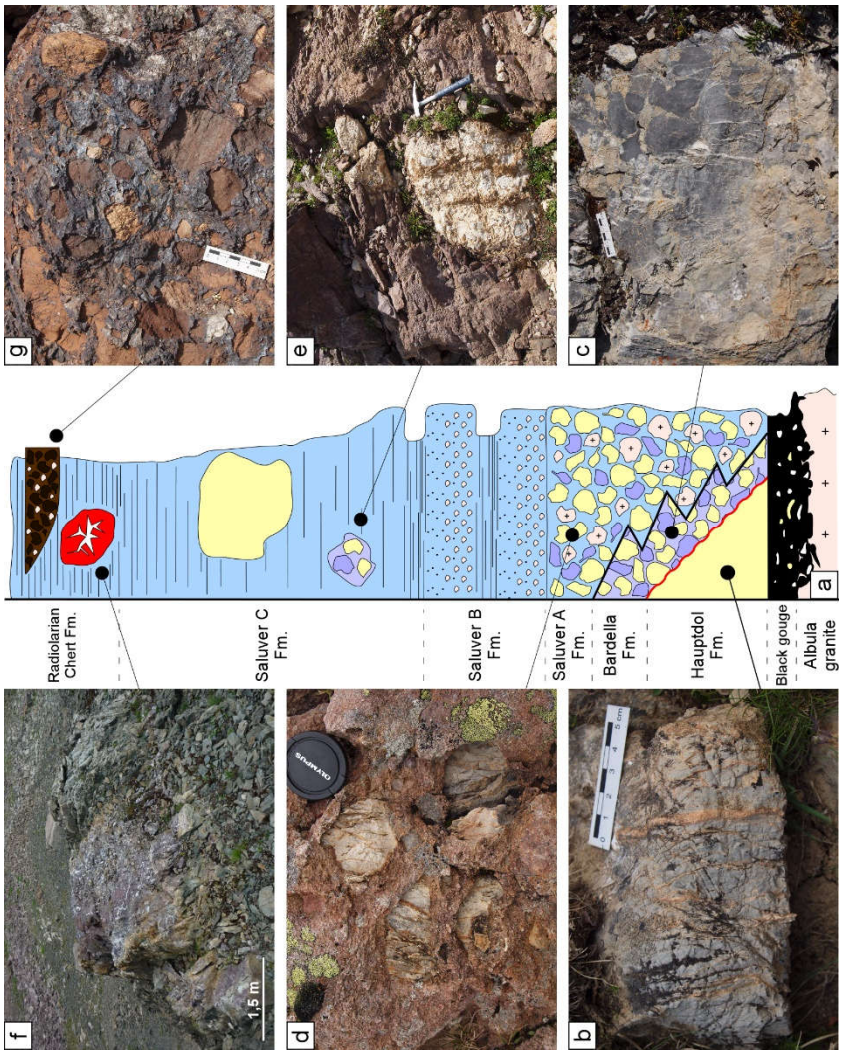

Fig. 4.7 - (a) Stratigraphic log, not to scale, of the Fuorcla Cotschna area based on transects A and B described in the text and shown in Fig. 4.6. (b) Massive dolostones belonging to the Hauptdolomit Fm. crossed by randomly oriented fractures filled with orange-yellow saddle dolomite. (c) Bardella Fm.: sedimentary clast-supported breccias made up of Triassic carbonate clasts. (d) Saluver A Fm.: clasts- to matrix-supported conglomerates with carbonate and basement-derived clasts in a coarse sandy matrix. Note veins within clasts stopping at clast edges. (e) Decimeter-sized block of Bardella Fm. reworked in the red sandstones of the Saluver Fm. (f) Thick-bedded conglomerates constituted of carbonate and basement-derived clasts showing

a peculiar brownish color of the carbonate clasts. The shiny black portion is silicified matrix. (g) Big "nodule" of chert within the lowermost part of Radiolarian Cherts crossed by an irregular network of quartz-filled fractures. Scales: hammer (33 cm long), lens cap (6 cm in diameter).

Both the basal sandstone and the overlying breccias show mm-thick sub-vertical injections of black fine-grained material, which is derived from the gouge that caps the exhumed granite. Moreover, the breccias are crosscut by a dense network of mm-thick and some meters long veins filled with quartz and saddle dolomite (Fig. 4.9 a). The presence of basement-derived material constituting the matrix of the breccia, allows to ascribe this body to the Saluver A Formation (Masini et al 2011, 2012, Finger 1978; Fig. 4.6). Clasts are crosscut by dolomite- and quartz-filled veins that stop at the edge of clasts showing the same features already described from Piz Val Lunga. Worth mentioning in the Saluver A unit is the presence of several meter-large blocks of Triassic dolostones in which cm- to dm-large grossly tabular bodies of crackle to mosaic breccias occur with a cement of coarse dull luminescent saddle dolomite, yellowish in outcrop (Fig. 4.7 e).

Upsection, the sedimentary succession defines a thinning and fining upward trend. Conglomerates and breccias are progressively replaced by thin- to medium-bedded reddish turbidites, composed of siliciclastic sandstones and pelitic interbeds referred to the Saluver B and C units (Masini et al. 2011, 2012; Finger 1978; Fig. 4.6). In the uppermost part of this succession, ghosts of radiolaria have been identified within reddish siliceous mudrocks and grey cherts, interbedded with sandstone beds, which should mark the onset of Radiolarian Cherts deposition (Masini et al. 2011, 2012; Finger 1978; Fig. 4.6). Nonetheless, much coarser deposits locally occur as scattered, several decimeter-sized blocks of carbonate breccias of the Bardella Formation or thick to very thick-bedded conglomerates or breccias composed of variable amounts of basement-derived or hanging wall derived carbonate clasts. One of these beds, a few meters above the first grey radiolarian cherts, is notable for the marked

lenticular geometry and for the brownish color of most carbonate clasts (Fig. 4.7 g; Fig. 4.11 a-b). Microprobe analyses show that this color is due to variable degrees of Fe and Mn oxide staining. The whole Saluver Formation is crossed by veins filled with quartz and subordinate saddle dolomite and is affected by a localized but intense silicification. This has been identified: 1) in the blocks of Triassic dolostones, where irregular dm-sized patches made of round-shaped clusters of quartz crystals up to 1 mm large occur; 2) in the lenticular brownish breccia bed where the space among clasts is black, markedly weathers out, and consists of very fine-grained quartz (Fig. 4.11 c-d) in which dolomite rhombs, some 100's μm long, are scattered; 3) in the lowermost, grey, radiolarian chert beds, where a large "nodule" of chert, over 2 m-long and about 1 m thick occurs (Fig. 4.7 f). It is whitish at the outer edge and reddish in its inner part where it shows a crackle to mosaic breccia structure with white quartz veins up to over 1 cm large. The reddish chert consists of very fine-grained quartz whereas the veins are filled with isopachous, botryoidal chalcedony, which rims the vein walls, and a mosaic of quartz crystals (up to over 1 mm large) in the inner parts of the veins. Interestingly, dm-sized clasts, showing the same features, are found in the lower, coarse, part of the thick turbiditic beds locally present in the Saluver C unit. Concentric, septarian-like fractures also occur in these clasts (Fig. 4.10 a-d).

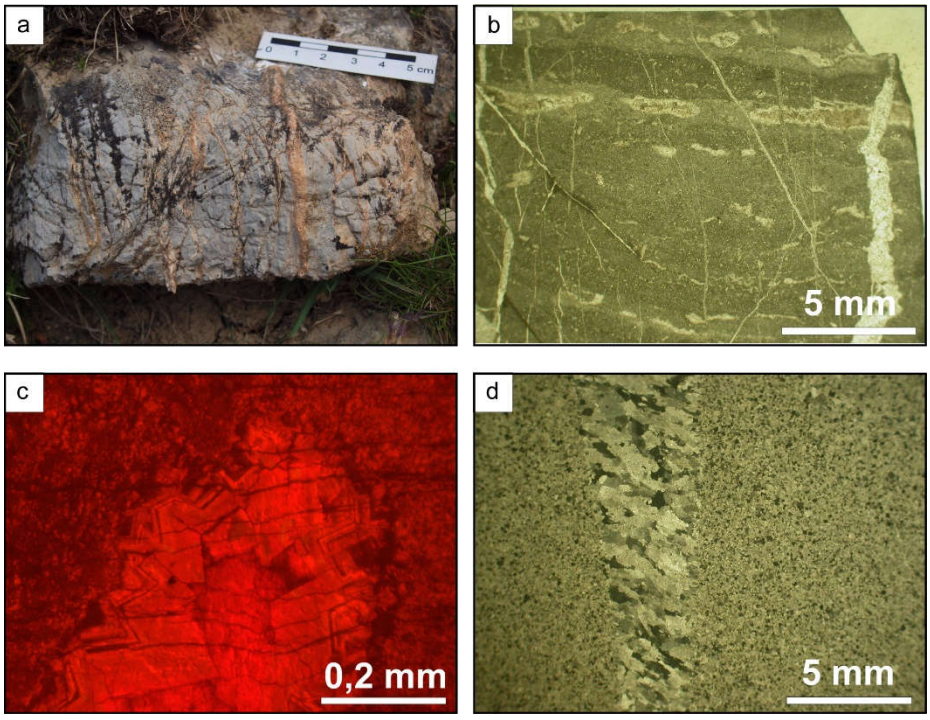

Fig. 4.8 - (a) Massive dolostones belonging to the Hauptdolomit Fm. crossed by randomly oriented fractures filled with orange-yellow saddle dolomite. (b) TL image of finely crystalline dolostone with shrinkage pores filled with dolomite cement. (c) CL detail of a shrinkage pore filled with concentrically zoned dolomite cement showing alternaces of bright to dull reddish orange zones. (d) TL image of a sucrosic dolostone of the Hauptdolomit Fm. crossed by a coarsly crystalline saddle dolomite vein.

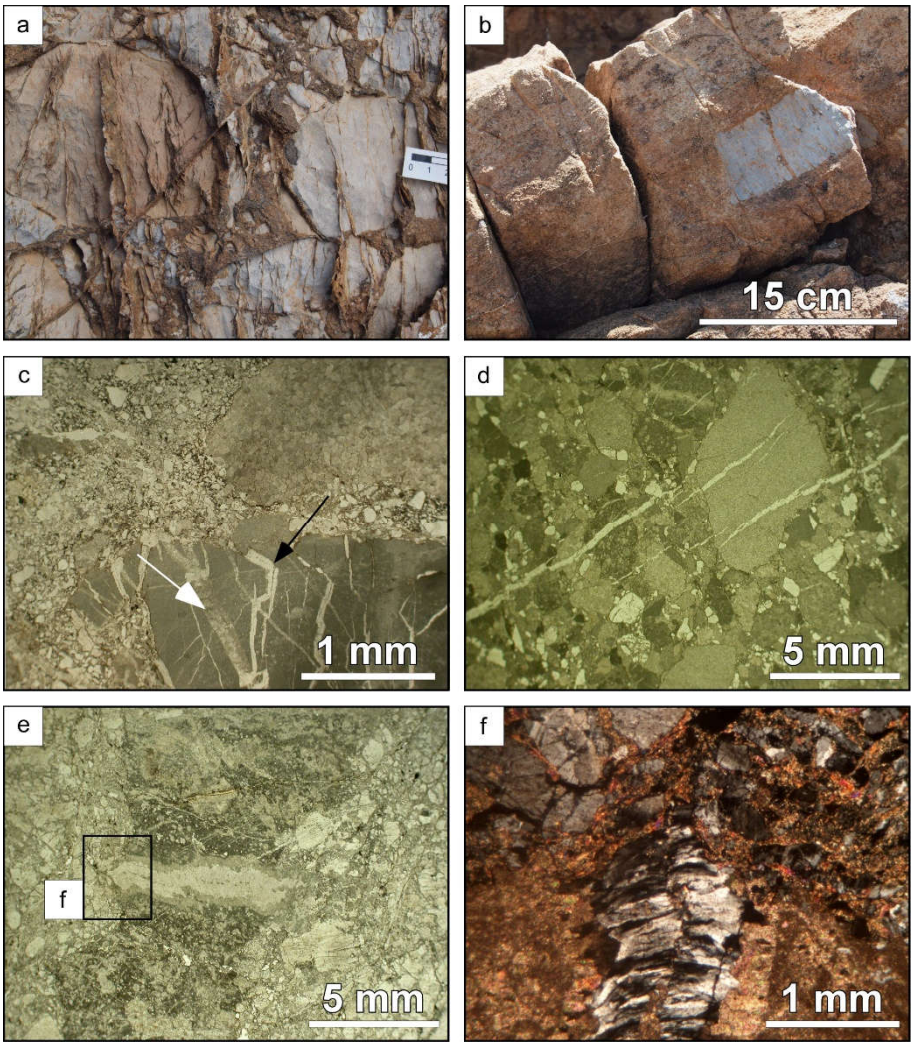

Fig. 4.9 - Saluver Fm.: (a) Clast-supported conglomerates composed of mainly carbonate-derived material with a fine grained siliciclastic matrix. Some dolomite and quartz veins are confined within the clasts whereas others crosscut both the clasts and the matrix. (b) Upper part of the Saluver Fm. composed of turbidites beds in which some cm- to dm-large clasts occur. The whole rock mass is cut by dolomite and quartz veins. (c) TL image of carbonate clasts in the Bardella Fm. with dolomite (white arrow) and quartz (black arrow) veins that stop at the edge of the clast. (d) TL image of quartz veins crosscutting both clasts and matrix in the Saluver Fm. (e) TL and (f) crossed polarizers detail of multiphase filling of a vein within a clast in the Saluver Fm.: a first, 200 μm rhick, isopachous rim of dolomite is followed by a fibrous quartz infill.

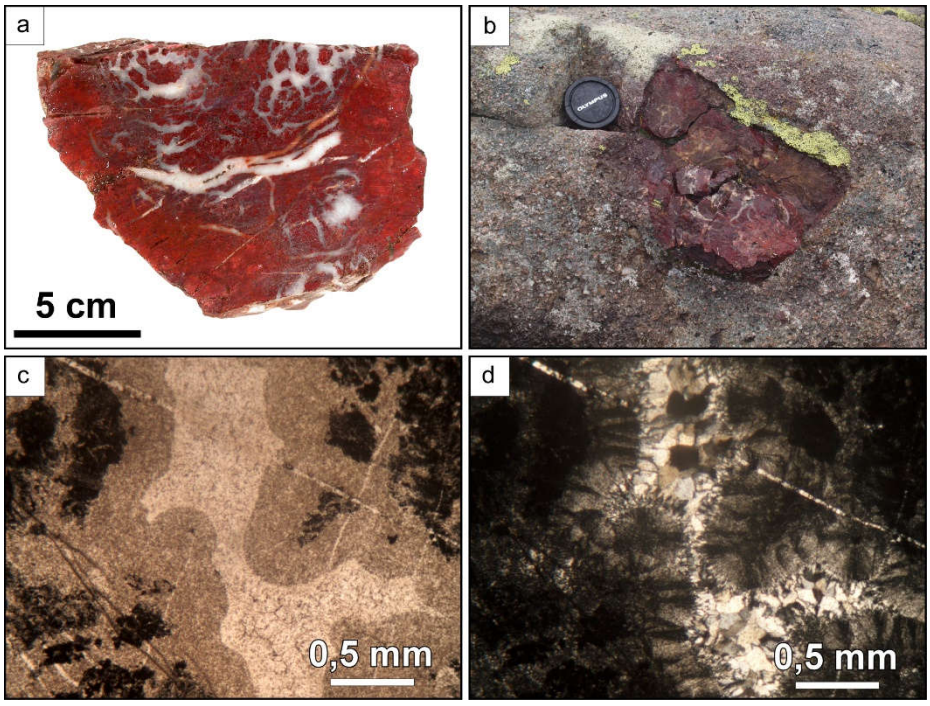

Fig. 4.10 - (a) Hand specimen and (b) field occurrence of septarian-like concretions in the uppermost part of Saluver Fm. (c) TL and (d) crossed polarizers images of the septarian-like fracture fill. Isopachous, botroidal chalcedony rims the cavity and is followed by a coarse mosaic of quartz crystals in the inner part of the cavities.

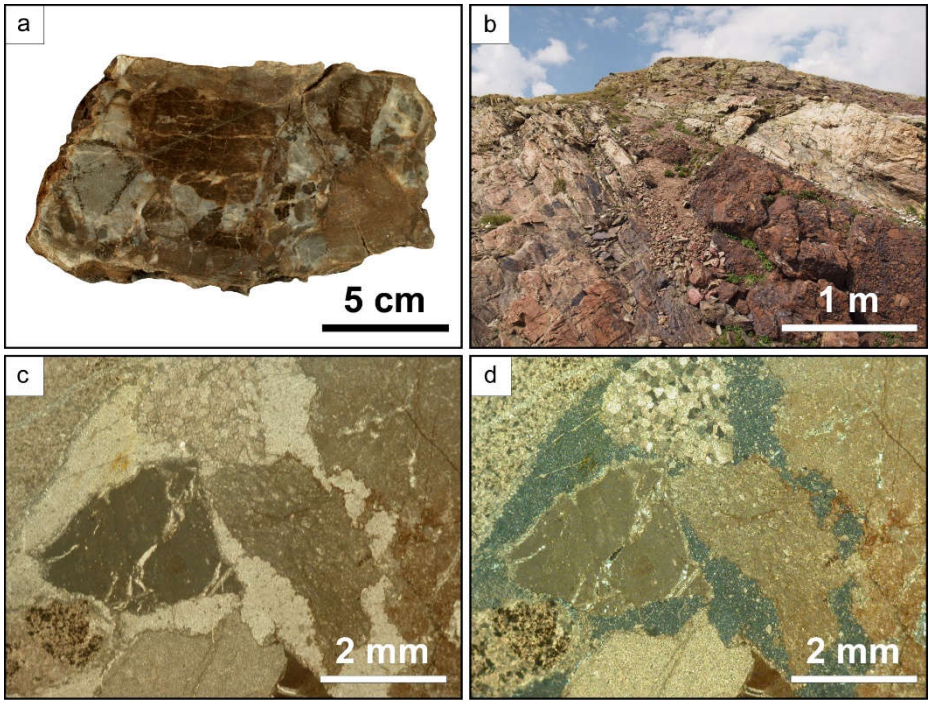

Fig. 4.11 - (a) Hand specimen and (b) field occurrence of polymict brownish calciruditic bed in the uppermost part of Saluver Fm. and in basal part of the Radiolarian Chert Fm. (c) TL and (d) crossed polarizers images highlighting the polymict origin of the clasts and their Fe-Mn oxide coating, and the finely silicified matrix.

4.3 ISOTOPE GEOCHEMISTRY AND FLUID INCLUSION DATA

4.3.1 O and C isotopes

Oxygen and carbon isotope analyses have been performed on calcite and dolomite occurring in different portions of the studied rocks in both the Fuorcla Cotschna and the Piz Val Lunga sections. Analyzed dolomite includes Upper Triassic samples of fine grained and sucrosic dolostones of the Hauptodolomit and Kössen Formations and dolomite veins occurring within them, as well as clasts of these formations in breccias and in the Bardella Formation. The calcite samples correspond to sparry cement of breccias, to veins crosscutting the whole

succession and to the replacement of former dolomite. The results are shown in Fig. 4.12 and ANNEX A. All the data are characterized by slightly negative to positive $\delta^{13}C$ values (-0.23‰ VPDB to 3.07‰ VPDB) and slightly to strongly negative $\delta^{18}O$ values (-1.01‰ VPDB to -12.05‰ VPDB).

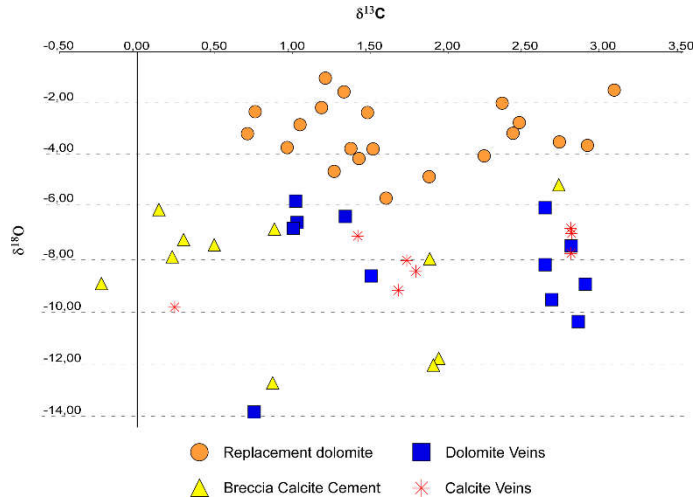

Fig. 4.12 - Stable isotope data: $\delta^{18}O$ versus $\delta^{13}C$ cross plot for dolomite and calcite minerals from Piz Val Lunga (PVL) and Fuorcla Cotschna (FCT) areas. Values relative to VPDB standard.

4.3.2 Sr isotopes

$^{87}Sr/^{86}Sr$ isotope analyses have been performed in order to better characterize fluid flow circulation paths. Three samples of replacement dolomite, two of dolomite veins in the Hauptdolomit Formation and four of calcite cement of breccias and dedolomite were analyzed. All these samples show $^{87}Sr/^{86}Sr$ values comprised between 0.708723±0.000011 (Fuorcla Cotschna dolostone) and 0.713137±0.0000238 (Fuorcla Cotschna, dolomite vein), which are markedly higher than expected for Triassic and Jurassic seawater (maximum values for Upper Triassic and Lower Jurassic 0.708000, McArthur et al., 2012; ANNEXES C).

4.3.3 He isotopes

Analyses were carried out on saddle dolomite veins within the Hauptdolomit Fm., dedolomite and septarian-like concretion cements. All the results show a $^{3}He/^{4}He$ between 0.027 Ra and 0.100 Ra (ANNEX D).

4.3.4 Fluid inclusion microthermometry

More than 80 fluid inclusions from 12 doubly-polished sections have been measured to find their homogenization temperatures with a standard heating method (Goldstein and Reynolds, 1994). Primary fluid inclusions of useful size for microthermometry (i.e. more than 2 μm in diameter; Goldstein and Reynolds, 1994) were found in the replacement dolomite and dolomite cement of fenestral pores in the Hauptdolomit Formation, which have been gathered because of their genetic relationships and represent set 1, in the calcite cement of breccias representing set 2, and in the calcite due to dedolomitization corresponding to set 3. The very small size of inclusions hindered low-temperature runs aimed at determining the fluid composition. As shown in Fig. 4.13 and ANNEX B, set 1 homogenization temperatures ranges from 88°C to 152°C with the highest frequency between 120°C and 130°C. The calcite cement (set 2) shows values from 77°C to 203°C with the highest frequency between 130°C and 140°C whereas dedolomite calcite (set 3) ranges from 96°C to 114°C.

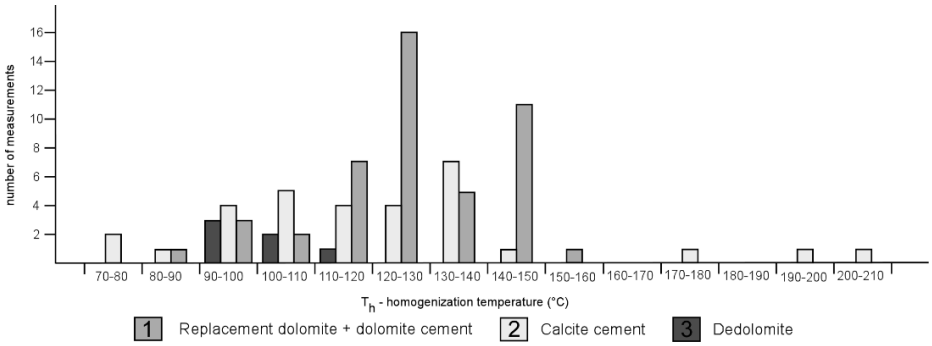

Fig. 4.13 - Histogram of the homogenization temperatures for replacement dolomite and dolomite cement, calcite cement and de-dolomite.

4.4 FIRST ORDER INTERPRETATION

4.4.1 Dolomite

Two styles of dolomitization were distinguished: the first gave rise to finely crystalline dolostones with preservation of primary depositional textures, the second led to the formation of coarse crystalline sucrosic dolostones and zoned cements of fenestral pores. The preservation of CL zoning in the pore-filling dolomite cement clearly demonstrates that no subsequent recrystallization took place. The non-destructive fine-grained dolomite likely formed very early after deposition in a peritidal environment (Tucker & Wright, 1990 and references therein). Conversely, the fabric-destructive coarse-grained replacement dolomite and the pore-filling cements are interpreted to have formed much later as the result of hydrothermal fluid flow. This is clearly documented by fluid inclusion microthermometry, O and Sr isotopes (see “Discussion”).

4.4.2 Dedolomitization

Dedolomitization has been observed only at Piz Val Lunga within the Upper Triassic dolostones. Its occurrence is twofold: at the base of the allochthon close to the detachment fault it forms localized dm-sized patches and selective replacement of coarse dolomite crystals in the cataclasites; in the overlying rubble breccias as partly dedolomitized clasts. Here, the presence of dedolomitized clasts side by side with dolomitic ones shows that dedolomitization is not related to telogenetic processes associated with recent exposure at the surface but occurred before the formation of the breccias. This observation implies a change in the physico-chemical parameters of fluids compared to those responsible for the dolomitization described above. This is confirmed by fluid inclusions, which document considerably lower temperatures in calcite.

4.4.3 Breccias

Leaving aside sedimentary breccias of the Bardella and Saluver Fm., breccias are common at Piz Val Lunga in the Upper Triassic dolostone of the allochthon where they show a quite wide array of features, which document different genetic processes. The dilational character of monogenic crackle and mosaic breccias, which are matrix-free and whose clasts mostly fit to each other (jigsaw breccias), suggests mechanisms of *in situ* hydro-fracturing. Polygenic, matrix-free rubble breccias, containing clasts from different beds of the original stratigraphic succession are interpreted as due to hydro-fracturing associated to some degree of vertical displacement of clasts. A third type of breccia, characterized by the presence of a fine-grained matrix, very poor sorting, and somewhat rounded clasts, is interpreted to be related to cataclastic processes affecting the lower part of the allochthon just above the detachment fault. The absence of cataclasites and breccias formed by hydrofracturing at Fuorcla Cotschna is probably related to the much smaller thickness of the Piz Val Lunga allochthon compared to the studied allochthon situated at Fuorcla Cotschna. At Piz Val Lunga the pre-rift Triassic succession, comprised between the black gouge and the base of the Bardella Formation, is maximally a few tens of meters thick. The burial depth of the Triassic dolomites at Piz Val Lunga was thus very small and overpressured fluids flowing upwards along the detachment fault could easily overcome the internal strength of the overlying rocks inducing hydrofracturing. At Fuorcla Cotschna, conversely, the base of the allochthon is not exposed and consequently the cataclasites that presumably developed at the boundary with the footwall of the detachment, cannot be observed. Furthermore, the hundreds of meters-thick Triassic succession possibly hindered the formation of hydraulic breccias.

4.4.4 Calcite cement

Calcite cement mainly occurs at Piz Val Lunga associated with crackle, mosaic and rubble breccias, the latter including dedolomitized clasts. The petrographic

and CL features, coarse equant calcite spar with a distinct zoning, document a process of cement filling an open framework in static conditions. Given the relatively low abundance of calcite in the studied rocks, the comparable CL features and $\delta^{18}O$ values in calcite cements and dedolomite, it is suggested that dedolomitization and infilling of open pores in breccias are related to the same event of circulation of fluids supersaturated in calcite.

4.4.5 Veins

Veins are widespread and abundant throughout the Triassic-Jurassic sedimentary succession. Crosscutting relationships evidence that veining arises as a complex process, which can be subdivided in two main stages, each one being poly-phase. Particular attention has therefore been paid not only to establish a relative chronology among vein systems but also their relation to stratigraphic markers. The veins within clasts of the Bardella and Saluver Fms. document that a first stage of veining took place before reworking of the host rocks i.e. in a time interval comprised between the top of the Agnelli Formation (TAF) and the base of the Bardella Fm. (BBF; Incerpi et al. 2017; Fig. 4.14), which most probably corresponds to a significant hiatus in sedimentation. Conversely veins crosscutting the studied succession show that subsequent stages of fracturing were recorded by breccias and conglomerates of the Bardella and Saluver Fms respectively. The style of vein filling, mostly consisting of mosaics of unoriented crystals, reflects a prevailing process of passive infill of open fractures in static conditions. Nevertheless, much less frequent, syn-kinematic fibrous crystals perpendicular to fracture walls also exist. Lastly, but importantly, the different mineralogy of the vein-filling phases (dolomite, calcite, quartz, albite) documents significant changes in fluid composition and consequently circulation paths. In fact, a trend through time has been detected from pre-BBF veins dominated by saddle dolomite to post-BBF veins, which are dominantly filled with quartz. This clearly points to an increasingly stronger interaction of fluids with basement rocks in which breakdown of less stable minerals such as feldspars delivered large amounts of silica to the fluids. Calcite-filled veins that

crosscut all the stratigraphic succession and cannot be constrained chronologically, could be related to Alpine orogenesis and were not studied in detail.

4.4.6 Silicification

The products of an early diagenetic silicification are widespread in both sites and at different stratigraphic levels. In fact, 4 types of cherts can be observed : 1) clasts of echinoderm-and sponge spicule-bearing grey cherts within the Bardella Fm. at Piz Val Lunga; 2) clasts of reddish cherts within the Saluver C Fm at Fuorcla Cotschna commonly characterized by a brecciated, locally septarian-like, structure; 3) very large red chert nodules in the lower part of the Radiolarian Chert Fm. at Fuorcla Cotschna; and 4) silicified matrix of calciruditic beds in the Bardella Fm. at Piz Val Lunga and in the Radiolarian Chert Fm. at Fuorcla Cotschna.

Type 1 cherts are easily referred to the Agnelli Fm. and result from early diagenesis of a sponge spicule opal A-rich succession taking place before its erosion and reworking as clasts in the Bardella Fm. The reddish color of type 2 cherts conversely excludes provenance from the Agnelli Fm. and suggests a provenance from silicified clay-rich portions of the red turbidites of the Saluver C. The early, syn-depositional origin of type 2 and 3 cherts is documented by the reworking of type 2 cherts as clasts and by the transitional boundary of type 3 cherts with the encasing sediments, which indicate precompactional growth. The provenance of red cherts from the turbiditic Saluver C Fm., the relative scarcity of radiolarian-rich beds even in the Radiolarian Chert Fm. and the anomalous features of chert nodules (large size, dilational character, locally septarian-like, of brecciation with quartz-filled fractures) show that biogenic opal could not be the source for such silicifications, which conversely must have been extraformational. Massive removal of silica from the quartzo-feldspatic footwall of the detachment on which the syn-rift sedimentary succession lies, seems the obvious and most likely source for silicification. At the present state of

knowledge, however, it cannot be excluded that a contribution of silica came from serpentinization of mantle peridotites (Pinto et al. 2015). The brecciated textures moreover document processes of hydraulic fracturing developed in these cherts, which were forming at very shallow burial depths, in a similar way to what happened in the brecciated Triassic dolostones at Piz Val Lunga. In this scenario, quartz veins crossing subvertically the underlying succession could therefore, at least in part, represent the feeding system of SiO_2–rich fluids flowing upward towards the sea floor. Here, the interaction with shallow buried, fine grained, highly porous sediments could give rise to chert nodules, which in turn could be exposed by erosion and resedimented as clasts, or to silicification of breccia matrixes.

4.4.7 Fe-Mn oxide coating

Different degrees of mineralization, from staining of the clast edges to intense replacement of the whole clast, point to a Fe-Mn oxide precipitation before deposition of the calciruditic deposits occurring close to the Saluver C-Radiolarian cherts boundary at Fuorcla Cotschna. This mineralization likely took place during a period of non-deposition and exposure of sediments at the seafloor. It points to a significant reduction in the supply of clastic sediments to the supra-detachment basin that could be related to the substantial termination, or at least a sharp decrease, of fault activity and the consequent change of the sedimentary system to a basically pelagic one.

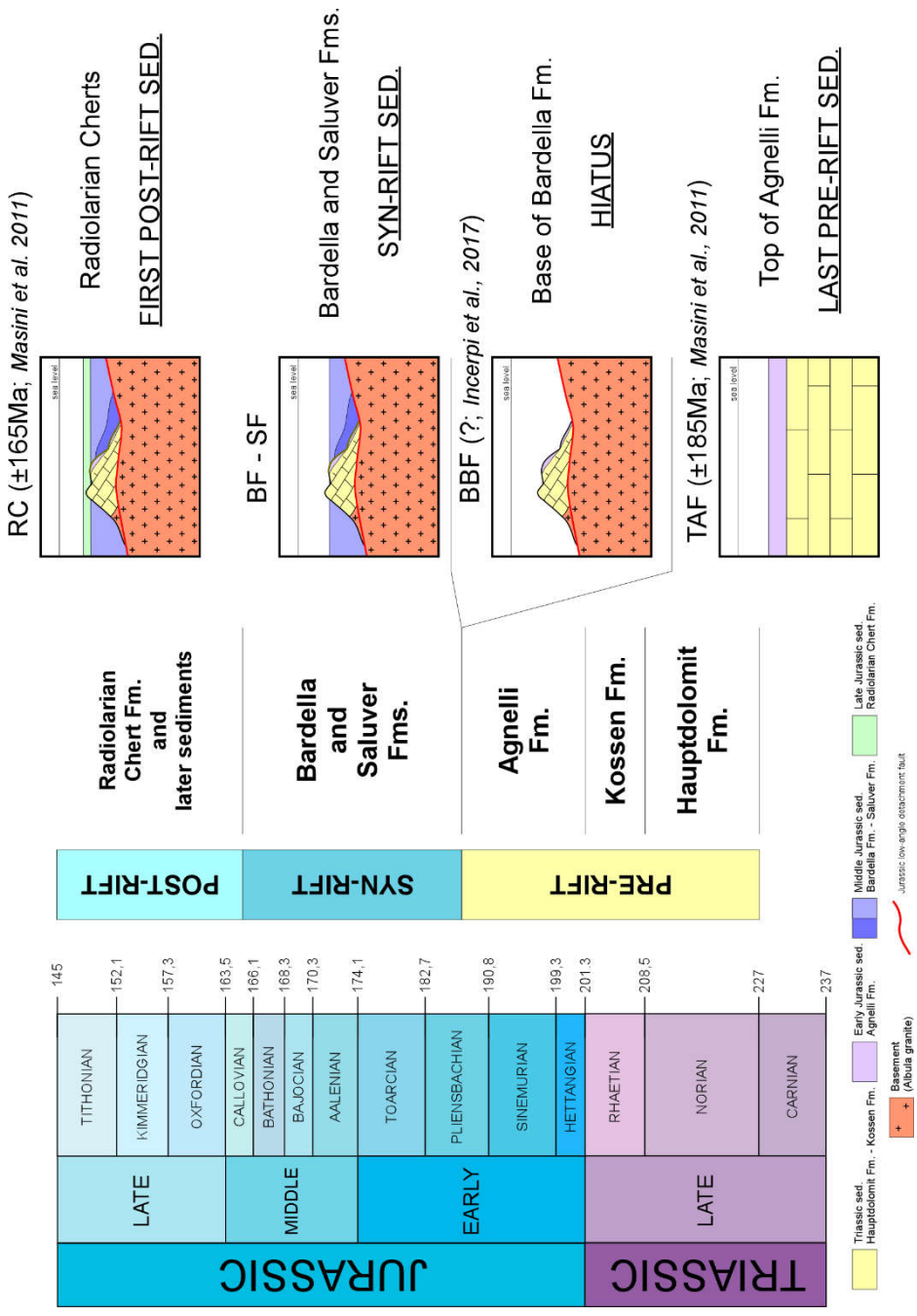

Fig. 4.14 - Stratigraphic evolution of the Adriatic central distal margin as recorded at Piz Val Lunga and Fuorcla Cotschna areas. TAF: Tof of Agnelli Fm.; BBF: Base of Bardella Fm.; RC: Radiolarina Chert Fm.

5. The outer distal margin

5.1 MAL PASS AREA

5.1.1 Stratigraphy and petrography

The Mal Pass area belongs to the Lower Err unit. The present-day overturned section, due to Alpine tectonic, is composed of mantle-related rocks at the base, and an extensional allochthon, sealed by a syn-rift sedimentary succession, at the top. In between, an Alpine D1 thrust fault occurs even if not clearly exposed in this area. The hangingwall is here characterized by an extensional allochthon made up of pre-rift Triassic carbonate rocks which are stratigraphically overlain by Jurassic syn-rift sediments (Fig. 5.1 a-b; Dietrich, 1969; Froitzheim and Manatschal, 1996; Manatschal and Nievergelt, 1997). Differently from the present-day architecture, during the Jurassic evolution of the Adriatic margin the allochthon was floored by an extensional detachment fault whose footawall was constituted of continental crust (Albula granite).

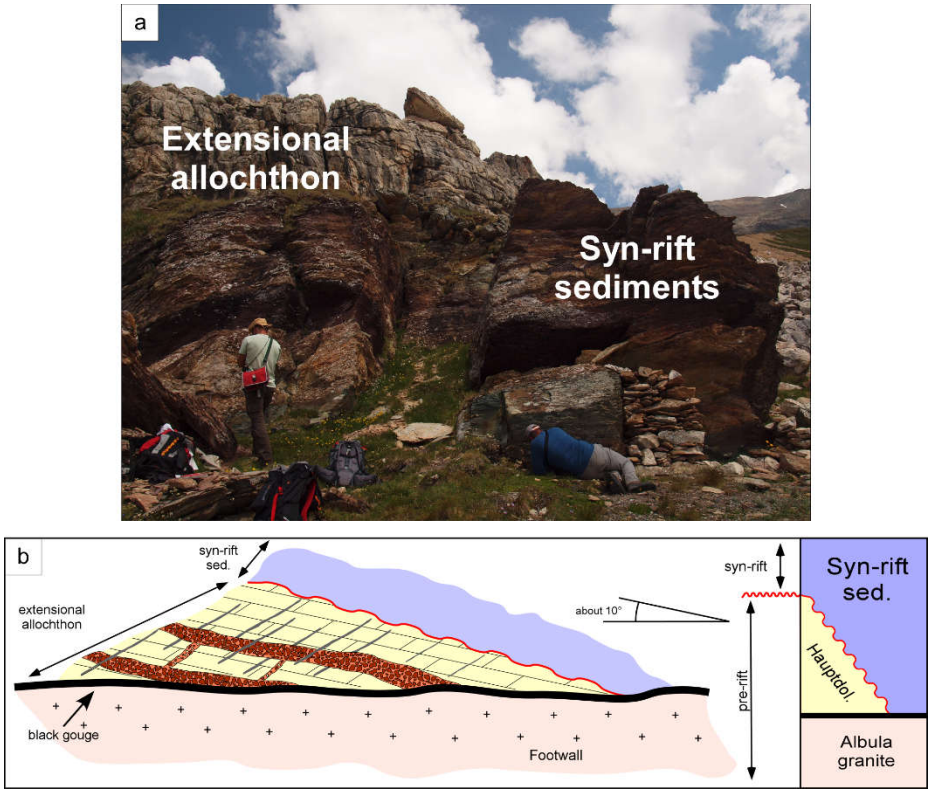

Fig. 5.1 - (a) Photograph of Mal Pass area where the stratigraphic contact between the extensional allochthon, made of Hauptdolomit Fm., and the syn-rift sediments is preserved. The present-day overturned position is due to the Alpine deformation. (b) Schematic sketch, not to scale, representing the main features observed at Mal Pass area.

The extensional allochthon is mainly constituted by alternation of finely crystalline and thinly laminated dolostones, which preserve shrinkage pores filled with dolomite cement. These features allow to assign these rocks to the Upper Triassic peritidal Hauptdolomit Formation. The Hauptdolomit Fm. shows always a homogeneous dark orange color in cathodoluminescence (CL) whereas the shrinkage pores are locally characterized by a polyphase infill (Fig. 5.2 a-d). The first filling stage consists of a thin (few tens of microns) fringe of dolomite cement that is concentrically zoned in CL. It is followed by a geopetal fill of fine grained, dolomitized sediment; the upper part of the pores, not completely filled

with sediment are plugged by a homogeneous, dark orange luminescent, saddle dolomite cement. Locally, the Hauptdolomit Fm. is characterized by a coarser size of dolomite crystals (up to 150-200 μm) that show a concentrical CL zoning.

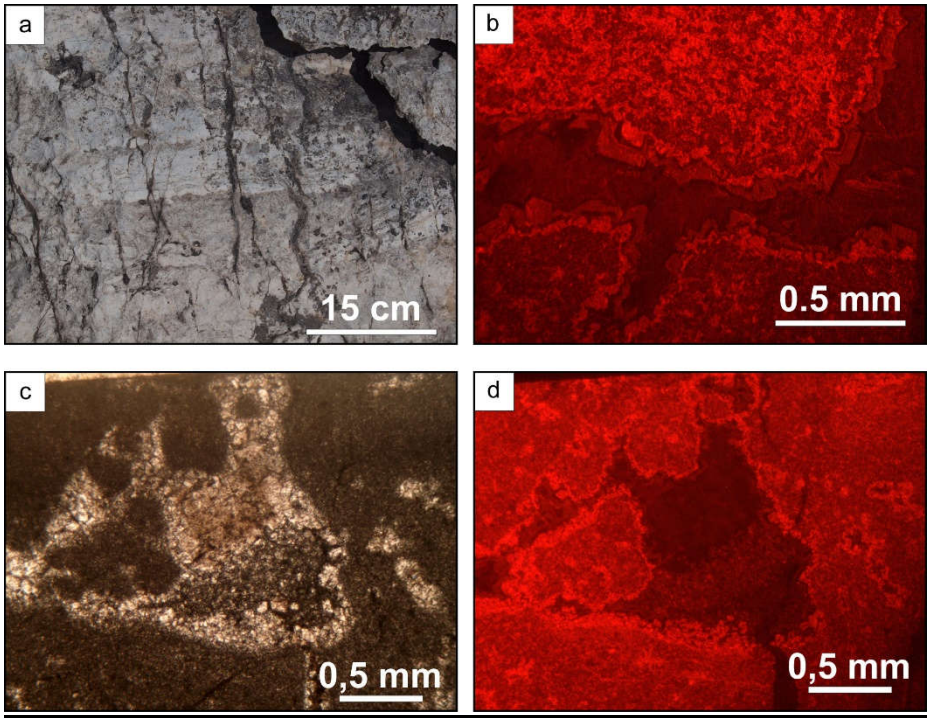

Fig. 5.2 - (a) Finely crystalline and thinly laminated Hauptdolomit Fm. constituting the extensional allochthon. (b) CL detail of shrinkage pore, cemented with dolomite, within the Hauptdolomit Fm. (c) TL and (d) CL images of polyphase, geopetally filled pores in the Hauptdolomit Fm. The filling is made of a first dolomite cement fringing the pore followed by fine grained, dolomitized sediment.and a last pore-filling dull dolomite cement.

The peritidal Triassic dolomites then show the presence of neptunian dykes and sills (Fig. 5.1 b). Sills are decimeter- to meter-wide and decameters-long (Fig. 5.3 a). They are filled with finely dolomitized reddish wackestones in which sponge spicules and radiolaria ghosts are still recognizable. Some pores filled with zoned dolomite are present even if their origin (as dissolution of former

bioclasts) is not always clear. Most of the sill infills are fractured and give rise to clast-supported breccias. The clasts, from rounded to slightly angular in shape, range from some millimeter to decimeter in size (Fig. 5.3 b). Close to the boundary with the sills, the Hauptdolomit Fm. is brecciated too and the clasts, ranging in size from some millimeter to decimeter, are separated by a scarce reddish, fine-grained matrix compositionally comparable to the sill infill (Fig. 5.3 c-d). Neptunian dykes, nearly orthogonal to Hauptdolomit bedding, are far smaller and less frequent; they are less than 20 cm in width, can be traced vertically for a few decimeters, and consist of clast-supported breccias with Hauptdolomit clasts and the reddish fine-grained matrix.

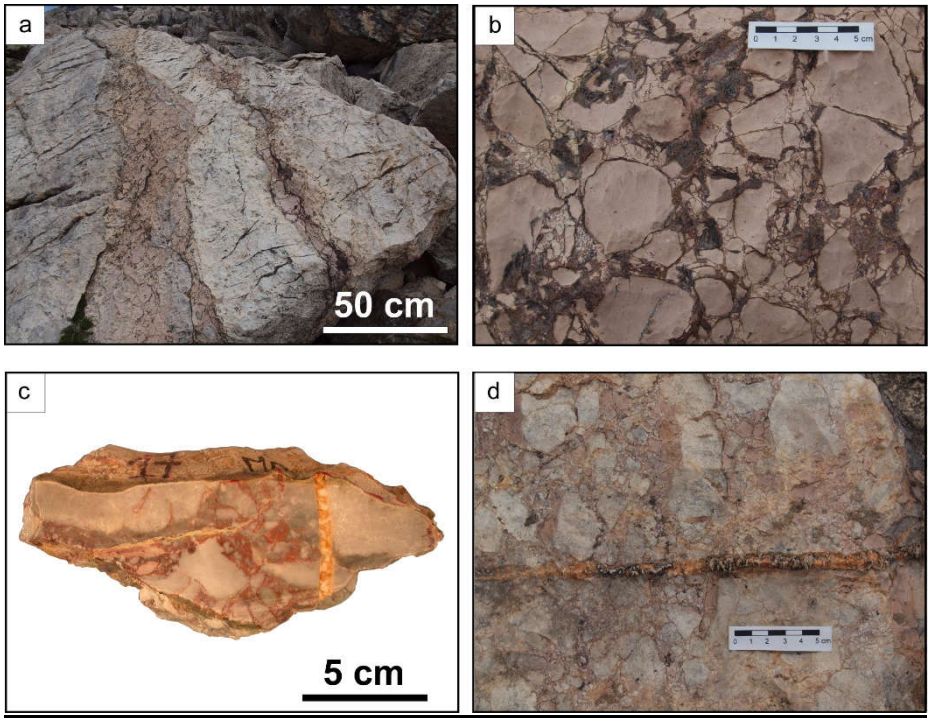

Fig. 5.3 - (a) Neptunian dykes and sills in the Hauptdolomit Fm. filled by brecciated, reddish dolomitized wackestones (b). (c) Hand specimen and (d) field photograph of quartz-dolomite vein cutting through the brecciated Hauptdolomit Fm.

The whole extensional allochthon exposed in Mal Pass area is crosscut by several generations of veins that can be gathered in, at least, two main sets which

are themselves polyphase. The first, affecting mainly the Hauptdolomit Fm., seems to predate the opening of the dykes and sills and is characterized by saddle dolomite cements. It occurs as meters-long and cm-large grey veins that cut bedding almost perpendicularly. CL investigations show the presence of at least two generations of saddle dolomite cements with a dark to bright orange CL luminescence (Fig. 5.4 a-d). The dolomite crystals can reach some millimeters in size. The second set consists of those veins cutting through the whole rock mass (i.e. dykes, Hauptdolomit Fm. and the first set of veins; Fig. 5.5 a-d). It is filled with saddle dolomite and quartz whose crystals are mm-large. Finally, a common feature of both sets of veins is that they sharply stop at the top of the allochthon (Fig. 5.1 b).

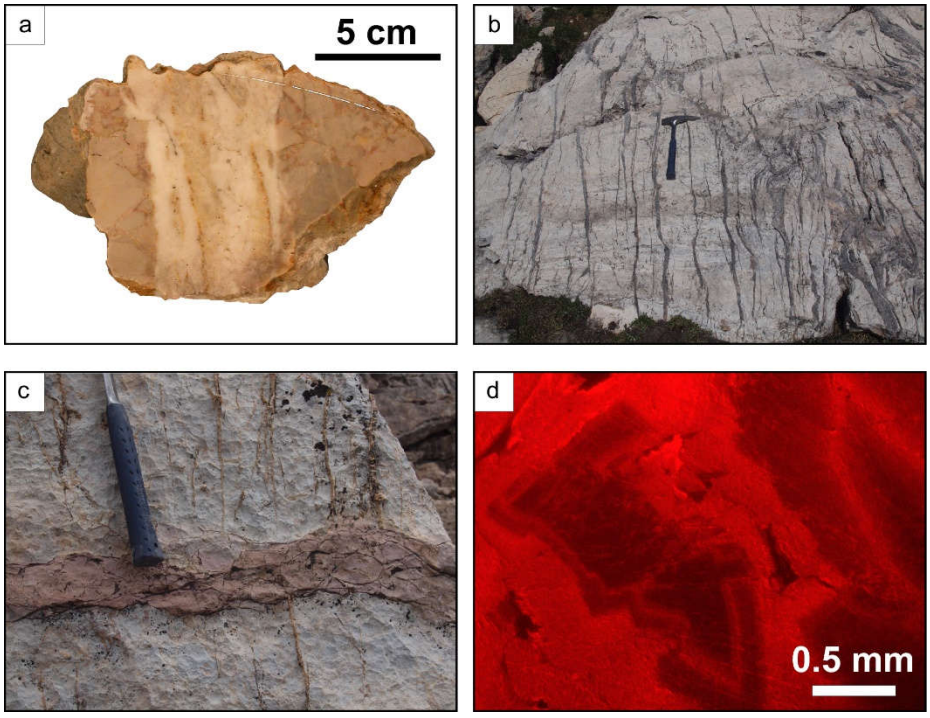

Fig. 5.4 - Dolomite veins within the Hauptdolomit Fm. in the extensional allochthon. (a) Hand specimen, (b-c) field photograph, and CL images (d) of polyphae saddle dolomite filling.

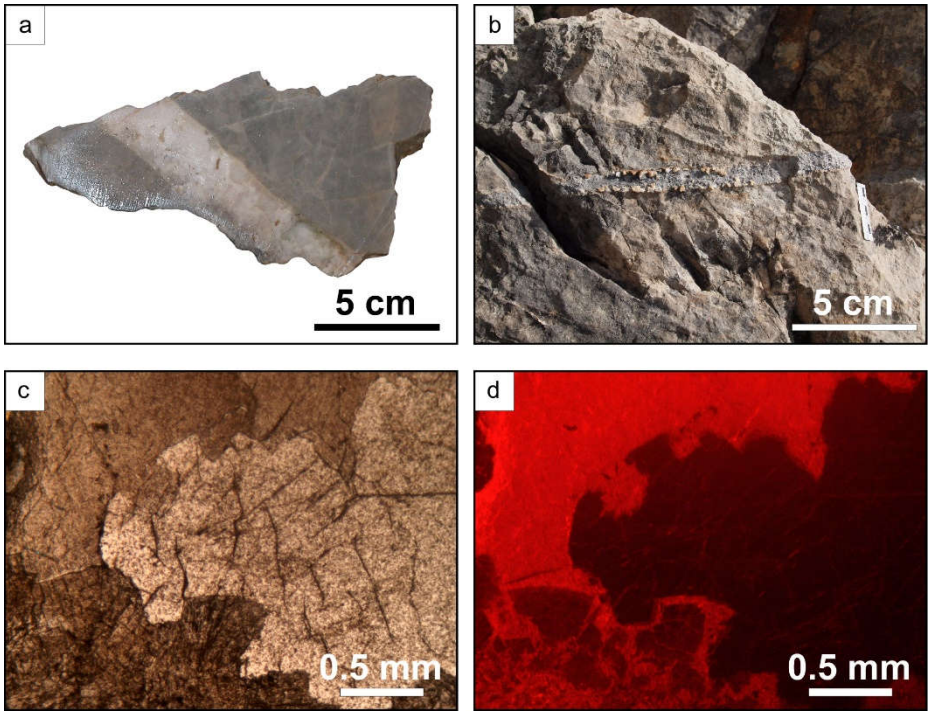

Fig. 5.5 - Quartz-dolomite veins within the extensional allochthon cutting through both Hauptdolomit Fm. and neptunian sills and dykes. (a) Hand specimen, (b) field photograph, (c) TL and (d) CL images of vein filling.

The syn-rift sediments lie directly onto the extensional allochthon with a primary depositional contact. At Mal Pass area, the sedimentary succession above the Triassic Hauptdolomit Formation is never thicker than about 10 meters. It consists of alternation of greenish, yellowish to reddish finely laminated marly to arenitic sediments in which rudite beds occur (Fig. 5.6 a). These coarser beds are polimict and matrix- to clast-supported. The clasts, mm- to cm- in size, are made of diverse lithologies among which sucrosic dolomites, micrites, and cherts locally showing septarian-like, quartz-filled fractures. Some of the carbonate clasts preserve cavities and/or shrinkage pores filled with dolomite cements comparable to those observed in the underlying allochthon, and quartz-dolomite veins that stop at the edge of the clasts. In some chert clasts few radiolaria ghosts have been observed. Dolomite rhombs up to 150 μm in size,

are also recognized in the completely silicified matrix of the breccia levels. The matrix is marly to arenitic and contains angular quartz grains. Where the matrix is scarce, clasts are tightly packed. The matrix appears silicified but at a closer view this appears to be due to swarms of veinlets, few tens of microns thick, filled with finely crystalline quartz and developed at clast boundaries.

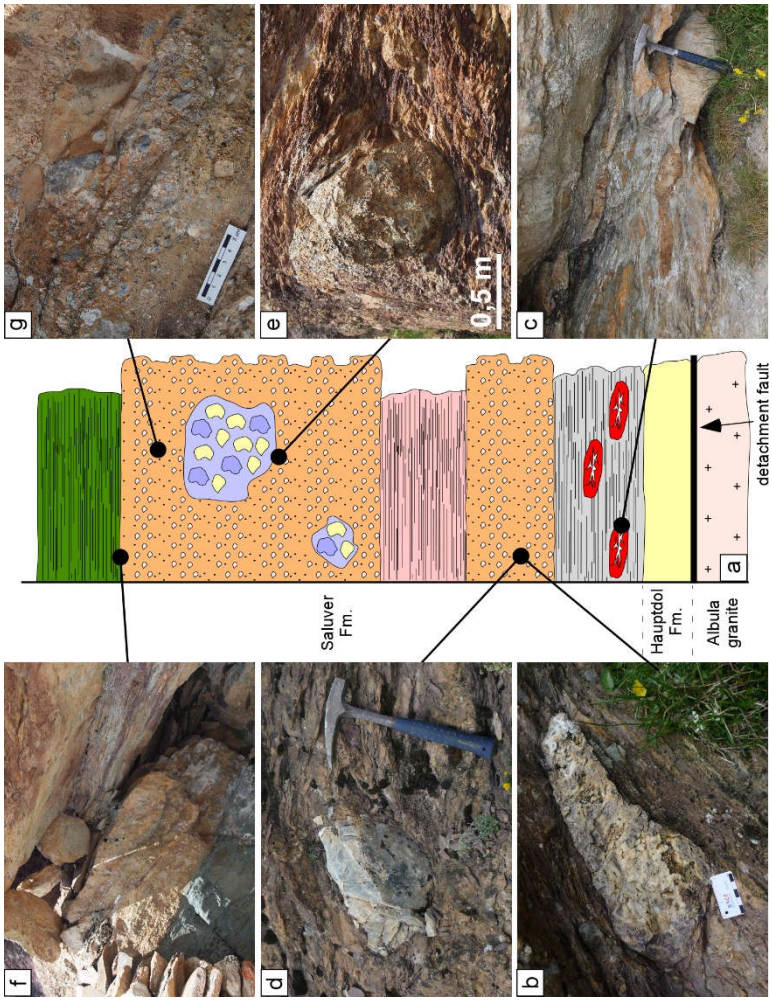

Fig. 5.6 - (a) Stratigraphic log, not to scale, of the Mal Pass area. (b) Clast of brecciated chert nodule within the rudite beds . (c) Septarian-like concretions occurring in the marly sediments right onto the extensional allochthon. (d) Chert clast in the rudite beds. (e) Meter-scale block of Bardella Fm. embedded in turbidite deposits. (f) Stratigraphic contact between greenish mudrocks and coarse-grained sediments. (g) Detail of coarse-grained sediments.

From the base to the top of the syn-rift sequence, three are the main worth noting features: (1) the first decimeters of the sedimentary succession are characterized by marly sediments in which several, cm- to dm-size, septarian-like concretions are aligned parallel to the bedding (Fig. 5.6 c). These concretions show both wedge-shaped fractures, pinching out towards the edge, and concentric ones filled with a mosaic of drusy quartz crystals elongated perpendicularly to the fracture wall, and saddle dolomite (up to 2 mm in size; Fig 5.7 a-d). The quartz/saddle dolomite ratio can vary from one concretion to the other even if quartz is always the first filling phase. The marly sediments embedding the septarian concretions contain thin layers of arenites with angular quartz grains, fine-grained carbonate lithoclasts, 100-200 μm in size, as well as radiolarian

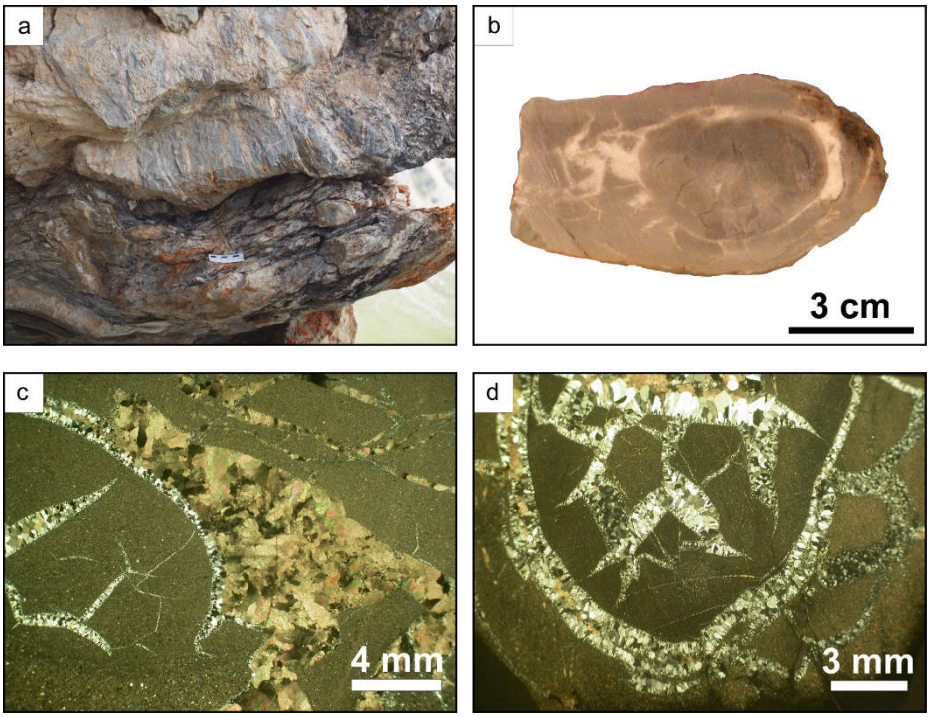

Fig. 5.7 - (a) Stratigraphic contact between the extensional allochthon and the syn-rift sediments. The first decimenters of the sedimentary succession are characterized by the presence of many (b) septarian-like concretions. The septarian cracks are filled by quartz and saddle dolomite. (c) and (d) TL images showing the cements filling the septarian cracks.

molds filled with chalcedony. (2) Moving upsection, the sediments become coarser and dominated by many mass flow/turbidite deposits that rework either carbonate clasts (in which carbonate and quartz veins are preserved), and greyish to reddish cherts locally showing quartz-filled, septarian-like cracks (Fig. 5.6 b and d-g). On the basis of the texture and the composition of these sediments, which contain common quartz grains, they can be referred to the Saluver Formation (Masini et al., 2011, 2012). Meter-scale blocks of breccias composed only of carbonate lithoclasts are also present and may be referred to the Bardella Formation (Masini et al., 2011, 2012). Some laminated beds are widely dolomitized with dolomite rhombs up to 100µm (Fig. 5.8 a-c). (3) Differently from what has been observed and described at Fuorcla Cotschna, the syn-rift sediments are not crossed by fractures and/or veins.

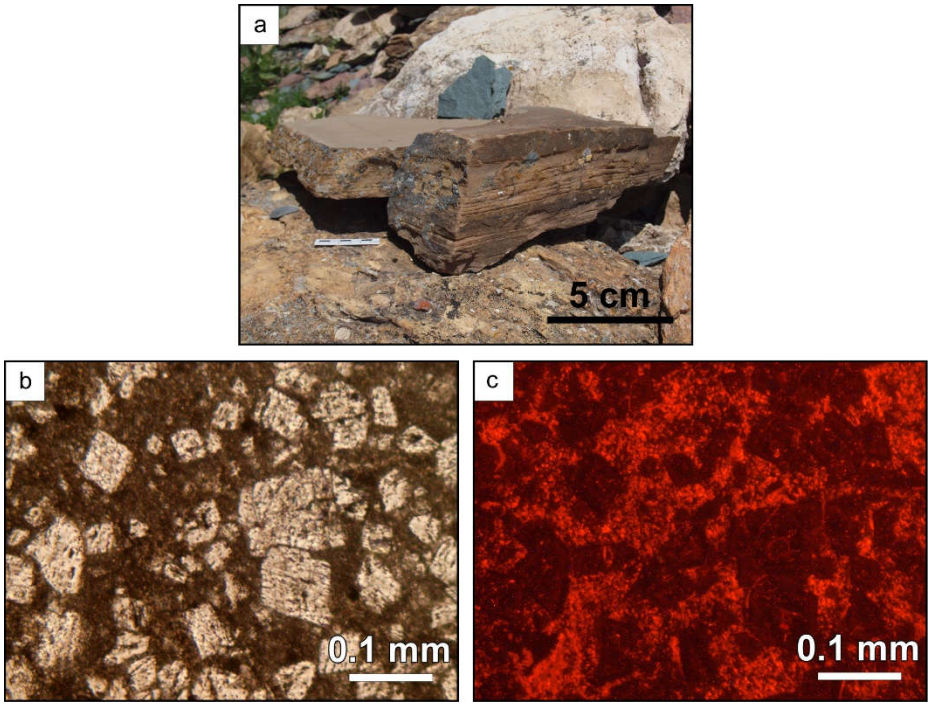

Fig. 5.8 - (a) Hand specimen of laminated syn-rift sediments. (b) TL and (c) CL images highlighting the pervasive dolomitization affecting the syn-rift sediments

5.2 ISOTOPE GEOCHEMISTRY AND FLUID INCLUSION DATA

5.2.1 O and C isotope

Oxygen and carbon isotope analyses (Fig. 5.9 and ANNEX A) have been performed on dolomite occurring as a replacement phase of former Hauptdolomit Fm., dolomite cement in veins and on saddle dolomite filling fractures in the septarian-like concretions. One measurement has been carried out also on the calcite cement of the ophicalcite. All the data show a slightly negative to positive $\delta^{13}C$ values (-0.19‰ to 2.51‰ VPDB) and slightly to strongly negative $\delta^{18}O$ (-3.47‰ to -15.02‰ VPDB).

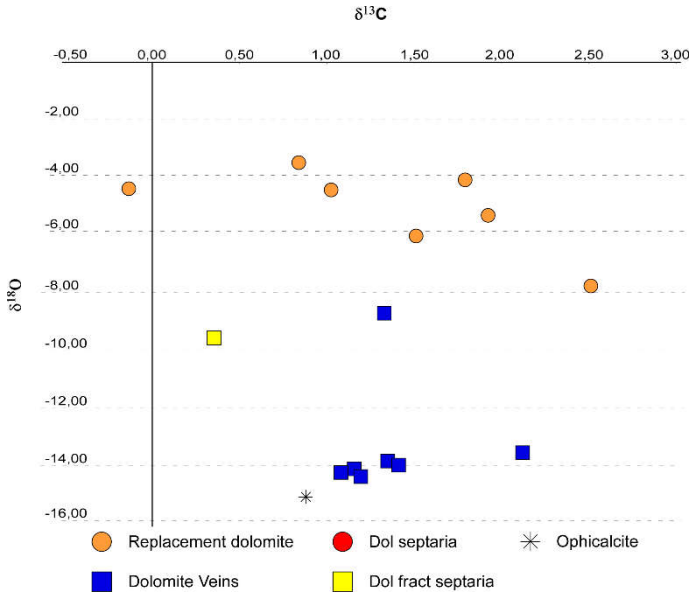

Fig. 5.9 - Stable isotope data: $\delta^{18}O$ versus $\delta^{13}C$ cross plot for dolomite and calcite minerals from Mal Pass (MP) area. Values relative to VPDB standard.

5.2.2 Sr isotopes

$^{87}Sr/^{86}Sr$ isotope analyses have been performed (ANNEX C) on replacement dolomite (0.708254±0.000188 to 0.712604±0.000349), saddle dolomite veins (0.708968±0.000142 to 0.716308±0.000246), calcite (ophicalcite, 0.709924±0.000536) and saddle dolomite fractures filling in septarian-like concretion (0.708529±0.000131). All the analyzed samples show values that are

strongly higher than those of Upper Triassic and Lower Jurassic seawater (maximun value 0.708000, McArthur et al. 2012).

5.2.3 He isotopes

Analyses were carried out on veins dolomite cement of set 1 and on both quartz and dolomite cements of veins set 2. All the $^{3}He/^{4}He$ ratios range in between 0.022 Ra and 0.039 Ra (ANNEX D).

5.2.4 Fluid inclusion microthermometry

About 80 primary fluid inclusions were found and measured in saddle dolomite and quartz cements of septarian-like concretions (Fig. 5.10) and veins (Fig. 5.11; ANNEX B). Quartz cement of septarian-like concretions shows values ranging from 112°C to 190°C with highest frequency between 140°C and 150°C and in the range 150-160°C for dolomite. Veins homogenization temperatures ranges from 119°C to 205°C for the quartz cement (highest frequency between 130°C and 140°C) and from 138°C to 159°C for the saddle dolomite (highest frequency between 140°C and 150°C).

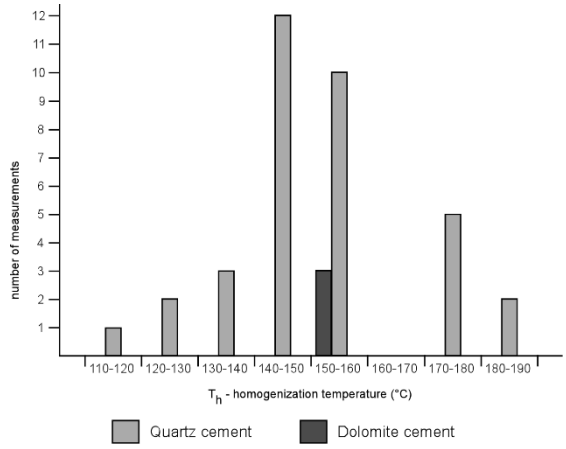

Fig. 5.10 - Histogram of the homogenization temperatures obtained by standard heating method (Goldstein and Reynolds, 1994) for quartz cement in septarian-like concretions in syn-tectonic sediments.

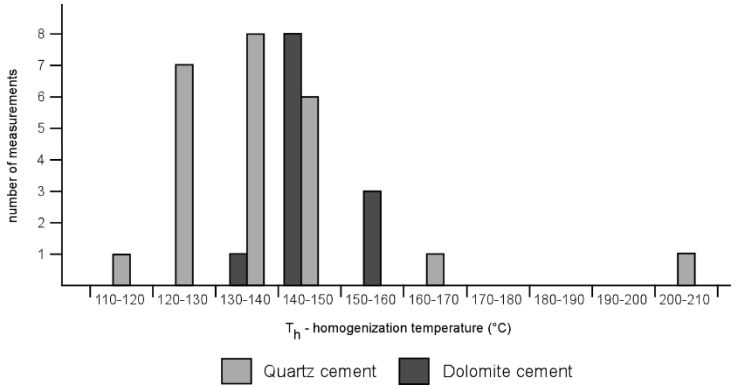

Fig. 5.11 - Histogram of the homogenization temperatures obtained by standard heating method (Goldstein and Reynolds, 1994) for quartz and dolomite cements of veins in the Hauptdolomit Fm.

5.3 FIRST ORDER INTERPRETATION

5.3.1 Dolomite

Four different dolomite types occur at Mal Pass:

1) Finely crystalline replacement dolomite in the extensional allochthon occurs as fabric retenctive process allowing the preservation of the former depositional features of the Hauptdolomit Fm. and sills (e.g. lamination, shrinkage pores, skeletal grains). It possibly occurred right after the deposition of the dolostones similarly to what has been described at Piz Val Lunga and Fuorcla Cotschna areas.

2) Coarsely crystalline dolomite locally occurs in the Hauptdolomit Fm. and neptunian dykes as fabric-destructive replacement, which obliterates primary textures. In the syn-rift succession it is widespread as substituting euhedral mineral phase within laminated fine-grained deposits.

3) Coarsely crystalline dolomite cement of shrinkage pores in the Hauptdolomit Fm. and of biomoldic pores in sills. The preservation of the well-defined CL zoning excludes a later recrystallization.

4) Lastly, saddle dolomite crystals occur as cement in syn-rift septarian-like concretion cracks.

5.3.2 Neptunian dykes and breccias

The occurrence of sills and dykes in the extensional allochthon is genetically related to tectonic events, which affected the host Hauptdolomit Formation. To be formed, they require a stage of fracturation enabling the creation of open spaces and the infiltration of the reddish pelagic sediments. Findings of sponge spicules and radiolarian ghosts in the sill-filling sediments suggest the correlation of the internal sediments with the sponge spicule-bearing Agnelli Formation. Therefore, the opening of the fissures could be dated to the early Early Jurassic when the sedimentary environment was deeper than that of in Late Triassic. Ongoing tensional stresses led to the brecciation of sills and dykes infill.

5.3.3 Veins

Veins represent the most widespread feature in Mal Pass area even if they only occur within the extensional allochthon. Indeed, it is affected by a huge amount of both saddle dolomite and dolomite-quartz veins that, due to the style of vein filling (mosaic of mainly unoriented crystals), point to a precipitation in static conditions and in open fissures. Taking the neptunian dykes as a relative time marker, the occurrence of two main phases of veining, which are themselves polyphase, can be established. A first stage (set 1), preceding the formation of the dykes, is characterized by saddle dolomite cements and affects pervasively the Hauptdolomit Fm. in the extensional allochthon. The second stage (set 2), which crosscuts both the Hauptdolomit Fm. and the neptunian dykes, postdate the formation, sediment filling and brecciation of fissures. It also marks a change in the chemistry of the fluids, as the presence of quartz cements in this second generation of veins documents. The relationships between quartz and dolomite cements are not always unambiguous, implying that the two mineral phases could be co-genetic in origin. Conversely, from time to time, because of the presence of corrosion gulfs, well-defined growth zones and CL zoning it is

possible to suggest that dolomite predates the precipitation of quartz. To this second stage, finally, can be related the formation of the quartz-rich septarian-like concretions and the dolomitization of the syn-rift sediments.

Type 4 dolomite, as discussed above, is suggested to be related to fracturation and development of vein set 2 in the allochthon. The strong difference in behavior of the allochthon and the overlying syn-rift sediment (Saluver Fm.) to the passage of fluids, which resulted in veins in the former and in formation of concretions and a diffuse dolomitization in the latter, shows that the Saluver Fm. was not lithified at all and thus most likely buried under a very limited thickness of younger sediments. This inference, together with fluid inclusion microthermometry performed on dolomite and quartz cements of veins and on dolomite-quartz filling cracks in syn-rift concretions, point to consider such fluids as hydrothermal. No analytical data are available for dolomite type 2 in the syn-rift sediments but, since its precipitation can be linked to the same physico-chemical conditions of dolomite type 4, hydrothermal fluids should be also responsible for the replacement process.

5.3.4 Septarian-like concretions and silicification

Many septarian-like concretions have been found in the basal part of syn-rift sediments right onto the top of the extensional allochthon.

The mechanisms responsible for septarian cracking are still the object of controversies. Several hypotheses have been advanced among which dehydration and shrinkage (Raiswell, 1971), excess pore pressures (Astin, 1986; Hounslow, 1997), and synsedimentary seismic shocks (Pratt, 2001). More recently Hendry et al. (2006) proposed that volume contraction and resulting crack formation is due, at very shallow burial depths, to syneresis of clay-bearing sediments enhanced by the decay of bacterial EPS. The septarian concretions of Mal Pass largely consist of silicified sediments with cracks filled with quartz and dolomite and as such differ from most of those described in literature, which are cemented by calcite. However, the geometry of the cracks is

definitely the same and the bacterially-aided syneresis hypothesis by Hendry et al. (2006) seems to fit the features of the Mal Pass concretions.

The presence of both quartz and dolomite in septarian cracks allows to interpret their formation as related to the second stage of veining (set 2). Keeping in mind that the veins stop sharply at the top of the allochthon, it can be suggested that overpressured fluids opened their way through the allochthon, made of fully lithified rocks, flowing within discrete fractures. This channelized, focused, flow abruptly changed at the boundary with the fine-grained syn-rift succession where it became diffuse and found open spaces where quartz and dolomite could precipitate in the pores of the not fully cemented concretion bodies and especially in the cracks.

At Mal Pass, in addition to septarian concretions, early diagenetic silicification is also documented in the matrix of ruditic beds in the syn-rift succession lying above the extensional allochthon, and especially by the occurrence of chert clasts in the ruditic beds. Since dolomite rhombs are still preserved within the quartz matrix, it can be assumed that silicification was preceded by a partial dolomitization. These processes took place at very shallow burial depths (probably decimeters to meters) so that the resulting cherts could be eroded and included in the coarsest beds of the syn-rift succession. The temperatures obtained by fluid inclusion microthermometry in quartz crystals support a hydrothermal nature also for silicifying fluids.

6. The proximal margin

6.1 IL MOTTO AREA

6.1.1 Stratigraphy and petrography

The study area is located in the central part of the Ortler nappe west of Livigno (Il Motto area, N Italy) and belongs to the Upper Austroalpine domain. Here, the structures of the former proximal Adriatic rifted margin are preserved in a well-exposed section in which the relationships between the sediment infill and the main high-angle normal fault bounding the basin are exposed (Eberli, 1987, 1988; Fig. 6.1). The syn-rift sedimentary sequence is characterized by thinning- and fining-upward cycles as well as a thinning and fining away from the fault zone. Furthermore, an inversion of the clast stratigraphy is observed in the basin due to erosion and re-deposition of the footwall block during progressive exhumation along the fault (Eberli, 1988). In the present-day architecture, the Ortler nappe is under- and overlain along Alpine tectonic contacts by other Upper Austroalpine units, the Quattervals nappe above and the Campo nappe below.

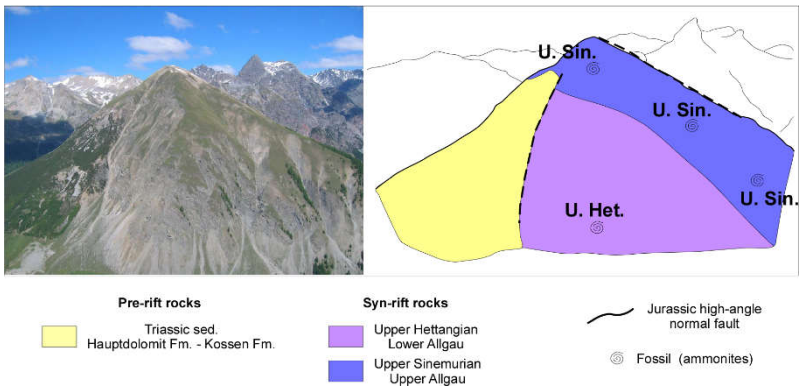

Fig. 6.1 - (a) Panoramic picture and interpreted drawing of Il Motto area in order to show the averall architecture of the area characterized by a high-angle normal fault bounding a half-graben basin. Modified after Mohn et al. (2010).

At Il Motto area, samples in the footwall of the high-angle fault bounding the sedimentary basin were collected. The prevailing lithotype is represented by grey, finely laminated dolostones preserving shrinkage pores that, by their lithofacies and stratigraphic position, can be referred to the Triassic Hauptdolomit Formation. Here, the footwall alternates portions in which it preserves the pristine features (e.g. bedding and lamination) with others where it occurs as slightly to strongly disrupted and dolomitized. The bedding of the Hauptdolomit Formation is cut almost perpendicularly by two different types of breccias. The first type occurs as subvertical cm- to dm-wide bodies and consists of monomict crakle to mosaic breccias (*sensu* Morrow, 1982) cemented by dolomite (Fig. 6.2 a-d). The clasts, angular to sub-angular in shape, some mm- to cm in size, consist of medium to coarsely crystalline dolostones that completely replace the former rock hindering the recognition of any sedimentary structures. Under cathodoluminescence, the replacement dolomite is dull to non-luminescent. Conversely, the dolomite cement, with euhedral, up to 1 mm-large rhomb, shows dull to bright orange luminescing concentric zones. Within some clasts, dolomite veins are preserved showing a dark orange to dull luminescence. Finally, these breccias (both clasts and cement) are cut by mm-wide veins made of homogeneous dull luminescent dolomite.

The second type of breccia is constituted by polymict rubble breccia (Fig. 6.3 a-d; *sensu* Morrow, 1982), which is the result of a polyphase mechanism of disruption. Indeed, some clasts are composed of wackestone to packstone with bivalve shell fragments actually replaced by dolomite/calcite whereas others are made of a former mosaic breccia whose clasts still consist of wackestone/packstone cemented by finely to coarsely crystalline, dark orange to non-luminescent dolomite and thus different from the type 1 crackle breccia. Some carbonate veins confined within the clasts also occur. This rubble breccia is cemented by sparry calcite showing a CL concentric zoning, from dark to very bright orange.

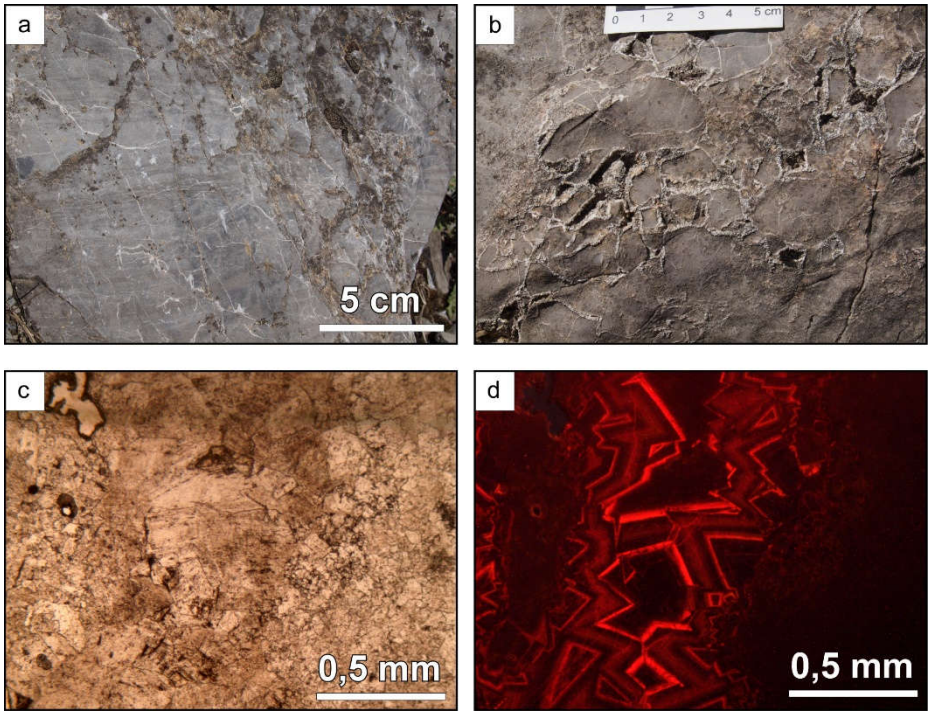

Fig. 6.2 – Field photograph of (a) crackle and (b) mosaic breccias. (c) TL and (d) CL images of the dolomite cement of the breccia.

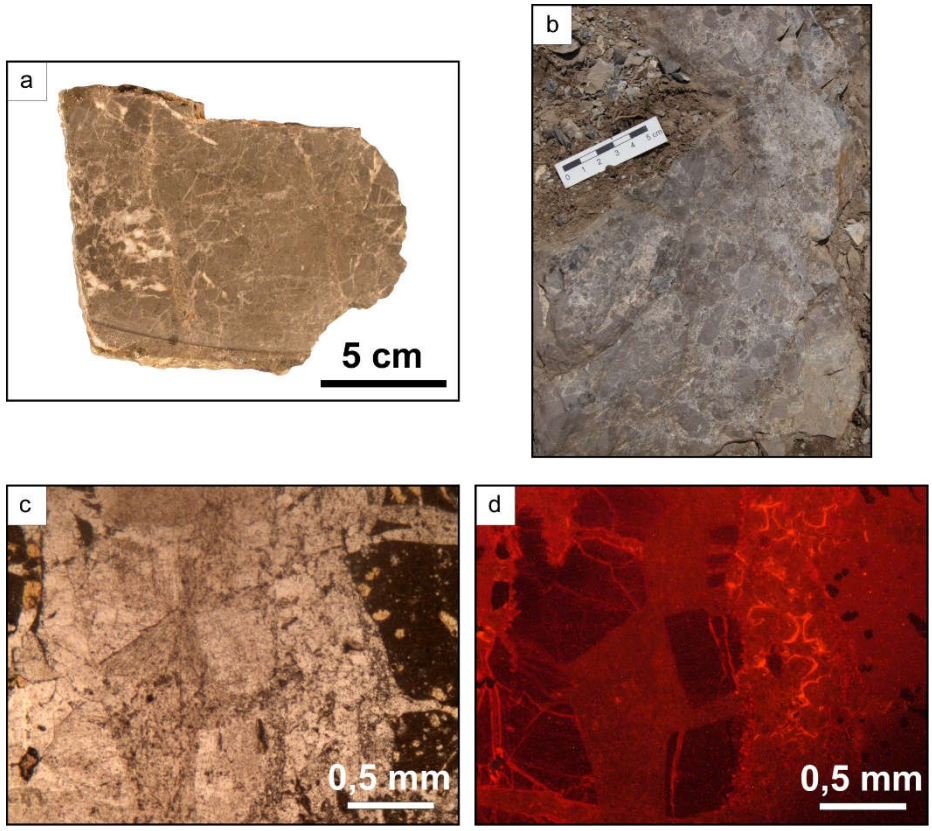

Fig. 6.3 –. (a) Hand specimen and (b) field photograph of rubble breccia. (c) TL and (d) CL images highlighting the polyphase cementation (dolomite and calcite) of the breccia.

6.2 ISOTOPE GEOCHEMISTRY AND FLUID INCLUSION DATA

6.2.1 O and C isotopes

Oxygen and carbon isotope analyses have been performed on dolomite occurring as replacement phase of former Hauptdolomit Fm. of type 1 breccia and its dolomite cement (Fig. 6.4 and ANNEX A). The Hauptdolomit Fm. shows slightly positive $\delta^{13}C$ values (1.66‰ to 2.04‰ VPDB) and slightly positive to negative $\delta^{18}O$ (0.05‰ to -0.76‰ VPDB). The breccia dolomite cement has slightly positive $\delta^{13}C$ values (2.84‰ VPDB) and quite negative $\delta^{18}O$ (-5.55‰ VPDB).

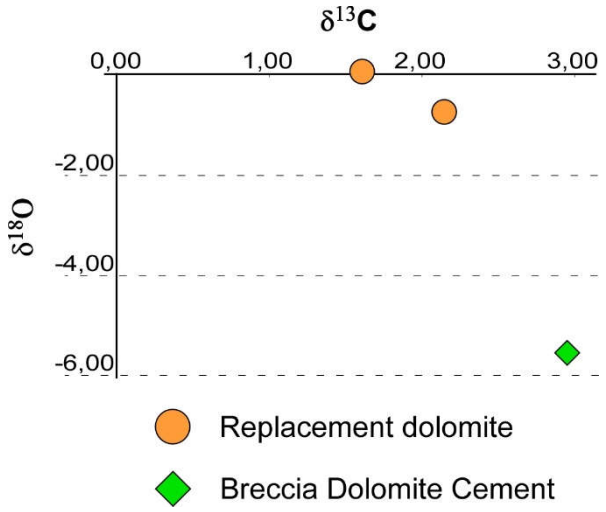

Fig. 6.4 - Stable isotope data: $\delta^{18}O$ versus $\delta^{13}C$ cross plot for dolomite minerals from Il Motto (MO) area. Values relative to VPDB standard.

6.2.2 Sr isotopes

$^{87}Sr/^{86}Sr$ isotope analyses have been performed on replacement dolomite (0.709106±0.000611) and breccia dolomite cement (0.708750±0.000639; ANNEX C). All the analyzed samples show values that are strongly higher than those of Upper Triassic and Lower Jurassic seawater (maximun value 0.708000, McArthur et al. 2012).

6.2.3 Fluid inclusion microthermometry

About 30 primary fluid inclusions were measured in the dolomite cement of type 1 breccias. Homogenization temperatures ranges from 86°C to 206°C (highest frequency between 130°C and 140°C; Fig. 6.5 and ANNEX B).

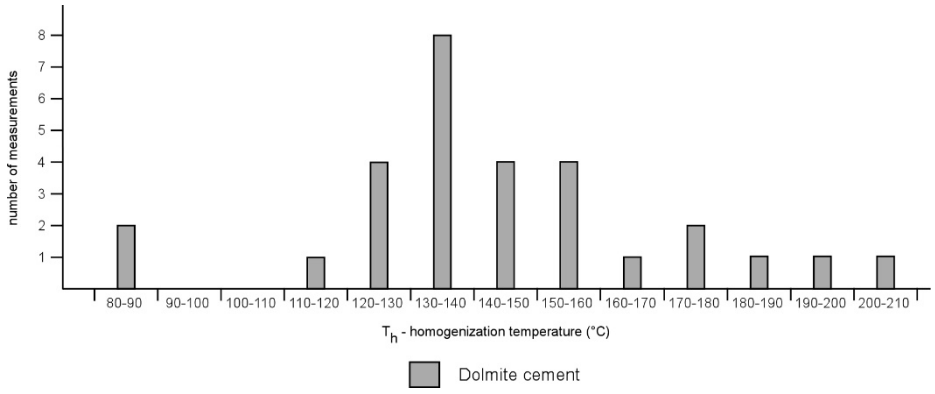

Fig. 6.5 - Histogram of the homogenization temperatures obtained by standard heating method (Goldstein and Reynolds, 1994) for dolomite cements of breccias in the Hauptdolomit Fm.

6.3 FIRST ORDER INTERPRETATION

6.3.1 Dolomite

Two styles of dolomitization occur at the Il Motto area. The first is responsible of the finely crystalline dolomitization, which allows the preservation of pristine features of the Hauptdolomit Fm. The second gives rise to medium to coarsely crystalline dolostones replacing the former Hauptdolomit Formation. It is a fabric destructive replacement since no former features of the rock (e.g. lamination, shrinkage pores, fossils) are preserved and is always related to type 1 breccias.

6.3.2 Breccias

The two types of breccias are matrix-free with clasts that, by their shape and spatial organization, suggest complex and repeated *in situ* hydro-fracturing

mechanism obviously related to the pulsating activity of the Il Motto normal fault, which in the earliest Jurassic generated the well known half graben basin. Different degrees of displacement of the clasts resulted in crackle to rubble breccias and are likely associated to the proximity with the fault damage zone and thus to more or less focused and repeated fluid fluxes.

6.3.3 Dolomite and calcite cements

The petrographic features of both dolomite and calcite cements enable to consider their precipitation in an open framework and in static conditions. Since their well-defined CL zoning is still preserved, it can be assumed that no subsequent recrystallization took place. The dolomite cement of type 1 breccias shows the more depleted $\delta^{18}O$ value of the dataset. Homogenization temperatures and O isotopes point to the presence of hydrothermal fluids that possibly flowed through the fault damage zone as main pathway.

6.3.4 Veins

Veining is not a pervasive process at Il Motto area. However, the presence of veins that stop at the edge of the clasts in type 1 breccias, and others that cut also through the dolomite cement, allows to consider the occurrence of at least two fracturing stages right before and after the emplacement of overpressured, dolomite-rich fluids to which the brecciation is related.

7. The inner distal margin

7.1 PIZ ALV AREA

7.1.1 Stratigraphy and petrography

The Piz Alv area belongs to the Bernina unit that is made of Carboniferous to Early Permian igneous rocks intrusive into polymetamorphic Variscan basement (Spillmann and Büchi, 1993; von Quadt et al. 1994). Mesozoic sediments occur only locally as slices at the Piz Alv area, where a complete pre-rift succession is preserved (Fig. 7.1) including: Permian rhyolites, massive shallow marine Triassic dolomites and Upper Triassic lagoonal sediments, overlain by Lower Jurassic limestones (Agnelli Formation).

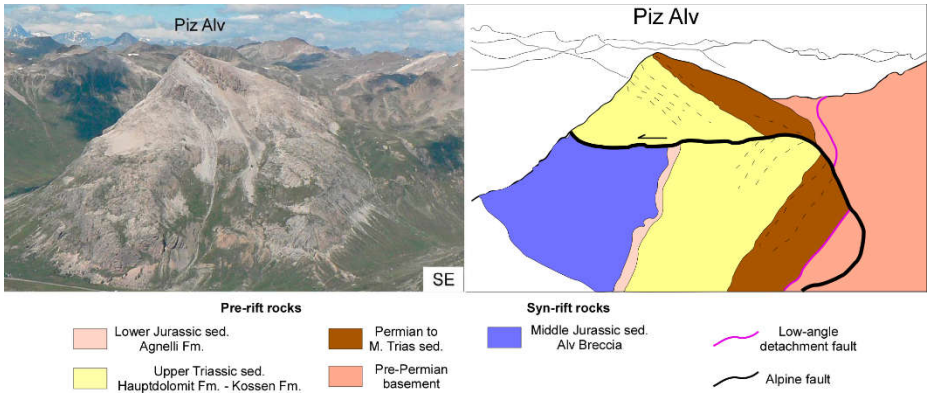

Fig. 7.1 - Photograph and drawing of Piz Alv area showing the large-scale structure viewed from the SW in order to highlight the relationships between the pre- and syn-rift sediments. Modified after Mohn et al. 2012.

The whole sequence is 600 to 800 m thick and shows, except for the Agnelli Fm., a very similar evolution to that observed in the more proximal parts of the Adriatic margin (e.g. Ortler and Ela units). Syn-rift sedimentation began with the deposition of 200 to 300 m thick breccias, referred to as the Alv Breccia

(Schüpbach, 1974) at Piz Alv. The occurrence of a detachment fault at the interface between basement rocks and a complete pre-rift succession, allowed Mohn et al. (2012) to interpret Piz Alv as an extensional allochthon.

The Piz Alv breccia is a megabreccia, with clasts of Triassic and Lower Jurassic carbonates that range in size from few millimeters to tens of meters. Although it has not been studied in detail, some features are worth noting, which show a high degree of complexity of the Piz Alv breccia. The largest blocks mainly consist of dolostones (crystal size around 50-100 μm) crossed by mm-thick veins filled with saddle dolomite (crystal size around 400 μm) and locally showing a brecciated structure. The vein dolomite (Fig. 7.2 a-b) shows a well-defined CL zoning similar to that of dolomite cements of type 1 breccias at Il Motto (proximal margin). The blocks are separated by dm-thick beds of polygenic breccias, with mm- to dm-large angular clasts, interlayered with thinner bedded fine-grained, light grey limestones. Clasts mainly consist of the same dolostones observed in the large blocks but other textures are also common. These include intensely dolomitized wackestones with bioclasts. In spite of dolomitization, bivalve shells (Fig. 7.2 c-d) and benthic foraminifera (*Triasina*?) may be identified, which allow to refer these clasts to the Rhaetian Kössen Fm. Some breccia beds differ from the previous ones because clasts have rounded edges and are mainly composed of wackestones with echinoderm fragments (Fig. 7.2 e-f) and sponge spicules, which may be strictly compared to the Lower Jurassic Agnelli Fm. facies. The rounded clasts, moreover, show a brighter few millimeter thick, halo in their outer part that can possibly be related to oxidation of the organic matter content. SEM-EDS analyses do not highlight compositional changes along these portions.

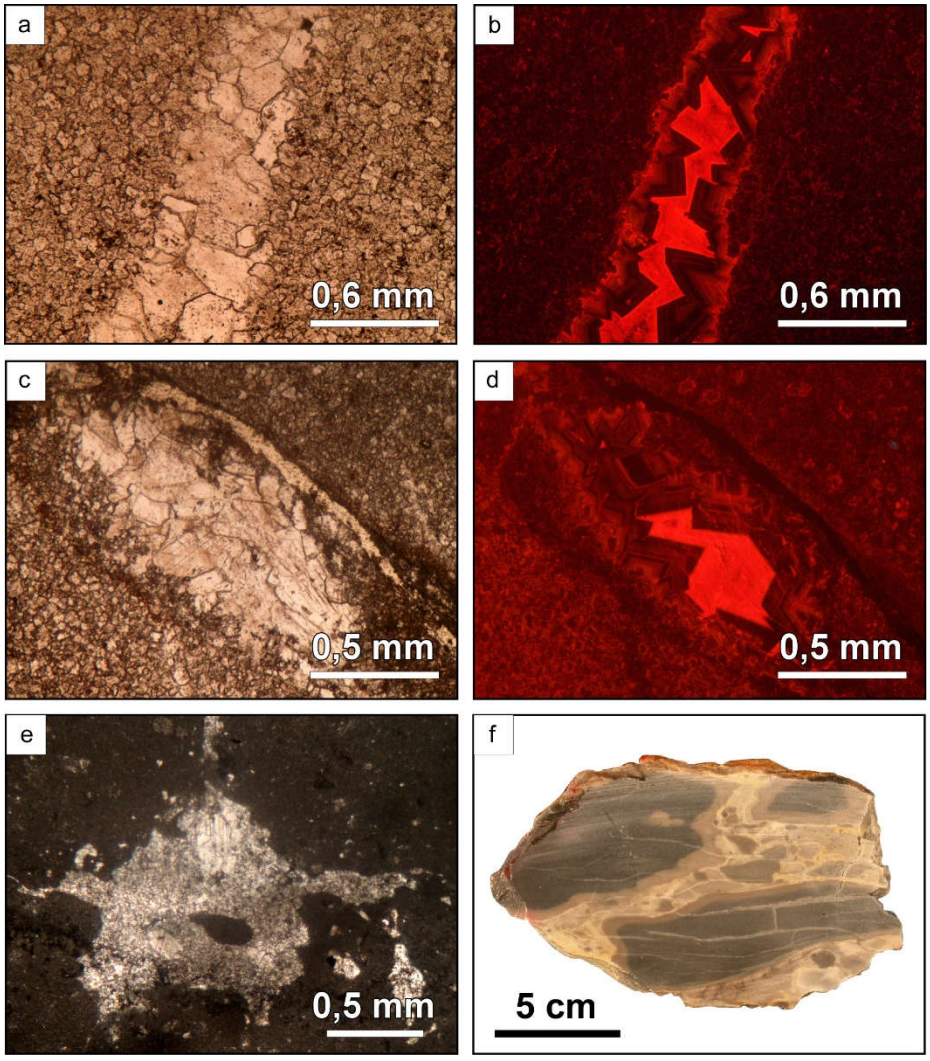

Fig. 7.2 - (a) TL and (b) CL images of saddle dolomite vein within a clast of the Piz Alv breccia. The vein dolomite shows a well-defined CL zoning similar to that of dolomite cements of type 1 breccias at Il Motto (proximal margin). (c) TL and (d) CL images of bivalve preserved within a clast made of dolomitized wakestone (Kössen Fm.). (e) TL detail of a clast of Agnelli Fm. Within the pore, echinoderm fragments are recognizable. (f) Hand specimen of breccia made of rounded dark grey clasts of Agnelli Fm. that show a brighter, few millimeter thick, halo in their outer part.

Another relevant difference is that these clasts are not dolomitized but show a slight recrystallization confined to the matrix, giving rise to microsparitic

textures. Rounded cavities, corresponding to unrecognizable former bioclasts, are filled with a calcite blocky spar characterized by a marked CL zoning from non-luminescent to bright yellow and dull orange (Fig. 7.3 a-d). The fine-grained beds are mudstones to wackestones with scattered echinoderm fragments up to 1 mm large. The former micrite presently appears as a mosaic of calcite crystals 10 to 30 µm in size with a homogeneous dull orange cathodoluminescence. Scattered grains of detrital quartz about 50 µm large also occur. These breccias, and the interlayered fine-grained limestones, commonly show evidence of shear.

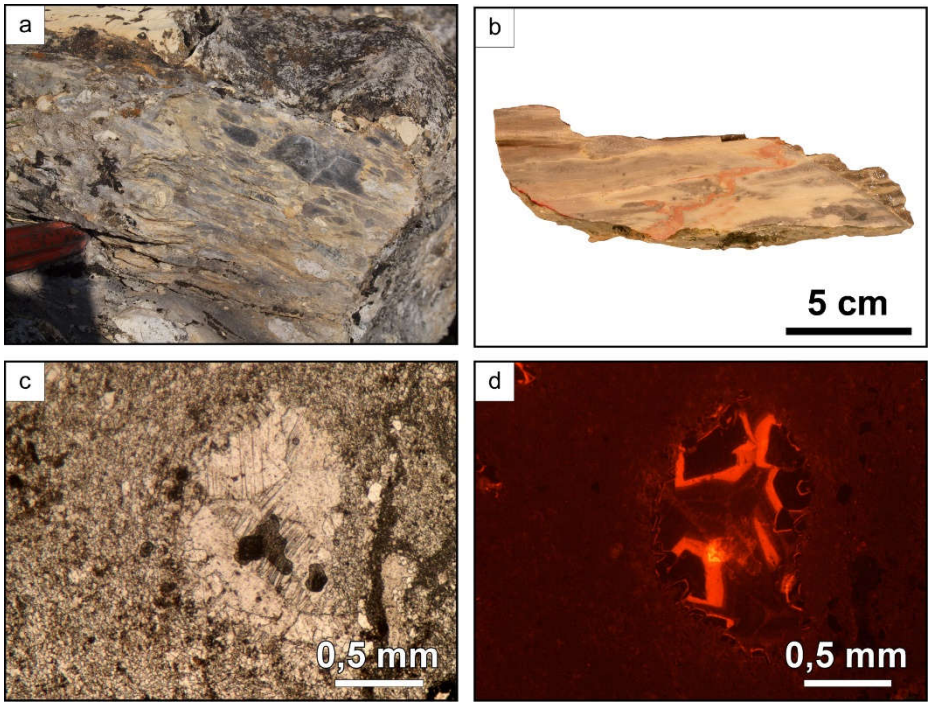

Fig. 7.3 - (a) Field occurrence and (b) hand specimen of non-dolomitized breccias. Recrystallization occurs only within the matrix. (c) TL and (d) CL photomicrographs of rounded cavities, corresponding to unrecognizable former bioclasts, in the clasts. They are cemented by a calcite spar showing a well defined CL zoning from non-luminescent to bright yellow and dull orange.

Both large blocks and breccia beds are crossed by a network of neptunian sills and dykes, from less than 1 mm to several decimetres thick, filled with pink to brick red sediment (Fig. 7.4 a-b). This red sediment also occurs as a matrix in breccias close to dykes (7.4 c). Some of the dykes are filled with breccias with angular clasts of the encasing rock that fit together, separated by a homogeneous red sediment. Veins filled with saddle dolomite in the host rock are crosscut by these dykes. The largest dyke infills show mm-thick lamination, highlighted by slightly darker and lighter reddish colours, or even bedding with alternation of red fine-grained homogeneous sediments and lithoclastic breccias with mm- to cm-sized angular clasts of the encasing rocks and red fine-grained matrix. The laminated parts commonly show convolutions (Fig. 7.4 d). Locally, these breccias include clasts of the reddish sediment. These red sediments locally contain abundant silt-sized grains of quartz and minor mica and show different degrees of dolomitization with development of euhedral to subhedral dolomite crystals, 30 to 50 μm large characterized by a moderate to dull orange colour. CL also allows to recognize sphaerical structures, about 30 μm in diameter, which can be referred to calcisphaeres. The dykes are further crosscut by smaller, mm-thick, fissures, filled with an analogous reddish dolomitized sediment preceded by a thin dolomite cement rimming the fissure walls, or veins, filled with 100 μm large dolomite crystals and calcite spar. These dolomite cements are clearly zoned in CL showing a range of colours from nearly non luminescent to bright reddish orange (Fig. 7.4 e-f). The smaller, mm-thick dykes, which cross the fine-grained recrystallized beds, conversely, are light pink in colour and are not dolomitized.

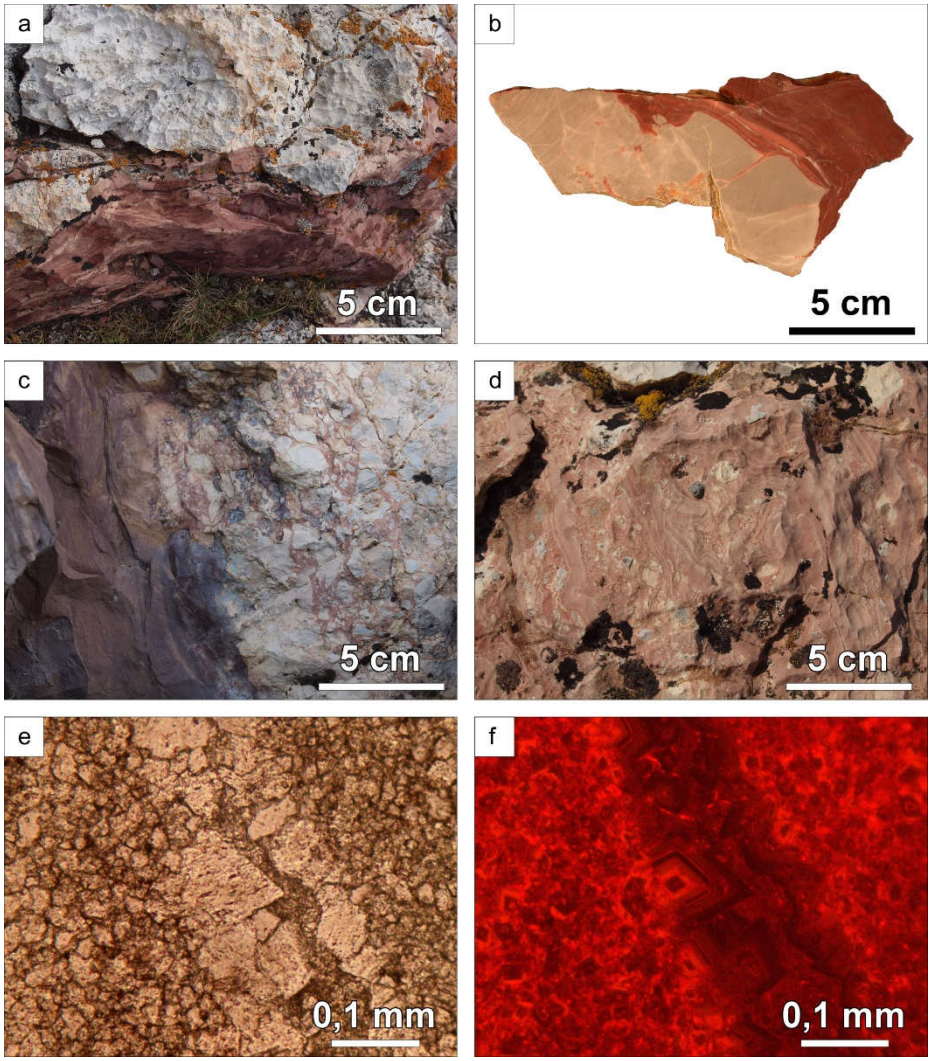

Fig. 7.4 - (a) Field photograph and (b) hand specimen of neptunian dyke cutting through both the large blocks and breccia beds. (c) The red sediment also occurs as matrix of the brecciated host rocks close to the dykes (d) The laminated infill of the neptunian dykes commonly shows convolution. (e) TL and (f) CL images of dolomitized reddish sediment cut by dolomite vein. The dolomite cement shows CL zoning from non luminescent to bright orange.

7.2 ISOTOPE GEOCHEMISTRY

7.2.1 O and C isotopes

Oxygen and carbon isotope analyses (Fig. 7.5 and ANNEX A) have been performed on dolomite occurring as replacement phase of former Hauptdolomit Fm., dolomitized sill and dykes, and the calcite cement of grey breccias with rounded clasts. The Hauptdolomit Fm. shows slightly positive $\delta^{13}C$ values (1.66‰ VPDB) and slightly negative $\delta^{18}O$ values (-0.76‰ VPDB). The breccia calcite cement has slightly positive $\delta^{13}C$ values (2.41‰ to 2.76‰ VPDB) and quite negative $\delta^{18}O$ (-1.66‰ to -1.91‰ VPDB). The dolomitized fillings of sills and dykes show $\delta^{13}C$ values in the range 2.11‰ to 3.43‰ VPDB and $\delta^{18}O$ ranging in between -2.52‰ and -4.90‰ VPDB.

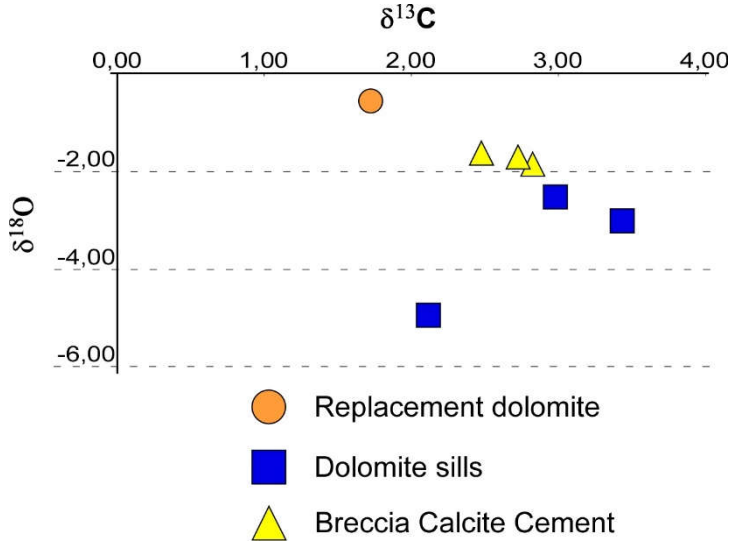

Fig. 7.5 - Stable isotope data: $\delta^{18}O$ versus $\delta^{13}C$ cross plot for dolomite and calcite minerals from Piz Alv area. The orange dot corresponds to the dolomite replacing the host Hauptdolomit Fm. The blue squares refer to dolomite sills and dikes cutting through the Alv Breccia. The yellow squares represent the recrystallized matrix of the Alv breccia.

7.2.2 Sr isotopes

$^{87}Sr/^{86}Sr$ isotope analyses have been performed on replacement dolomite (0.710336±0.000383), on reddish sediment (0.709319±0.000269) and on calcite replacing former matrix of breccias (0.71149±0.00040). All the analyzed samples show values that are much higher than those of Upper Triassic and Lower Jurassic seawater (maximun value 0.708000, McArthur et al. 2012; ANNEX C).

7.3 FIRST ORDER INTERPRETATION

The Piz Alv Breccia is a very complex deposit and has not been studied in detail. However, some field and petrographic features enable to put some constraints on its genesis and age. The Piz Alv Breccia overlies the Agnelli Fm., which may be interpreted as an outer ramp deposit. Actually the Piz Alv Breccia consists of two different types of ruditic deposits: 1) the first is constituted of massively bedded megabreccias with large blocks, up to several meters in size, of Hauptdolomit and Kössen Formations that are widely dolomitized and crossed by neptunian dykes filled with dolomitized sediments; 2) the second is organized in thinner beds made of smaller clasts (up to 10 cm large) of the only Agnelli Formation, which, as well as the small neptunian dykes crosscutting the breccias, do not show dolomitization. On the basis of their paleontological content (calcisphaeres, echinoderms), albeit very scarce and poorly preserved, the neptunian dyke infillings are attributed to an open marine environment. The red and pink colour is thus not suggestive of subaerial exposure but of oxygenated conditions. The fine-grained texture moreover documents low energy levels during the deposition of internal sediments that may be defined as pelagic.

The overall evolution of Piz Alv area (Fig. 7.6) can be summarized assuming in the Early Jurassic a first stage of fragmentation of the Triassic carbonate platform and drowning of the remnants into a pelagic environment. This event was associated to fracturing, sediment infilling, and hydrothermal dolomitization

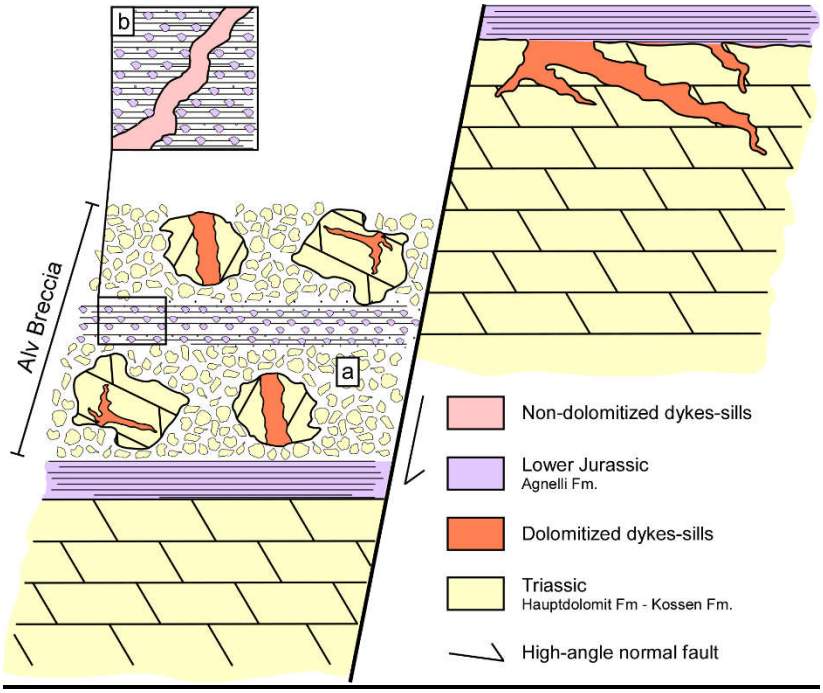

Fig. 7.6 - Schematic interpretation, not to scale and based on field observations and petrographic study, of Piz Alv area at the time of deposition of the Alv Breccia. The Alv Breccia is mainly composed of two types of sedimentary breccias: a) megabreccias with large blocks, up to several meters, made of Hauptdolomit and Kössen Fms. crossed by dolomitized neptunian dykes; b) thinner bedded breccias whose clasts, up to a decimeter in size, are made of the only Agnelli Fm. These breccias are then crosscut by a new generation of dykes which are not dolomitized.

(strongly suggested by negative $\delta^{18}O$ and radiogenic $^{87}Sr/^{86}Sr$ isotope values) taking place concomitantly. Seismic activity along rift-related normal faults provoked the gravitational collapse of the steep margins of such submerged structural highs and gave rise to the accumulation of megabreccias at the toes of the escarpments. These catastrophic rock fall events took place along with sedimentation of the Agnelli Formation, which was also affected by gravitational instabilities resulting in debris flows of semilithified sediments. Minor fracturing and infilling by pink pelagic sediments could affect also these beds short after deposition.

8. U-Pb dating

8.1 THE DATASET

U-Pb datings were performed on different hydrothermal minerals strictly related to the tectonic phases that characterised the evolution of the Adriatic continental rifted margin (Fig. 8.1 and ANNEX E). Their petrographic features, stratigraphic position and significance in the frame of the Triassic-Jurassic Adriatic margin extension have been already described in previous sections. In particular, three mineral phases with the right amount of U and Pb allowed the definition of satisfying concordia lines and then reliable ages, such as: replacement dolomite substituting the host Hauptdolomit Formation throughout the entire margin in the different paleogeographic domains (proximal margin, inner, central and outer distal margin), calcite cement of breccias and dedolomite at Piz Val Lunga (central distal margin), and saddle dolomite cements in veins at Piz Val Lunga and Fuorcla Cotschna (central distal margin). In Fig. 8.1 all the results are plotted in combination with the geological time scale (Cohen et al., 2013; updated). Measurements were performed also on quartz filling veins but the amount of U and Pb were not enough too provide reliable data. As a general consideration, the better results were obtained from the replacing minerals such as replacement dolomite and dedolomite whereas the void-filling minerals (cements of breccias and veins) do not seem to be the suitable target for this kind of analysis.

Considering the Late Triassic and Middle Jurassic times as lower- and upper ages bracketing the tectonic evolution of the Adriatic margin (e.g. deposition of the Hauptdolomit Fm. and Radiolarian Cherts respectively), it is evident that some data fall within this time lapse whereas others spread over a much wider time interval. Thus, the dataset can be subdivided in three main groups based on their significance with respect to the well-established steps that constrain the

extensional evolution of the Adriatic margin (e.g. TAF, RC; Masini et al., 2011; BBF, Incerpi et al., 2017).

To the first group (Group 1 in Fig. 8.1) belong those data, between the middle Late Triassic to Middle Jurassic time, obtained from replacement dolomite of host Hauptdolomit Fm. and saddle dolomite cement of veins. Using the major time lines described in Masini et al. (2011; TAF and RC) and Incerpi et al. (2017; BBF), it is possible to establish the occurrence of three sub-groups (SG): SG_1, pre-TAF and ranging from Rhaetian to middle Pliensbachian, includes ages of the replacement dolomite from each paleogeographic domain (proximal margin, inner, central and outer distal margin); SG_2, post-TAF and pre-BBF ranging from middle Pliensbachian to late Toarcian, is composed of coarse-grained replacement dolomite samples from the extensional allochthon at Piz Val Lunga and Fuorcla Cotschna (central distal margin); SG_3, post-BBF to RC, has only one data which is referred to the vein-cementing saddle dolomite within the extensional allochthon at Fuorcla Cotschna (central distal margin).

Group 2 (post-RC) gathers all the samples, from the only distal margin, with ages younger than Middle Jurassic, but mainly Cretaceous and younger. They consist of replacement dolomite, most of the calcite cement of breccia and dedolomite, and saddle dolomite cement of veins.

Group 3 is composed of those samples with ages older than middle Late Triassic which refer to calcite cement of breccia (Piz Val Lunga) and saddle dolomite of veins (Fuorcla Cotschna).

8.2 DISCUSSION AND INTERPRETATION

Taking the middle Late Triassic to Middle Jurassic as the time range in which the extensional phases took place in the Adriatic rifted margin, only Group 1 shows values with a “geological meaning” in the terms of processes related to Triassic-Jurassic continental extension.

Ages from Group 2 and 3 cannot be associated to the extensional evolution of the margin since they are younger than post-rift Radiolarian Chert Fm. and older than Norian Hauptdolomit Fm., respectively. Rasbury and Cole (2009) stated that an isotope system may be disturbed by diagenetic alteration of the original mineral (e.g. further fluid circulation). The fluids responsible for the alteration may add or remove either parent or daughter isotope or both resulting in younger or older ages of the analysed minerals. Such disturbance may not be associated to any recrystallization, as the petrography of the here analysed minerals documents. Therefore, based on strong geological constrains, also the minerals of Group 2 and 3 are surely related to the extensional evolution of the Adriatic margin even though their U-Pb ages suggest a re-opening of the radiogenic system possibly related to Alpine orogenic processes.

As previously said, Group 1 can be divided in three sub-groups. SG_1 shows the most homogeneous ages and, furthermore, some of the lowest standard deviation. Most of the data plot around the Triassic-Jurassic boundary with ages of about 200 Ma. As demonstrated and described in previous chapters, the replacement dolomitization of the host Hauptdolomit Formation is supposed to be related to hydrothermal fluids (based on fluid inclusions microthermometry, O and Sr isotopes). U-Pb datings allow to document that deep fluid circulation cells started to be active right after the deposition of the Hauptdolomit Fm. (and syn-deposition of the Kössen Formation) and affected the whole margin. The fluid flow and dolomitization processes continued even after the deposition of the Agnelli Formation, in a time when water depth increased but before the onset of detachment faulting as the predominant tectonic style dissecting the continental margin.

SG_2 ages, middle Pliensbachian to Toarcian in age (TAF-BBF range), from the extensional allochthon in the distal margin, can be explained as a dolomitization event that in the distal margin is strictly related with the emplacement of the extensional allochthons onto the detachment fault and is characterised by nearly

the same physico-chemical conditions of the older dolomitizing event as demonstrated by petrography, CL, fluid inclusion and stable isotopes.

SG_3, spanning from Aalenian to Callovian, can be related to the products of fluid flow, which affected the syn-rift sediments in the distal margin. The only sample belonging to this subgroup refers, interestingly, to saddle dolomite cement of vein crosscutting the extensional allochthon at Fuorcla Cotschna. It can therefore confirm the fact that the fracturing and veining, easily identifiable in the syn-rift sedimentary succession, were also recorded within the extensional allochthon.

Beltrando et al. (2015) described for the Southern Alps several stages of extensional faulting from Middle Triassic to the Sinemurian in the Adriatic plate, followed by a more focused deformation in the Late Pliensbachian-Toarcian. The authors established the occurrence of various heating-cooling cycles among which one is dated at 215-200 Ma (ZHe data). Such a thermal perturbation was coeval with the onset of rift-related deformation at lower crustal levels, which predated normal faulting at upper crustal levels by about 10-15 Ma. Extensional deformation at all crustal levels started from about 185 to 180 Ma leading to complete crustal excision at about 165 Ma. These thermal events reported by the authors match quite precisely with our U-Pb ages. Indeed, SG_1 can further support the occurrence of the Late Triassic-Early Jurassic thermal stage whereas SG_2 refers to processes that occurred when the deformation localized in the distal part of the Adriatic margin.

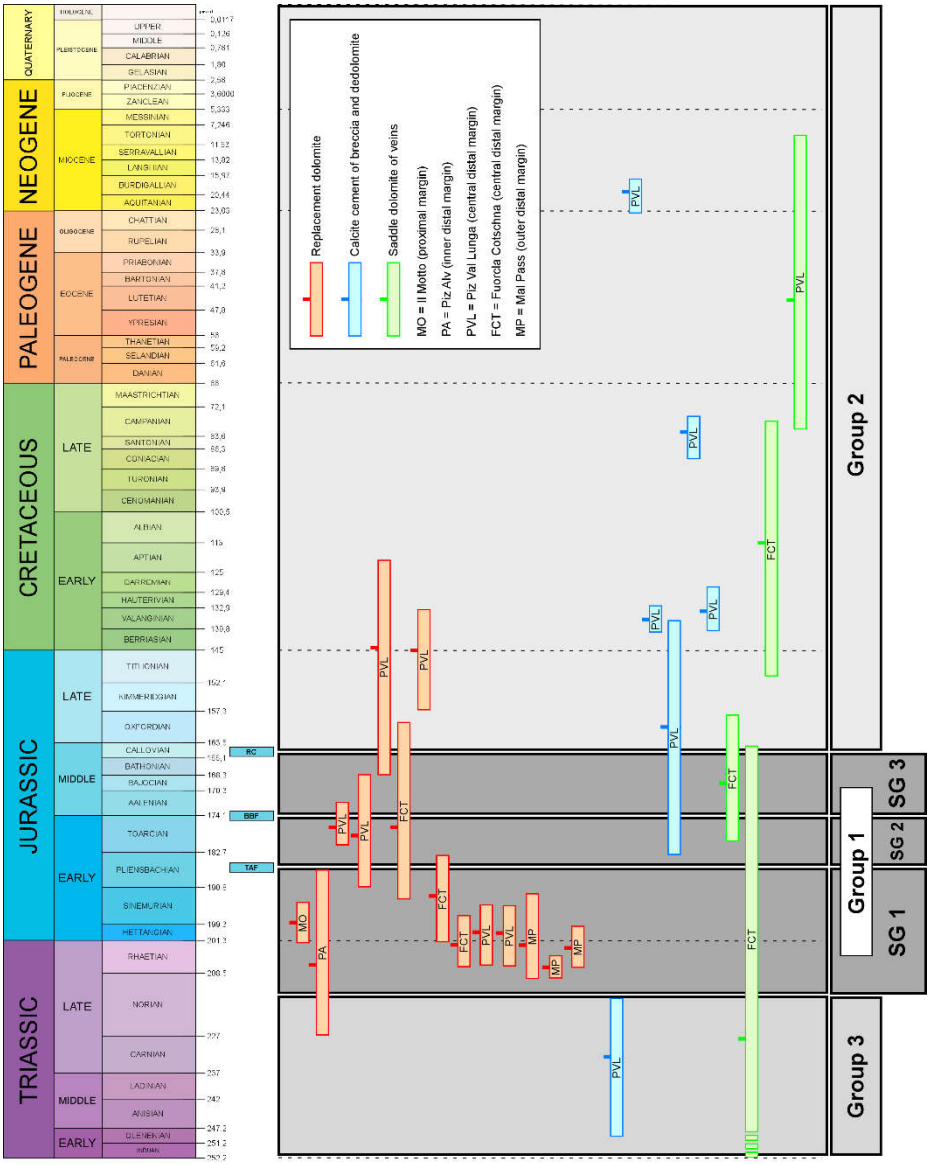

Fig. 8.1 - U-Pb dating results have been gathered in three main groups as discussed in the text. On the basis of the major time lines TAF-BBF-RC (Fig. 4.14), the Group 1 is furthermore divided into three subgrups (SG1-2-3). The data are plotted in combination with the geological time scale (Cohen et al., 2013; updated). TAF: Top of Agnelli Fm.; BBF: Base of Bardella Fm.; RC: Radiolarian Chert Fm.

9. Trace elements and REE

9.1 INTRODUCTION

Geochemical analyses of main, trace and rare earth elements (REE) were performed on the whole rock (bulk rock composition) of different lithotypes (ANNEXES F-G). Such method allows to get an overall dataset of the composition of the samples even if it can be affected by "impurities". This problem is obviously intrinsic of the method itself, since about 100 gr of material are required to accomplish the measurements. Where possible (e.g. cements of vein) the mineral phase representing the target of the analyses was separated from the enclosing rock. In other cases, the cataclasite for instance, both clasts and matrix were analysed together. This must be kept in mind during the interpretation of the dataset.

The rare earth elements consist of yttrium (Y) and the lanthanide series (La to Lu). The low-atomic number lanthanides (La-Eu) are conventionally termed light REE (LREE), whereas their heavier counterparts (Gd-Lu) are referred to as heavy REE (HREE). Y was integrated in the REE pattern between Dy and Ho. Y has a trivalent state in hydrothermal fluids and its enrichment has the same origin as that of the other trivalent REE also because its geochemical behaviour is similar to that of REE and especially Ho (Jochum et al., 1986; Govindaraju, 1989). The chondrite-normalized REE patterns were generated by using the chondritic values of Anders and Grevesse (1989) and showed in diagrams with a logarithmic vertical scale. Calculation of Ce and Eu anomalies is based on Taylor and Mclennan (1985) where CN represents the chondrite normalized values:

$$Ce/Ce^* = Ce_{CN}/(La_{CN} \times Pr_{CN})^{1/2}$$

$$Eu/Eu^* = Eu_{CN}/(Sm_{CN} \times Gd_{CN})^{1/2}$$

9.2 ANALYSED SAMPLES

The analyses were performed on different rocks belonging to the different paleogeographic domains of the Adriatic margin and include: Hauptdolomit Formation (HD), dolomitized sediment filling sills and dykes (SILL), clasts of Hauptdolomit Formation within the black gouge of the detachment fault (HD GOUGE), cataclasite (HD CAT), dedolomite (DEDOL), dolomite veins within the allochthon (DOL VEIN), silicified matrix of syn-rift calciruditic beds (SILIC), septarian-like concretions and chert nodules (SEPT), clasts coated by Fe-Mn oxides (Fe-Mn) and ophicalcites (OPH). As previously described, all the analysed samples have to be considered as the result of fluid-related processes that altered the former rocks or generated new forming minerals. When the same rock type comes from different paleogeographic domain it will be specified (e.g. HD DIST = Hauptdolomit Fm. in the distal margin). Since more than one sample was analysed for each fluid-related product, they were gathered together to make the understanding and description of each set as easiest as possible. Lastly, oxydes are expressed in wt% while trace and rare earth elements in ppm (parts per million). Elements below the detection limit were considered as absent.

9.2.1 Reference samples

To get a comparison with "unaltered" samples, two specimens of Hauptdolomit Fm. (REF HD) sampled far from Triassic-Jurassic faults (Lombardian basin and Quattervals nappe, courtesy of Prof. Fabrizio Berra), and hence from active fluid activity, have been analysed in order to have a signal as undisturbed as possible. Furthermore, data from Pinto et al. (2015) are here considered for black gouge of detachment fault (REF GOUGE) and cataclasite (REF CAT) affecting the Albula granite in the distal margin domain and for post-rift Radiolarian Chert Fm. (REF RAD).

The two REF HD samples are characterized by the lowest amount of trace elements with appreciable concentration only in Ba, Sr, V, Pb and Zn.

As to REE, these samples show the lesser total amount of rare earth elements (ΣREE = 2.35 ppm) also considering that Eu, Tb, Y and Ho are below the detection limit. For such reason it has not been possible to calculate the Y/Ho ratio nor consider the Eu anomaly. A slightly negative Ce anomaly occurs (Ce/Ce* = 0.763).

REF CAT and GOUGE show trace elements patterns strongly enriched compared to the analysed samples (e.g. Ba, Rb, Zr) with smaller maxima in Ga, Sr, V, Cu, Ni. Pb, Zn. Total REE contents are 199 and 213 ppm for REF CAT and GOUGE, respectively. Y/Ho ratio is slightly super-chondritic (> 26-28). LREE are slightly fractionated relative to HREE (La/Yb = 7 to 10), no Ce anomaly (Ce/Ce* = 0.99) occurs whereas negative Eu anomaly is present (Eu/Eu* = 0.59 to 0.62).

REF RAD are strongly enriched in Ba, Rb, Zr and Ni. Other relevant trace elements are V, Co, Cu and Zn. Generally, REF RAD shows higher concentrations than the samples analysed in this Thesis.

ΣREE is almost 100 ppm, Y/Ho is lower than that of chondrite (Y/Ho = 25), no Ce anomaly occurs (Ce/Ce* = 1.01) whereas negative Eu anomaly is present (Eu/Eu* = 0.66), La/Yb ratio is 10 (LREE/HREE).

9.3 THE HAUPTDOLOMIT FM. ALONG THE ADRIATIC CONTINENTAL MARGIN

Analyses were performed on the Hauptdolomit Fm. all over the Adriatic margin (proximal domain, central and outer distal domain) where it occurs in the footwall of the main fault at the Il Motto area and as extensional allochthons at Piz Val Lunga, Fuorcla Cotschna and Mal Pass areas.

All the samples show trace elements concentrations higher than that of REF HD (Fig. 9.1 a). Some elements, such as Ba, Cr, Rb, Sr, Zr, Cu, Pb and Zn show about the same values all over the margin even if a slight increase occurs

moving from the proximal part towards the outer domains. Conversely, V, As and Mo have higher amount in the samples of the proximal margin.

Concerning the REE (Fig. 9.1 b), all the HD samples show always the lowest amount of rare elements (ΣREE < 20 ppm) compared to all the others analysed samples with the only exception of the REF HD (ΣREE = 2.35 ppm). As well as the trace elements, an increase in the total amount of REE from the proximal domain to the distal one occurs. All the samples do not show Ce anomaly (nor negative or positive) whereas negative Eu anomalies occur (Eu/Eu* = 0.63 to 0.85) as well as super-chondritic Y/Ho ratio (> 26-28) and relative enrichment of light rare earth elements compared to heavy rare earth elements (La/Yb = 10 to 15).

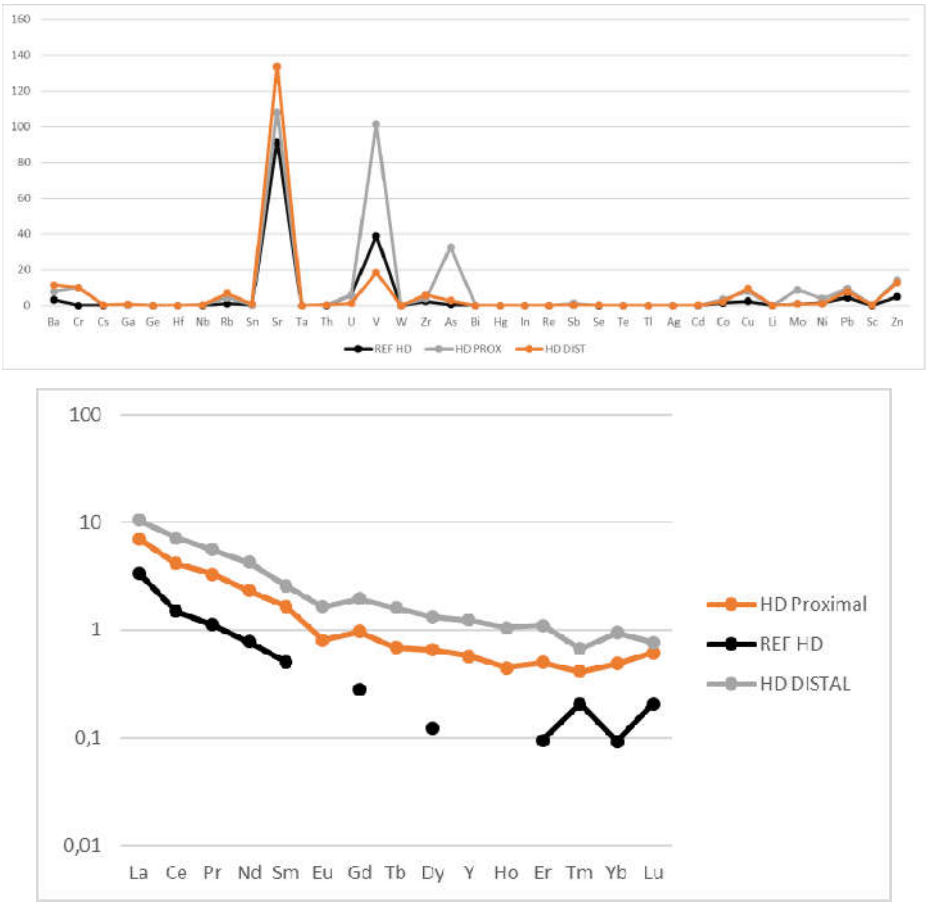

Fig. 9.1 - Trace elements content (in ppm) and chondrite-normalized REE patterns of

Hauptdolomit Fm. along the Adriatic continental margin. HD: Hauptdolomit Fm.; REF: reference sample (courtesy of Prof. Fabrizio Berra); PROX: proximal margin; DIST: distal margin.

9.4 THE HAUPTDOLOMIT FM. IN THE DISTAL MARGIN

Focusing on the distal domain of the Adriatic continental margin, it is useful to look at those rocks representing modifications of the HD DIST such as: clasts of Hauptdolomit Fm. within the black gouge (HD GOUGE), the cataclasite (HD CAT) and the dedolomite (DEDOL). As already described, such modifications are due to the interaction between the extensional allochthon and overpressured fluids related to the detachment fault activity.

HD DIST and HD CAT have lower amounts of trace elements compared to DEDOL and HD GOUGE and are characterized by an almost identical trend showing enrichment in Sr, V, Ba, Cr, Rb, Co and Zn. Conversely, HD GOUGE and DEDOL are strongly enriched in Ba, Sr, Pb and Zn with minor maxima in Cr, V, As. HD GOUGE, furthermore, is the only sample that shows particular enrichment in some oxides such as SiO_2, Fe_2O_3, Al_2O_3. Interestingly, DEDOL occurring at the base of the allochthon at Piz Val Lunga area is strongly enriched in Ba (about 370ppm) showing values almost identical to those of REF GOUGE and REF CAT in the basement. These latter have always higher concentrations of trace elements than the carbonates except for Sr, V and Zn, which are comparable (Fig. 9.2 a).

Rare earth elements reflect the same patterns observed for trace elements (Fig. 9.2 b). HD DISTAL and HD CAT have the lowest amount of REE (ΣREE about 10 ppm) compared to that of DEDOL and HD GOUGE, the latter being the richer sample within the distal margin with total amount of REE (ΣREE = 50 ppm). Indeed, it is almost three times higher than the others. In any case, LREE are slightly enriched relative to HREE (La/Yb = 5 to 12), the ratio Y/Ho is always super-chondritic with the only exception of HD CAT (Y/Ho = 20). Ce never shows a clear anomaly (Ce/Ce* = 0.87 to 0.94), whereas all the samples

have negative Eu anomaly (Eu/Eu* = 0.58 to 0.78) whilst HD GOUGE shows a positive one (Eu/Eu* = 1.37).

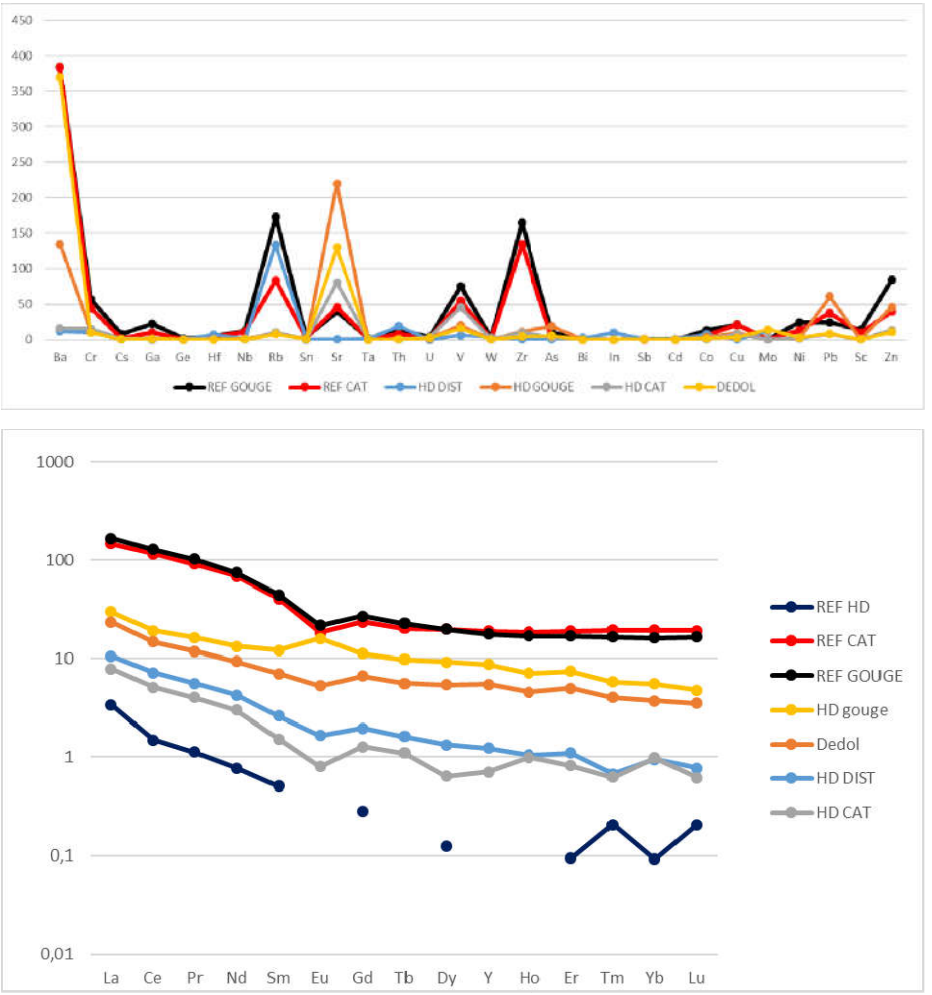

Fig. 9.2 - Trace elements content (in ppm) and chondrite-normalized REE patterns of Hauptdolomit Fm. in the Adriatic distal margin. REF GOUGE and CAT: reference samples of black gouge and cataclasite from Pinto et al. (2015); REF HD: reference samples of Hauptdolomit Fm. (courtesy of Prof. Fabrizio Berra); HD DIST: Hauptdolomit Fm. in the distal margin; HD GOUGE: clasts of Hauptdolomit FM. within the black gouge; HD CAT: cataclasite made of Hauptdolomit Fm.; DEDOL: dedolomite.

Particular attention has to be paid to the filling of sills and dykes (SILL) occurring at Piz Alv area (inner distal margin). This sample shows the highest total amount of both trace elements and rare earth elements. Indeed, it is strongly enriched in Ba, Cr, Rb, Sr, V, Zr with minor maxima on Cs, Ga, Co, Cu, Li, Ni, Sc and Zn and up to 14% of SiO_2, Al_2O_3, K_2O and Fe_2O_3. As to REE, it shows a total amount that is almost six times that of the other samples (ΣREE = 116.18 ppm). It shows slightly super-chondritic Y/Ho ratio (28,63), positive and negative Ce and Eu anomaly respectively (Ce/Ce* = 1.39; Eu/Eu* = 0.64).

9.5 DOLOMITE VEINS IN THE DISTAL MARGIN

Analyzed dolomite veins from the distal margin (DOL VEIN DIST) are encased within the extensional allochthons.

Veins and the host HD DISTAL show basically the same pattern of trace elements even if DOL VEIN has higher conent in Ba, Cr, Sr, Pb and Zn whereas the host rock has higher values of Cu (Fig. 9.3 a).

Concerning the REE (Fig. 9.3 b), the total amount DOL VEIN DIST is almost double than that of HD DISTAL (about 20 ppm vs 12 ppm). In both cases, LREE are enriched relative to HREE (La/Yb = 11) with no Ce anomaly (Ce/Ce* = 0.93), negative Eu anomaly (Eu/Eu* = 0.67 to 0.72) and super-chondritic Y/Ho ratio (Y/Ho = 22 to 35).

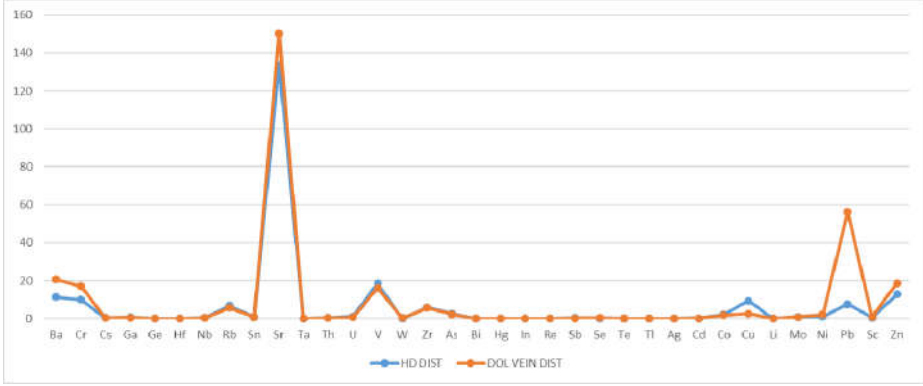

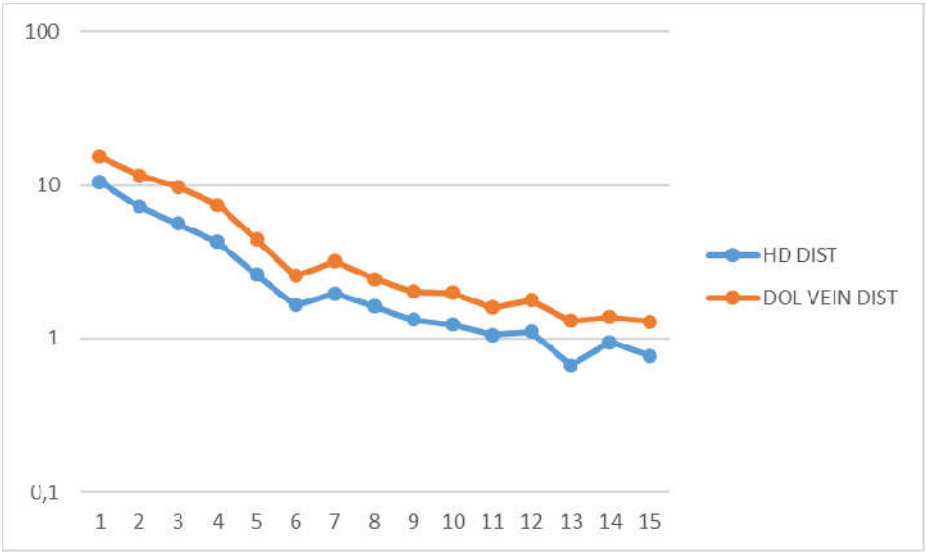

Fig. 9.3 - Trace elements content (in ppm) and chondrite-normalized REE patterns of the Hauptdolomit Fm. in the distal margin (HD DIST) and of dolomite veins within the extensional allochthon in the distal margin (DOL VEIN DIST).

9.6 SILICIFICATION

Within this group is possible to distinguish two different sets of samples: 1) fine grained silicification affecting the matrix of calciruditic beds (SILIC) and 2) silicification related to the formation of chert nodules and septarian-like concretions (SEPT) both occurring in the uppermost part of the sedimentary sequence (syn- to post-rift) at Fuorcla Cotschna and Mal Pass areas.

Both sets of data show enrichment in the same trace elements even if some differences occur (Fig. 9.4 a). SEPT show a double amount of Ba, Rb, V and Cu whilst is depleted in Sr. SILIC is slightly enriched in Cr relative to SEPT. Other relevant elements are Zr, Pb and Zn. As a comparison, REF RAD show higher values of Ba, Rb, Zr, Co, Ni whereas similar amount of Cr, V, Pb and Zn. Conversely, Sr is almost absent.

As to the rare earth elements (Fig. 94 b), SILIC represents the second group of the whole dataset for total abundance (ΣREE about 72 ppm). It is more than

three times that of SEPT (ΣREE = 22 ppm). Both SILIC and SEPT show evident anomalies in Ce and Eu (Ce/Ce* = 0.35 to 1.42; Eu/Eu* = 0.60 to 0.63), super-chondritic Y/Ho ratios in the range 33-38 and LREE higher than HREE (La/Yb = 9 to 14).

9.7 FE-MN OXIDES

Compared to the trace elements of REF RAD, Fe-Mn coated clasts show lesser amount of Ba, Cr, Rb, Zr, Co, Cu and Zn, higher concentrations in Sr and Pb and similar values of V (Fig. 9.4 a).

Fe-Mn has a total amount of REE of about 24 ppm that is very similar to that of SEPT (Fig. 9.4 b). LREE-HREE fractionation is relatively slight with ratio of La/Yb = 8. No Ce anomaly occurs (Ce/Ce* = 0.91) while Eu show negative anomaly (Eu/Eu* = 0.72).

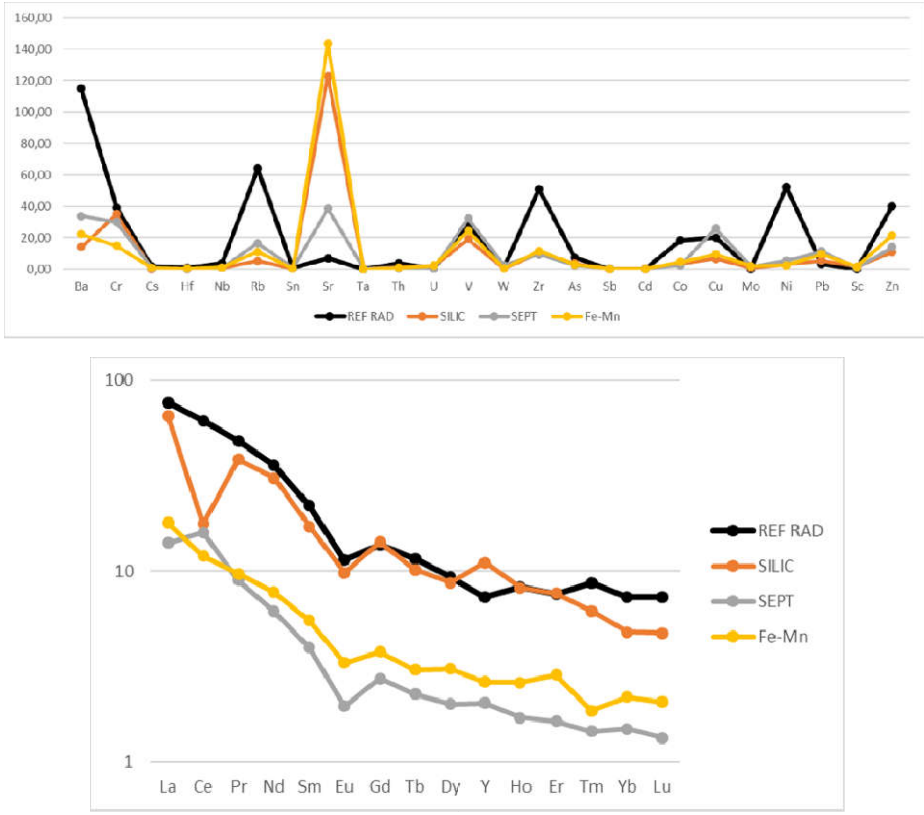

Fig. 9.4 - Trace elements content (in ppm) and chondrite-normalized REE patterns of

reference sample of Radiolarian Chert Fm. (REF RAD) from Pinto et al. (2015), silicified matrix of calciruditic beds (SILIC), spetarian-like concretions (SEPT) and Fe-Mn oxides coating (Fe-Mn).

9.8 DISCUSSION AND INTERPRETATION

The rare earth elements (REE) are powerful tracers in the study of the evolution of geochemical systems and have been widely used to identify sources of oceanic REE and mixing processes within the oceans (Elderfield, 1988). Since the first publication of REE data in hydrothermal fluids by Michard et al. (1983), REE studies have been conducted on fluids from many different oceanic hydrothermal areas including the Mid-Atlantic Ridge at Lucky Strike (Klinkhammer et al., 1995), Broken Spur (James et al., 1995), TAG (Mitra, 1991; Mitra et al., 1994), Snakepit or MARK (Campbell et al., 1988 a; Mitra, 1991; Mitra et al., 1994), the East Pacific Rise (Michard et al., 1983; Michard and Albaréde, 1986), and the Lau Back-Ark Basin of the South-West Pacific (Fouquet et al., 1993). All of these investigations reported that the chondrite-normalized REE (REE_{CN}) patterns of acidic hydrothermal fluids exhibit LREE-enriched patterns with positive Eu anomalies. Furthermore, REE concentrations in hydrothermal fluids are greatly enriched compared to seawater (Elderfield and Greaves, 1982; De Baar et al., 1985; Piepgras and Jacobsen, 1992).

Positive Eu anomaly, which is supposed to be a clear signal of hydrothermal activity, is likely to reflect the Eu^{2+}/Eu^{3+} ratio in the fluid (Zhong and Mucci, 1995), which is in turn strongly dependent on temperature. Eu^{2+}/Eu^{3+} equilibrium is established at about 250°C (Sverjensky, 1984; Bau, 1991; Bau & Möller, 1992) so that positive Eu anomalies in a fluid need a temperature of more than approximately 250°C. Said that, Michard et al. (1983) showed that hydrothermal fluids produced by low-temperature hydrothermal alteration (below 200°C) display weak or no Eu anomalies. Looking at the homogenization temperatures of fluid inclusions presented in this Thesis, the absent or weakly negative Eu anomalies can be justified by the occurrence of low temperature

hydrothermal fluids. Because of its larger ionic radius and different charge, Eu^{2+} has a lower affinity for sorption or incorporation into secondary minerals during water–rock interaction than Eu^{3+}, and, relative to its trivalent REY neighbours, Eu^{2+} preferentially partitions into the dissolved phase (Bau, 1991; Bau and Möller, 1992). A positive Eu anomaly in a hydrothermal fluid is, therefore, a typical result of high-temperature water-rock interaction and cannot develop in low-temperature aqueous systems. Because of the extremely low oxygen fugacities required for significant Eu^{3+} reduction at low temperature (Bau, 1991), carbonate-precipitating fluids with positive Eu anomalies are even very rare in extremely reducing natural systems such as methane ("cold") seeps (e.g., Feng et al., 2008, 2009; Himmler et al., 2010). The HD GOUGE, on the contrary, shows positive Eu anomaly. Manatschal (1999) and Manatschal et al. (2000) described temperatures for the detachment fault and the black gouge as high as 250°C. Such temperature could then be responsible for the positive Eu anomaly. Furthermore, positive Eu anomaly has been related to fluid-rock interactions such as breakdown of plagioclase (McLennan, 1989). Alteration of plagioclase widely occurred within the Albula granite in the Err Nappe in response to the detachment fault activity. Negative Eu anomaly of the analysed samples from the Adriatic margin can be also explained, even if in contrast to what has just been mentioned, based on Lüders et al. (1993) who stated that carbonates formed from fluids which interacted with granites may show a negative Eu anomaly.

The hydrothermal characteristics of the studied minerals and by inference of the fluids seem to be strongly confirmed by super-chondritic Y/Ho ratio of the whole dataset (the only exception is HD CAT), which is typical of hydrothermal systems (Bau and Dulski, 1995). The enrichment of the LREE relative to HREE observed in the whole dataset can be attributed to the greater stability of HREE complexes in hydrothermal solutions and is a common feature of hydrothermal fluids (Douville et al., 1999). Low content of REE, which is a characteristic of the presented samples, can give some indication about the residence time of fluids within the aquifer that was possibly fast recharged.

Due to oxidizing conditions in seawater, Ce^{2+} is oxidized in Ce^{3+}, which is less mobile resulting in Ce depletion of the seawater itself. Therefore, marine water commonly possesses a negative Ce anomaly (Elderfield and Greaves, 1982; De Baar et al., 1985; Hu et al., 1988), which is then inherited by carbonates formed in a marine environment. Converserly, positive Ce anomalies mainly occur due to detrital input (Nath et al 1997; Madhavaraju and Ramasamy, 1999; Madhavaraju and Lee, 2009; Madharavarju et al. 2010), diagenesis (Armstrong-Altrin et al., 2003) and scaveging processes (Masuzawa and Koyama, 1989), and paleo-redox conditions (Liu et al., 1988). Only two sets of samples show evident Ce anomalies within the whole dataset: SILIC and SEPT with negative and positive anomalies respectively. All the other samples show very weak to no anomalies.

The clear difference in total amount of REE (ΣREE) of HD REF relative to the other samples as well as the absence of Y and Ho (below the detection limit) suggest that the so far described fluid-related processes (e.g. replacement dolomitization, dedolomitization) which affected the Hauptdolomit Fm. were key processes leading to the enrichment of REE as well as trace elements.

9.8.1 The distal margin

With a more detailed look at the distal margin preserved at Piz Val Lunga, Fuorcla Cotschna and Mal Pass areas, it becomes evident how the portions of HD more involved in the activity of the detachment fault recorded higher concentration of both trace and rare earth elements. Indeed, both HD GOUGE and DEDOL are strongly enriched. In the first case the enrichment can be related to fluids circulated along the detachment and/or interaction with the black gouge. In the second case, fluids responsible of dedolomitization of both HD and HD CAT may be ascribed for the enrichment too.

Pinto et al. (2015) widely described, for the detachment system in the distal domain of the Adriatic continental margin, the occurrence of elements as Cr, Ni, V, Co, Cu, Sc as related to serpentinization processes affecting and depleting the

exhuming mantle. Such enrichment occurred in response to fluid migration along the Err detachment fault system, which allowed the enrichment of both cataclasites and black gouges of the detachment itself. Findings of such elements also within the analysed samples of this study could suggest that also the carbonates lying above the detachment fault recorded such serpentinizing event. Furthermore, the staining of carbonate clasts by Fe-Mn oxides within the upper part of the syn-rift succession, point to important involvement of "mantle-related" fluids even far from the detachment surface. Indeed, Pinto et al. (2015) suggest the occurrence of "poisoning" of the seawater in response to venting related to serpentinization, which may confirm the "mantle overprint" recorded at the syn- to post-rift sediments transition.

The presented dataset highlights also the occurrence of crustal-related elements (e.g. Ba, Sr, Rb, Pb) that should testify and confirm a deep fluid circulation within the Albula granite (e.g. footwall of the detachment fault). In particular, the strong enrichment in Ba should confirm the occurrence of hydrothermal circulation (Plank and Langmuir, 1998)

Both SILIC and SEPT show strong enrichment in Sr. The explanation can be found considering those "impurities" mentioned at the beginning of this chapter. Petrographic studies allowed to recognize a dolomitization stage that occurred prior to the fine grained silicification (as demonstrated by the occurrence of dolomite rhombs within the silicified matrix of calciruditic beds and chert nodules). Carbonates generally contain high amount of Sr, which could have been inherited, giving that high Sr content even after the almost complete silicification of the rocks. SEPT samples contain both sparse dolomite rhombs and saddle dolomite cementing fractures in septarian-like concretions. Such carbonate content can be responsible for high Sr values.

Further *in situ* measurements are required to better characterize and constrain the geochemical history of fluids involved in the extensional phases affected the Adriatic continental margin.

10. Discussion: Fluid characteristics and flow pathways

10.1 INTRODUCTION

While post-depositional processes such as dolomitization, veining, and silicification are observed in different paleo-geographic domains of the Adriatic continental margin, others are exclusive of only one site. The cataclastic breccias, calcite cementation, dedolomitization are observed only at Piz Val Lunga area and Fe-Mn oxide coating only at Fuorcla Cotschna area. Other individual features are the absence of veining in syn-rift sediments at Mal Pass area, and the lack of quartz at Il Motto area. Each of these aspects sheds light on the mechanical and chemical processes that acted in an articulated rifting history that, depending on sites, is recorded by different tectono-stratigraphic settings. Each outcrop is a window over different segments of such a complex system and enables to observe what happened at the base and within the allochthon, in the lower part of the syn-tectonic sedimentary succession or in its upper, younger part. Everywhere, however, circulating fluids clearly appears to have been of primary importance in determining the final aspects of the rocks. Isotope geochemistry and fluid inclusion microthermometry, trace elements and REE enable to constrain some characteristics of these fluids, their circulation patterns and also the timing.

10.2 CONSTRAINTS ON THE HYDROTHERMAL FEATURES OF THE FLUIDS

$\delta^{13}C$ values of all the analyzed samples from the different paleogeographic domains fall in the range of 0 to +4 ‰ which is characteristic of normal marine sedimentary carbonates and show no significant contribution of organic matter decomposition. $\delta^{18}O$ values, conversely, are all negative showing a quite wide range from 0 to -16 ‰. Nonetheless, a common trend can be observed (Fig.

10.1) throughout the entire Adriatic margin based on $\delta^{18}O$. The less depleted values are always those related to the replacement dolomite whereas the more depleted ones refer to the new forming minerals (e.g. calcite and dolomite cements of breccias and veins). Looking at Fig. 10.1 it is evident that from the proximal towards the outer distal margin, a constant decrease in $\delta^{18}O$ values in replacement and authigenic minerals occurs even if the distinction between the two is always well recognizable.

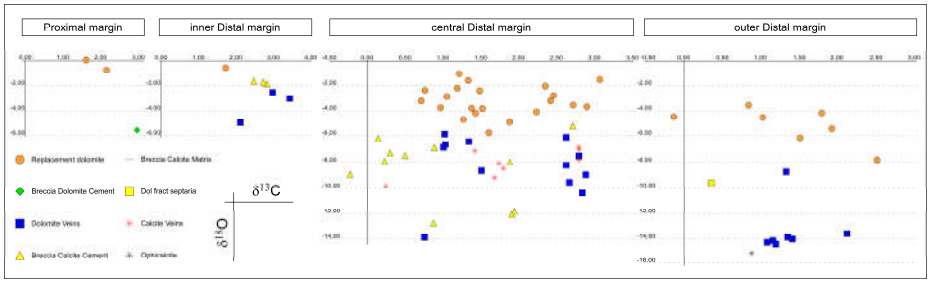

Fig. 10.1 - Stable isotope data: $\delta^{18}O$ versus $\delta^{13}C$ cross plot for dolomite and calcite minerals from the whole Adriatic continental margin. Values relative to the VPDB standard. A detailed description of each group of data is given in previous chapters.

Both finely and coarsely crystalline dolomites ("Replacement dolomite" in Fig. 10.1) show the least ^{18}O-depleted values of the whole dataset which, however, are lower than those reported in present day settings where dolomite is forming and ranges from 0 to +4 ‰ (e.g. Tucker and Wright, 1990; Meister et al., 2013). The study of fluid inclusions indeed provides temperature constraints to these dolomites, with formation temperatures averaging 120-130°C. These dolomites, in the distal domain (Piz Val Lunga, Fuorcla Cotschna, Piz Alv) already occur as clasts in the Bardella Fm. and thus they could not have been buried more than the cumulative thickness of the Kössen and Agnelli Formations, which does not exceed a few 100's meters. Burial temperatures reached by Upper Triassic dolostones before middle Early Jurassic were thus surely significantly lower than those documented by fluid inclusion microthermometry and a dolomitization event related to the upward advection of hydrothermal fluids is thus supported (e.g. Lopez-Horgue et al., 2010). The hydrothermal

characteristics of the fluids are also confirmed by REE systematics (e.g. Y/Ho, LREE/HREE, weak Eu anomaly). Furthermore, such an event is strongly constrained by U-Pb ages, which point to a dolomitizing stage, widely affecting the Hauptdolomit Formation, at about 200 Ma which interestingly corresponds to a thermal event documented by Beltrando et al. (2015) on the basis of ZHe data in the western part of the Southalpine domain. Keeping in mind this fundamental time constrain and that it is recorded within dolostones presently preserved all over the Adriatic margin, the replacement event described also at Mal Pass and Il Motto areas, also characterized by negative $\delta^{18}O$ values, can be assumed to be related to the same hydrothermal system described for the distal margin, in spite of the lack of homogenization temperatures of fluid inclusions. The Hauptdolomit Formation in the proximal and distal margins, when the replacement dolomitization took place, was not deeply buried so that also in these areas the occurrence of a hydrothermal circulation can be postulated.

All the samples of the second group (dolomite and calcite veins, calcite cements and dedolomite) plot in an area of more ^{18}O-depleted values but the variability internal to each analyzed subgroup of samples (veins, cement etc.) is so large that it is impossible to separate it from the others on the basis of O or C isotope values alone. Homogenization temperatures of fluid inclusions confirm that also these mineral phases precipitated from high-T fluids. Crosscutting relationships inferred by field and petrographic observations, as well as U-Pb dating, clearly show that these hydrothermal products postdate the replacement processes affecting the Hauptdolomit Fm.

Calculations of the isotope composition of fluids responsible for dolomite and calcite precipitation, made by applying the equation of Horita (2014) and Anderson and Arthur (1983) respectively for dolomite and calcite, provide O isotope values for fluids from slightly to markedly positive (+2 to about +12 ‰ SMOW). Such positive signature may be related to different processes such as evaporative enrichment (e.g. McKenzie, 1991), clay mineral diagenesis (Dählmann and de Lange, 2003; Hensen et al., 2007), and to the interaction with

silicate minerals of siliciclastic and crystalline rocks (Clayton *et al*., 1966; Land and Prezbindowski, 1981; Hitchon *et al*., 1990; Haeri-Ardakani et al., 2013). In the context of an extending continental margin, meteoric waters may be ruled out and the only reasonable source of fluids feeding the complex fracture-controlled circulation system was seawater. In particular, the stratigraphy of the studied sections, where deepwater sediments occur also directly over basement rocks topped by the detachment faults, leads to exclude the first two hypotheses. The highly radiogenic Sr isotope values of dolomite and calcite occurring as replacing and authigenic minerals, conversely, demonstrate a fundamental contribution by feldspars and thus support a circulation of fluids within the quartzo-feldspatic basement rocks of the Albula granite and/or Permian siliciclastics. Trace elements analyses show enrichments in some elements (e.g. Ba, Sr, Pb) which inevitably ask for an important interaction between fluids and crustal rocks.

On the whole, the quite wide range of variability of $\delta^{18}O$ values is suggested to depend on the characteristics of the flow paths. Many variables are to be taken into account such as depth and rate of circulation of fluids in the basement in addition to mixing with seawater. All these factors, which govern the degree of fluid-rock interaction and hence temperature and enrichment in ^{18}O, interact in such a complex way that is probably impossible to model in detail.

10.3 EVOLUTIONARY MODEL

On the basis of the considerations exposed above, the following scenario for the Triassic-Jurassic evolution of the Adriatic continental margin preserved in the Err nappe may be suggested. Two main stages in the post-depositional evolution can be distinguished (Fig. 10.2) according to the extensional deformation phases ature of fluids. 1) The first affects the pre-rift successions (Hauptdolomit, Kössen, Agnelli Formations) before their reworking and resedimentation as clasts within the syn-rift sequences (Bardella and Saluver Formations). This stage (pre-BBF; Rhaetian to late Early Jurassic) mainly involves fluids rich in

carbonate and includes several processes such as dolomitization of calcareous sediments, dolomite cementation of pores, veining (formation of fractures and filling with saddle dolomite), formation and cementation of breccias with dolomite and calcite, and minor quartz precipitation in veins. It may be related to the early phases of rifting (SG_1 U-Pb ages) recorded in the proximal margin and to the phase of localization of the deformation in the distal domain (SG_2 U-Pb ages). 2) The second stage (post-BBF; Middle to early Late Jurassic) affects the whole succession (pre-, syn- and post-rift) although it is best recognized in syn- to post-rift sediments. It took place during and after the deposition of Bardella, Saluver and Radiolarian Cherts Formations, documenting an involvement of large amounts of SiO_2 into the system with resulting precipitation of quartz (veins, septarian-like concretions, diffuse silicification). To this stage is also related the income of mantle-related elements (e.g. Fe-Mn oxides).

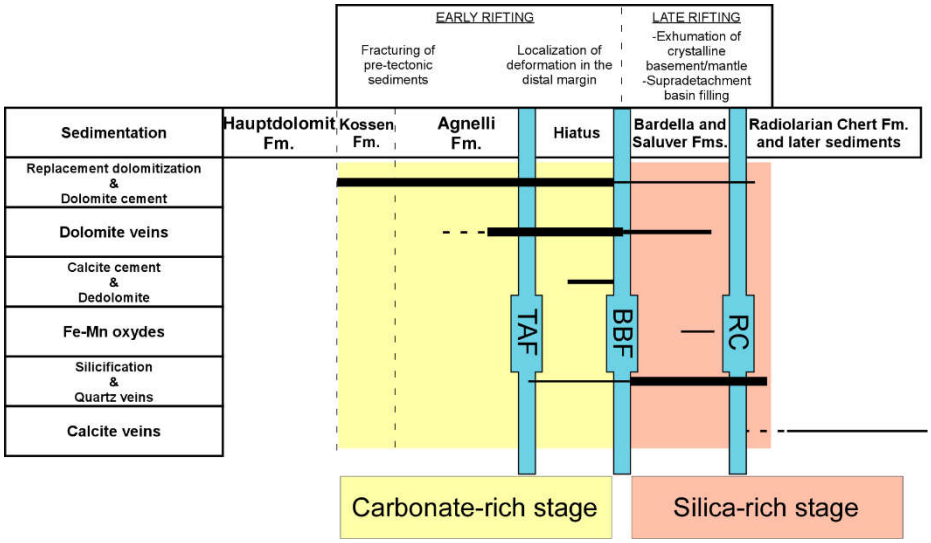

Fig. 10.2 - Paragenetic sequence showing the relative timing of post-depositional processes and related products affecting the pre- to post-tectonic sediments of the Adriatic continental margin. This interpretation is based on the data of the different analysed paleogegraphic domain. The width of the lines is qualitatively proportional to the magnitude of each process (modified after Incerpi et al., 2017). TAF = Top of Agnelli Fm.; BBF = Base of Bardella Fm.; RC = Radiolarian Cherts.

10.3.1 Similar conditions but different products: why?

Both the carbonate- and silica-rich stages, and hence their diagenetic products, are characterized by comparable physico-chemical features as: similar homogenization temperatures of fluid inclusions, negative $\delta^{18}O$, high Sr^{87}/Sr^{86} ratios, trace elements and REE signature. This dataset, as already discussed, clearly allow to consider the studied fluids as hydrothermal in response to deep circulation through faults and fracture systems and strong interaction with basement rocks. Despite these similarities, the first diagenetic stage is carbonate-dominated whereas the second is almost uniquely related to silica-rich fluids. Then, one important question arises: why apparently similar conditions produced so different mineralogies within the diagenetic products? In order to give an answer, the tectono-stratigraphic architecture of the margin at the time when the two different diagenetic stages occurred has to be taken into account.

The first carbonate-rich diagenetic stage refers to the first rifting events (SG1 and SG2), which segmented the continental margin leading to the formation of half graben basins bounded by high angle normal faults (Fig. 10.3). These main structures, that penetrated within the crust for some kilometers, are composed of different minor faults each one accommodating displacements in the order of hundreds of meters. Seawater, penetrated through these high angle faults and their damage zones. Fluids were consequently heated and chemically modified by exchanges with basement rocks, as documented by $\delta^{18}O$ and Sr^{87}/Sr^{86}. In their way up within convective cells, seawater, which is per se a dolomitizing fluid (Land, 1985; Purser et al., 1994; Machel, 2004) was hot enough to overcome the kinetic barrier to dolomitization. CO_2 degassing, promoted by pressure decrease while approaching the surface, possibly triggered this process.

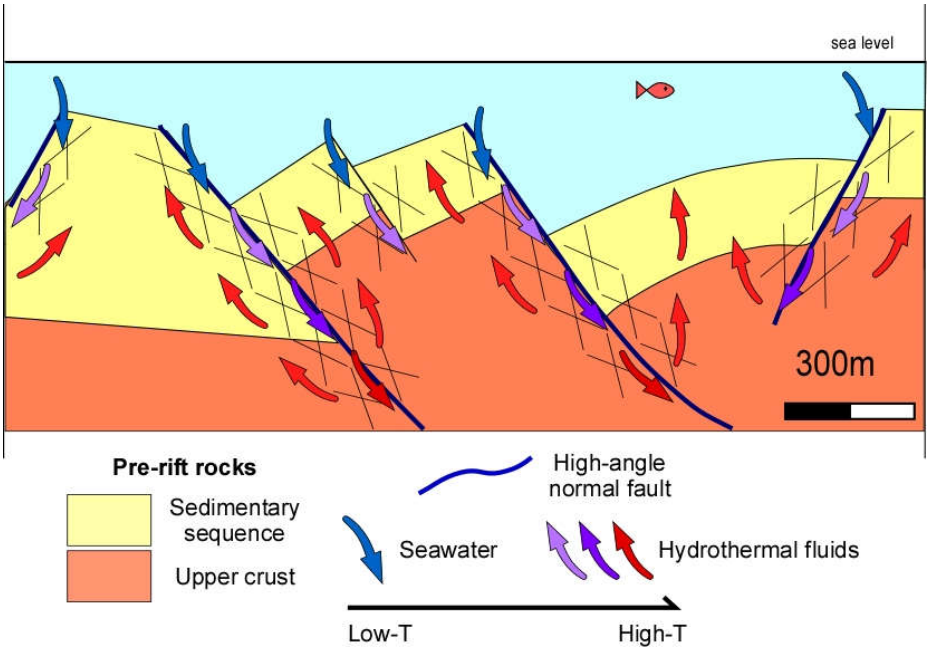

Fig. 10.3 - Schematic representation of the Adriatic continental margin architecture and fluid flow circulation during the first diagenetic stage.

The second silica-rich diagenetic stage, occurring during low-angle detachment faulting (SG3), is characterized by a greater amount of tectonic displacement that is mainly horizontal and one order of magnitude higher than that of the first stage (Fig. 10.4). The volume of cataclastic belts in the crystalline basement was much greater and consequently the degree of breakdown of feldspars. Moreover, in this frame, the flux of seawater was probably shallower and much more active resulting in stronger fluid-rock interaction in turn producing a massive silica enrichment in the fluids.

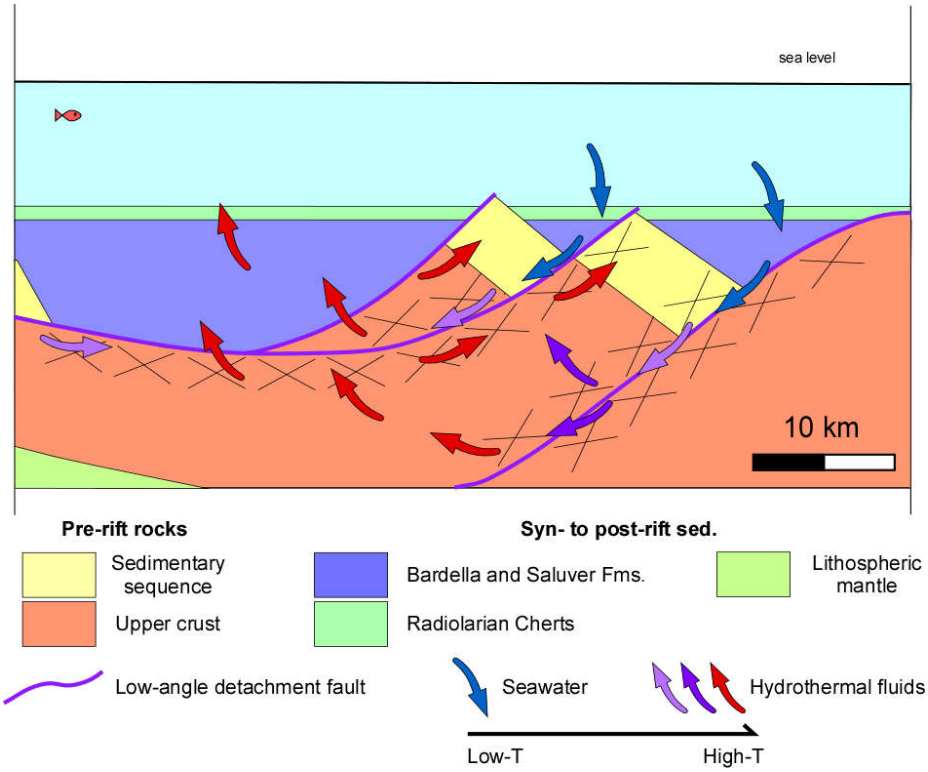

Fig. 10.4 - Schematic representation of the Adriatic distal margin architecture and fluid flow circulation duringthe second diagenetic stage.

10.3.2 The two diagenetic stages along the Adriatic continental margin

10.3.2.1 The central distal margin

The Hauptdolomit Fm., preserved as extensional allochthons in the distal domain of the Adriatic margin, has been affected by diffuse replacement dolomitization and dolomite cementation of pores (first diagenetic stage). As documented by U-Pb ages, these hydrothermal events are coeval with the early rifting phases affecting the margin in late Triassic-early Jurassic. Such dolomitizing processes took place when the carbonate platform started to be tectonized leading to the drowning of the Hauptdolomit Fm., as documented by the deposition of the deeper facies of the Kössen and especially Agnelli Fms.

Furthermore, to this tectonic phase is strictly related also the formation of neptunian dykes and sills well recorded at Piz Alv and the Mal Pass area, which are, in turn, widely dolomitized. At this time, the architecture of the margin was characterized by structural highs and subsiding areas, both of them in a pelagic to hemi-pelagic environment. When the deformation started to localize towards the future distal domains, the base of the forming extensional allochthons underwent intense friction between the basement and the overriding carbonate rock masses generating cataclastic deformation. Fluid circulation locally induced dedolomitization. Fault-valve mechanisms (Sibson 1992) along the detachment fault may have caused a cyclic, abrupt release of overpressured fluids, which resulted in hydraulic fracturing of the overlying dolostones and filling of fractures or spaces among breccia clasts by saddle dolomite and calcite spar (e.g. Lopez-Horgue et al., 2010). Petrographic, isotopic, fluid inclusion and REE data of dolomite and calcite show that they are of hydrothermal origin. Nonetheless, low temperatures as measured in fluid inclusions and a lesser enrichment in ^{18}O of dedolomite could point to a mixing of fluids involved in more superficial circulation cells, such as along the extensional detachment fault, with those flowing up from deeper parts of the rock column.

The second diagenetic stage mainly involves silica, which occurs as filling of veins crosscutting the whole syn-rift succession (Bardella and Saluver Fms.). It occurs also as a replacement of still very soft and porous sediments that developed at a very shallow burial depth in the upper part of the syn-tectonic succession (Saluver B-C Fms.). Occurrences of septarian-like concretions (both as clasts and in place) and silicified calciruditic bodies in the Saluver C and Radiolarian Cherts Fms. point to a persistent fluid activity even after the deposition of the first post-rift sediments. The Fe-Mn oxydes staining of the clasts within calciruditic beds suggest also an input related to the exhumation of the mantle in the outermost part of the margin (ocean-continent transition; Pinto et al. 2015). Trace elements seem to confirm such connection by the occurrence of mantle-derived metals as Cr, V, Ni.

10.3.2.2 The outer distal margin

In the Mal Pass area, the first carbonate-rich diagenetic stage (pre-BBF) is dominated by dolomite fluids, which led to the dolomitization of the Hauptdolomit Formation, dykes and the filling of pores. It is also responsible of the formation of remarkable amounts of multiphase saddle dolomite veins (set 1) cutting through the allochthon.

The second stage (silica-rich and post-BBF) is characterized by dolomite-quartz mixed fluids giving rise to different and possibly contemporaneous products in the allochthon and overlying syn-rift sediments. The allochthon shows a second set of veins (set 2) cemented by saddle dolomite and quartz. Since they cut through the Hauptdolomit Fm. and the brecciated sills and dykes, it had inevitably to occur after their formation. The release of these fluids in the syn-rift succession, finally, contributed to the formation of the septarian-like concretions and the dolomitization of the marly beds in a very early stage after their deposition.

10.3.2.3 The proximal margin

The medium to coarsely crystalline dolostones replacing the former Hauptdolomit Fm. at Il Motto area, by similarities with those observed in others domains of the Adriatic margin and by U-Pb ages, are referred to the first carbonate-rich stage (pre-BBF).

The textures of the described breccias and the mineralogy of the cements point to the presence of hydrofracturing processes related to the upflow of overpressured carbonate-rich fluids. Microthermometry and negative O isotopic values of breccia dolomite cement (type 1) document the involvement of hydrothermal fluids. Even if there are not unequivocal proofs about the ages of the breccias and related cements, their strict association with the master fault bounding the half-graben seems to constrain their formation to the Hettangian tectonic activity occurring at Il Motto. By that moment, the thickness of the Hauptdolomit Formation of which the footwall consisted was not more than

1000-1500 m and hence the obtained homogenization temperatures of fluid inclusions are not justified by burial depths. It can be assumed that the fluid flow was forced by the activity of the fault itself, which behaved as main circulation pathway (e.g. Lopez-Horgue et al., 2010). Finally, the occurrence of two compositionally different cements in the breccias point to a change in the chemistry of the system from a dolomite-rich to a calcite-dominated one. An Alpine age for the latter cannot be excluded.

At the Il Motto area, the second silica-dominated diagenetic stage (post-BBF) is not recorded. In order to further constrain or confute such observation, it would be useful to investigate the lowermost portion of the sedimentary column close to the contact with the Permian siliciclastics, where possibly silica-rich diagenetic products could have been formed.

Based on the above considerations it is evident that the study of the most distal portions of the Adriatic margin enables to reconstruct a long-lasting history characterized by complex tectono-stratigraphic and fluid-related features. These characteristics refer to several stages of the margin evolution, from the very first to the last stages of extension, which led to the exhumation of mantle rocks. The evolution of the fluids (e.g. the chemistry) appears to be directly connected with the tectono-stratigraphic evolution of the margin. Depending on which kind of rocks have been exhumed (e.g. Albula granite or mantle rocks), seawater composition changed leaving diagnostic signals in the precipitating minerals. Our results suggest that the fluids promptly responded to any changes of the surrounding environment giving detailed information about the processes responsible for the different parts of the margin. Furthermore, they may have played a fundamental role in the thermal history of the continental margin focusing heat fluxes and inducing diagenetic processes (e.g. dolomitization and silicification) otherwise not possible. Such role has strong consequences in terms

of maturation of organic matter and increase/decrease of porosity, which are fundamental parameters that control oil and gas migration and storage.

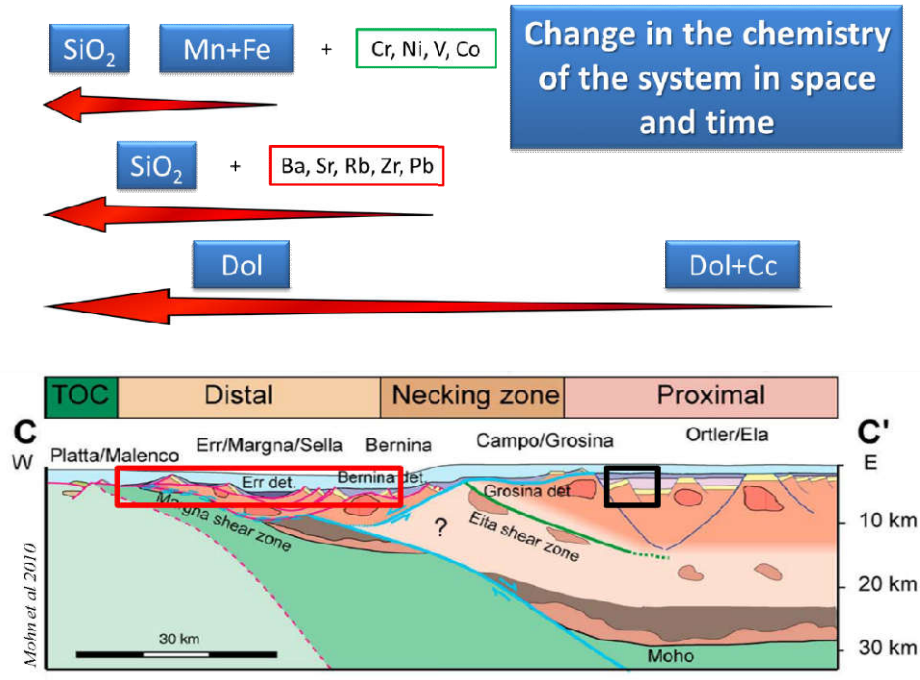

Fig. 10.5 - Reconstructed paleogeographic section across the Adriatic continental margin (modified after Mohn et al. 2010). The black and red rectangles show the domain analysed in this Thesis. The red arrows highlight, schematically, the chemistry of the fluids as depicted by the multi-disciplinary approach adopted in this work. The main changes occurred simoultaneously to the exhumation of continental crust and mantle-related rocks in response to detachment fault activity.

11. The Pyrenean hyper-extended rift system

11.1 INTRODUCTION

The Pyrenees are a continental fold and thrust belt resulting from the collision of the Iberian and European plate during the Late Cretaceous to Tertiary (Choukrune and ECORS Team, 1989; Muñoz, 1992; Deramond et al., 1993; Roure and Choukroune, 1998; Teixell, 1998). Triassic and Jurassic aborted rift events predated the development of a major Cretaceous crustal thinning stage, which gave rise to a counter-clockwise displacement of Iberia relative to Europe (Puigdefàbregas and Souquet, 1986; Vergés and Garcia-Senz, 2001), coeval with the onset of oceanic spreading in the Bay of Biscay between approximately 125-83 Ma (Le Pichon et al., 1970; Choukroune and Mattauer, 1978; Olivet, 1996; Gong et al. 2008; Jammes et al., 2009).

11.2 THE BAY OF BISCAY-PYRENEAN DOMAIN

The present-day Bay of Biscay–Pyrenean domain results from the polyphasic Triassic to Early Cretaceous rift system, which led to the formation of hyper-extended basins and oceanic crust in the western Bay of Biscay (Vergés and Garcia-Senz, 2001; Sibuet et al., 2004; Jammes et al., 2009; Filleaudeau et al., 2012; Vissers and Meijer, 2012a, b; Clerc and Lagabrielle, 2014; Mouthereau et al., 2014; Tugend et al., 2015; Vacherat et al., 2016). This system was reactivated during latest Cretaceous to Oligocene time by N-S directed compression due to the convergence of the European and Iberian plates. Although the Pyrenean compressional overprint resulted in the inversion of the Lower Cretaceous basins and reactivated most of the rift-related structures, it has the advantage that it uplifted and exposed the basal parts of a former hyper-extended rift basin. Similar to the Alps, the Bay of Biscay-Pyrenean domain can

be considered to represent a natural laboratory to investigate hyper-extended rift systems (Fig. 11.1).

Lithospheric break-up and seafloor spreading in the Bay of Biscay occurred simultaneously to hyper-extension further to the east in the Pyrenean domain. These processes are described both offshore (Parentis: Pinet et al., 1987; Bois et al., 1997; Brunet and Boillot, 1991; Bois and Gabriel, 1994; Jammes et al., 2010a; Roca et al., 2011) and onshore (e.g. the Aulus basin: Lagabrielle and Bodinier, 2008; Lagabrielle et al., 2010; Clerc et al., 2012; the Arzacq-Mauléon basin: Daignères et al., 1994; Jammes et al., 2009, 2010b; Lagabrielle et al., 2010; Debroas et al., 2010; Masini et al., 2014; Tugend et al., 2014; and the Basque-Cantabrian basin; Pedreira et al., 2007; Roca et al., 2011).

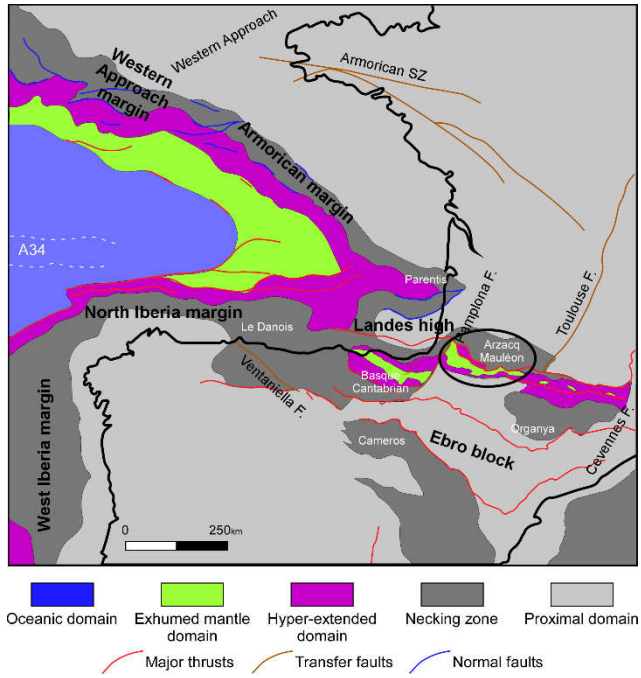

Fig. 11.1 - Map of the rift domains preserved in the Bay of Biscay and their fossil analogues from the Pyrenean domain. Extensional rift structures and thrust faults from the Armorican and Western Approach margins are based on the work of Thinon (1999). Modified after Tugend et al. (2014).

The Parentis basin, located at the NE termination of the Bay of Biscay, is a 100 km wide, weakly reactivated, offshore basin bordered to the north by the Western Approach and Armorican margins and to the south by the North Iberian margin (Fig. 11.1). The geometry of the Parentis basin, well imaged in the ECORS-Bay of Biscay profile (Bois et al., 1997) and East-West Expanding Spread profiles (ESPs, Marillier et al., 1988), shows that extreme crustal thinning to less than 10 km occurred. Furthermore, the interpretation of seismic profiles highlights the strong asymmetry of the basin, which is characterized by an upper and a lower plate sag basin architecture with its southern part floored by a low-angle extensional detachment fault (Jammes et al., 2009, 2010a).

The Arzacq-Mauléon rift system, located further to the SE, is a reactivated and partly exposed analogue of the Parentis Basin showing similar geophysical, tectonic and sedimentary features (Jammes et al., 2009, 2010a, b; Fig. 11.1). As for the Parentis Basin, the Arzacq-Mauléon rift system appears to be strongly asymmetric. Several authors suggested the occurrence of rift-related detachment faults in the Arzacq-Mauléon Basin (e.g., Ducasse and Vélasque, 1986a; Johnson and Hall, 1989a, b; Claude,1990; Jammes et al., 2009; Lagabrielle et al,. 2010; Masini et al., 2014). Its western part was reactivated during the Pyrenean inversion in late Cretaceous to Tertiary time (Choukrune and ECORS Team, 1989; Muñoz, 1992; Deramond et al., 1993; Roure and Choukroune, 1998; Teixell, 1998) as a large pop-up structure explaining the weak orogenic overprint. Here, consequently, there is a direct access to mantle, middle and upper crustal rocks as well as to the complete stratigraphic record including pre- to post-rift sediments.

11.2.1 Large-scale rift architecture of the Arzacq-Mauléon system

Masini et al. (2014) subdivided the Arzacq-Mauléon basin in 4 main domains, which, from north to south, are (Fig. 11.2):

1. The Arzacq Basin, extending over the European continental crust, is characterized by the progressive crustal thinning from 25 km in the north to less

than 20 km in the south leading to a progressive increase in the amount of Mesozoic extension moving southward (Daignières et al.,1994; Teixell, 1990). This is also supported by the southward thickening of the Lower and Middle Cretaceous sedimentary sequences (e.g., Biteau et al., 2006). One of the main characteristics of this basin is that the pre-rift sequences (pre-Aptian) can be imaged and were drilled throughout the entire Arzacq Basin (Daignières et al., 1994; BRGM et al., 1974). This suggests that the upper crust was weakly stretched, which contrasts with the observed crustal thinning responsible for progressive subsidence of the basin from the Aptian onward (Jammes et al., 2009).

2. The Grand Rieu High, is the boundary between the Arzacq and the hyper-extended Mauléon Basin located to the south. This domain is partially lacking the pre- to syn-rift sequences and, locally, is directly sealed by post-rift sediments (e.g., Cardesse 2 drillhole in BRGM, 1974; Serrano et al., 2006). It suggests that this domain acted as a topographic barrier until post-rift time. During Pyrenean convergence, the sedimentary cover of the Grand Rieu High was decoupled and thrust northward.

3. The Mauléon Basin is part of a complex E-W directed trough system bounded by two paleohighs: the Grand Rieu High to the north and the Axial domain to the south. The Mauléon Basin corresponds to a major Cretaceous basin formed over hyper-extended Iberian crust. It differs from the Arzacq Basin by a more complex rift history, with pre-rift sediments that are discontinuous and show a strongly variable syn-rift stratigraphic architecture. Jammes et al. (2009) showed that this basin formed as a hyper-extended basin with local exhumation of middle crustal and mantle rocks in the northern part of the basin. The authors also demonstrated the occurrence of a long-offset extensional detachment fault. Masini et al. (2014) showed that a second, large-scale detachment system can be traced across the southern margin of the Mauléon Basin. In this Thesis, the investigations will focus on the easternmost part of the Mauléon Basin, the so-called Chaînons Béarnais.

4. The Axial domain, further to the south, corresponds to the western equivalent of the Axial Zone of the Central and Eastern Pyrenees. It corresponds to the southern border of the former hyper-extended basin. One of the key characteristics is the occurrence of a major hiatus and the unconformable deposition of the Upper Cretaceous (Cenomanian and younger) post-rift carbonate platform over Paleozoic basement.

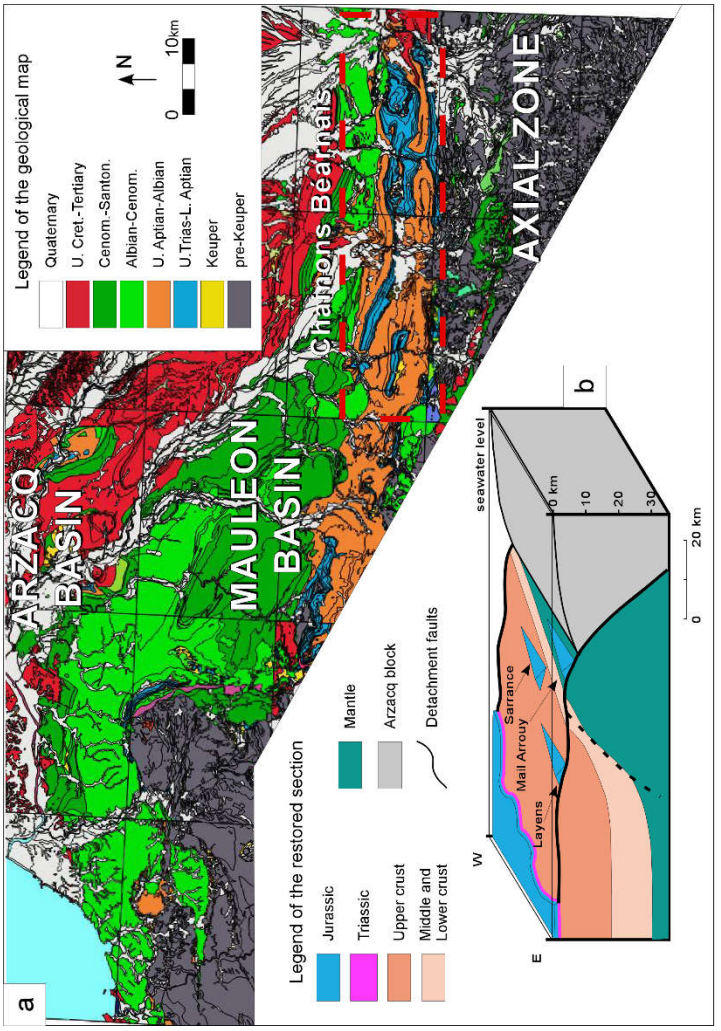

Fig. 11.2 - (a) Simplified geological map of the Arzacq-Mauleon rift system preserved in the western Pyrenees (modified after Jammes et al., 2010b). (b) Schematic restoration of the Mauléon Basin prior the onset of pyrenean compression. Only the pre-rift basement and sedimentary rocks are represented (modified after Jammes et al., 2009).

11.2.2 The stratigraphy of the Arzacq-Mauléon basin

11.2.2.1 Metamorphic basement

The Paleozoic metasediments consist of thick successions of low metamorphosed siliciclastic, shaly and calcareous deposits ranging from anchizonal to lower greenschist facies (Heddebaut, 1973). These rocks are mainly exposed south of the Mauléon Basin. The post-Variscan evolution is related to the activity of strike-slip/transform faults throughout the Late Carboniferous to the Early Permian that strongly structured the lithosphere (Arthaud and Matte, 1975, 1977; Burg et al., 1994 a, b).

11.2.2.2 Pre-rift sequence (Permian to early Aptian)

This sequence shows strong thickness variations and cannot be mapped as a continuous horizon. The Triassic sediments show the classical transgression of the Muschelkalk carbonate platform over the continental deposits of the Buntsandstein made of shales, sandstones and conglomerates (e.g., Germanic Facies: Curnelle, 1983; Fréchengues, 1993). Keuper evaporites, overlying the Muschelkalk carbonate platform, represent an important weak layer acting as a decoupling horizon during the subsequent extensional (e.g., Canérot et al., 2001; Jammes et al., 2010b) and compressional events (Casteras, 1969; Casteras et al., 1970a, b, 1971; Le Pochat et al., 1978). Voluminous time equivalent tholeiitic magmatic activity, also known as the "ophitic" intrusions, can be found associated with the evaporites (Rossi et al., 2003 and references therein). The occurrence of the evaporitic facies is threefold: (1) above upper crustal rocks and Lower Triassic sediments within a stratigraphic context (e.g., the Axial Zone), (2) in diapiric structures inside Cretaceous sediments, or (3) at the base of a massive Rhaetian to lower Aptian sequence (e.g., Chaînons Béarnais) separated tectonically from mantle derived rocks or Cretaceous sediments. Most of the contacts between the Keuper sediments and the underlying and overlying units are tectonized. A Late Triassic transgression resulted in the development of a second carbonate platform (up to 1500 m thick and composed of alternations of

dolomites, limestones and marls) starting from Raethian time. Regionally, E-W trending subsiding basins started to develop from Tithonian onward (e.g., BRGM et al., 1974; James et al., 1996; Biteauet al., 2006; Jammes et al., 2009). In the Arzacq-Mauléon domain, a single large-scale depocenter developed north of the future Arzacq Basin. This led to a complete Neocomian sedimentary record whereas a major regression is recorded to the south in the future Mauléon Basin. This is mostly shown by the development of a major erosional unconformity with, locally, the formation of bauxites (Biteau and Canérot, 2007; Canérot, 2008 for a review). Barremian and Lower Aptian sediments record a general south directed transgression with the development of Annelides carbonates and Sainte Suzanne marls, which have been interpreted to be deposited in a shallow marine environment (Cassou, 1968). The depocenter was still localized in the Arzacq Basin where more than 1 km of Sainte Suzanne Marls have been accommodated (e.g., Biteau et al., 2006 and references therein). In the southern part of the domain, Barremian to Lower Aptian carbonates are either condensed within some meters or locally absent (e.g., Canérot, 2008). The top of the Lower Aptian carbonates represents the second important time marker that can be mapped throughout the basin. This marker corresponds to the base of the syn-rift sequence. As already shown by Ducasse and Velasque (1988), the Lower Cretaceous Fms. were already folded in the Mauléon Basin before being eroded and unconformably overlain by the Upper Aptian carbonates and marls. This is often interpreted to be linked to salt mobility (e.g., Ducasse and Vélasque, 1986a; Canérot, 1989; James and Canérot, 1999; Canérot et al., 2001; Biteau et al., 2006; Teixell et al., 2016) during earlier local rift events.

11.2.2.3 Syn-rift sequence (Upper Aptian to Lower Albian)

The late early Cretaceous carbonate facies record a major change in the tectonic, sedimentary and isostatic evolution of the Arzacq–Mauléon rift system. From that time onward, the Arzacq and Mauléon Basins started to be disconnected. The Arzacq Basin, located north of the Grand Rieu High, records an increased subsidence (Brunet, 1984); carbonate platforms developed on highs surrounded

by more subsiding basins were filled by marls and formation of salt diapirs (e.g., Biteau et al., 2006). In the Mauléon Basin, the Upper Aptian carbonates and marls (Urgonian facies) record a crustal extension phase associated with the formation of tilted blocks and extensional fault-bounded basins. Their base corresponds to an important unconformity that can be observed throughout the Mauléon Basin. The Albian carbonate system consists of carbonate platform and marl deposits (Esquevin et al., 1971; Canérot et al., 1990; Claude, 1990 and references therein). Upsection and to the south, the marls are progressively replaced by siliciclastic turbiditic beds, known in the literature as Flysch Noir, which are in turn replaced by more proximal conglomeratic facies (up to 900m of conglomerates mainly formed by Paleozoic metasediments derived from the uplift and erosion of the Axial Zone; Boirie and Souquet, 1982). The transition from the Albian-Cenomanian conglomerate fan deposits in the south to shales and turbidites in the north suggests the existence of a complete depositional sedimentary system ranging from the platform across the slope into a deep marine fan. However, the existence of blocks composed of Jurassic to Aptian limestone (the Chaînons Béarnais ridges), interpreted by Jammes et al. (2009) as extensional allochthons, seems to control the distribution of the conglomerate fan deposits and its transition with the deep marine facies. Although Flysch Noir deposits occur throughout the Mauléon Basin, they were not found further north across the Grand Rieu High (Serrano et al., 2006). The intrusive and extrusive alkaline rocks are time equivalent to the Flysch Noir and mainly occur in the northern part of the Mauléon Basin and above the Grand Rieu high (Serrano et al., 2006; Montignyet al., 1986).

11.2.2.4 Post-rift sequence (Cenomanian onward)

A new transgression over the Axial domain resulted in a progressive cessation of the siliciclastic input that was replaced by thick carbonate platform deposits. This event is recorded in the Mauléon Basin by a platform-driven sedimentation and the development of calciturbiditic and hemipelagic systems. The occurrence of these sediments over the Grand Rieu High (e.g., Razin, 1989; Claude, 1990;

Mulderet al., 2009) suggests that in Cenomanian time, the Grand Rieu High was not acting anymore as a high separating the Mauléon and the Arzacq Basins. A significant amount of post-rift subsidence over the Grand Rieu high is also shown by the thick Turonian succession in this domain (e.g., Serrano et al., 2006). In the Arzacq Basin, no major changes were recorded with the continuation of the carbonate-dominated sedimentation (Biteau et al., 2006).

11.2.3. Mantle-derived rock occurrences in the Mauléon Basin

In the Mauléon Basin a number of outcrops showing mantle-derived serpentinized peridotites can be found. In contrast to the mantle rocks exposed in the eastern Pyrenees (e.g. Lherz), the mantle rocks in the western Pyrenees are not associated with North Pyrenean Variscan Massifs (Saint Barthelemy, Trois Seigneurs, Milhas; Fabriès et al., 1998), nor with the Pyrenean fault zone. These bodies are commoly found at the base of east-west trending ridges composed of Upper Triassic to Lower Cretaceous sediments (Chaînons Béarnais ridges) and only locally register the HT-LP metamorphism conversely widely diffused in the eastern part of the chain (Fortane et al., 1986; Thiebaut et al., 1992; Lagabrielle et al., 2010). Such metamorphic event was characterized by a temperature peak barely exceeding 400°C (Clerc, 2012). Petrological and geothermobarometric studies of these ultramafic bodies show that they underwent a two-step exhumation with a first rise from 60 to 25 km depth, probably during late Hercinian times, followed by a further step from 25 km to shallower and cooler levels (Fabriès et al., 1998) from 117 to 109 Ma (Visers et al., 1997; Fabriès et al., 1998). In the past, various scenarios have been proposed for their emplacement: from purely tectonic mechanisms, such as solid intrusion of mantle rocks into sediments during strike-slips events (Vielzeuf and Kornprobst, 1984), to tectonosedimentary processes in which mantle rocks were exhumed during Variscan time (Mattauer and Choukroume, 1974, Fontane et al., 1986) and reworked in a middle Cretaceous flysch (Fontane et al., 1986). More recently, Lagabrielle and Bodinier (2008) and Jammes et al. (2009, 2010)

proposed that these rocks were exhumed during Albian time to the seafloor before they were reworked and deposited in the overlying younger sediments.

11. 3 THE CHAÎNONS BÉARNAIS

The Chaînons Béarnais form a series of E-W trending fold-thrust structures made of continuous late Triassic- to Lower Cretaceous sediments (Fig. 11.3). These ridges are floored by a south-verging Pyrenean faults tipically occurring within the Triassic evaporites (Teixell et al., 2016). The three ridges comprise from north to south: the Mail Arrouy, the Sarrance and the Layens. The base of the Mesozoic sequence is represented by the Triassic Keuper facies with shales, evaporites, breccias and ophites, followed by Jurassic to Aptian platform limestones and dolomites. These sediments represent the original pre-rift cover of the northern Iberian margin (Canerot and Delavaux, 1986, Canerot et al., 1978), now entirely detached from the Palaeozoic basement (Lagabrielle et al., 2010; Teixell et al., 2016). This sedimentary succession is intimately associated with peridotite (lherzolite) bodies and scarse Palaeozoic basement rocks, most of them located at the base of the Mesozoic sequence. As a whole, the Chaînons Béarnais represent remnants of the most distal part of the Iberian continental margin. Within this context, the three ridges are considered as extensional allochthons (Jammes et al. 2009; Lagabrielle et al., 2010; Masini et al., 2014; Teixell et al., 2016) over hyper-thinned continental crust as well as exhumed mantle.

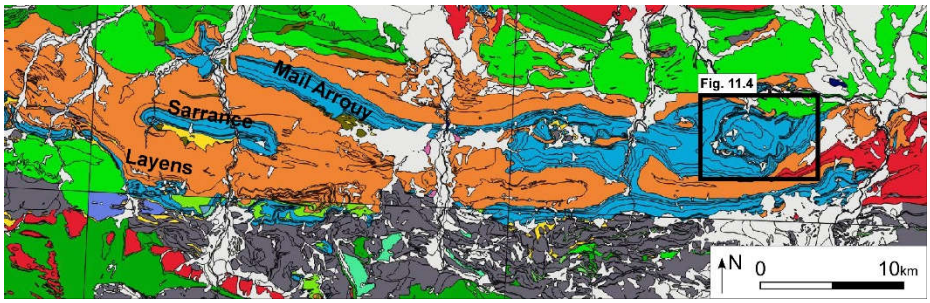

Fig. 11.3 - Simplified geological map of the Chaînons Béarnais cropping out in the easternmost part of the Mauléon basin (map modified after the BRGM 1/50,000

geological map of Oloron-Ste-Marie and Lourdes). The legend corresponds to that of Fig. 11.2a.

11.3.1 The study area

The focus of this study is the easternmost part of the Chaînons Béarnais ridges (Fig. 11.3), near the town of Lourdes (France). Here, it is not possible anymore to distinctly recognize the three ridges since Mail Arrouy and Sarrance are merged. The study area, geographically part of the Forêt de Tres Court, is characterized by a folded pre-rift stratigraphic succession (Keuper to Kimmeridgian). In the whole area, only one slice of basement rocks has been described in the northeastern part of the Foret des Tres Crouts, at the base of the Mesozoic succession. It is constituted of slaty schists dated as Ordovician and ascribed to be part of the Paleozoic basement (Casteras et al., 1970b; Fig. 11.4).

Because of the very scarse outcrop conditions and the lack of a detailed geological map (mapping was beyond the purpose of the Thesis), in the following the focus will be on the main features clearly related to fluid circulation that affected the study area. For a more detailed description of the stratigraphic succession, the reader can refer to *Notices Explicative de la Carte Géologique au 1/50.000 Feuille Lourdes* (Casteras et al. 1970b). In this section, some interesting "windows" where fluid-related, post-depositional modifications affected the host rocks are well recognizable will be described. In particular, the most interesting fluid-related products were found associated to the lithostratigraphic units: Ophites, I_1, I_{2-3}, J_{7-3} and J_8 (Casteras et al. 1970b) that, from now on, will be defined as Sedimentary Breccia Unit (Ophites, I_1 and I_{3-2}), Black Dolomites Unit (J_{7-3}) and Black Limestones Unit (J_8). Within the latter, Casteras et al. (1970b) distinguished one sub-unit (J_{8m}), which refers to not better defined "metamorphic limestones" possibly making part of the Hercynian basement.

For each Unit, a stratigraphic and petrographic description will be given as well as a first order interpretation based also on analytical data (stable isotopes and

fluid inclusions), when available. To conclude, an overall summary of the evolution of the area will be proposed.

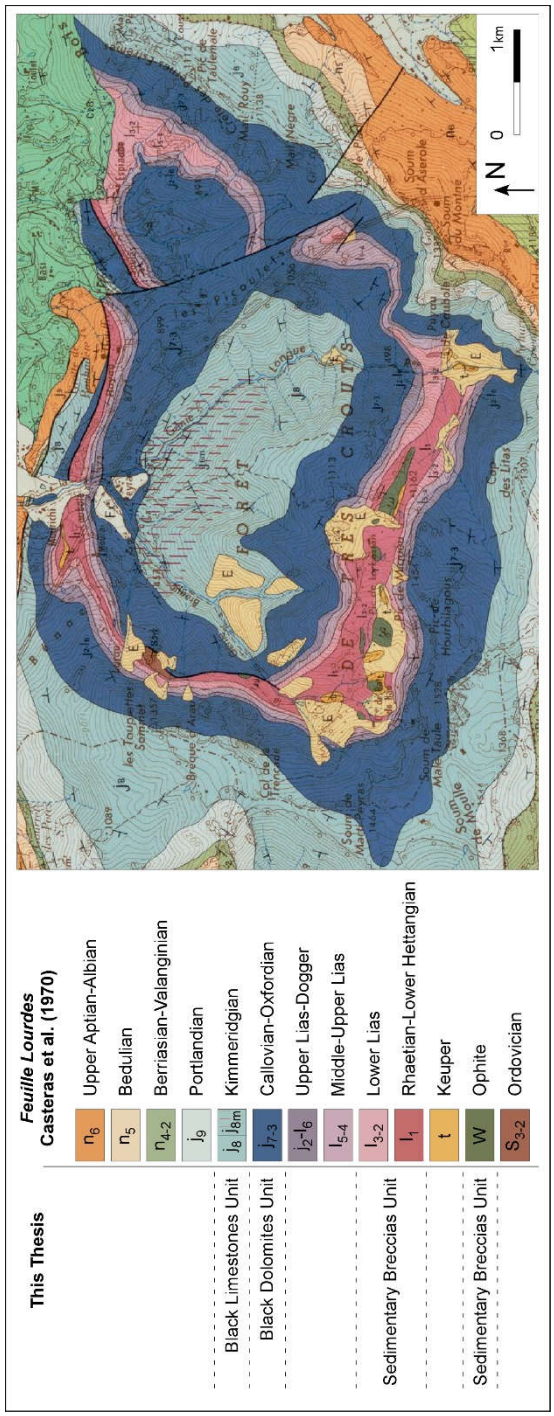

Fig. 11.4 - Detail of the geological map of the *Feuille Lourdes* BRGM 1/50.000 showing the study area which is geographically part of the Foret des Tres Crouts.

THE RESULTS

12. Black Dolomites Unit

(Callovian-Oxfordian)

12.1 STRATIGRAPHY AND PETROGRAPHY

This lithostratigraphic unit is composed of coarse to very coarse crystalline, pyrite-rich, black dolostones that never show a well-defined bedding and can reach, in the *Feuille Lourdes* (Castéras et al., 1970), a maximun thickness of 400m. On the weathered surface they show a karstic appearance and locally alternate with dolomitic limestones. These dolomites were not dated by their fossil content but only relatively to the over- and underlying sediments. So that, they were assigned to the Callovian-Oxfordian (Castéras et al., 1970).

In the study area, the Black Dolomites Unit is characterized by a coarsely crystalline, subhedral to euhedral, replacement dolomite whose crystals can reach 300µm in size. Under CL it is not luminescent. These dolostones show different degrees of disruption of the rock. Where it is less deformed, the Black Dolomites Unit is affected by randomly oriented, few µm wide, fracture sets (only visible by CL investigation) filled by dolomite cement, bright orange under cathodoluminescence (Fig. 12.1). These micro-fissures usually occur along the crystal contacts even if they also cut through them. Locally, some open spaces occur. They are cemented by dolomite whose crystals, 100-200 µm large, show a bright orange, very poorly zoned CL luminescence (Fig. 12.1). By their features, these portions of the rock mass can be considered as incipient crackle breccias (*sensu* Morrow, 1982).

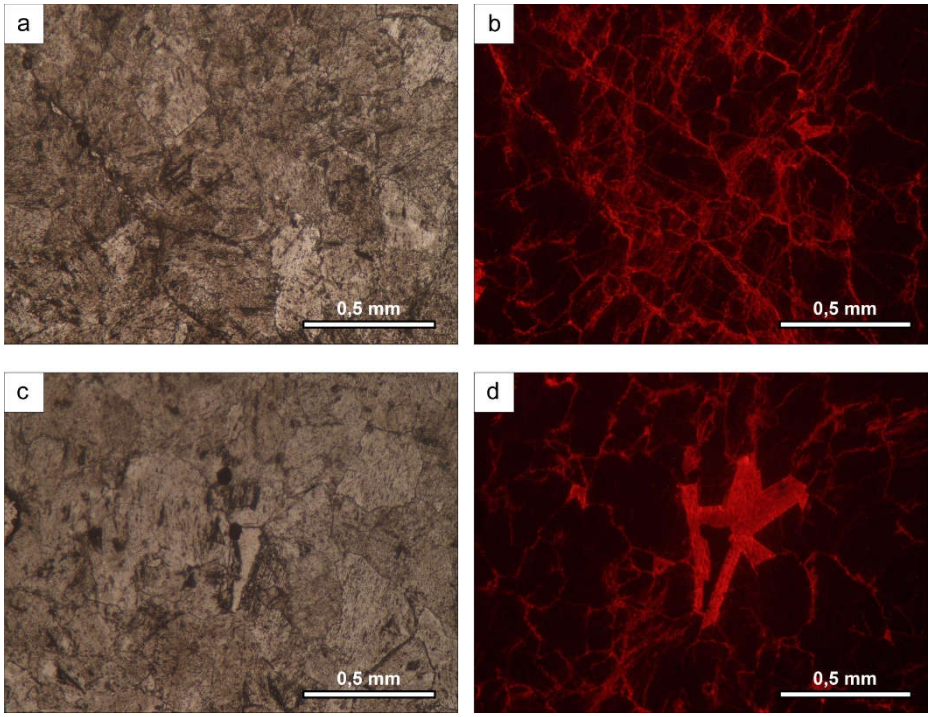

Fig. 12.1 - Crackle breccias: (a) TL and (b) CL images highlighting the diffuse fissure sets developed along crystal contacts and within them, cemented by orange luminescing dolomite. The host rock (Black Dolomites Unit) is dull in CL. (c) TL and (d) CL images showing cavities within the host rock filled with orange, poorly zoned, dolomite cement.

Where the deformation is stronger, mosaic to rubble breccias (*sensu* Morrow, 1982) affect the Black Dolomites Unit. These breccias were never observed in place but only as clasts within the Genie Longue torrent. Nonetheless, they are clearly constituted by the previously described black dolostones. Indeed, they are made of millimeter- to some centimeter- large, coarsely crystalline dolomite clasts, angular in shape and dull in CL. Within some clasts, ooids are still recognizable (Fig. 12.2). The clasts themselves show different degree of internal deformation: from almost preserved dolostones to strongly fractured and brecciated clasts cemented by bright orange luminescing dolomite.

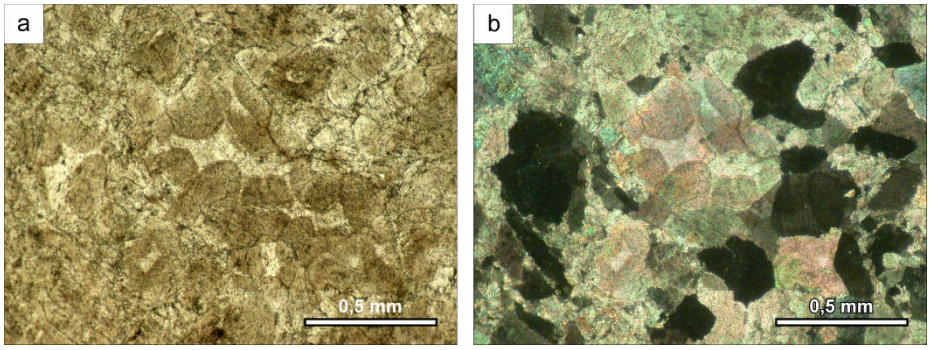

Fig. 12.2 - Locally, within the clasts of the mosaic-rubble breccias, ooids are still recognizable despite the diffuse replacement dolomitization.

The mosaic to rubble breccias (Fig. 12.3) are cemented by two generations of saddle dolomite. The first, almost isopachous and up to 500 µm thick, shows CL zoning from bright to dark orange. Commonly, in between the clasts and the first dolomite cement, a geopetally filling, dolomitized fine-grained sediment occurs. The second cement, finally, is still dolomite and is characterized by a bright, poorly zoned, orange luminescence (Fig. 12.3 b-f).

In few cases, a third cement made of dark orange/brown luminescing calcite occurs (Fig. 12.3 g-h). It is not always easy to define the timing of precipitation of this calcite cement since it occurs both between the two dolomite cements or before the first one. In any case, it occurs as calcite spar with crystals size ranging between tens to hundreds of microns. Locally, some fractures are filled with the first dolomite cement fringing the cavitiy walls followed by a yellow to dark brown zoned calcite cement.

The whole breccias (e.g. clasts and cements) are then crosscut by several randomly oriented dolomite veins that are recognizable only by CL observation. They occur as tens to hundreds microns wide fractures filled with an almost homogeneous orange dolomite cement. Lastly, tens of microns wide calcite veins, with a dark brown to dull luminescence in CL, are present.

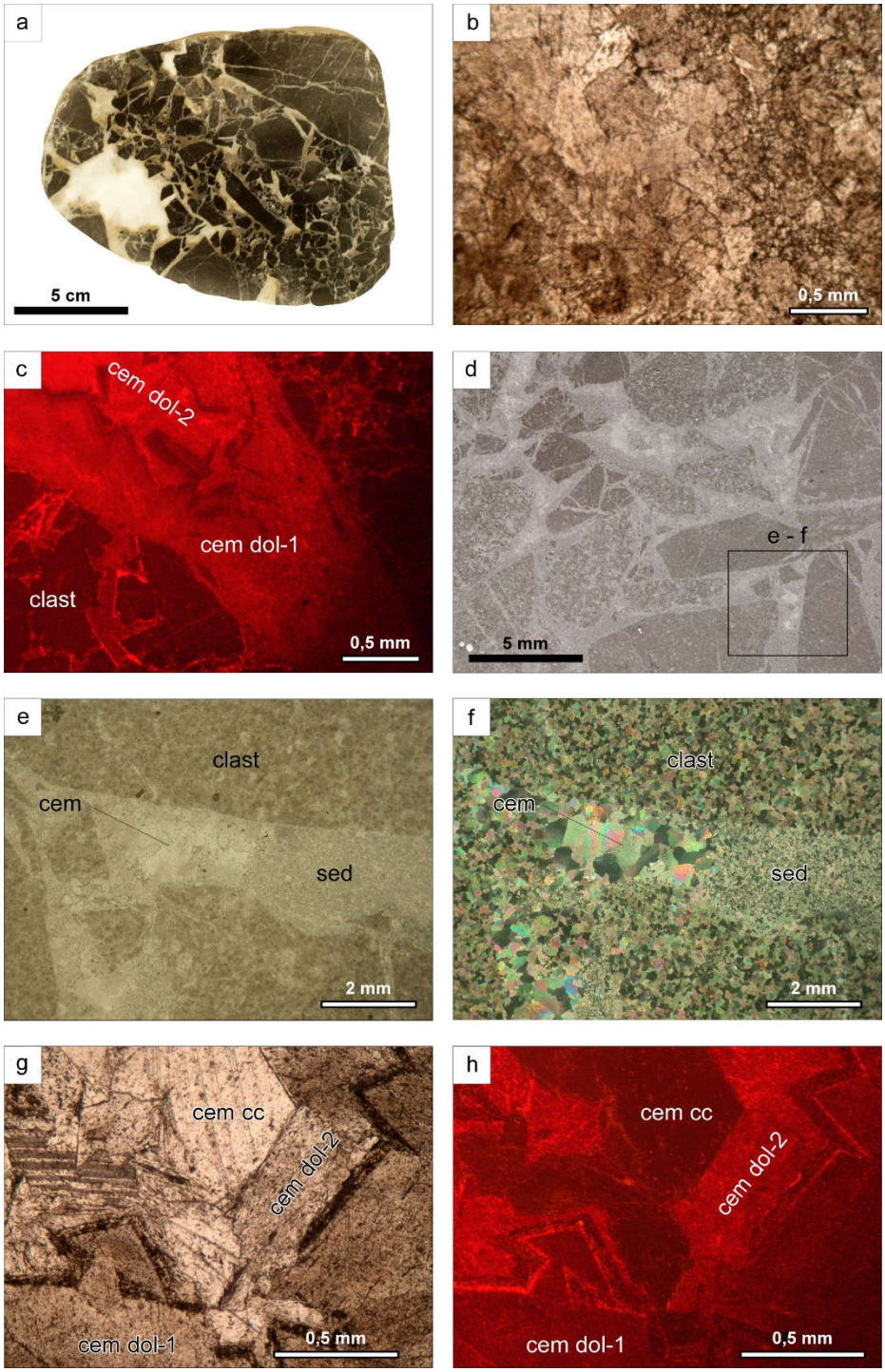

Fig. 12.3 - Mosaic to rubble breccias. (a) Hand specimens. (b) TL and (c) CL images showing the two generations of dolomite cements of the breccias. The clasts are dull

in CL. (d) TL photomicrograph showing the relationship among the clasts, the internal dolomitized sediment and the dolomite cement. e) TL and (f) crossed polarizers details of (d). (g) TL and (h) CL details of the cements. The dark orange/brownish calcite cement, as described in the text, occurs in different "stratigraphic" positions.

12.2 STABLE ISOTOPE GEOCHEMISTRY

12.2.1 O and C isotopes

Oxygen and carbon isotope analyses have been performed on the host Black Dolomites Unit and on dolomite and calcite cements of breccias (Fig. 12.4, ANNEX H). The host dolomite shows slightly positive $\delta^{13}C$ values (2.27‰ to 3.29‰ VPDB) and negative $\delta^{18}O$ ones (-3.37‰ to -7.79‰ VPDB). The dolomite cement has slightly positive $\delta^{13}C$ values (1.38‰ to 2.16‰ VPDB) and quite negative $\delta^{18}O$ (-8.60‰ to -12.10‰ VPDB).

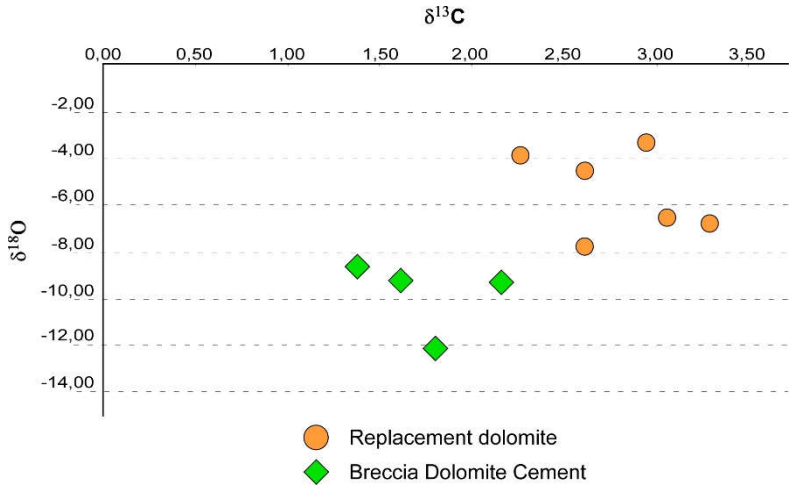

Fig. 12.4 - Stable isotope data: $\delta^{18}O$ versus $\delta^{13}C$ cross plot for dolomite minerals of Black Dolomites Unit. Values relative to VPDB standard.

12.3 FIRST ORDER INTERPRETATION

12.3.1 Dolomite

One main style of dolomitization was detected within the Black Dolomites Unit. The rock mass was widely dolomitized leading to the present-day coarse crystalline texture (Fig. 12.1). Such recrystallization, and the related increase of crystal size, asks for the presence of (high-T?) fluids as driving process. This hypothesis may also be supported by the negative O isotopes values (Fig. 12.5).

12.3.2 Breccias

After the almost complete recrystallization, the Black Dolomites Unit underwent modifications related to the emplacement of overpressured carbonate-rich fluids, which gave rise to different textures. Where the circulation was less intense it generated μm large, randomly oriented fractures along the dolomite crystals contacts and/or within the crystals themselves (crackle breccias; Fig. 12.1). Such a pervasive infiltration could have been facilitated by inter-crystalline porosity related to the previous pervasive dolomitizing event. Conversely, where the flow was more concentrated and/or overpressured, a higher degree of disruption occurred by hydraulic deformation that resulted in the formation of mosaic and rubble breccias (Fig. 12.3). The occurrence of sediment geopetally filling the cavities (Fig. 12.3 d-f) of the breccias suggests the hydrofracturation took place close to the seafloor. Overpressured fluids generated the open framework texture of the breccias, which was in close vicinity and connected to the water-sediment interface that allowed the infiltration of sediment. The fact that the internal sediment is dolomitized suggests the infiltration occurred concomitantly with the circulation of fluids (e.g., Barale et al., 2016).

12.3.3 Dolomite and calcite cements

Since the dolomite cements within the inter- and intra-crystalline fissures of the host rock and the first cement of the mosaic-rubble breccias show similar CL features (Fig. 12.1 a-d and Fig. 12.3 b-c), it allows to consider the two cements as related to the same fluid flow event. The petrographic features and the quite

well defined zoning of the first dolomite cement (type 1) suggest that the precipitation occurred in open spaces and in static conditions. New fluid pulsations generated the second dolomite cement (type 2) as well as the calcite one (Fig. 12.3 g-h). Even if the timing of precipitation is not obvious, it documents a change in the chemistry of the fluids. Possibly, as the calcite cement has been found both before and after the first dolomite cement, it may be assumed a multi-stage occurrence for the $CaCO_3$-rich fluid circulation.

12.3.4 Veins

Veins are not abundant within the Black Dolomites Unit and seem to be confined to those portions of the host rock that experienced the more intense fluid circulation. Both dolomite and calcite veins were found cutting through the breccias implying the fracturing stage and subsequent circulation of fluids took place after the formation of the breccias themselves.

13. Black Limestones Unit

(Kimmeridgian)

13.1 INTRODUCTION

The Black Limestones Unit crops out in the central part of the study area and shows an overall thickness of 200-300 meters (Casteras et al., 1970b). It is made of fine-grained, well-bedded limestones alternated with black to reddish marly limestones. Locally it is also dolomitized. The fossil content includes: serpulides, *Exogyra virgule*, *Pseudocyclammina virgulina*, *Haplophragmium*, *Pseudocyclammina* gr. *jaccardi-personata*. *Valvulinella jurassica* is common throughout the Unit and allowed Casteras et al. (1970b) to date this lithostratigraphic unit to the Kimmeridgian. These limestones, on the whole, are microsparitic, dark orange in CL and cut by dolomite and calcite veins hundreds of μm large (Fig. 13.1 a-b). Bivalve shells, echinoderm and gastropod fragments, oncoids and cortoids are preserved even if recrystallized. Some bioclasts are coated by pyrite. Locally, the Black Limestones Unit is characterized by the occurrence of several, up to 300 μm long, "sandwiches" made of fibrous calcite growing perpendicularly to and encasing fibrous aggregates of Mg-rich alumino-silicates (Fig. 13.1 c-d). The first results of Raman spectroscopy investigations revealed that such silicates are hydrated and characterized by spectra similar to that of talc and chlorite.

As shown in the *Feuille Lourdes* (Casteras et al., 1970b), the Black Limestones Unit in the study area is supposed to be deformed by a main syncline structure. In its inner part (Fig. 11.4), "metamorphosed limestones" were reported by Casteras et al. (1970b), which represent the main focus of the following description. Indeed, for about 2 km from the dam of Peyras towards the top of the Genie Longue torrent, the Black Limestones Unit has been described as

recrystallized white, scapolite-rich marbles that were also the target of exploitation (two abandoned quarries are present in the area). With the present work, it will be clarified that the white marbles represent only one of the many different post-depositional modifications experienced by the Black Limestones Unit.

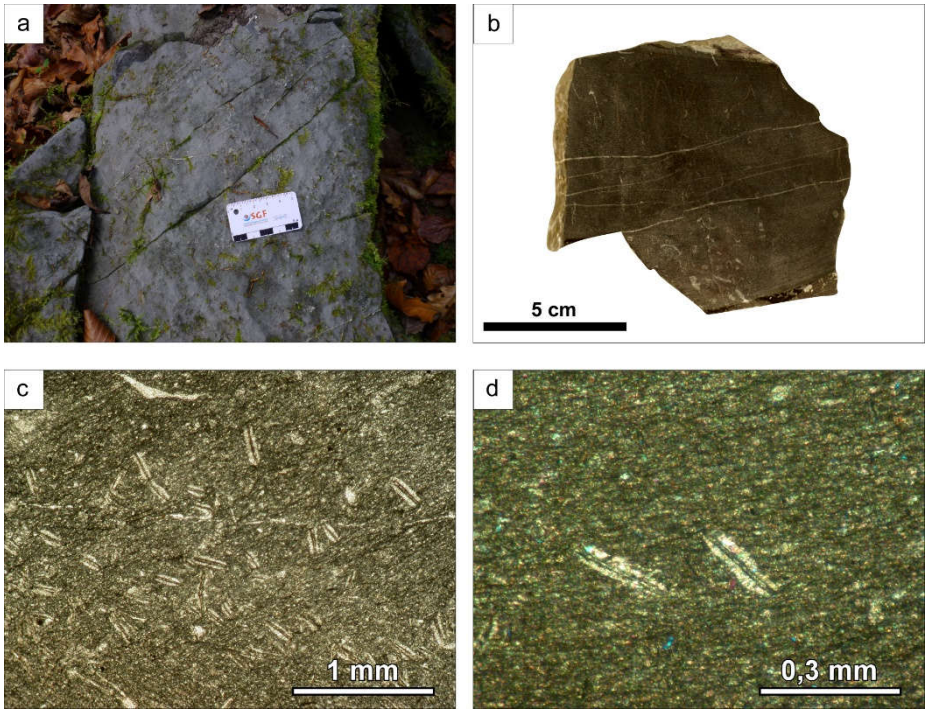

Fig. 13.1 - Black Limestones Unit: (a) Field occurrence and (b) hand specimen. (c) TL and (d) crossed polarizers images of the "sandwiches" within the limestones. The inner part, made of Mg-rich alumo-silicates, is encased within perpendicularly growing, fibrous calcite.

Two are the main sites where it was possible to investigate the post-depositional modification affecting the Black Limestones Unit within the "metamorphosed area". The first, in its northern part, comprises two quarries located along the Genie Longue river (Quarries area). The second, south of the quarries and developing only for some tens of meters along the riverbed, is characterized by new and different types of rocks (Riverbed area).

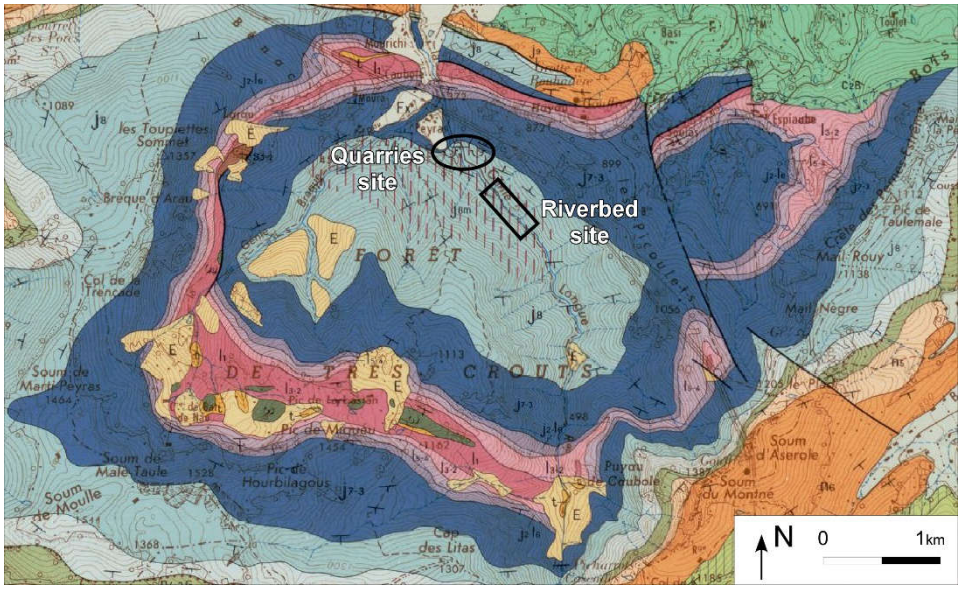

Fig. 13.2 - Localization of the investigated sites in the Black Limestones Unit: the Quarries site and the Riverbed site. The geological map and its legend are the same of Fig. 11.5.

13.2 THE QUARRIES AREA

13.2.1 Stratigraphy and petrography

Here, the highest variety of rock types occur, even if the vegetation always hides the transition from one to the others. Entering the first quarry, from the left to the right side, a section from slightly deformed and altered limestones towards strongly deformed rocks is observable. The main product of such deformation/alteration is represented by hydrofracturing and sedimentary breccias. More precisely, the former are composed of at least 3 different types of breccias, which differ each other because of the composition of the clasts and the cements. 1) The first type is made of clasts ranging in size from some centimeters to some decimeters (Fig. 13.3 a-b), strongly angular in shape and constituted by microsparitic limestones. The clasts are cemented by very coarse, sparry calcite crystals that can reach some centimeters in size (Fig. 13.3 c-d). Locally, a dolomite rim, zoned in CL, fringes the clasts and is always coupled

with a hundreds μm thick rim of dolomitized fine-grained sediment. Both the clasts and the calcite cement show a homogeneous orange CL luminescence.

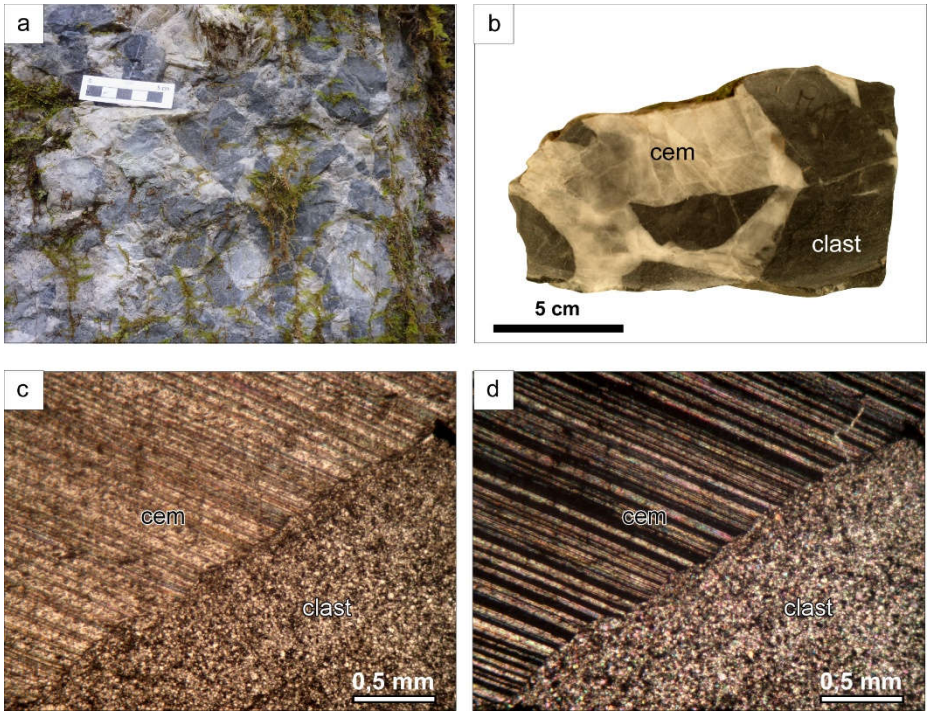

Fig. 13.3 - Breccia type 1. (a) Field occurrence and (b) hand specimen. The clasts are made of limestone whereas the cement is made of sparry calcite. (c) TL and (d) crossed polarizers images of the clasts and the calcite cement.

2) The second type of breccias (Fig. 13.4 a-c), occurring only few meters far from the previous one, is made of already dolomitized clasts that by their petrographic and cathodoluminescence features can be referred to the Black Dolomites Unit. The clasts, angular in shape and up to 5 cm in size, are cemented by a fine-grained (few tens of microns), homogeneous orange/brownish luminescing, calcite. Within the clasts, some cavities are cemented by type 1 dolomite already described in the Black Dolomite Unit. Some detrital dolomite crystals (200 μm in size; Fig. 13.4 d), still encased within the calcite cements, show a few μm large, bright orange, dolomite overgrowth, evidenced only by CL investigations. Within the calcite cement, some large

detrital crystals (2,5 mm large) made of a former dolomite cement are also present.

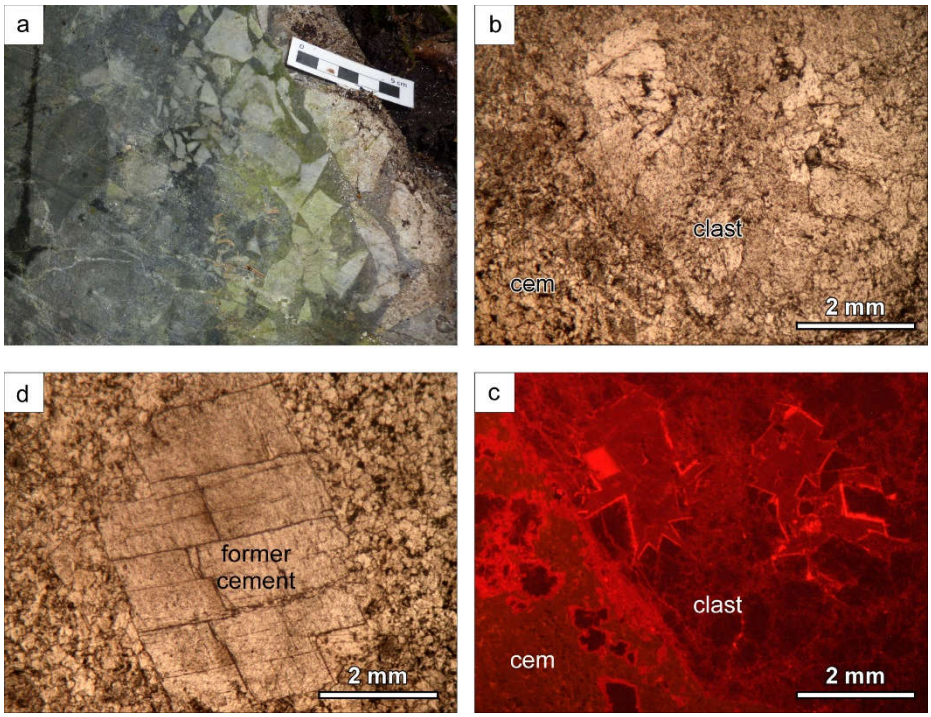

Fig. 13.4 - Breccia type 2. (a) Field image. (b) TL and (c) CL images of non-luminescing dolomite clasts of Black Dolomites Unit within the dark orange calcite cement. In the latter, some mm-large crystals of a former dolomite cement are present (d).

Locally, type 2 breccia clasts are characterized by a stronger internal deformation giving rise to poorly sorted, brecciated textures composed of hundreds of μm large, almost rounded clasts within a bright orange luminescing dolomite cement (Fig. 13.5 a-b-c-d). These portions of the rock are also interested by different, diachronous, vein sets cemented by dolomite and calcite. The former is characterized by a poorly zoned orange luminescence whereas the latter shows well defined, yellow to brownish, concentric zoning (Fig. 13.5 e-f).

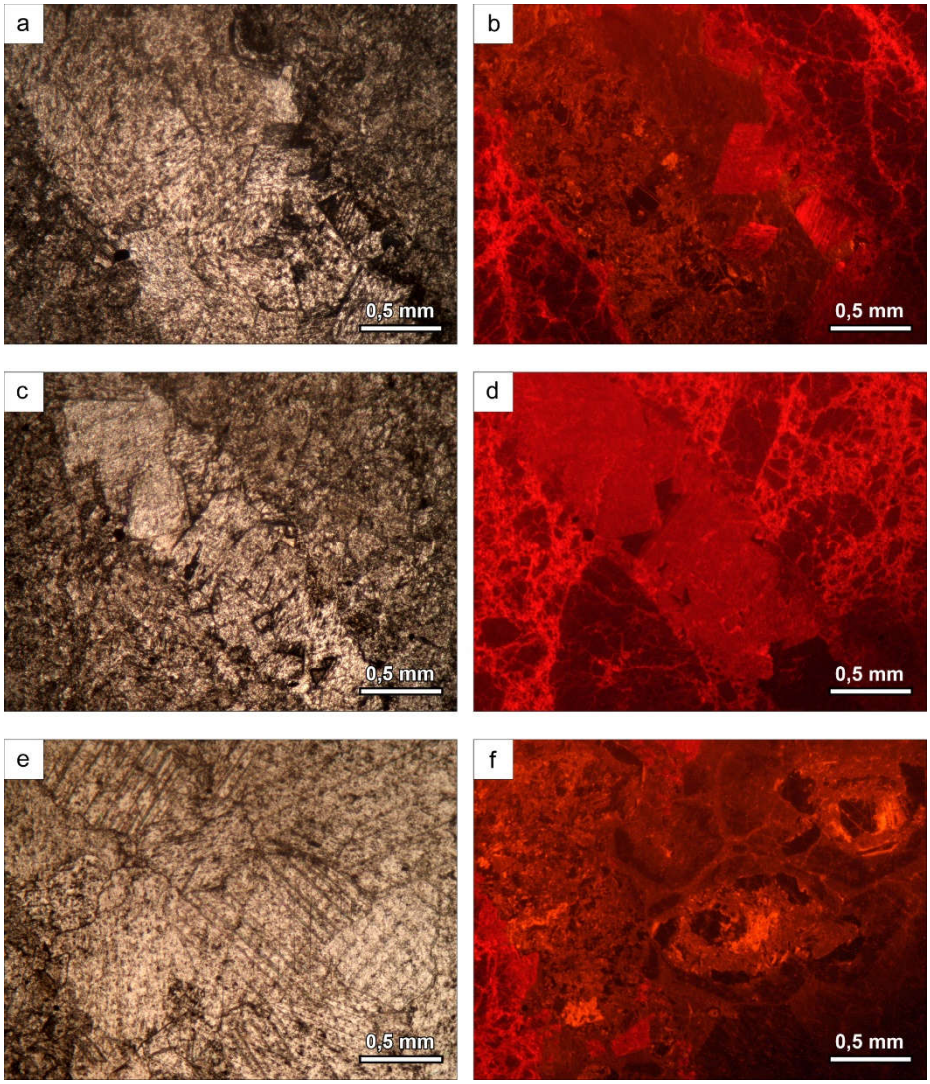

Fig. 13.5 - Detail breccia type 2. (a-c) TL and (b-d) CL images of poorly sorted breccias crosscut by fractures filled with dolomite and calcite cements. (e) TL and (f) CL details of the orange to brown zoning of the calcite cement.

3) The third type is a polimict breccia made of larger clasts, cm to dm in size, bluish on the weathered surface composed of micro-crystalline limestones, and smaller, mm to cm in size, ones made of fine grained dolostones (Fig. 13.6 a-b). The clasts are within a complex cement composed of i) coarse grained dolomite

crystals (up to 500 µm) with dark orange, poorly zoned, luminescence, and ii) yellowish to dark orange luminescing sparry calcite (300 µm; Fig. 13.6 c-d).

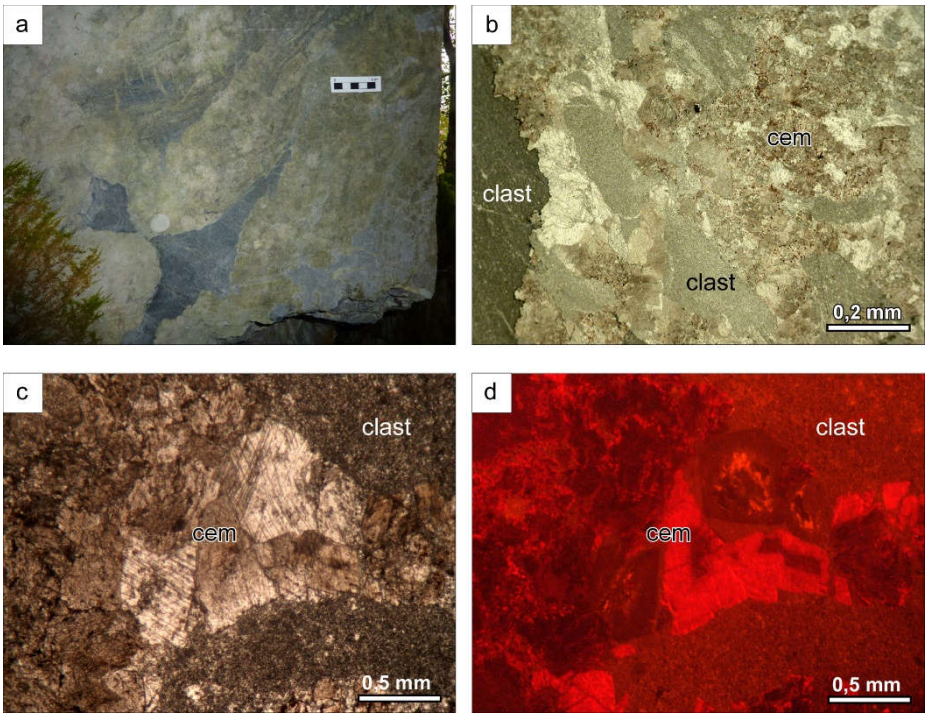

Fig. 13.6 - Breccia type 3. (a) Field image. (b), (c) TL and (d) CL images of the polimict clasts (limestones and dolostones) of the breccia cemented by dolomite and calcite.

About ten meters from the three types of hydrofracturing breccias, the second main type of breccia crops out. It is a carbonate sedimentary breccia presently slightly to strongly deformed by compaction and shearing (Fig. 13.7 a-b). The mm-large clasts, made of crystalline dolomite (with veins that stop at the edge of the clasts) within a micritic matrix, show stylolitic contacts due to compaction and/or tectonic deformation (Fig. 13.7 c-d-e-f). Pyrite, often oxidized, is also quite abundant. Both the clasts and matrix are orange in CL with the clasts slightly brighter than the matrix. In the latter, some detrital dolomite crystals occur surrounded by an overgrowth marked by CL orange luminescence. Lastly, cm-large calcite and dolomite veins cut through the whole rock mass.

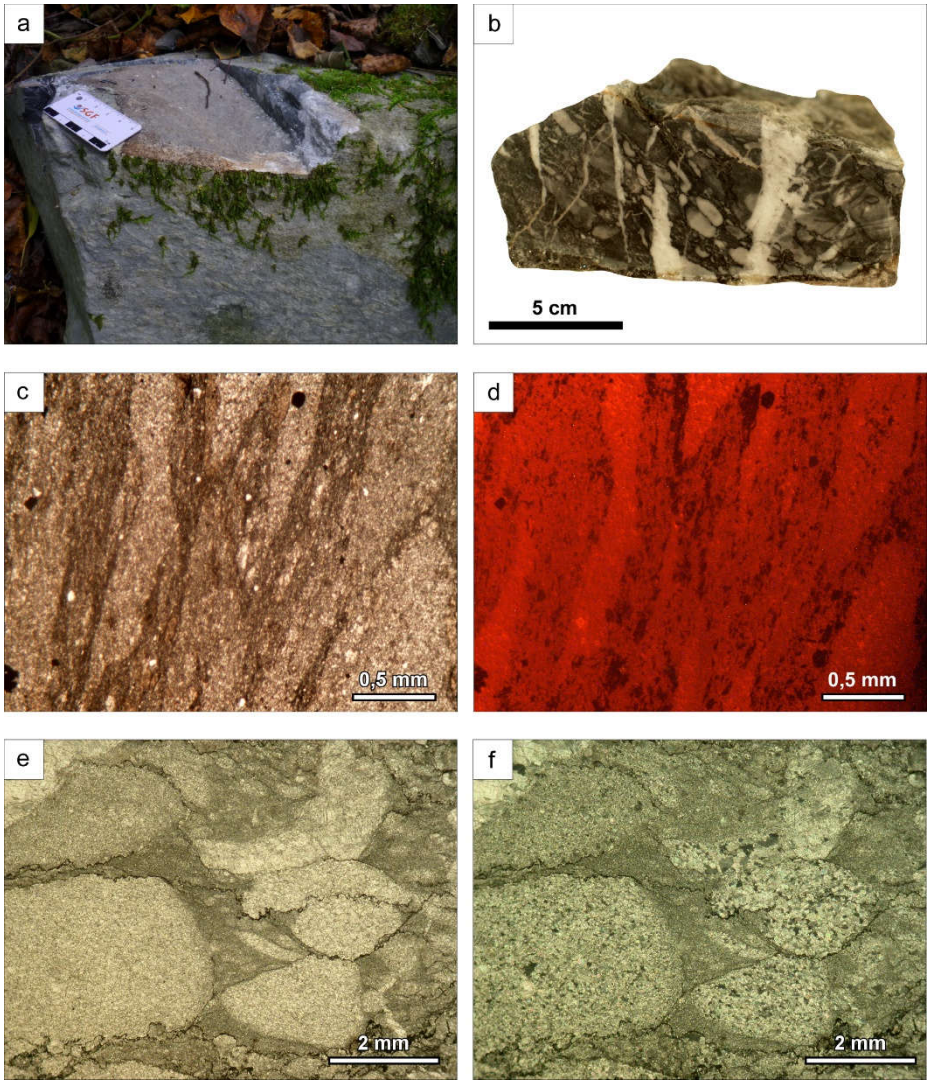

Fig. 13.7 - Deformed sedimentary breccia. (a) Field image and (b) hand specimen. In (b) is evident that carbonate veins crosscut the whole breccia. (c) TL and (d) CL images showing that deformation (compaction and shearing) affected the sedimentary breccia. The clasts are brighter in CL. (e) TL and (f) crossed polarizers images showing stylolites at the clasts boundaries and within the matrix.

13.3 ISOTOPE GEOCHEMISTRY AND FLUID INCLUSION DATA

13.3.1 O and C isotopes

Oxygen and carbon isotope analyses have been performed on the host Black Limestones Unit and on calcite cements of type 1 hydrofracturing breccias (Fig. 13.8 and ANNEX H). The host limestones show slightly positive $\delta^{13}C$ values between +0.5 ‰ to +3 ‰ and negative $\delta^{18}O$ ranging from 0 ‰ to -8 ‰. The calcite cement has $\delta^{13}C$ values in the range -2 ‰ to +2 ‰ and quite to strongly negative $\delta^{18}O$ (-6 ‰ to -14 ‰).

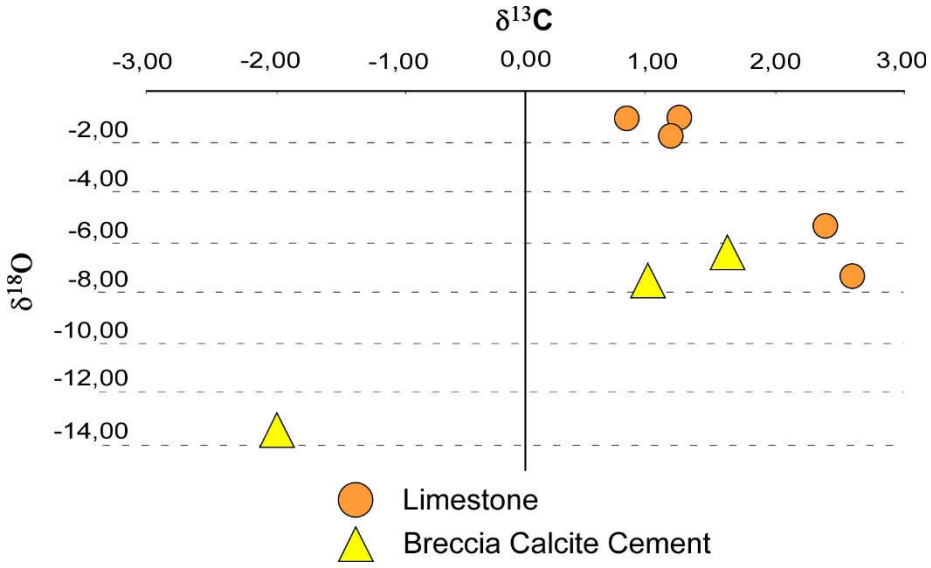

Fig. 13.8 - Stable isotope data: $\delta^{18}O$ versus $\delta^{13}C$ cross plot for calcite clasts and cements from the Quarry sites. Values relative to VPDB standard.

13.3.2 Fluid inclusion microthermometry

More than 40 primary fluid inclusions were measured on calcite and dolomite cements of the hydrofracturing breccias type 1 and 3, respectively (Fig. 13.8 and ANNEX H). As shown in Fig. 13.9, homogenization temperatures of dolomite cement range from 152°C to 203°C with the highest frequency between 180°C

and 190°C. The calcite cement shows higher values from 227°C to 249°C with the highest frequency between 240°C and 250°C.

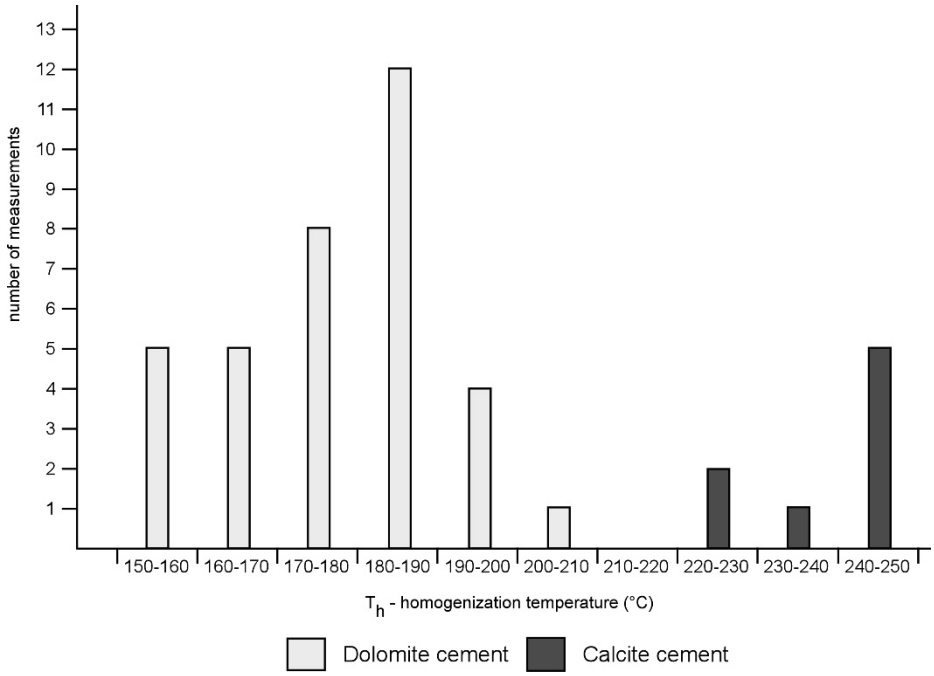

Fig. 13.9 - Histogram of the homogenization temperatures for calcite and dolomite cements of breccia types 1 and 3 respectively.

13.4 FIRST ORDER INTERPRETATION

13.4.1 Breccias

Two different kinds of breccias can be distinguished in the Quarries area: i) hydrofracturing breccias and ii) sedimentary breccias. The first type is the more complex because it is composed of further three different types of breccias based on the composition of the clasts and the cements (Fig. 13.3, 13.4 and 13.6). Nonetheless, the forming process seems to be the same. Indeed, the shape of the clasts and their spatial organization within the cements ask for overpressured fluids disrupting the former host rocks. The fact that the clasts are not made of the only Black Limestones Unit but also of the stratigraphically underlying

Black Dolomites Unit, suggests that a conspicuous vertical displacement through the sedimentary column took place.

The contact between the hydraulic and sedimentary breccias was never observed. The sedimentary breccias (Fig.13.6), nonetheless, on the basis of their deformed texture could represent a shear zone/tectonic contact.

In any case, the two main types of breccias found in the Quarries area are younger in age than both the encasing Black Limestones and Black Dolomites Units as demonstrated by the composition of the clasts of breccia type 2 and 3. Hence, a post-Kimmeridgian age is suggested.

13.4.2 Calcite and dolomite cements

The different cements of the hydrofracturing breccias were precipitated in open spaces and in static conditions. Finding of breccias cemented by chemically different mineral phases, in close vicinity one to the others, imply a change in the physico-chemical properties of the fluids even if always in a carbonate-dominated system. The dolomite cement of breccia type 3 (Fig.13.6) as well as the calcite cement of breccia type 1, shows homogenization temperature anomalously high also considering that the overall thickness of the post-Kimmeridgian succession cannot supply for such values only by sedimentary overburden. Furthermore, the negative O isotopic values (Fig. 13.8) support the idea that the cements precipitated from hydrothermal fluids.

13.4.3 Veins

Veins are not widespread in the Quarries area and mainly affect the sedimentary breccias. The definition of the exact timing of their formation is so far not clear.

13.5 THE RIVERBED SITE

13.5.1 Stratigraphy and petrography

In the northern part of the study area within the talweg of the Genie Longue torrent and only for some tens of meters, strongly recrystallized carbonate rocks

crop out. In the *Feuille Lourdes* (Castéras et al., 1970), they were included within the sub-unit "metamorphosed limestones". In the few spots where they were observed, they look discordant, by variable angles, with respect the surrounding lithotypes (Black Limestones Unit and their modifications). The stratigraphic or tectonic contact with these sediments has never been observed.

These rocks show a regular and planar foliation where dm- to m-large whitish and bluish layers alternate each other (Fig. 13.10 a). Whitish layers are composed of finely crystalline dolomite with some scattered authigenic quartz crystals (up to 400 μm large) that poikilotopikally includes the carbonate matrix. Sulphide and opaque minerals also occur (from few μm to tens of μm). Fine grained quartz (detrital?) is also present between the dolomite crystals. Under cathodoluminescence and excluding the non-luminescent quartz, the rock appears with a homogeneous orange colour. The bluish layers are still made of fine grained dolomite in which coarser stretched and parallel to the bedding, policrystalline porphyroclasts made of dolomite crystals, up to 500 μm large, exist (Fig. 13.10 b-c-d). Quartz is still present both in the porphyroclasts and in the matrix (Fig. 13.10 g-h). Some relicts of possible former scapolite (Casteras et al., 1970b), 500 μm large and presently completely replaced by fine grained aggregates of K-rich alumo-silicates, occur (Fig. 13.10 e-f). Such porphyroblasts include poikilotopically the carbonate matrix.

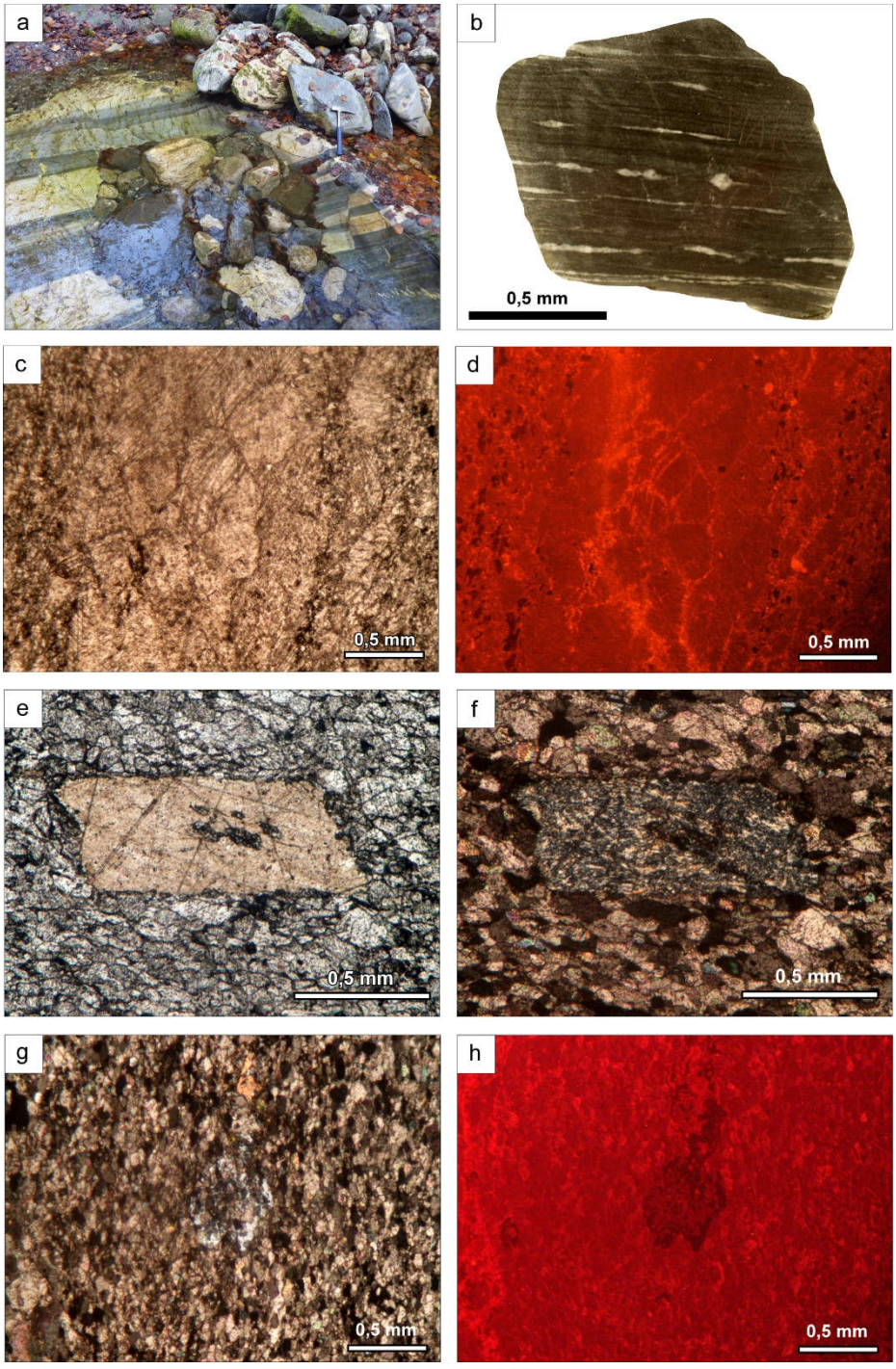

Fig. 13.10 - (a) Field image and (b) hand specimen of carbonate mylonites. In the bluish layers porphyroclasts of the former coarse-grained rock are preserved. (c) TL and (d) CL details of the porphyroclasts. (e) TL and (f) crossed polarizers images of

porphyroblasts of former scapolite presently replaced by assemblages of K-rich alumo-silicates. (g) Crossed polarizers and (h) CL images of authigenic quartz, poikilotopikally including the carbonate matrix.

Out of the riverbed and in an area comprised between the Genie Longue and Braque torrents before their confluence, few spotty occurrences of white, coarse crystalline dolomite marbles were found. The crystals, up to 500 μm, are characterized by a dark orange CL luminescence (Fig. 13.11). Brighter luminescing zones correspond to crystal contact. On the whole, the rock is made of almost equant crystals with sutured boundaries; only locally, planar boundaries occur. Where observed, the marbles are massive and do not show a well-defined bedding nor a foliation.

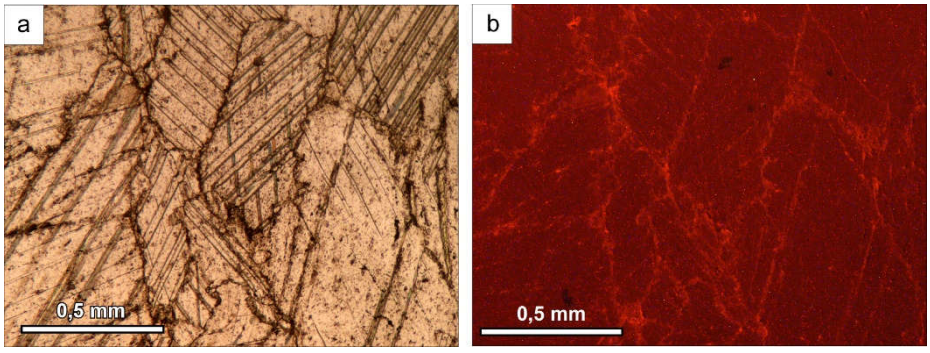

Fig. 13.11 - (a) TL and (b) CL images of dolomite marbles. Note the coarse grained textures and the sutured contact among the crystals.

13.6 STABLE ISOTOPE GEOCHEMISTRY

13.6.1 O and C isotopes

Oxygen and carbon isotope analyses were performed on mylonites and marbles (Fig. 13.12 and ANNEX H). The only available data on marbles show positive $\delta^{13}C$ values (about +3 ‰) and negative $\delta^{18}O$ (almost -7 ‰). The pale bands of the mylonite have slightly positive $\delta^{13}C$ values (1.67‰) and slightly negative

$\delta^{18}O$ (-1.11‰). The bluish bands show always a slightly positive $\delta^{13}C$ values while $\delta^{18}O$ values are more depleted (about -7 ‰).

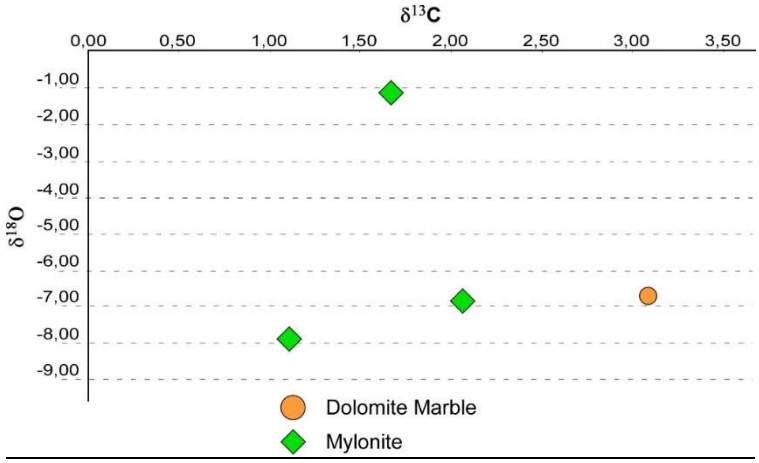

Fig. 13.12 - Stable isotope data: $\delta^{18}O$ versus $\delta^{13}C$ cross plot for dolomite marbles and mylonites. Values relative to VPDB standard.

13.7 FIRST ORDER INTERPRETATION

13.7.1 Marbles and Carbonate mylonites

The regular and planar foliation, the fine-grained matrix with coarser grained porphyroclasts (percentage of matrix compared to porphyroclasts of 50-90%) and the monomineralic composition of the layered rocks found within the Genie Longue torrent, allow to define these rocks as carbonate mylonites (Burlini and Kunze, 2000; Sibson, 1977; Scholz, 1988; Schmid and Handy, 1991; Fig. 13.9). The present-day, fine-grained texture is suggested to derive from a more coarse-grained parent rock in response to intra-crystalline deformation and recrystallization. Finding of marbles (Fig. 13.11) in the close vicinity of the mylonites may support such hypothesis. The porphyroclasts could then represent resistant relics of a more coarse-grained original fabric of former rock. The presence of quartz and former scapolite (Fig. 13.10 e-f-g-h) that poikilotopikally grew over the carbonate matrix suggests the involvement of fluids after the "mylonitization" process that affected the precursor rock.

14. Sedimentary Breccias Unit

14.1 STRATIGRAPHY AND PETROGRAPHY

Based on the *Feuille Lourdes* (Casteras et al., 1970b), along the southern ridge of the study area as well as its northeastern part, evaporites, ophites and sedimentary breccias widely crop out. The ophites and the evaporites are assigned to the Keuper, whereas the breccias are described by the authors as Rhaetian to Sinemurian in age.

In this area three types of sedimentary breccias have benn distinguished: ophitic monomictic, polimictic and carbonate monomictic. The Ophite unit, conversely to what has been proposed in the *Feuille Lourdes* (Casteras et al., 1970b), occurs as monomict clast-supported sedimentary breccia, with an overall thickness of about 20 meters. It is constituted exclusively of almost rounded ophitic clasts ranging in size from some centimeters to around a meter (Fig. 14.1 a). Laterally, the ophitic breccia passes to clast- to matrix-supported, polimict sedimentary breccias mainly composed of carbonate clasts, and subordinately ophitic clasts. On average, the clasts are mm- to cm-large, even if some larger, mainly ophitic clasts can be up to some decimeter (Fig. 14.1 b and Fig. 14.2 c-d). Compositionally, the carbonate clasts are mainly made of micritic to microsparitic limestones, oolitic limestones showing different degrees of dolomitization, and finely to coarsely crystalline dolostones (Fig. 14.2 a-f). Locally gastropods and bivalve shells are still recognizable, even if recrystallized. Dolomite veins, confined within the clasts, are common and characterized by orange luminescencing crystals, up to few hundreds of μm in size (Fig. 14.2 a-d). Among the siliciclastic material, clasts made of polycrystalline quartz occur (Fig. 14.3 a-b). The crystals, up to 10 μm large, subhedral to euhedral, show a particular grain organization: the larger crystals are in the center of the clasts whereas, moving towards the edge, the grain size

decreases progressively. Around some carbonate and ophitic clasts, pressure shadows filled with mm-long, elongated crystals of calcite are present (Fig. 14.3 c). The matrix of this mixed breccia is a grainstone made of the same material of the clasts and detrital quartz. It is important to note the occurrence of authigenic quartz (30-40 μm large) and albite that poikilotopically grow over the matrix, including carbonate crystals (Fig. 14.2 g-h and Fig. 14.3 d-e-f). The albite, chemically almost pure, is euhedral and randomly oriented, up to 2 mm long, showing the characteristic Roc Tourné twinning and dull luminescence under CL. It occurs within the clasts, the matrix and across the contact of the two. Also authigenic opaque minerals (sulphides up to 500 μm large) are widely distributed. Lastly, some dolomite veins crosscut the entire breccia body (e.g. both clasts and matrix).

A third sedimentary breccia type (Fig. 14.1 c), stratigraphically above the previously described ophitic and polimict breccias, occurs in the study area. It is clast-supported and composed solely of carbonate clasts within a matrix that shows the same features of the polimict breccias (e.g. authigenic quartz, albite and opaque minerals). The clasts, which generally range in size from few mm to cm, are made of micrities, microsparitic limestones and fine grained laminated dolostones preserving the pristine features of the rock (e.g. shrinkage pores, fossils). Some clasts show borings possibly referable to *Lithophaga* at the edge. Within some clasts, dolomite veins occur. Other clasts, conversely, are strongly recrystallized and the recognition of pristine features is no longer possible. It is the case of coarse grained, sucrosic dolostones that under CL are almost non-luminescent and preserve some cavities filled with orange luminescing dolomite cement. By their petrographic and CL features, such clasts are clearly referable to the Black Dolomites Unit. Few dolomite veins, characterized by a concentric CL zoning alternating dull and bright orange CL zones, cut through the whole rock mass.

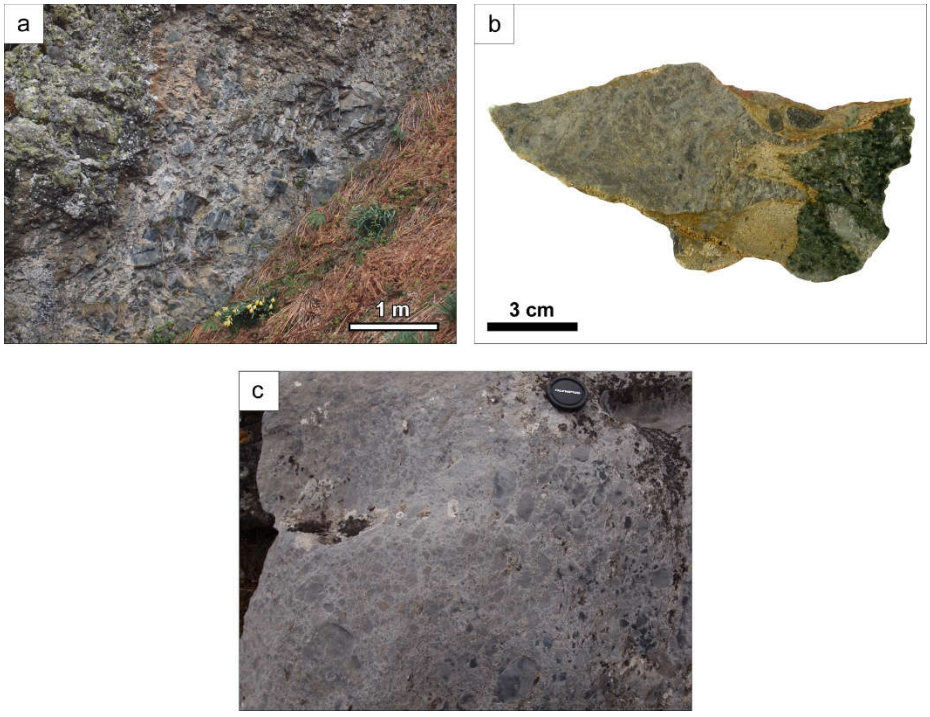

Fig. 14.1 - (a) Field photograph of monomict ophitic breccias. (b) Hand specimen of polimict breccias. The green clast is made of ophite, which is encased within the matrix that is mainly made of carbonate. (c) Field picture of monomict carbonate breccias.

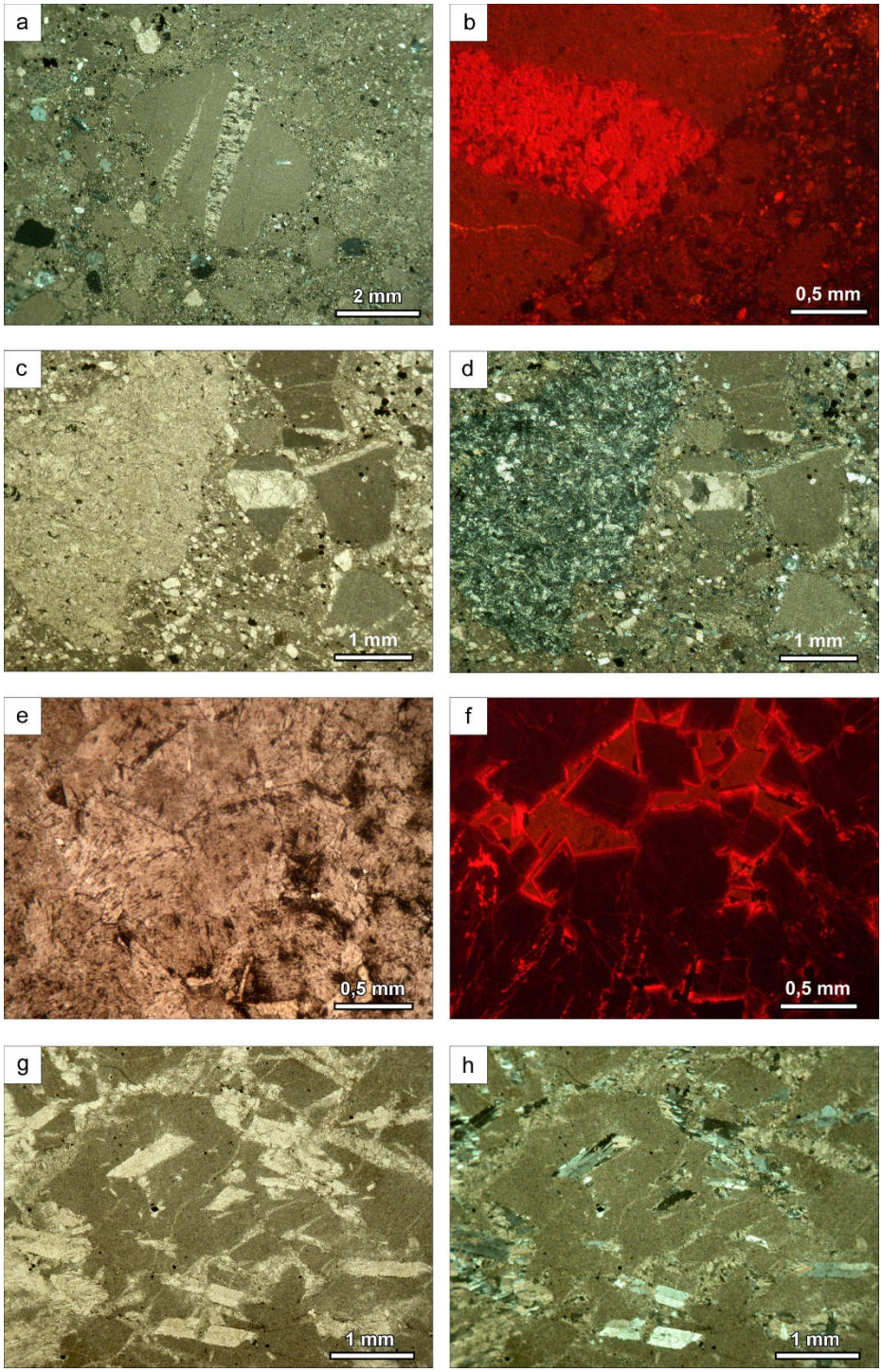

Fig. 14.2 - (a) TL and (b) CL images of polimict breccia. The carbonate clasts preserve dolomite veins characterized by a bright orange luminescence. (c) TL and (d)

crossed polarizers images of polimict breccia made of carbonate clasts, with dolomite veins preserved, and larger ophite clasts. (e) TL and (f) CL images of a clast made of coarse-grained dolostone belonging to the Black Dolomite Formation. (g) TL and (h) crossed polarizers images of authigenic, randomly oriented, albite crystals grown within carbonate clasts and over the clast-matrix boundaries.

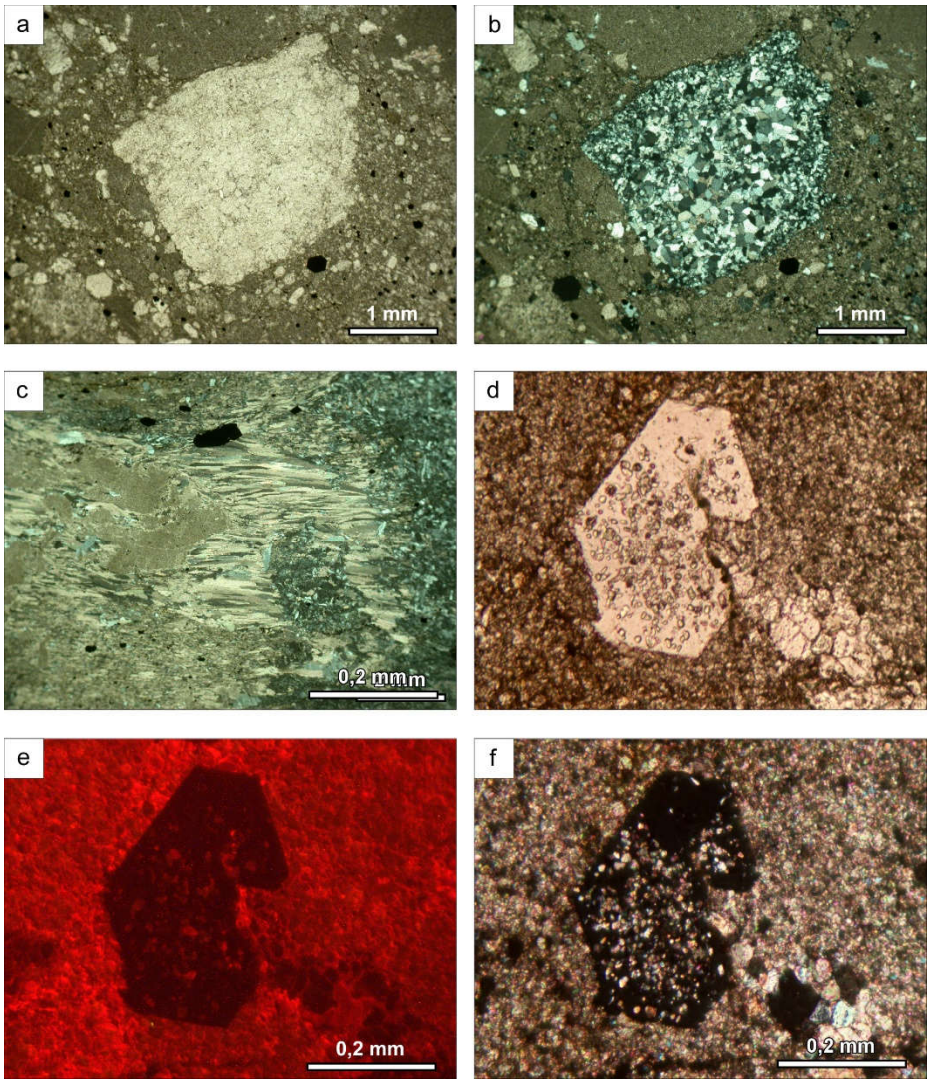

Fig. 14.3 - (a) TL and (b) crossed polarizers images of a clast made of polycrystalline quartz. Note the decreasing grain size towards the edge of the clast. Within the matrix, euhedral opaque minerals are easily recognizable. (c) Crossed polarizers image of

pressure shadows filled with elongated calcite crystals. (d) TL (e) crossed polarizers and (f) CL details of the authigenic quartz poikilotopikally including carbonate crystals within the matrix of the breccias.

14.2 FIRST ORDER INTERPRETATION

14.2.1 Breccias

As already shown in the introduction of this chapter, Casteras et al. (1970b) considered the Sedimentary Breccias Unit older than the Black Dolomite and Black Limestones Units only on the basis of their stratigraphic relationships. Conversely, the here presented petrographic study and field observation shed light on the possibility to re-interpret the stratigraphy of the area. Indeed, findings of clasts belonging to the Black Dolomite Unit as well as carbonates clasts possibly belonging to other Jurassic lithostratigraphic units, represent the strongest argument in order to assign a younger age to these sedimentary breccias (e.g. not older than Kimmeridgian). The composition and the stratigraphic relationships among the three types of breccias allow to consider the occurrence of two different source areas available at the time of their formation: the Ophites and the carbonate sedimentary succession. As a consequence, the overall structure of the study area should to be revisited in the light of these new interpretations.

14.2.2 Fluid-related products

In terms of fluid circulation, the features described for the three types of breccias allow to distinguish at least three main stages in the fluid history of the studied area.

1) A first fluid flow event took place within the sedimentary column before its erosion and re-deposition as documented by the dolomite veins preserved within the clasts (Fig. 14.2 a-d). Apparently, such fluid flow did not lead to recrystallization of the host rocks but occurred only through discrete fractures in

the rock mass. Nonetheless, some portions of the sedimentary sequence underwent pervasive recrystallization as the occurrence of coarse-grained Black Dolomites Unit clasts records (Fig. 14.2 e-f).

2) The second stage occurred after the deposition of the breccias. It is documented by the formation of authigenic minerals (quartz, albite and sulphides) that grew over both the matrix and the clasts of the breccias (Fig. 14.2 g-h and Fig. 14.3 d-f). Such mechanism suggests that the breccias were not completely lithified insofar allowing a diffuse circulation of fluids.

3) The elongated calcite crystals within the pressure shadows (Fig. 14.3 c) suggest its precipitation in a time of ongoing tectonic activity. It could be related to later stages connected to the compressional pyrenean evolution. This stage is possibly related also to the formation of those carbonate veins that cut through the whole rock package.

15. Discussion: Stratigraphy and Fluid flow evolution

15.1 INTRODUCTION

Despite the very poor outcrop conditions, many lines of evidence point to the occurrence of a strong fluid activity within the study area (Forêt de Tre Crouts). Such circulation led to significant post-depositional modifications of the host rocks: pervasive and almost complete replacement dolomitization, micro- to mesoscale fracturation and veining, strong hydrofracturation, recrystallization and variable degrees of ductile deformation. Each process reflects different physico-chemical conditions as demonstrated by the several different resulting textures and fluid-related mineral phases. Unfortunately, it was not possible to truly understand the geometric relationships among the different rock types so that only general considerations can be proposed. Nonetheless, the results of the present work provide undisputable proofs for a strong fluid-related history in the rocks that derive from the former hyper-extended domain. The provided interpretations, albeit not fully constrained by a complete analytical dataset (e.g. lack of fluid inclusion microthermometry and U-Pb dating), will take advantage and based on those proposed for the better studied Alpine counterpart presented in this Thesis and on the recent study of Salardon et al. (2017) on the Pyrenees. As already discussed in the introductory part (cfr. 11.3), the Chaînons Béarnais ridges have been interpreted to represent extensional allochthons lying over detachment faults in the most distal part of the Iberian continental margin (Jammes et al. 2009). For such reason, it is possible to compare the tectono-stratigraphic architecture of the study area, as well as the fluid-related products, with that of the distal domain of the Adriatic rifted margin preserved in the Alps.

15.2 CONSTRAINTS ON THE HYDROTHERMAL FEATURES OF THE FLUIDS

15.2.1 Black Dolomites and Black Limestones Units

$\delta^{13}C$ values of all the analyzed samples from the Black Dolomites and Black Limestones Units show values between 0 and +3,5 ‰, which is characteristic of normal marine sedimentary carbonates with no significant contribution of organic matter decomposition. Only one sample of calcite cement of breccia type 1 (Black Limestones Unit) has a slightly negative $\delta^{13}C$ value (about -2 ‰). On the contrary, $\delta^{18}O$ isotopic values are always negative within a wide range from 0 to -14 ‰. Excluding for a while the mylonites and marbles, and based only on $\delta^{18}O$ values, two main groups of data can be distinguished: the less depleted values belonging to the host rocks (limestones and replacement dolomite) and the more depleted ones referring to new forming minerals, such as calcite and dolomite, which precipitated in open fractures of the hydraulic breccias. The two groups are slightly overlapping, expecially for the Black Dolomite Unit. As previously stated and even if not constrained by fluid inclusion microthermometry, the replacement dolomitization affecting the dolostones could be related to hot fluid circulation to which the observed depletion of oxygen isotopes may be related. Indeed, the replacement dolomite shows $\delta^{18}O$ values that are lower than those documented in present day settings where dolomite is forming (0 to +4‰; Tucker and Wright, 1990; Meister et al., 2013). Comparing this dataset with the one described in the Alpine areas (Fig. 10.2), it looks evident that the overall trend is completely similar. The replacement minerals, which inherited the former $\delta^{18}O$ signature of the precursor rock, are always less depleted than the void filling ones cementing veins and breccias, which, on the contrary, are pure new forming phases.

Calculations of the isotopic composition of fluids (for the only Black Limestones Unit) responsible for dolomite and calcite precipitation, made by applying the equation of Horita (2014) and Anderson and Arthur (1983) respectively, provide O isotope values for fluids markedly positive (+9 ‰ SMOW for dolomite to

about +12 ‰ SMOW for calcite). Such positive signature may be related to different processes such as evaporative enrichment (e.g. McKenzie, 1981), clay mineral diagenesis (Dählmann and de Lange, 2003; Hensen et al., 2007), and to the interaction with silicate minerals of siliciclastic and crystalline rocks (Clayton *et al*., 1966; Land and Prezbindowski, 1981; Hitchon *et al*., 1990; Haeri-Ardakani et al., 2013). Taking into account the model of Jammes et al. (2009) where the Chaînons Béarnais were considered to be extensional allochthons in a hyper-extended domain, the only reasonable source of fluid feeding the hydrothermal system is seawater. As for the Alpine areas, also in this case an interaction with basement rocks could be addressed as the main reason to explain such positive signature. In this case, moreover, the occurrence of Keuper evaporites at the base of the Mesozoic sedimentary column likely provided a contribution in determining the positive isotopic signature.

15.2.2 The mylonites and marbles

The carbonate mylonites and their precursors (marbles) show the same O and C isotopic pattern. The same negative O isotopic values shown by both rock types suggest that the mylonites derived from the deformation of an already recrystallized rock. Interestingly, the pale bands of the carbonate mylonites are less depleted than both the dark ones and marbles. In any case, two different steps characterized the evolution of these rocks. The first led to the complete recrystallization of the former protolith giving rise to dolomite marbles and their negative $\delta^{18}O$ values. The second stage involved the already recrystallized rock mass and was related to a strong ductile deformation event resulting in the development of mylonitic texture. The very coarse crystal size of the marbles and the subsequent mylonitization are both processes that need a “hot environment” to occur as well as involment of fluids. The occurrence of quartz and former scapolite (?) poikilotopikally grown over the carbonate foliation point to consider a silica-rich fluid flow event after or at least simultaneously to the mylonitization. Former scapolite (?), presently replaced by microcrystalline

assemblages of K-rich alumo-silicates highlight that new fluid-rock interaction took place within these rocks in a later stage of their evolution.

15.2.2 Sedimentary Breccias Formation

No geochemical data are available for the Sedimentary Breccias Unit. However, petrography and cathodoluminescence investigations shed light on some important aspects related to fluids circulation. Apart from authigenic quartz and sulphides, the widespread occurrence of authigenic albite is noteworthy. Albite is quite common in high-grade diagenetic to low-grade metamorphic carbonate rocks (Spötl et al., 1999). Euhedral habit, chemical composition and crystallographic properties are the major lines of evidence that allow to distinguish detrital albite from the authigenic one. Indeed, the latter is almost compositionally pure (Kastner, 1971; Spötl et al., 1999) and commonly shows the peculiar Roc-Tourné twinning, which is not present in magmatic or metamorphic albites (Kastner, 1971). Furthermore, it is characterized by the absence of CL luminescence due to its chemical purity (Richter et al., 2002). The carbonate grains poikilotopikally included within the authigenic albites, represent remnants of the host rock and provide one more distinctive feature with respect to the magmatic ones (Kastner, 1971). Albite crystals are present both in the carbonate clasts and in the carbonate matrix, and in some cases they grow across the clast-matrix boundary. This provides a further evidence of a post-depositional growth of albite crystals. Concerning the mechanism of authigenesis in carbonate rocks, two different models have been proposed: the first is based on isochemical transformation of the host rock (Kastner & Siever, 1979), whereas the second takes into account metasomatic transformation due to migration of brines (Kastner & Siever, 1979; Spötl et al., 1999). In the eastern Pyrenees, albitites are known as a product of fluid/rock interactions occurring during a syn-extensional metasomatic event dated at about 100 Ma (Boulvais et al., 2007; Fallourd et al., 2014; Poujol et al., 2010). The geographical distribution of albitites closely matches that of talc/chlorite mineralizations related to a hydrothermal event of regional extent during mid-Cretaceous time

(Schärer et al., 1999). Interestingly, also in the study area albite occurrences are stratigraphically close to the Mg-rich alumo-silicates ("sandwiches") affecting the Black Limestones Unit, which are likely to be talc and chlorite. Such ore deposits have been attributed by Boulvais et al. (2006) as due to seawater modified by chemical exchange with crustal rocks. The albitizing fluids are considered to be related to hot (200-300 °C) Na- and Si-rich fluids with high salinity (Spötl et al., 1999; Rais et al., 2008). This high salinity is supposed to be referable to a primary magmatic feature (Hall et al., 1988; Aslund et al., 1995), to an interaction of aqueous metamorphic/magmatic fluids with evaporite levels (Oliver, 1995; Barton and Johnson, 1996), or should represent a primary characteristic of surface-derived brines (McLelland et al., 2002).

15.3 NEW INTERPRETATION OF THE STRATIGRAPHIC SETTING OF THE STUDY AREA

Finding of clasts made of unaltered limestones and dolostones, strongly dolomitized rocks, dolomite and calcite cements identical to those which have been described for Black Limestones and Black Dolostones Unit within the Sedimentary Breccias Unit has strong implications in terms of stratigraphic architecture of the area. Indeed, Casteras et al. (1970b) assigned a Rhaetian-Sinemurian age to these sedimentary breccias only on the base of the stratigraphic relationships with the over- and underlying rocks (Aalenian-Toarcian limestones and Keuper evaporites and ophites, respectively). As demonstrated by field observations and petrographic studies carried out in the present Thesis, these breccias cannot be older than the younger rocks that compose the clasts and the matrix, i.e. at least the Callovian-Oxfordian Black Dolomites unit.

The evolution of the Pyrenean hyper-extended rift system is characterized by different aborted rifting events in the Triassic and Upper Jurassic time before the major Cretaceous crustal thinning stage (Puigdefàbregas and Souquet, 1986; Vergés and Garcia-Senz, 2001). Such rifting events were obviously associated

with tectonic activity, which exposed different rocks to erosional processes at different times. The Sedimentary Breccias Unit could therefore be interpreted as the sedimentary product of erosion and re-sedimentation of the Triassic-Jurassic sedimentary sequence tectonically involved in the ongoing extensional events. As already demonstrated in the Alps (Pinto et al., 2015; Incerpi et al., 2017; this Thesis) and in the Basque Cantabrian Basin and Pyrenees (e.g., Lopez-Horgue et al., 2010; Salardon et al., 2017), every tectonic stage that characterizes the extensional evolution of hyper-extended domains is related to strong fluid circulation. Such circulation took place over a long time and a large area and affected the whole sedimentary column (e.g. pre-, syn- and post-rift sediments). In this frame, the fluid-related products described in the Sedimentary Breccias Unit can be the proof for a long-lasting fluid activity that took place in the sedimentary column before and after its erosion. For such reason, the breccias cannot be considered as part of the pre-rift sequence. Based on the presented observations, this Unit is most likely related to erosional episodes connected with the mid-Cretaceous extensional tectonic. Such hypothesis is also supported by the post-depositional albitization affecting the breccias, which was dated as mid-Cretaceous (Boulvais et al., 2007; Fallourd et al., 2014; Poujol et al., 2010).

15.4 EVOLUTIONARY MODEL

Based on the observations and related interpretations exposed in the previous sections, the following evolutionary model for the study area can be proposed (Fig. 15.1).

1) Carbonate-rich stage:

- First event of circulation of (hot) fluids to which the pervasive and fabric-destructive dolomitization of the Black Dolomites Unit is related.
- Second event of circulation of dolomite-rich fluids and formation of crackle, mosaic and rubble breccias within the Black Dolomites Unit. These fluids, strongly overpressured, could also be possibly responsible for the formation of hydrofracturing breccias type 3 within the overlying

Black Limestones Unit. Indeed, such breccias are the only one cemented by dolomite. The clasts of these breccias are polimict including not only the Black Dolomites Unit but also the Black Limestones Unit. Therefore, a flow of overpressured fluids thorough the two lithostratigraphic units can be inferred which led to a conspicuous amount of disruption and vertical displacement in post-Kimmeridgian time.

- First phase of circulation of calcite-rich fluids as documented by the cement within mosaic to rubble breccias of the Black Dolomites Unit and that of breccia types 1, 2 and 3 within the Black Limestones Unit.

Hydrofracture breccias have been widely documented in the pre-rift sedimentary sequence preserved at Il Motto area and within the extensional allochthon at Piz Val Lunga area of the Adriatic continental margin. Also in those cases, overpressured fluids generated crackle, mosaic and rubble breccias to which a vertical displacement of the clasts was associated. The study area, as well as the whole Chaînons Béarnais (Salardon et al., 2017), interestingly recorded the same processes even on a larger scale. Indeed, both clasts and cement crystals are larger in size possibly implying higher amount of fluids and/or overpressure. In the Adriatic distal margin, hydraulic fracturing has been genetically related to the activity of the Err detachment fault. Also for the Pyrenean study area the same scenario could be envisaged (e.g. circulation of fluids related to mid-Cretaceous hyper-extension). Indeed, in the Chaînons Béarnais Salardon et al. (2017), after a first fracturing event which is the result of the first rifting phases affecting the rift system, described a second major fracturing event that affected the Liassic to Albian sediments to which an increase in temperature of the fluids and depletion of $\delta^{18}O$ are associated. The authors attribute a diffuse replacement dolomitization as well as the dolomite-calcite cementation of hydraulic breccias and veins to this stage. On the basis of chemical exchanges due to serpentinization presented by Pinto et al. (2015) and the occurrence of serpentinized lherzolites in the Chaînons Béarnais

(Lagabrielle et al., 2010), the source of Mg enabling such dolomitization could then be related to serpentinizing processes that took place in mid-Cretaceous time during mantle exhumation (Masini et al., 2014). The tectonic activity, to which the fluid circulation is strictly connected, was also the trigger responsible for the erosion of the sedimentary column and the subsequent deposition of the Sedimentary Breccias Unit.

2) Na- and SiO_2-rich stage:

- First event of circulation of Na- and Si-rich fluids as poikilotopic growth of quartz and albite over the matrix and clasts of the Sedimentary Breccias Unit attest. The occurrence of authigenic sulphides demonstrates that the chemistry of the circulating fluids was even more complex.

In the Fuorcla Cotschna area (Adriatic distal margin), rare authigenic albite has been found within veins cutting through the extensional allochthon. It was not possible to date precisely that stage of fracturation so the authigenesis could have occurred both prior or after the BBF (i.e. affecting only the pre-rift rocks of the allochthon or also the syn-rift sequence). Since the Sedimentary Breccias Unit that can be tentatively defined as syn-rift sediments, is affected by diffuse albitization and knowing that such process in the eastern Pyrenees has been described in relation to mid-Cretaceous metasomatic event, it can be assumed that also in the Chaînons Béarnais domain it took place during the hyper-extension phases.

One more important stage characterized the evolution of the study area even if it is very difficult to place in the frame proposed so far: the marble and mylonite formation. Despite still being related to hydrothermal fluids, these rocks underwent a completely different mechanism of deformation. Indeed, all the other described rocks are the result of brittle hydrofracturation whereas the marbles were affected by a completely ductile deformation leading to

mylonitization. Such ductile deformation characterized, to a lesser extent, also the sedimentary breccias found in the Quarries site.

Many questions remain open, based on the available data and field observations: What is the relation between the marbles-mylonites and the surrounding Black Limestones Unit? Is there any link between the mylonites and the deformed sedimentary breccias of the Quarries site? Do they represent a shear gradient within the same fault zone? Are they really part of the same lithostratigraphic unit? If not, what is the real architecture of the study area? Are the mylonites and marbles part of a tectonic slice of pre-Keuper succession?

To answer all these questions and to better constrain the evolution of the whole area more analyses are required as well as more fieldwork. Field activity should allow to better understand the tectono-stratigraphic architecture of the area by the re-definition of the lithostratigraphy and highlighting the reciprocal relationships among all the different “new and old” units. U-Pb dating will be fundamental in order to constrain chronologically all the described evolutionary steps as well as Sr isotopes in order to define the amount of interaction with crustal basement rocks and/or evaporites. Because of the abundance of mantle-related rocks in close vicinity to the study area and the Chaînons Béarnais in general, He isotopes will eventually permit to comprehend if mantle-derived fluids played a role within the here presented hydrothermal system as suggested by Salardon et al. (2017).

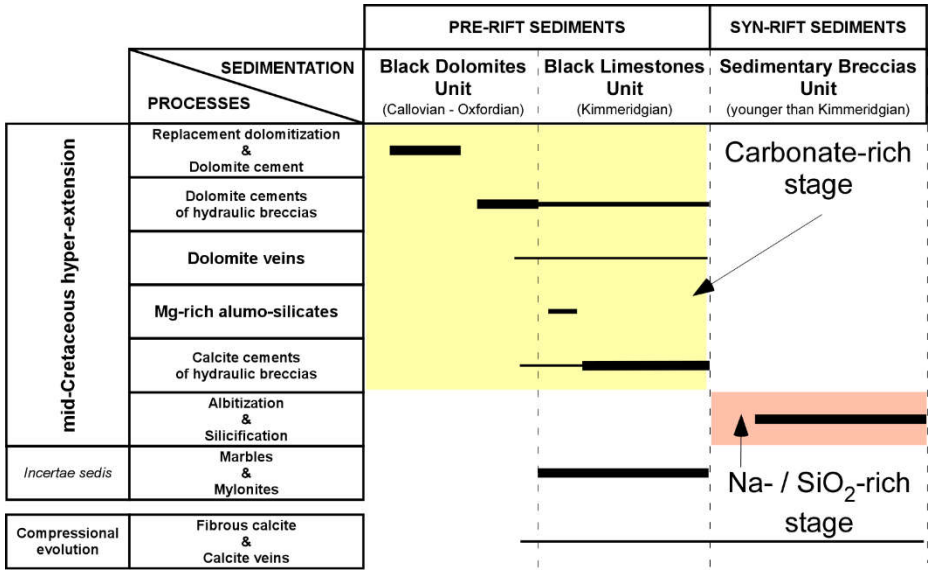

Fig. 15.1 - Paragenetic sequence showing the relative timing of post-depositional processes and related products affecting the pre- to syn-tectonic sediments of the Pyrenean hyper-extended rift system. The width of the lines is qualitatively proportional to the magnitude of each process.

16. Summary of the results and future perspectives

16.1 AIM OF THE THESIS

The present Thesis focused on the hydrothermal systems in continental rifted margins. Despite the advanced knowledge of their tectono-stratigraphic architecture and evolution, some fundamental aspects are still missing. In fact, the role of fluids has never been the target of investigations except for hydrothermal vents along mid-ocean ridges. Understanding the exact role of fluids along the whole evolution of a continental margin is of major importance in terms of diagenetic processes, heat fluxes and thermal evolution of the sedimentary cover. In the Thesis the major focus was on the syn- to post-depositional modifications of the rocks due to circulation of fluids. Two fossil analogues were chosen as targets of the research: the Adriatic paleo-rifted margin and the Pyrenean hyper-extended rift system.

16.2 THE RESULTS

16.2.1 The Adriatic rifted margin

The main focus of the Thesis is the Adriatic distal margin in its central and outer parts. To get a more complete understanding of the system, observations and analyses were also performed in the proximal margin and the inner distal margin.

16.2.1.1 The distal margin

Four sites were chosen within the distal margin. From the inner part and moving oceanwards they are: Piz Alv, Piz Val Lunga, Fuorcla Cotschna and Mal Pass. Apart from the Piz Alv area, where only syn-rift sediments were studied (Piz Alv breccia), in the other sites the investigations focused on extensional

allochthons mainly made of peritidal dolomites of the Norian Hauptdolomit Fm. and on the Lower to Middle Jurassic syn- to post-rift sediments filling supra-detachment basins (Bardella and Saluver Fms., Radiolarian Cherts). Both the extensional allochthons and the syn-rift sediments directly overlie low-angle detachment faults. The Bardella and Saluver Fms. consist of gravitational deposits related to the erosion of the extensional allochthon and basement-derived material from the footwall of the detachment, respectively. The tectono-stratigraphic evolution of a supra-detachment basin is confined within two major time lines: TAF - Top of Agnelli Fm. (e.g. the last pre-rift sediments in the distal margin, ~185 Ma) and the RC - Radiolarian Cherts (e.g. the first post-rift sediments, ~165 Ma). The study of the fluid activity in the distal margin allowed to depict a complex fluid-related history that led to different processes to which the precipitation of different mineral phases is due. Some of these fluid-related products were found only within the extensional allochthons whereas others affected also the syn- to post-rift sedimentary sequence. For such reason, a new fundamental time line, that corresponds to a *hiatus* in the sedimentation, has been introduced in order to truly understand the polyphase evolution of the system: the BBF - Base of Bardella Formation (e.g., the base of the first syn-rift sediments in the distal margin). Based on this, two main stages in evolution of the Adriatic distal margin were recognized:

1) First, carbonate-rich, stage

Pre-TAF:

- Deposition of the Hauptdolomit Fm.
- Rhaetian-Hettangian tectonic activity leading to the formation of neptunian dykes and sills in the Hauptdolomit Fm. as recorded at Piz Alv and Mal Pass areas.
- Diffuse replacement dolomitization and dolomite cementation of pores of the Hauptdolomit Fm. and neptunian dykes.

Post-TAF and pre-BBF:

- Onset low-angle detachment faults activity to which cataclastic deformation at the base of those pre-rift volumes of rocks, which will become extensional allochthons, and abrupt release of overpressured fluids (e.g. fault-valve mechanism) are related. The latter is documented by hydraulic brecciation with development of calcite cement, partial dedolomitization of the Hauptdolomit Fm. and cataclasite, fracturation and vein filling with saddle dolomite cements.

2) Second, silica-rich, stage (syn- to post-BBF)

- Ongoing tectonic activity generated topography and following erosion of the extensional allochthons resulting in the deposition of the syn-rift Bardella and Saluver Fms.
- Fracturation events and formation of quartz veins throughout the whole syn-rift sedimentary sequence and within the extensional allochthons.
- Formation of silica-rich septarian-like concretions and Fe-Mn oxides coating of clasts of calciruditic beds in the uppermost part of the syn-rift sequence.
- Deposition of post-rift Radiolarian Cherts.
- Persistence of fluid activity and subsequent formation of syn-depositional chert nodules.
- Further silicification and dolomitization processes within the matrix of calciruditic beds in the basal part of the Radiolarian Cherts.

The BBF does not mark only a temporal constrain in the evolution of the distal margin but also an important change in the chemistry of the fluid system through time. In fact, the pre- to syn-BBF stages are characterized by carbonate-dominated fluids with only minor occurrence of silica. On the contrary, the post-BBF diagenetic stage is strongly silica-rich and lasted, at least, until the deposition of the first post-rift sediments.

Geochemical analyses and fluid inclusion microthermometry were performed on different fluid-related products, belonging to the pre- and post-BBF stages, in order to characterize the physico-chemical properties of the fluids.

- O and C isotopes analyses performed on replacement dolomite and new forming minerals (dolomite and calcite cements of breccias and veins) show a common trend all over the distal margin. Slightly positive $\delta^{13}C$ is in the range of normal marine carbonates; $\delta^{18}O$, on the contrary, is slightly to strongly negative. The replacement dolomite shows always the less depleted $\delta^{18}O$ values (up to -6‰ VPDB), whereas the more depleted ones refer to dolomite and calcite cements of breccias and veins (up to -16‰ VPDB).
- Homogenization temperatures of fluid inclusions measured on the replacement dolomite, calcite cement and dedolomite, dolomite and quartz of veins as well as septarian-like concretions show values in the range of 100°C to 150°C. Such values cannot be explained only by the sedimentary overburden that was few 100's of meters at the time of the fluid circulation. Therefore, the occurrence of hydrothermal fluids is strongly suggested. This hypothesis is also confirmed by REE systematics (Y/Ho, LREE/HREE, weak Eu anomaly).
- Calculation of the isotopic composition of the fluids responsible for dolomite and calcite precipitation provides slightly to strongly positive O isotope values (+2 to +12‰ SMOW). These results, supported by the highly radiogenic Sr isotope values of the same mineral phases, point to an intense interaction between the fluids and the granitic footwall of the detachment faults. Such interpretation is further constrained by the "crustal" values of the He isotopes.
- Geochemical analyses on trace elements seem to confirm this hypothesis as demonstrated by enrichment in some elements (e.g. Ba, Sr, Pb) typical of crustal rocks. Moreover, elements like Cr, V, Ni seem to shed light on a possible interaction of fluids with mantle-related rocks. The

occurrence of Fe-Mn oxides found in the upper part of the syn-rift sedimentary succession may have the same origin.

- Finally, U-Pb dating on replacement dolomite gave constrains about the timing of emplacement of dolomitizing fluids. Most of the analyses on samples belonging to the Hauptdolomit Fm. from different paleo-geographic domains indicate that the replacement process took place at about 200 Ma. Thus, this event may coincide with the onset of rifting, which is well preserved in the proximal margin, and lasted until the late Early Jurassic when deformation localized in the future distal margin.

On the basis of the described observations and data, it is important to underline how the Adriatic distal margin records a long-lasting and multi-stage fluid-related history. These characteristics refer to different stages in the margin evolution, from the very first phases in the proximal margin to the last extensional events in the distal margin, simultaneous with the exhumation of mantle rocks. The evolution of the fluids, and hence their chemistry, is directly connected with the tectono-stratigraphic evolution of the margin.

16.2.1.2 The proximal margin

The proximal margin, preserved at the Il Motto area, is characterized by a half-graben basin bounded by a high-angle normal fault that was active during the Hettangian, representing the onset of rifting along the Adriatic margin. Samples of Hauptdolomit Fm. from the footwall of the main fault highlight the occurrence of two main fluid-related processes: i) pervasive and fabric-destructive replacement dolomitization followed by ii) hydraulic brecciation of the host rock, which gave rise to breccias cemented by dolomite and calcite.

The petrographic features of the replaced Hauptdolomit Fm., similar to those of the others domains of the Adriatic margin, allow to ascribe the replacement dolomitization to the pre-BBF stage. U-Pb ages (~200 Ma) support this hypothesis. The textures of the breccias related to hydrofracturing, the negative $\delta^{18}O$ isotopic values (about -6‰ VPDB) and the microthermometric results (T_h

in the range 130-140°C) of the dolomite cement require the occurrence of overpressured hydrothermal fluid circulation. As for the distal margin, the sedimentary column was not sufficiently thick to justify the obtained temperatures by burial only. Fluid flow may have been triggered by the activity of the main faults bounding the half-graben basins, which rooted down in the basement, allowing the fluids to get highly radiogenic Sr isotope values. At the Il Motto area, finally, the post-BBF silica-rich diagenetic stage has not been observed.

16.2.2 The Pyrenean hyper-extended rift system

The study area (Chaînons Béarnais) is localized in the eastern termination of the Mauléon Basin, which is a hyper-extended supra-detachment basin formed in response to the mid-Cretaceous aborted rifting predating Pyrenean collision. The focus of the study is the pre-rift, Upper Triassic to Lower Cretaceous, sedimentary sequence preserved as extensional allochthons. As for the Alpine area, the target is the post-depositional modification of the sediments due to fluid circulation. Because of the poor outcrop conditions, only discontinuous observations were possible. Three lithostratigraphic units, in particular, were affected by diffuse fluid circulation: the Black Dolomites Unit (Callovian-Oxfordian), the Black Limestones Unit (Kimmeridgian) and the Sedimentary Breccias Unit (post-Kimmeridgian?).

16.2.2.1 The Black Dolomites Unit

The Black Dolomites Unit is made of coarse crystalline dolostones, which are the result of an almost complete replacement dolomitization of the former host rocks. Such replacement represents the first fluid-related event recorded in the area. Even if homogenization temperatures of fluid inclusions are missing, the increase of crystal size may be explained by the occurrence of hot fluids. After the dolomitization, the Unit underwent strong brecciation. The breccias are genetically related to the circulation of overpressured carbonate-rich fluids as the polyphase dolomite and calcite cements document. The occurrence of sediment

geopetally filling the cavities of the breccias allow to consider that the hydrofracturation took place at shallow levels in the sedimentary column and in connection with the seafloor. Since the internal sediment is dolomitized, its deposition should have occurred concomitantly with the circulation of dolomitizing fluids.

O-C isotopic values of replacement dolomite and dolomite cement of breccias show the same trend already described for the Adriatic margin. $\delta^{13}C$ values are slightly positive whereas $\delta^{18}O$ values are slightly (replacement dolomite up to -8‰ VPDB) to strongly negative (dolomite cement up to -13‰ VPDB). Despite the absence of homogenization temperatures of fluid inclusions, stable isotope geochemistry may support a hydrothermal character for the fluids responsible of replacement and brecciation.

16.2.2.2 The Black Limestones Unit

The Black Limestones Unit is stratigraphically above the Black Dolomites Unit and consists of fine-grained well-bedded limestones, locally containing fibrous aggregates of Mg-rich alumo-silicates (talc and chlorite). The Unit shows the most abundant diversity in terms of rock types and fluid-related processes of the whole study area. For such reason, two different sites have been distinguished: the Quarries area and the Riverbed area.

The Quarries area

The Quarries area is mainly constituted of hydrofracturing and sedimentary breccias. The first type is further composed of three different types of breccias depending on the mineralogy of the clasts and the cements. Type 1 is made of clasts of limestones within a coarse calcite cement, type 2 is made of already dolomitized clasts of the Black Dolomite Unit encased in a fine-grained calcite cement, type 3 is a polimict breccias whose clasts are made of limestones and dolostones within a complex cement made of dolomite and calcite. All the three types of breccias, because of their textures, had to be formed by circulation of overpressured carbonate-rich fluids.

The second rock type is a deformed carbonate sedimentary breccia made of sheared dolomite clasts within a micritic matrix and is closely associated to the first one. O and C isotope analyses were performed on the host limestone and the calcite cement of type 1 hydraulic breccia. The slightly positive $\delta^{13}C$ and the negative $\delta^{18}O$ (up to -14‰ VPDB) combined with homogenization temperatures in the range of 180-190°C for dolomite cement of breccia type 3 and 240-250°C for calcite cement of breccia type 1 suggest a hydrothermal fluid circulation.

The Riverbed area

In close proximity to the breccias, strongly recrystallized carbonate rocks occur. Because of their strongly foliated texture these rocks are considered as mylonites. Some relicts of possible former scapolite are presently replaced by fine-grained aggregates of K-rich alumo-silicates. Authigenic quartz is also present. The rock is completely dolomitized. In close vicinity with the mylonites, coarse crystaline dolomite marbles were found. These marbles could represent the protolith of the mylonites as demonstrated by the porphyroclast within the mylonites as well as the nearly identical O and C isotopic signature ($\delta^{13}C$ between 1 and 3‰ VPDB; $\delta^{18}O$ about -7‰ VPDB).

16.2.2.3 The Sedimentary Breccias Unit

Within this Unit two different lithostratigraphic units that in the literature were assigned to the Rhaetian-Sinemurian, were gathered together. By the present work, it has been possible to propose a re-interpretation of the age of the unit. It is made of three types of sedimentary breccias that are: 1) monomict ophitic breccia, 2) polimict carbonate-ophitic breccia, and 3) polimict carbonate breccia. Findings of clasts made of Black Dolomites and Limestones Units within breccias type 2 and 3 allowed to assign a younger age to this Unit (e.g. at least Kimmeridgian). In terms of fluid circulation, this Unit records different interesting stages:

- A first fluid flow event affected the sedimentary column before its erosion and re-deposition as the dolomite veins within the clasts of the

breccias document. Some portions of the sedimentary sequence underwent pervasive dolomitization as the coarse-grained clasts made of Black Dolomites Unit records.

- The second stage occurred after the deposition of the breccias. It is documented by authigenic minerals (quartz, albite and sulphides) that grew over the matrix and clasts. Diffuse albitization has been described in the eastern Pyrenees connected to a mid-Cretaceous HT-LP metamorphic event.
- Elongated calcite crystals within pressure shadows around some carbonate and ophitic clasts suggest its precipitation in a time of ongoing tectonic activity. This could be considered as a later stage connected to the compressional Pyrenean evolution. The formation of the carbonate veins cutting through the whole rock package may be possibly related to this stage.

On the whole, the Pyrenean study area registered two main polyphase stages related to fluid circulation:

1) Carbonate-rich stage led to the fabric-destructive replacement dolomitization of the Black Dolomites Unit. New pulsations generated the hydraulic breccias within the same Unit. This stage could also be responsible of the formation of breccia type 3 in the Black Limestones Unit. Calcite cements in the breccias of Black Dolomites Unit and Black Limestones Unit document that the physico-chemical features of fluids changed to calcite-prone.

2) Na- and SiO_2-rich stage is documented by diffuse authigenesis of quartz and albite in the Sedimentary Breccias Unit. Moreover, the occurrence of sulphides makes the chemistry of the fluid even more complex.

In summary, the main result of this thesis is to confirm the fundamental role of faults, and the associated fracture zones, as plumbing structures of the hydrothermal system. However, the style of faulting seems to importantly

control the chemistry of fluids and therefore the composition of the diagenetic products that the circulation of fluids generates within the highest part of the hydrothermal system, i.e. the pre-tectonic sedimentary rocks and the syn-tectonic sediments. In the early rifting stage, tectonically dominated by normal faults, fluids are seawaters that penetrate at some kilometer depths within basement rocks where they are heated, insofar acquiring a dolomitization potential over carbonate sediments that are met along the upward flowing part of the hydrothermal cell. In the second stage of the rifting process, when faults merge at depth into detachment faults, the volume of cataclastic crustal rocks is much greater and consequently much more massive is the fluid-rock interaction with basement rocks which mainly involves feldspar alteration and delivers silica to the fluids. In the absence of solid evidence about the direct involvement of mantle rocks and/or fluids in the hydrothermal circulation system, this mechanism appears as the more likely to explain the marked change in space and time of the diagenetic products from carbonate-rich to quartz-rich along extensional continental margin transects.

16.3 OPEN QUESTIONS AND FUTURE PERSPECTIVE

The multidisciplinary approach adopted in this project allowed to understand how the fluid circulation during continental extension is strong and pervasive. Many lines of evidence point to the same conclusion: hydrothermal fluids played a key role in the syn- to post-depositional modification of the pre- to post-rift sedimentary rocks constituting the margins. Even if a quite detailed evolutionary model has been proposed, some open questions still remain unsolved for both the Adriatic and Iberian margin.

Adriatic proximal margin:

- How far from the fault surface is the fluid flow developed?
- Is the fluid circulation affecting only the footwall or also the Lower Jurassic turbiditic deposits of the hanging wall?

- Is the second diagenetic stage really not recorded?

Adriatic distal margin:

- Is the entire supra-detachment basin affected by the same processes described in this Thesis?
- Do they depend on the thickness of the sedimentary succession?
- Are the post-tectonic sediments really post-tectonic?

Pyrenean hyper-extended rift system:

- What is the absolute age (U-Pb dating) of the hydrothermal minerals affecting the pre- and syn-rift sediments?
- Did the fluids interact with the continental basement (Sr isotopes)?
- Are mantle-related fluids involved in the hydrothermal system (He isotopes)
- What is the geochemical signal recorded within the sediments (main, trace and rare earth elements)?
- What is the relation between the marbles-mylonites and the other Units?

As a future perspective, it would be very interesting to compare the here presented dataset to the present-day hyper-extended margins. One of the targets could be the present-day Iberia continental margin since it shows similar tectono-stratigraphic features to those of the Adriatic margin. Furthermore, not only the overall architecture makes the comparison of great interest. Indeed, in the ODP Leg 103 (Boillot et al., 1988), which drilled the distal part of the Iberia margin, a diffuse hydrothermal dolomitization is described. Petrographic characteristics as well as stable isotope geochemistry are completely similar to those presented in this work. The analytical dataset, on the contrary, is much less developed; it would thus be useful to apply the here presented methodologies.

References

Anders, E. and Grevesse, N. (1989). Abundances of the elements: Meteoric and solar. *Geochimica et Cosmochimica Acta, 53,* 197-214.

Anderson, T.F., & Arthur, M.A. (1983). Stable isotopes of oxygen and carbon and their application to sedimentologic and paleoenvironmental problems. In: Arthur, M.A., Anderson, T.F., Kaplan, I.R., Veizer, J., Land, L.S., eds., Stable isotopes in sedimentary geology, 10, Columbia, SEPM Short Course, 1-151.

Armstrong-Altrin, J.S., Madhavaraju, J., Lee, Y.I., Ramasay, S. (2003). Geochemistry of Upper Miocene Kudankulam Limestones, Southern India. *International Geology Review, 45,* 16-26.

Aslanian, D., Moulin, M. Olivet, J.-L, Unternehr, P., Matias, L., Bache, F., Rabineau, M., Nouzé, H., Klingelhoefer, F., Contrucci, I., & Labails, C., (2009). Brazilian and African passive margins of the Central Segment of the South Atlantic Ocean: kinematic constraints. *Tectonophysics (Special Issue: role of magmatism), 468*, 98-112.

Astin, T.R. (1986). Septarian crack formation in carbonate concretions from shales and mudstones. *Clay Minerals, 21,* 617-631.

Arthaud, F., and Matte, P. (1975). Les décrochements tardi-hercynien du sud–ouest de l'Europe. Géométrie et essai de reconstitution des conditions de deformation. *Tectonophysics, 25,* 139-171, doi:10.1016/0040-1951(75)90014-1.

Arthaud, F., and Matte, P. (1977). Late Paleozoic strike-slip faulting in southern Europe and northern Africa: Result of a right-lateral shear zone between the Appalachians and the Urals. *Geological Society of America Bulletin, 88*, 1305-1320.

Aslund, T., Oliver, N.H.S., Cartwright, I. (1995). Metasomatism of the Revenue Granite and aureole rocks, Mt Isa Inlier, Queensland: syndeformational fluid flow and fluid–rock interaction. *Australian Journal of Earth Sciences, 42,* 291-299.

Barale, L., Bertok, C., Talabani, N.S., d'Atri, A., Martire, L., Piana, F., Preat, A. (2016). Very hot, very shallow hydrothermal dolomitization: An example from the Maritime Alps (north-west Italy-south-east France). *Sedimentology, 63,* 2037-2065.

Barnolas, A. and Chiron, J.C. (1996). Synthèse géologique et géophysique des Pyrénées: cycle hercynien. *Bureau de Recherches Géologiques et Minières* (Eds.), Orléans.

Barton, M.K. and Johnson, D.A. (1996). Evaporitic-source model for igneous-related Fe oxide–(REE–Cu–Au–U) mineralization. *Geology, 24,* 259-262.

Bau, M. (1991). Rare-earth elements mobility during hydrothermal and metamorphic fluid-rock interaction and the significance of the oxidation state of europium. *Chemical Geology, 93,* 219-230.

Bau, M. and Dulski, P. (1995). Comparative study of yttrium and rare-earth element behaviours in fluorite-rich hydrothermal fluids. *Contributions to Minerlogy and Petrology, 119,* 213-223.

Bau, M., and Möller, P. (1992). Rare earth elements fractionation in metamorphogenic hydrothermal calcite, magnesite and siderite. *Mineralogy and Petrology, 45,* 231-246.

Baumgartner, P.O. (1987). Age and genesis of Tethyan Jurassic radiolarites. *Eclogae Geologicae Helvetiae, 80,* 831-879.

Beltrando, M., Rubatto, D., Manatschal, G. (2010). From passive margins to orogens: The link between ocean-continent transition zonesand (ultra)high pressure metamorphism. *Geology, 38(6),* 559-562.

Beltrando, M., Frasca, G., Compagnoni, R., Vitale-Brovarone, A. (2012). The Valaisan controversy revisited: Multi-stage folding of a Mesozoic hyper-extended margin in the Petit St. Bernard pass area (Western Alps). *Tectonophysics, 579,* 17-36.

Beltrando, M., Stockli, D.F., Decarlis, A., Manatschal, G. (2015). A crustal-scale view at rift localization along the fossil Adriatic margin of the Alpine Tethys preserved in NW Italy. *Tectonics, 34,* 1927-1951.

Bill, M., O'Dogherty, L., Guex, J., Baumgartner, P.O., & Masson, H. (2001). Radiolarite ages in Alpine-Mediterranean Ophiolites; constrains on the oceanic spreading and the Tethys-Atlantic connection. *Geological Society of America Bulletin*, 113, 129-143.

Biteau, J.J., Le Marrec, A., Le Vot, M., Masset, J.M. (2006). The Aquitaine Basin. *Petroleum Geoscience, 12,* 247-273.

Biteau, J.J. and Canérot, J. (2007). La chaîne des Pyrénées et ses avants-pays d'Aquitaine et de l'Ebre: caractéristiques structurales, evolution géodynamique et tectono-sédimentaire. *Géologues*, *155*, 16-28.

Boillot, G., E. L. Winterer, and A. W. Meyer (1988), *Proceedings of the Ocean Drilling Program, 103 Initial Reports*, Proceedings of the Ocean Drilling Program, edited by G. Boillot, E. L. Winterer, and A. W. Meyer, Ocean Drilling Program.

Boirie, J.M. and Souquet, P. (1982). Les poudingues de Mendibelza: dépôs de cônes sous-marins du rift Albien des Pyrénées. *Bulletin des Centres de Recherches Exploration Production Elf Aquitaine*, *6(2),* 405-435.

Bois, C., Gariel, O., Lefort, J.P., Rolet, J., Brunet, M.F., Masse, P., Olivet, J.L. (1997). Geologic contribution of the Bay of Biscay deep seismic survey: a summary of the main scientific results, a discussion of the open questions and suggestions for further investigations. *Société Géologique de France Mémoires, 171*, 193-209.

Bois, C., and Gariel, O. (1994). Deep seismic investigation in the Parentis Basin (Southwestern France). In: Hydrocarbon and Petroleum Geology of France, *Special Publication of the European Association of Petroleum Geoscience, 4,* edited by A. Mascle, pp. 173–186.

Boulvais, P., de Parseval, P., D'Hulst, A., Paris, P. (2006). Carbonate alteration associated with talc-chlorite mineralization in the eastern Pyrenees, with emphasis on the St. Barthelemy Massif. *Mineralogy and Petrology, 88*, 499-526.

Boulvais, P., Ruffet, G., Cornichet, J., Mermet, M. (2007). Cretaceous albitization and dequartzification of Hercynian peraluminous granite in the Salvezines Massif (French Pyrenees). *Lithos, 93,* 89-106.

Breitenbach, S.F.M., & Bernasconi, S.M. (2011). Carbon and oxygen isotope analysis of small carbonate samples (20 to 100 μg) with a GasBench II preparation device. *Rapid Communications in Mass Spectrometry, 25*, 1910-1914.

B.R.G.M., Esso, Snpa (1974). Géologie du bassin d'Aquitaine. Orléans, France

Brunet, M.F. (1984). Subsidence history of the Aquitaine basin determined from subsidence curves. *Geological Magazine, 121*, 421-428.

Brunet, M.F. and Boillot, G. (1991). Subsidence et géodynamique du basin d'Aquitaine. Relations avec l'ouverture de l'Atlantique. Thèse d'Etat, Université de Paris 6, Paris, France.

Burg, J.P., Van-Den-Driessche, J., Brun, J.P. (1994a). Syn- to post-thickening extension: Modes and structural consequences. *Compte Rendus de l'Académie des Sciences, 319,* 1019-1032.

Burg, J.P., Van-Den-Driessche, J., Brun, J.P. (1994b). Syn- to post-thickening extension in the Variscan Belt of western Europe: Modes and structural consequences. *Geologie de la France, 3,* 33-51.

Burlini, L., Kunze, K. (2000). Fabric and seismic properties of Carrara marble mylonite. *Physics and Chemistry of the Earth, 25,*133-139.

Campbell, A., Palmer, M.R., Klinkhammer, G.P., Bowers, T.S., Edmond, J.M., Lawrence, J.R., Casey, J.F., Thompson, G., Humphris, S., Rona, P., Karson, J.A. (1988). Chemistry of hot springs on the Mid-Atlantic Ridge. *Nature, 335,* 514-519.

Canérot, J. (1989). Rifting éocrétacé et halocinèse sur la marge ibérique des Pyrénées Occidentales (France). Conséquences structurales. *Bulletin des Centres de Recherches Exploration Production Elf Aquitaine, 13,* 87-99.

Canérot, J. (2008). Les Pyrénées—Histoire Géologique. Atlantica, BRGM (Eds.), pp. 516.

Canérot, J. and Delavaux, F. (1986). Tectonique et se´dimentation sur la marge nord-ibe´rique des chaıˆnons be´arnais (Pyrénées basco-béarnaises). Remise en question de la signification des lherzolites du sommet de Saraillé. *Compte Rendu de l'Académie des Sciences*, *302*, 951-956.

Canérot, J., Peybernès, B., Ciszak, R. (1978). Présence d'une marge méridionale à l'emplacement de la zone des Chaînons béarnaise (Pyrénées basco-béarnaises). *Bulletin de la Société Geologique de France, 5*, 673-676.

Canérot, J., Villien, A., Lenoble, L. (1990) Sequence stratigraphy and sedimentary unconformities: western Pyrenees (field data) and southern Aquitanian basin (subsurface data): examples. *Bulletin de la Société Géologique de France, 8,* 995-1000.

Canérot, J., Majeste-Menjoulas, C., Ternet, Y., James, V., Fabre, R., Desrumaux, C., Lebourg, T. (2001). Les glissements rocheux du versant sud du Layens (Vallée d'Aspe, Pyrénées occidentales). *Bulletin de la Société Géologique de France, 172,* 779-.784

Cannat, M., Manatschal, G., Sauter D., & Peron-Pinvidic, G. (2009). Assessing the conditions of continental breakup at magma-poor rifted margins: What can

we learn from slow spreading mid-ocean ridges? *Compte Rendus Geoscience, 341*, 406-427.

Cassou, A.-M. (1968). La formation des ‘‘marnes de Sainte-Suzanne’’ et ses faciès latéraux en Aquitaine Occidentale. Essai de zonation et de datation. *Centres de Recherches Exploration Production Elf Aquitaine, 2,* 263-281.

Casteras, M. (1969). Geological map sheet of Mauléon-Licharre, 1/80000. *Bureau de Recherche Géologique et Minières,* Orléans, France.

Casteras, M., Canérot, J., Paris, J.P., Tisin, D., Azambre, B., Alimen, H. (1970a). Feuille d’Oloron Sainte Marie (1051). Carte géologique de France au 1/50 000, Orléans, France.

Casteras, M., Godechot, Y., Villanova, M. (1970b). Feuille de Lourdes (1052), Carte géologique de la France 1/50,000. *Bureau de Recherche Géologique et Minières*, Orléans, France.

Casteras, M., Gottis, M., Clin, M., Guignard, J.D., Paris, J.P., Galharague, J., Frey, M. (1971). Feuille de Tardets Sorholus. Carte Géologique de France au 1/50 000, Orléans, France.

Choukroune, P. and ECORS Team (1989). The ECORS Pyrenean deep seismic profile reflection data and the overall structure of an orogenic belt. *Tectonics, 8,* 23-39, doi:10.1029/TC008i001p00023.

Choukroune, P. and Mattauer, M. (1978). Tectonique des plaques et Pyrénées: Sur le fonctionnement de la faille transformante nord-pyrénéenne; comparaisons avec des modèles actuels. *Bulletin de la Société Géologique de France, 7,* 689-700.

Claude, D. (1990). Etude stratigraphique, sédimentologique et structural des dépôts mésozoïques au Nord du massif du Labourd. Rôle de la faille de Pamplona (Pays Basque). PhD thesis, Université de Bordeaux III, pp. 252.

Clerc, C., Lagabrielle, Y., Neumaier, M., Reynaud, J-Y., de Saint Blanquat, M. (2012). Exhumation of subcontinental mantle rocks: evidence from ultramafic-bearing clastic deposits nearby the Lherz peridotite body, French Pyrenees. *Bulletin de la Société Géologique de France, 183(5),* 443-459.

Clerc, C. and Lagabrielle, Y. (2014). Thermal control on the modes of crustal thinning leading to mantle exhumation. Insights from the Cretaceous Pyrenean hot paleomargins, *Tectonics*, *33*, 1340-1359, doi:10.1002/2013TC003471.

Clayton, R.N., Friedman, I., Graf, D.L., Mayeda, T.K., Meents, W.F., & Shimps, N.F. (1966). The origin of saline formation waters: Isotopic composition. *Journal of Geophysyc Research, 71*, 3869-3882.

Cohen, K.M., Finney, S.C., Gibbard, P.L., Fan, J.X. (2013; updated). The ICS International Chronostratigraphic Chart. Episodes 36, 199-204.

Contrucci, I., Matias, L., Moulin, M., Géli, L., Klingelhoefer, F., Nouzé, H. et al. (2004). Deep structure of the west African continental margin (Congo, Zaire, Angola), between 5°S and 8°S, from reflection/refraction seismic and gravity data. *Geophysical Journal International, 158*, 529-553.

Cornelius, H.P. (1932). Geologische Karte der Err-Juliergruppe 1:25000. *Schweiz. Geologische Kommunikation, Spezialkarte 115A*.

Cornelius, H.P. (1935). Geologie der Err-Julier gruppe: Das baumaterial (stratigraphie und petrographie, excl. quartär). *Beitrage. Geologischen Karte Schweiz NF, 70(1),* 1-321.

Curnelle, R. (1983). Evolution structuro-sédimentaire du Trias et de l'infra-Lias d'Aquitaine. *Bulletin des Centres de Recherches Exploration Production Elf Aquitaine, 7,* 69-99.

Dählmann, A., & de Lange, G.J. (2003). Fluid-sediment interactions at Eastern Mediterranean mud volcanoes: a stable isotope study from ODP Leg 160. *Earth and Planetary Science Letters, 212*, 377-391.

Daignières, M., Seguret, M., Specht, M., Team E (1994). The Arzacq-Western Pyrenees ECORS deep seismic profile. *Publ European Association of Petroleum Geology Memories, 4,* 199-208.

De Baar, H.J.W., Bacon, M.P., Brewer, P.G. (1985). Rare earth elements in the Pacific and Atlantic Oceans. *Geochimica et Cosmochimica Acta, 49,* 1943-1959.

Debroas, E.J., Canérot, J., Billote, M. (2010). Les brèches d'Urdach, témoins de l'exhumation du manteau pyrénéen dans un escarpement de faille vraconien-cénomanien inférieur (Zone Nord Pyrénéenne, Pyrénées Atlantiques, France). *Géologie de France, 2,* 53-65.

Demény A. (1995). H isotope fractionation due to hydrogen-zinc reactions and its implications on D/H analysis of water samples. *Chemical Geology, 121 (1/4)*, 19–25.

Demény A. and Siklósy Z. (2008). Combination of off-line preparation and continuous flow mass spectrometry: D/H analyses of inclusion waters. *Rapid Communications in Mass Spectrometry*, 22, 1329–1334.

Déramond, J., Souquet, P., Fondecave-Wallez, M.-J., Specht, M. (1993). Relationships between thrust tectonics and sequence stratigraphy surfaces in foredeeps: Model and examples from the Pyrenees (Cretaceous-Eocene, France, Spain). *Geological Society London Special Publications, 71(1),* 193–219, doi:10.1144/GSL.SP.1993.071.01.09.

Desmurs, L., Manatschal, G., Bernoulli, D. (2001). The Steinmann Trinity revisited: mantle exhumation and magmatism along an ocean-continent transition: the Platta nappe, eatern Switzerland. *Geological Society London Special Publications, 187(1),* 235-266.

Demurs, L., Fudral, S., Lagabrielle, Y., Marthaler, M., Sartori, M. (2002). Onset of magmatic accretion within a magma-poor rifted margin: a case study from the Platta ocean-continent transition, eastern Switzerland. *Contributions to Mineralogy and Petrology, 144,* 365-382.

Dietrich, V. (1969). Die ophilithe des Oberhalbsteins (Graubünden) und das Ophiolithmaterial der ostschweizrischen Molasseablagerungen, ein petrgraphisher Verleig. Europäisch Hochschul-Schriften, 17 Verlag Herbert, Bern, 179.

Dommergues, J., Meister C., & Manatschal, G. (2012). Early Jurassic ammonites from Bivio (Lower Austroalpine unit) and Ardez (Middle Penninic unit) areas: a biostratigraphic tool to date the rifting in the Eastern Swiss Alps. *Revue de Paléobiologie, Genève, Vol. spéc. 11*, 43-52.

Douville, E., Bienvenu, P., Charlou, J.L., Donval, J.P., Fouquet, Y., Appriou, P., Gamo, T. (1999). Yttrium and rare earth elements in fluids from various deep-sea hydrothermal systems. *Geochimica et Cosmochimica Acta, 63,* 627-643.

Ducasse, L., Vélasque, P. (1986a). Glissement de couverture et panneaux basculés dans la région des Arbailles (Pyrénées occidentales): un modèle évolution crétacé de la marge nord-ibérique à l'Est de la transformante de Pamplona. *Compte Rendu de l'Académie des Sciences, 303(16),* 1477-1482.

Ducasse, L., Vélasque, P.C. (1986b). Tectonique et sédimentation dans la couverture des Pyrénées occidentale (Haute Soule). Arguments en faveur de la plaque ibérique sous la plaque européenne. *Compte Rendu de l'Académie des Sciences, 302(16),* 1027-1032.

Ducasse, L., Velasque, P.C. (1988). Géotraverse dans la partie occidentale des pyrénées de l'avant-pays aquitain au bassin de l'Ebre. Effet d'une inversion structurale sur l'édification d'une chaîne intracontinentale. PhD thesis, Université d'Aix-Marseille, Aix-en-Provence, France.

Eberli, G.P. (1987). Carbonate turbidite sequences deposited in rift-basins of the Jurassic Tethys ocean (eastern Alps, Switzerland). *Sedimentology, 34,* 363-388.

Eberli, G. (1988). The evolution of the southern continental margin of the Jurassic Tethys Ocean as recorded in the Allgäu Formation of the Austroalpine

Nappes of Graubünden (Switzerland). *Eclogae Geologicae Helvetiae., 81(1),* 175-214.

Edmonds, H.N. (2010). Chemical signature from hydrothermal venting on slow spreading ridges. In: Diversity of Hydrothermal Systems on Slow Spreading Ocean Ridges, vol. 188, pp. 27-42. AGU, Washington DC.

Elderfield, H. (1988). The oceanic chemistry of rare-earth elements. *Philolophical Transactions of the Royal Society of London, A325,* 105-126.

Elderfield, H. and Greaves M.J. (1982). The rare earth elements in seawater. *Nature, 296,* 214-219.

Esquevin, J., Fournie, P., de Lestang, J. (1971). Les séries de l'Aptien et de l'Albien des régions nord-pyrénéennes et sud-aquitaines (France Sud). *Bulletin des Centres de Recherches Exploration Production Elf Aquitaine, 5,* 87–151.

Fabriès, J., Lorand, J.P., Bodinier, J.L. (1998). Petrogenetic evolution of orogenic lherzolite massifs in the central and western Pyrenees. *Tectonophysics, 292,* 145-167.

Fallourd, S., Poujol, M., Boulvais, P., Paquette, J.-L., de Saint Blanquat, M., Remy, P. (2014). In situ LA-ICP-MS U–Pb titanite dating of Na–Ca metasomatism in orogenic belts: the North Pyrenean example. *International Journal of Earth Science. 103*, 667-682.

Feng, D., Chen, D., Peckmann, J. (2008). Rare earth elements in seep carbonates as tracers of variable redox conditions at ancient hydrocarbon seeps. *Terra Nova, 21,* 49-56.

Feng, D., Chen, D., Peckmann, J., Bohrmann, G. (2009). Authigenic carbonates from methane seeps of the northern Congo fan: microbial formation mechanism. *Marine and Petroleum Geology*. DOI:10.1016/j.marpetgeo.2009.08.006.

Ferreiro-Mählmann, R. (2001). The pattern of diagenesis and metamorphism by vitrinite reflectance and illite "crystallinity" in Mittelbünden and in the

Oberhalbstein: Part 2: Correlation of coal petrographical and of mineralogical parameters. *Schweizerische Mineralogishce und Petrographische Mitteilungen, 76,* 23-46.

Filleaudeau, P.Y., Mouthereau, F., Pik, R. (2012). Thermo-tectonic evolution of the south-central Pyrenees from rifting to orogeny: insights from detrital zircon U/Pb and (U-Th)/He thermochronometry. *Basin Research, 24*, 401-417.

Finger, W. (1978). Die Zone von Samedan (unterostalpine Decken, Graubünden) und ihre jurassischen Brekzien, PhD thesis, ETH Zürich, Zürich, doi:10.3929/ethz-a-000164017.

Fortane, A., Duée, G., Lagabrielle, Y., Coutelle, A. (1986). Lherzolites and the western ‘‘chaînons Béarnais’’ (French Pyrenees): Structural and paleogeographical pattern. *Tectonophysics, 129*, 81-98. doi:10.1016/0040-1951(86)90247-7.

Fouquet, Y., Von Stackelber, U., Charlou, J.L., Erzinger, J., Herzig, P.M., Mühe, R., Wiedicke, M. (1993). Metallogenesis in Back-Arc Environments: The Lau Basin example. *Economic Geology, 88,* 2154-2181.

Fréchengues, M. (1993). Stratigraphie séquentielle et micropaléontologie du Trias moyen-supérieur des Pyrénées franco-espagnoles. PhD thesis, Université de Toulouse 3, Toulouse, France.

Froitzheim, N. (1988). Synsedimentary and synorogenic normal faults within a thrust sheet of the Eastern Alps (Ortler zone, Graubünden, Switzerland). *Eclogae Geologicae Helvetiae, 81(3),* 593-610.

Froitzheim, N., and Eberli, G.P. (1990). Extensional detachment faulting in the evolution of a Tethys passive continental margin, Eastern Alps, Switzerland. *Geological Society of America Bullettin, 102(9)*, 1297-1308.

Froitzheim, N., Schmid, S.M., Conti, P. (1994). Repeated change from crustal shortening to orogenparallel extension in the Austroalpine units of Graubünden. *Eclogae Geologicae Helvetiae, 87(2),* 559-612.

Froitzheim, N., and Manatschal G. (1996). Kinematics of Jurassic rifting, mantle exhumation, and passive-margin formation in the Austroalpine and Penninic nappes (eastern Switzerland). *Geological Society of America Bulletin, 108*, 1120-1133.

Furrer, H. (1981). Stratigraphie und Fazies der Trias-Jura-Grenzschichten in den oberostalpinen Decken Graubündens. *Ph.D. dissertation*, Univ. Zürich, Zürich.

Gerdes, A. and Zeh, A. (2006) Combined U-Pb and Hf isotope LA-(MC-) ICP-MS analyses of detrital zircons: Comparison with SHRIMP and new constraints for the provenance and age of an Armorican metasediment in Central Germany. *Earth and Planetary Science Letters, 249,* 47-62.

Gerdes, A. and Zeh, A. (2009). Zircon formation versus zircon alteration – New insights from combined U-Pb and Lu-Hf in-situ La-ICP-MS analyses of Archean zircons from the Limpopo Belt. *Chemical Geology 261 (3-4)*, 230-243.

Goldstein, R.H., & Reynolds, T.J. (1994). Systematics of Fluid Inclusions in Diagenetic Minerals. SEPM Short Course 31, Tulsa, 199 pp.

Gong, Z., Langereis, C.G., Mullender, T.A.T. (2008). The rotation of Iberia during the Aptian and the opening of the Bay of Biscay. *Earth and Planetary Science Letters, 273,* 80–93, doi:10.1016/j.epsl.2008.06.016.

Govindaraju, K. (1989). Compilation of working values and sample description for 272 geostandards. *Geostandards Newsletter, 13,* 1-113.

Haeri-Ardakani, O., Al-Aasm, I., & Coniglio, M. (2013). Fracture mineralization and fluid flow evolution: an example from Ordovician-Devonian carbonates, southwestern Ontario, Canada. *Geofluids, 13*, 1-20.

Hall, D.L., Cohen, L.H., Schiffman, P. (1988). Hydrothermal alteration associated with the Iron Hat iron skarn deposit, eastern Mojave Desert, San Bernardino, California. *Economic Geology, 83,* 568-587.

Handy, M.R. (1996). The transition from passive to active margin tectonics; a case study from the zone of Samedan (Eastern Switzerland). *Geologische Rundschau, 85 (3)*, 832-851.

Handy, M.R., Herwegh, M., & Regli, C. (1993). Tektonische Entwicklung Der Westlichen Zone Von Samedan (Oberhalbstein, Graubünden, Schweiz). *Eclogae Geologicae Helvetiae, 86*, 785-817.

Heddebaut, C. (1973). Etudes géologiques dans les massifs Paléozoïques Basques. PhD thesis, Université des Sciences et Techniques de Lille, Lille, France.

Hendry, J.P., Pearson, M.J., Trewin, N.H., Fallick, A.E. (2006). Jurassic septarian concretions from NW Scotland record interdependent bacterial, physical and chemical processes of marine mudrock diagenesis. *Sedimentology, 53,* 537-565.

Hensen, C., Nuzzo, M., Hornibrook, E., Pinheiro, L., Bock, B., Magalhaes, V., & Bruckmann, W. (2007). Sources of mud volcano fluids in the Gulf of Cadiz-indications for hydrothermal imprint. *Geochimica et Cosmochimica Acta, 71*, 1232-1248.

Himmler, T., Bach, W., Bohrmann, G., Peckmann, J. (2010). Rare earth elements in authigenic methane-seep carbonates as tracers for fluid composition during early diagenesis. *Chemical Geology, 277,* 126-136.

Hitchon, B., Bachu, S., & Underschulz, J.R. (1990). Regional subsurface hydrogeology, Peace River area, Alberta and British Columbia. *Bulletin of Canadian Petroleum Geology, 38*, 196-217.

Horita, J. (2014). Oxygen and carbon isotope fractionation in the system dolomite-water-CO_2 to elevated temperatures. *Geochimica et Cosmochimica Acta, 129*, 111-124.

Hounslow, M.W. (1997). Significance of localized pore pressures to the genesis of septarian concretions. *Sedimentology, 44,* 1133-1147.

Hu, X., Wang, Y.L., Schmitt, R.A. (1988). Geochemistry of sediments on the Rio Grande Rise and the redox evolution of the South Atlantic Ocean. *Geochimica et Cosmochimica Acta, 52,* 201-207.

Incerpi, N., Martire, L., Manatschal, G., Bernasconi, S. (2017). Evidence of hydrothermal fluid flow in a hyperextended rifted margin: the case study of the Err nappe (SE Switzerland). *Swiss Journal of Geosciences*. DOI: 10.1007/s00015-016-0235-2.

James, R.H., Elderfield, H., Palmer, M.R. (1995). The chemistry of hydrothermal fluids from the Broken Spur site, 29°N Mid-Atlantic Ridge. *Geochimica et Cosmochimica Acta, 59(4),* 651-659.

James, V. and Canérot, J. (1999). Diapirisme et structuration post-triasique des Pyrénées occidentales et de l'Aquitaine méridionales (France). *Eclogae Geologicae Helvetiae, 92,* 63-72.

James, V., Canérot, J., Biteau, J.J. (1996). Données nouvelles sur la phase de rifting atlantique des Pyrénées occidentales au Kimméridgien. *Géolie de France, 3,* 66.

Jammes, S., Manatschal, G., Lavier, L., Masini, E. (2009). Tectono-sedimentary evolution related to extreme crustal thinning ahead of a propagating ocean; example of the western Pyrenees. *Tectonics 28* (TC4012).

Jammes, S., Lavier, L.L., Manatschal, G. (2010a). Extreme crustal thinning in the Bay of Biscay and the Western Pyrenees: from observations to modeling. G3 11.

Jammes, S., Manatschal, G., Lavier, L.L. (2010b). Interaction between prerift salt and detachment faulting in hyperextended rift systems: the example of the Parentis and Mauléon basins (Bay of Biscay and western Pyrenees). *American Association of Petroleum Geologist Bulletin, 94(7),* 957-975.

Jochum, K.P., Seufert, H.M., Spettel, B., Palme, H. (1986). The solar\-system abundances of Nb, Ta, Y, and the relative abundances of refractory lithophile

elements in differentiated planetary bodies. *Geochimica et Cosmochimica Acta, 50,* 1173-1183.

Johnson, J.A. and Hall, C.A. (1989a). The structural and sedimentary evolution of the Cretaceous North Pyrenean Basin, southern France. *Geological Society of America Bulletin, 101,* 231-247.

Johnson, J.A. and Hall, C.A. (1989b). Tectono-stratigraphic model for the massif d'Igountze-Mendibelza, western Pyrenees. *Journal of the Geological Society of London, 146,* 925-932.

Karner, G.D., & Driscoll, N.W. (2000). Style, timing and distribution of tectonic deformation across the Exmouth Plateau, northwest Australia, determined from stratal architecture and quantitative basin modeling. *Geological Society of London Special Pubblication, 164*, 271-311.

Kastner, M. (1971). Authigenic feldspars in carbonate rocks. *American Mineralogy, 56,* 1403-1442.

Kastner, M. and Siever, R. (1979). Low temperature feldspars in sedimentary rocks. *American Journal of Science, 279,* 435-479.

Kelley, D.S., Karson, J.A., Blackman, D.K., Fruh-Green, G.L., Butterfield, D.A., Lilley, M.D., Olson, E.J., Schrenk, M.O., Roe, K.K., Lebon, G.T., Rivizzigno, P., AT3-60 Shipboard Party (2001). An off-axis hydrothermal vent field near the Mid.Atlantic Ridge at 30°N. *Nature, 412,* 145-149.

Kelley, D.S. and Shank, T.M. (2010). Hydrothermal systems: A decade of discovery in slow spreading envirnments. In: Discovery of Hydrothermal Systems on Slow Spreading Ocean Ridges, col. 188, pp. 369-407, AGU, Washington DC.

Klinkhammer, G.P., Chin, C.S., Wilson, C., German, C.R. (1995). Venting from the Mid-Atlantic Ridge at 37°17'N: The Lucky Strike hydrothermal site. In: Parson, L.M., Walker, C.L., Dixon, D.R. Hydrothermal Vents and Processes

(Eds.), 87, pp.87-96. *Geological Society Special Pubblication No.87,* published by The Geological Society.

Lagabrielle, Y. and Bodinier, J.L. (2008). Submarine reworking of exhumed subcontinental mantle rocks; field evidence from the Lherz peridotites, French Pyrenees. *Terra Nova, 20(1),* 11-21.

Lagabrielle, Y., Labaume, P., De Saint Blanquat, M. (2010). Mantle exhumation, crustal denudation, and gravity tectonics during Cretaceous rifting in the Pyrenean realm (SW Europe): insights from the geological setting of the lherzolite bodies. *Tectonics, 29* (TC4012).

Land, L.S. (1985). The origin of massive dolomite. *Journal of Geological Education, 33*, 112-125.

Land, L.S., & Prezbindowski, D.R. (1981). The origin and evolution of saline formation waters, Lower Cretaceous carbonates, south–central Texas and southern New Mexico. *Hydrogeology Journal, 54*, 51–74.

Le Pichon, X., Bonnin, J., Francheteau, J., Sibuet, J.C. (1970), Une hypothèse dévolution tectonique du Golfe de Gascogne, In: Histoire Structurale du Golfe de Gascogne, 1.44, Technip, Paris.

Le Pochat, G., Heddebaut, C., Lenguin, M., Lorsignol, S., Souquet, P., Muller, J., Roger P. (1978). Feuille de St Jean Pied de Port. Carte Géologique de France au 1/50 000, Orléans, France.

Lemoine, M., Bas, T., Bourbon, M., Graciansky, P.C., Rudkiewicz, J., Megard-Galli, J., Tricart, P. (1986). The continental margin of the Mesozoic Tethys in the Western Alps. *Marine and Petroleum Geology, 3,* 179-199.

Lemoine, M., Tricart, P., Boillot, G. (1987). Ultramafic and gabbroic ocean floor of the Ligurian Tethys (Alps, Corsica, Apennines): in search of a genetic model. *Geology, 15,* 622-625.

Li, C., Kank, S., Zhanq, Q., Gao, S. (2015). Geochemical evidence on the source regions of Tibetan Plateau dusts during non-monsoon period in 2008/09. *Atmospheric Environment, 59,* 382-388.

Liu, Y.G., Miah, M.R.U., Scmhitt, R.A. (1988). Cerium, a chemical tracer for paleo-oceanic redox conditions. *Geochimica et Cosmochimica Acta, 52,* 1361-1371.

Lopez-Horgue, M., Iriarte, I., Schroder, S., Fernandez-Mendiola P.A., Caline, B., Corneyllie, H., Fremont, J., Sudrie, M., Zerti, S. (2010). Structurally controlled hydrothermal dolomites in Albian carbonates of the Ason valley, Basque Cantabrian Basin, Northern Spain. *Marine and Petroleum Geology, 27,* 1069-1092.

Lüders, V., Möller, P., Dulski, P. (1993). REE fractionation in carbonates and fluorites. In: Möller, P. and Lüders, V. (Eds.). Formation of hydrothermal vein deposits. *Monograph Series on Mineral Deposits Bornträger*, Berlin, pp. 133-150.

Ludwig, K.R. (2003) Isoplot 3.0, a geochronological toolkit for Microsoft Excel. *Berkeley Geochronology Center Special Publication, 4,* 1-71. (Version 3.7, released 2009).

Machel, H.G. (2004). Concepts and models of dolomitization: a critical reappraisal. In: Braithwaite, C.J.R., Rizzi, G., Darke, G. (eds) 2004. The Geometry and Petrogenesis of Dolomite Hydrocarbon Reservoirs. *Geological Society of London, Special Publications, 235,* 7-63.

Madhavaraju, J. and Ramasamy, S. (1999). Rare earth elements in limestones of Kallankurichchi Formation of Ariyalur Group, Tiruchirapalli Cretaceous, Tamil Nadu. *Journal of the Gelogical Society of India, 54,* 291-301.

Madhavaraju, J. and Lee, Y.I. (2009). Geochemistry of the Dalmiapuram Formation of the Uttatur Group (Early Cretaceous), Cauvery basin, southeastern

India: implications on provenance and paleo-redox conditions. *Revista Mexicana de Ciencias Geologicas, 26,* 380-394.

Madhavaraju, J., Gonzalez.Leon, C.M., Lee, Y.I., Armstrong-Altrin, J.S., Reyes-Campero, L.M. (2010). Geochemistry of the Mural Formation (Aptian-Albian) of the Bisbee Group, Northern Sonora, Mexico. *Cretaceous Research, 31,* 400-414.

Manatschal, G. (1999). Fluid- and reaction-assisted low-angle normal faulting; evidence from rift-related brittle fault rocks in the Alps (Err Nappe, Eastern Switzerland). *Journal of Structural Geology, 21*, 777-793.

Manatschal, G. (2004). New models for evolution of magma-poor rifted margins based on a review of data and concepts from west Iberia and he Alps. *International Journal of Earth Sciences, 93(3),* 432-466.

Manatschal, G., & Nievergelt, P. (1997). A continent-ocean transition recorded in the Err and Platta nappes (Eastern Switzerland). *Eclogae Geologicae Helvetiae, 90*, 3-27.

Manatschal, G. and Bernoulli, D. (1998). Rifting and early evolution of ancient ocean basins: the record of the Mesozoic Tethys and of the Galicia-Newfoundland margins. *Marine Geophysical Research,* 371-381.

Manatschal, G., Marquer, D., & Frueh-Green, G.L. (2000). Channellized fluid flow and mass transfer along a rift-related detachment fault (Eastern Alps, southeast Switzerland). *Geological Society of America Bullettin, 112*, 21-33.

Manatschal, G., Müntener, O., Desmurs, L. (2003). An ancient ocean-continent transition in the Alps: the Totalp, Err-Platta, and Malenco units in the eastern Central Alps (Graubünden and northern Italy). *Eclogae Geologicae. Helvetiae 96(1),* 131-146.

Manatschal, G., Engström, A., Desmurs, L., Schaltegger, U., Cosca, M., Müntener, O., Bernoulli, D. (2006). What is the tectono-metamorphic evolution

of continental break-up: The example of the Tasna Ocean-Continent Transition. *Journal of Structural Geology, 28(10),* 1849-1869.

Manatschal, G. and Müntener, O. (2009). A type sequence across an ancient magma-poor ocean-continent transition: the example of the western Alpine Tethys ophiolites. *Tectonophysics, 473(1-2),* 4-19.

Manatschal, G., Sauter, D., Karpoff, A., Masini, E., Mohn, G., Lagabrielle, Y. (2010). The Chenaillet ophiolite in the French/Italian Alps: an ancient analogue for an ocean core complex? *Lithos.*

Marillier, F., Tomassino, A., Patriat, P., Pinet, B. (1988). Deep structure of the Aquitaine shelf: constraints from expanding spread profiles on the ECORS Bay of Biscay transect. *Marine and Petroleum Geology, 5,* 65-74.

Masini, E., Manatschal, G., Tugend, J., Mohn, G., Flament, J-M. (2014). The tectono-sedimentary evolution of a hyper-extended rift basin: the example of the Arzacq–Mauléon rift system (Western Pyrenees, SW France). *International Journal of Earth Sciences,* DOI 10.1007/s00531-014-1023-8.

Masini, E., Manatschal, G., Mohn, G., Ghienne, J.F., & Lafont, F. (2011). The tectono-sedimentary evolution of a supra-detachment rift basin at a deep-water magma-poor rifted margin: the example of the Samedan Basin preserved in the Err nappe in SE Switzerland. *Basin Research, 23*, 652-677.

Masini, E., Manatschal, G., Geoffroy, M., & Unternehr, P. (2012). Anatomy and tectono-sedimentary evolution of a rift-related detachment system: The example of the Err detachment (central Alps, SE Switzerland). *Geological Society of American Bulletin, 124*, 1535-1551.

Masini, E., Manatschal, G., Mohn, G., Unternehr, P. (2013). The Alpine Tethys rifted margins: Reconciling old and new ideas to understand the stratigraphic architecture of magma-poor rifted margins. *Sedimentology, 60(1),* 174-196.

Masuzawa, T. and Koyama, M. (1989). Settling particles with positive Ce anomalies from the Japan Sea. *Geophyscal Research Letters, 16,* 503-506.

Mattauer, M. and Choukroune P. (1974). Les lherzolites des Pyrénées sont des extrusions de matériel ancien dans le Mésozoïque nord Pyrénées, paper presented at 2nd Réunion Annuelle des Sciences de la Terre, Société Géologique de France, Paris.

McArthur, J.M., Howarth, R.J., & Shields, G.A. (2012). Strontium Isotope Stratigraphy. In: Gradstein F.M., Ogg J.G., Schmitz M., Ogg G. (Eds.), *The Geologic Time Scale 2012*, 127-144, Elsevier.

McCaig, A.M.R., Cliff, J., Escartin, A., Fallick, E., MacLeod, C.J. (2007). Oceanic detachment faults focus very large volumes of black smoker fluids. *Geology, 35(10),* 935.

McKenzie, J.A. (1979). Holocene dolomitization of calcium carbonate sediments from the coastal sabkhas of Abu Dhabi, UAE: a stable isotope study. *Jour. Geol., 89*, 185-198.

McKenzie, J.A. (1991). The dolomite problem: an outstanding controversy. In: Muller, D.W., McKenzie, J.A., Weissert, H. (Eds.). Controversies in modern geology: evolution of geological theories in sedimentology. *Academic Press*, Londo, 37-54.

McLelland, J., Morrison, J., Selleck, B., Cunningham, B., Olson, C., Schmidt, K. (2002). Hydrothermal alteration of late- to post-tectonic Lyon Mountain Granitic Gneiss, AdirondackMountains, New York: Origin of quartz–sillimanite segregations, quartz–albite lithologies, and associated Kiruna-type low-Ti Fe-oxide deposits. *Journal of metamorphic Geology 20,* 175-190.

McLennan, S.M. (1989). Rare earth elements in sedimentary rocks: influence of provenance and sedimentary processes. In: Lipin, B.R. and McKay, G.A. (Eds.). Geochemistry and Mineralogy of Rare Earth Elements. *Review in Mineralogy*, pp. 1209-1264.

Meister, P., Mckenzie, J.A., Bernasconi, S.M. (2013). Dolomite formation in the shallow seas of the Alpine Triassic. *Sedimentology, 60,* 270-291.

Michard, A., Albaréde, F., Michard, G., Minster, J.F., Charlou, J.L. (1983). Rare-earth elements and uranium in high-temperature solutions from East Pacific Rise hydrothermal vent field (13°N). *Nature, 303,* 795-797.

Michard, A. and Albaréde, F. (1986). The REE content of some hydrothermal fluids. *Chemical Geology, 55,* 51-60.

Mitra, A. (1991). Rare earth element systematics of submarine hydrothermal fluids and plumes. PhD thesis. Univ. Cambridge, 119 pp.

Mitra, A., Elderfield, H., Greaves, M.J. (1994). Rare earth elements in submarine hydrothermal fluids and plumes from the Mid-Atlantic Ridge. *Marine Chemistry, 47,* 217-236.

Mohn, G., Manatschal, G., Müntener, O., Beltrando, M., & Masini, E. (2010). Unraveling the interaction between tectonic and sedimentary processes during lithospheric thinning in the Alpine Tethys margins. *International Journal of Earth Sciences, 99*, 75-101.

Mohn, G., Manatschal, G., Masini, E. (2011). Rift-related inheritance in orogens: a case study from the Austroalpine nappes in Central Alps (SE-Switzerland and N-Italy). *International Journal of Earth Sciences, 100(5),* 937-961.

Mohn, G., Manatschal, G., Beltrando, M., Masini, E., Kusznir, N. (2012). Necking of continental crust in magma-poor rifted margins: Evidence from the fossil Alpine Tethys margins. *Tectonics, 31(1),* TC1012, DOI: 10.1029/2011TC002961.

Montigny, R., Azambre, B., Rossy, M., Thuizat, R. (1986). K-Ar study of Cretaceous magmatism and metamorphism from Pyrenees; age and length of rotation of the iberian peninsula. *Tectonophysics, 129,* 257-274.

Morrow, D.W. (1982). Descriptive field classification of sedimentary and diagenetic breccias fabrics in carbonate rocks. *Bulletin of Canadian Petroleum Geology, 30*, 227-229.

Moulin, M., Aslanian, D., Olivet, J.L., Contrucci, I., Matias, L., Géli, L. et al. (2005). Geological constraints on the evolution of the Angolan margin based on reflection and refraction seismic data (ZaiAngo project). *Geophysical Journal International, 162*, 793-810.

Mouthereau, F., Filleaudeau, P.Y., Vacherat, A., Pik, R., Lacombe, O., Fellin, M.G., Castelltort, S., Christophoul, F., Masini, E. (2014). Placing limits to shortening evolution in the Pyrenees: role of margin architecture and implications for theIberia/Europe convergence. *Tectonics, 33*, 2283-2314.

Mulder, T., Zaragosi, S., Razin, P., Grelaud, C., Lanfumey, V., Bavoil, F. (2009). A new conceptual model for the deposition process of homogenite: application to a cretaceous megaturbidite of the western Pyrenees (Basque region, SW France). *Sedimentary Geology, 222,* 263-273.

Muñoz, J.A. (1992). Evolution of a continental collision belt: ECORS-Pyrenees crustal balanced section. In: McClay, K.R. (Eds.) Thrust tectonics. Chapman and Hall, London, pp. 235–246.

Müntener, O., Pettke, T., Desmurs, L., Meier, M., Schaltegger, U. (2004). Refertilization of mantle peridotite in embryonic ocean basins: trace element and Nd isotopic evidence and implications for crust-mantle relationships. *Earth and Planetary Science Letters, 221,* 293-308.

Nath, B.N. Bau, M., Ramalingeswara, R.B., Rao C.M. (1997). Trace and rare earth elemental variation in Araban Sea sediments through a transect across the oxygen minimum zone. *Geochimica et Cosmochimica Acta, 61,* 2375-2388.

Nonn, C. (2012). Architecture d'un système hyper-étiré: l'example des Chaînons Béarnais (bassins de Mauléon-Lourdes, Pyrénées). Master Thesis, Université de Strasbourg, Strasbourg, France

Oliver, N.H.S. (1995). Hydrothermal history of the Mary Kathleen Fold Belt, Mt Isa Block, Queensland. *Australian Journal of Earth Sciences, 42*, 267-279.

Olivet, J.L. (1996). La cinématique de la plaque Ibérique. *Bulletin des Centres de Recherches Exploration Production Elf Aquitaine, 20 (1),* 131-195.

Papp L., Palcsu L., Major Z., Rinyu L. and Tóth I. (2012). Noble gas measurements from different water amounts - from microlitres to millilitres and litres. *Isotopes Environmental Health Studies, 48(4)*, 494-511. doi:10.1080/10256016.2012.679935.

Pedreira, D., Pulgar, J.A., Gallart, J., Torné, M. (2007). Three-dimensional gravity and magnetic modeling of crustal indentation and wedging in the western Pyrenees–Cantabrian Mountains. *Journal of Geophysical Research, 112*. doi:10.1029/2007JB005021.

Peron-Pinvidic, G., & Manatschal G. (2008). The final rifting evolution at deep magma-poor passive margins from Iberia-Newfoundland: a new point of view. *International Journal of Earth Sciences, 98*, 1581-1597.

Piepgras, D.J. and Jacobsen, S.B. (1992). The behavior of rare earth elements in seawater: Precise determination of variations in the North Pacific water column *Geochimica et Cosmochimica Acta, 56,* 1851-1862.

Pinet, B., Montadert, L., Curnelle, R., Cazes, M., Marillier, F., Rolet, J., Tomassino, A., Galdeano, A., Patriat, P., Brunet, M.F., Olivet, J.L., Schaming, M., Lefort, J.P., Arrieta, A., Riaza, C. (1987). Crustal thinning on the Aquitaine shelf, Bay of Biscay, from deep seismic data. *Nature, 325,* 513-516.

Pinto, V.H., Manatschal, G., Karpoff, A.M., & Viana, A. (2015). Tracing mantle-reacted fluids in magma-poor rifted margin: The example of Alpine Tethyan rifted margin. *Geochemistry, Geophysics, Geosystems, 16*, 3271-3308.

Plank, T. and Langmuir, C.H. (1998). The chemical composition of subducting sediment and its consequences for the crust and mantle. *Chemical Geology, 145,* 325-394.

Poujol, M., Boulvais, P., Kosler, J. (2010). In-situ LA–ICP–MS U–Th–Pb dating of metasomatic fluid circulation: Evidence of regional-scale albitization in the Pyrenees. *Journal of the Geological Society, 167,* 751-767.

Pratt, B.R. (2001). Septarian concretions: internal cracking caused by synsedimentary earthquakes. *Sedimentology, 48,* 189-213.

Puigdefàbregas, C. and Souquet, P. (1986). Tecto-sedimentary cycles and depositional sequences of the Mesozoic and Tertiary from the Pyrenees. *Tectonophysics, 129,* 173-203.

Purser, B.H., Tucker, M.E. and Zenger, D.H. (1994). Dolomites - A Volume in Honour of Dolomieu. *International Association of Sedimentologists, Special Publications, 21.*

Rais, P., Louis-Schmid, B., Bernasconi, S.M., Reusser, E., Weissert, H. (2008). distribution of authigenic albites in a limestone succession of the Helvetic Domain, eastern Switzerland. *Swiss Journal of Geosciences, 101,* 99-106.

Raiswell, R. (1971). The growth of Cambrian and Liassic concretions. *Sedimentology, 17,* 147-171.

Rankenburg, K., Lassiter, J.C., Brey, G. (2004). Origin of megacrysts in volcanic rocks of the Cameroon volacanic chain - constraints on magma genesis and crustal contamination. *Contribution to Mineralogy and Petrology, 147(2),* 129-144.

Rasbury, E.T. and Cole, J.M. (2009). Directly dating geological events: U-Pb dating of carbonates. *Reviews of Geophysics, 43(3),* RG3001, doi:10.1029/2007RG000246.

Razin, P. (1989). Evolution tecto-sédimentaire alpine des Pyrénées basques à l'Ouest de la transformante de Pampelona. PhD thesis, Université de Bordeaux, Bordeaux, France.

Richter, D.K., Götte, T., Habermann, D. (2002). Cathodoluminescence of authigenic albite. *Sedimentary Geology, 150,* 367-374.

Ring, U. and Gerdes, A. (2016). Kinematics of the Alpenrhein-Bodensee graben system in the Central Alps: Oligocene/Miocene transtension due to formation of the Western Alps arc. *Tectonics, 35(6),* 1367-1394.

Roca, E., Muñoz, J.A., Ferrer, O., Ellouz, N. (2011). The role of the Bay of Biscay Mesozoic extensional structure in the configuration of the Pyrenean orogen: constraints from the MARCONI deep seismic reflection survey. *Tectonics, 30* (TC2001).

Rosenbaum, J., & Sheppard, S.M. (1986). An isotopic study of siderites, dolomites and ankerites at high temperatures. *Geochimica et Cosmochimica Acta, 50*, 1147-1150.

Rossi, P., Cocherie, A., Mark Fanning, C., Ternet, Y. (2003). Datation U-Pb sur zircons des dolarites tholéïtiques pyrénéennes (ophites) à la limite Trias-Jurassique et relation avec les tufs volcaniques dits “infra-liasiques” nord-pyrénéens. *Compte Rendu Géosciences, 335,* 1071-1080.

Roure, F. and Choukroune, P. (1998). Contribution of the ECORS seismic data to the Pyrenean geology: Crustal architecture and geodynamic evolution of the Pyrenees. *Memoires Société Geologique de France, 173,* 37-52.

Salardon, R., Carpentier, C., Bellahsen, N., Pironon, J., France-Lanord, C. (2017). Interactions between tectonics and fluid circulations in an inverted hyper-extended basin: Example of mesozoic carbonate rocks of the western North Pyrenean Zone (Chaînons Béarnais, France). *Marine and Petroleoum Geology, 80,* 563-586.

Schaltegger, U., Desmurs, L., Manatschal, G., Müntener, O., Meier, M., Frank, M., Bernouulli, D. (2002). The transition from rifting to sea-floor spreading within a magma-poor rifted margin: field and isotopic constraints. *Terra Nova, 14,* 156-162.

Schärer, U., de Parseval, P., Polvé, M., de Saint Blanquat, M. (1999). Formation of the Trimouns talc-chlorite deposit (Pyrenees) from persistent hydrothermal activity between 112 and 97 Ma. *Terra Nova, 11,* 30-37.

Schmid, S.M., Handy, M.R. (1991). Towards a genetic classification of fault rocks: geological usage and tectonophysical implications. In: Müller, D.W., McKenzie, J.A., Weissert, H. (Eds.). Controversies in modern geology, evolution of geological theories in sedimentology, earth history and tectonics. Academic Press, London, pp. 339-361.

Schmid, S.M. and Froitzheim, N. (1993). Oblique slip and block rotation along the Engadine line. *Eclogae Geologicae Helvetiae, 86,* 569-593.

Schmid, S.M., Fuegenschuh, B., Kissling, E., & Schuster, R. (2004). Tectonic map and overall architecture of the Alpine Orogen. *Eclogae Geologicae Helvetiae*, 97, 93-117.

Scholz CH (1988) The brittle-plastic transition and the depth of seismic faulting. *Geologische Rundschau, 77,*319-328.

Schübach, M.A. (1973). Comparison of slope and dbasinal sediments of a marginal cratonic basin (Pedregosa Basin, New Mexico) and a marginal geosynclinals basin (Southern border of Piemontais Geosyncline, Bernina nappe, Switzerland). Ph.D. thesis, Rice Univ. Houston, Texas.

Serrano, O., Delmas, J., Hanot, F., Vially, J., Herbin, J.P., Houel, P., Tourtiere, B. (2006). Le bassin d'Aquitaine: valorisation des données sismiques, cartographie structurale et potentiel pétrolier. BRGM, Orléans.

Sibson, R.H. (1977). Fault rocks and fault mechanisms. *Journal of the Geological Society of London 133,* 191-213.

Sibson, R.H. (1992). Implication of fault-valve behavior for rupture nucleation and recurrence. *Tectonophysics, 211*, 283-293.

Sibuet, J.C., Srivastava, S.P., Spakman, W. (2004). Pyrenean orogeny and plate kinematics. *Journal of Geophysical Research, 109*. doi:10.1029/2003JB002514.

Souquet, P., Debroas, E.J., Boirie, J.M., Pons, P., Fixari, G., Roux, J.C., Dol, J., Thieuloy, J.P., Bonnemaison, M., Manivit, H., Peybernès, B. (1985). The black flysh group (Albian-Cenomanian) of the Pyrenees. *Centres de Recherches Exploration Production Elf Aquitaine, 9,* 183-252.

Spillmann, P. and Büchi, H.J. (1993). The Pre-Alpine Basement of the Lower Austroalpine Nappes in the Bernina Massif (Grisons, Switzerland; Valtellina, Italy). The Pre-Mesozoic Geology in the Alps, 457-467.

Spötl, C., Longstaffe, F.J., Ramseyer, K., Rüdinger, B. (1999). Authigenic albite in carbonate rocks - a tracer fro deep-burial brine migration? *Sedimentology, 46,* 649-666.

Srivastava, S.P., Sibuet, J.C., Cande, S., Roest, W.R., Reid, I.D. (2000). Magnetic evidence for slow seafloor spreading during the formation of the Newfoundland and Iberian margins. *Earth and Planetary Science Letters, 182,* 61-76.

Sverjensky, D.A. (1984). Europium redox equilibria in aqueous solution. *Earth Planetary Science Letters, 67,* 70-78.

Staub, R. (1948). Ueber den Bau der Gebirge zwischen Samedan und Julierpass und seine Beziehungen zum Falknis- un Bernina-Raum. *Beiträge Geologische Karte Schweiz* N.F. Lief. 93.

Taylor, S.R. and McLennan, S.M. (1985). The continental crust: its composition and evolution. Blackwell, Oxford, 312 pp.

Teixell, A. (1990). Alpine thrusts at the western termination of the Pyrenean Axial Zone. *Bulletin de la Société Géologique de France, 8(6),* 241-249.

Teixell, A. (1998). Crustal structure and orogenic material budget in the western central Pyrenees. *Tectonics, 17,* 395-406.

Teixell, A., Labaume, P., Lagabrielle, Y. (2016). The crustal evolution of the west-central Pyrenees revisited: inferences from a new kinematic scenario. *Compte Rendu Geosciences, 348,* 257-267.

Thinon, I. (1999). Structure profonde de la Marge Nord Gascogne et du Bassin Armoricain. PhD thesis, Ifremer-IUEM, Brest, France.

Tucker, M.E., & Wright, V.P. (1990). Carbonate sedimentology. Blackwell, Oxford, 428 pp.

Tugend, J., Manatschal, G., Kusznir, N.J., Masini, E., Mohn, G., Thinon, I. (2014). Formation and deformation of hyperextended rift systems: Insights from rift domain mapping in the Bay of Biscay-Pyrenees. *Tectonics, 33,* DOI:10.1002/2014TC003529.

Tugend, J., Manatschal, G., Kusznir, N.J. (2015). Spatial and temporal evolution of hyperextended rift systems: Implication for the nature, kinematics, and timing of the Iberian-European plate boundary. *Geology, 43,* 15-18. doi: 10.1130/G36072.1

Vacherat, A., Mouthereau, F., Pik, R., Bellahsen, N., Gautheron, C., Bernet, M., Daudet, M., Balansa, J., Tibari, B., Pinna Jamme, R., Radal, J. (2016). Rift-to-collision transition recorded by tectonothermal evolution of the northern Pyrenees. *Tectonics, 35*. doi.org/10.1002/2015TC004016.

Varsányi I., Palcsu L. and Ó-Kovács L. (2011). Groundwater flow system as an archive of palaeo-temperature: Noble gas, radiocarbon, stable isotope and geochemical study in the Pannonian Basin, Hungary. *Applied Geochemistry, 26*, 91–104.

Vergés, J., García Senz, J.M. (2001). Mesozoic evolution and Cenozoic inversion of the Pyrenean Rift. In: Peri-Tethys memoir 6: Pery-Tethyan rift/wrench basins and passive margins. In: Ziegler, P.A., et al. (Eds.). *Memoires Muséum National d'Histoire Naturelle, 186,* pp. 187-212.

Vielzeuf, D. and Kornprobst J. (1984), Crustal splitting and the emplacement of Pyrenean lherzolites and granulites, *Earth and Planetary Science Letters, 67,* 87-96. doi:10.1016/0012-821X(84)90041-4.

Vissers R.L.M. and Meijer, P.T. (2012a). Iberian Plate kinematics and Alpine collision in the Pyrenees, *Earth Sci. Rev.*, *114(1–2)*, 61-83, doi:10.1016/j.earscirev.2012.05.001

Vissers R.L.M. and Meijer, P.T. (2012b). Mesozoic rotation of Iberia: Subduction in the Pyrenees? *Earth Sci. Rev.*, *110(1–4)*, 93–110, doi:10.1016/j.earscirev.2011.11.001

Von Quadt, A., Grünenfelder, M., & Büchi, H. (1994). U-Pb zircon ages from igneous rocks of the Bernina nappe system (Grisons, Switzerland). *Schweizerische Mineralogische und Petrographische Mitteilungen, 74*, 373-382.

Weissert, H.J. and Bernoulli, D. (1985). A transform margin in the Mesozoic Tethys: evidence from the swiss alps. *Geologische Rundschau, 74,* 665-679.

Wilson, R.C.L., Manatschal, G., Wise, S. (2001). Rifting along non-volcanic passive margins: stratigraphic and seismic evidence from the Mesozoic successions of the Alps and western Iberia. *Geological Society of London, Special Publications, 187(1),* 429-452.

Whitmarsh, R.B., Manatschal, G., Minshull, T.A. (2001). Evolution of magma-poor continental margins from rifting to seafloor spreading. *Nature, 413,* 150-154.

Zhong, S. and Mucci, A. (1995). Partitioning of rare earthe elements (REEs) between calcite and seawater solutions at 25°C and 1 atm, and high dissolved REE concentrations. *Geochimica et Cosmochimica Acta, 59,* 443-453.

ANNEXES

Annex A - O and C isotopic values of the Alpine samples. MO = Il Motto area; PA = Piz Alv area; PVL = Piz Val Lunga area; FCT = Fuorcla Cotschna area; MP = Mal Pass area.

Unit	$\delta^{13}C$	$\delta^{18}O$
	%	%
Repl. Dol.	*VPDB*	*VPDB*
M02	2,04	-0,76
M02	1,66	0,05
PA 1	1,72	-0,57
PVL 1	1,27	-4,60
PVL 2	1,88	-4,79
PVL 2	1,60	-5,62
PVL 4	1,38	-3,72
PVL 8	1,05	-2,81
PVL 9	0,76	-2,31
PVL 10	2,90	-3,60
PVL 11	3,07	-1,47
PVL 12	1,48	-2,33
PVL 12	1,43	-4,10
PVL 12	1,52	-3,73
PVL 17	2,46	-2,71
PVL 17	1,21	-1,01
PVL 26	2,71	-3,45
FCT 1	1,20	-2,15
FCT 3	0,98	-3,68
FCT 3L	0,73	-3,14
FCT 4	2,24	-3,99
FCT 4	2,42	-3,13
FCT 5	2,35	-1,97
FCT 75	1,34	-1,54
MP 8	-0,14	-4,40
MP 16	1,78	-4,05
MP 18	1,92	-5,30
MP 20	0,84	-3,47
MP 21	1,50	-6,04
MP 22	1,02	-4,43
MP 23	2,51	-7,79

Unit	$\delta^{13}C$	$\delta^{18}O$
	%	%
Cem Dol.	*VPDB*	*VPDB*
M02	2,84	-5,55
PA 1	2,97	-2,52
PA 1	2,11	-4,90
PA 5	3,43	-3,00
PVL 26	2,88	-8,92
PVL 26	2,84	-10,36
Cem Dol.		
PVL 26	2,79	-7,46
PVL 26	1,50	-8,62
PVL 26	2,62	-8,18
PVL 26	2,66	-9,51
PVL 26	2,62	-5,99
FCT 1	1,35	-6,33
FCT 3	1,03	-5,74
FCT 3	1,04	-6,56
FCT 3	1,02	-6,78
FCT 75	0,77	-13,84
MP 8	1,08	-14,30
MP 18	1,33	-8,74
MP 19	1,15	-14,24
MP 20	1,41	-14,00
MP 21	1,19	-14,41
MP 22	1,35	-13,91
MP 23	2,12	-13,59
MP 11	0,35	-9,57

Unit	$\delta^{13}C$	$\delta^{18}O$
	%	%
Cem Cc + Dedol	***VPDB***	***VPDB***
PA 8	2,41	-1,66
PA 10	2,65	-1,78
PA 10	2,76	-1,91
PVL 8	0,14	-6,07
PVL 9	-0,23	-8,90
PVL 3	0,51	-7,41
PVL 3	0,23	-7,90
PVL 4	0,30	-7,25
PVL 15	1,88	-7,97
PVL 15	1,91	-12,05
PVL 57	0,88	-6,85
PVL 59	1,94	-11,80
PVL 60	0,88	-12,72
PVL 61	2,71	-5,19
MP 24	0,88	-15,02
Calcite veins		
PVL 3	0,24	-9,81
PVL 4	0,22	-6,33
PVL 11	1,42	-7,08
PVL 26	2,79	-6,78
PVL 26	2,80	-6,98
PVL 26	2,79	-7,74
FCT 4	1,69	-9,16
FCT 5	1,74	-8,01
FCT 5	1,80	-8,44

ANNEX B - Homogenization temperature of fluid inclusions. MO = Il Motto area; PVL = Piz Val Lunga area; FCT = Fuorcla Cotschna area; MP = Mal Pass.

Sample	T_h	
	°C (±0,1)	
Proximal - Cem Dol		
M02	86	141,3
	86,2	144,3
	116,3	145,8
	120,8	146,2
	125,2	153,1
	127,8	155,5
	128,3	157,9
	135	158,8
	135,7	161,6
	137,6	170,2
	137,8	174,7
	138,8	186,9
	139	191
	139,2	205,9
	139,6	
Central dist- Repl Dol		
PVL 5-9-12	87,9	125,8
FCT 8	91	125,9
	93,2	126
	97,8	126
	107,6	127,6
	108,4	129,9
	113,7	131,4
	114,8	134,8
	116,8	135,2
	117,7	136
	118,2	136,8
	118,2	141,3
	120	142,2
	120,4	143

Sample	T_h	
	°C (±0,1)	
Central dist- Repl Dol		
	121	145,2
	121,2	145,5
	121,2	146
	121,4	146,7
	121,6	146,8
	121,8	147,3
	123,2	147,6
	124,8	147,7
	124,9	152,5
Central Dist - Cem CC + Dedol		
PVL 5-9-15	77,4	118,2
	78,3	118,5
	88,7	118,9
	91,5	122,5
	92,7	123
	95,5	125,5
	96,1	129,5
	97	131,5
	97,6	134,3
	99,6	134,5
	100,1	135,2
	100,3	137,5
	101,3	137,7
	104,2	139,5
	104,7	141,4
	105,7	171,7
	107,7	198
	113,6	202,8
	117,2	

Sample	T_h	
	°C (±0,1)	
Outer Dist - Qtz sept		
MP 11	112,1	151,6
	126,8	153,8
	129,2	153,8
	130,1	154
	133,9	154
	135,8	154,7
	140,2	156,4
	140,5	158,8
	141,1	158,9
	141,2	160
	141,7	170,2
	141,9	175,4
	144	175,6
	144,1	175,8
	145,5	176
	145,8	187,2
	148,1	189,2
	148,2	
Outer Dist - Dol sept		
MP 11	155,1	
	156,8	
	158,2	

Sample	T_h	
	°C (±0,1)	
Outer Dist - Vein Qtz		
MP 17	119,8	137,4
	120,8	138,8
	121	139
	121,6	139,3
	122,2	141,7
	125,3	141,7
	129,9	143,3
	130	145
	130,7	146,8
	135,1	149
	135,8	162,1
	137,1	204,5
Outer Dist - Vein Dol		
MP 17	138,2	146,1
	143,9	146,2
	144,6	147,8
	144,9	153,3
	145,2	157,5
	146	158,3

ANNEX C - Sr isotopic values for the Alpine samples

SAMPLE	87Sr/86Sri	± 2 S.E.
Proximal		
Dol cement	0,708750	0,000639
Repl dolomite	0,709106	0,000611
Inn Distal		
Calcite matrix	0,71149	0,0004
Dykes	0,709319	0,000269
Repl dolomite	0,710336	0,000383
Centr Distal		
Repl dolomite	0,708910	0,000244
	0,708723	0,000011
	0,709129	0,000013
Dolomite vein	0,713137	0,000238
	0,70892	0,00001
Cc cem - Dedol	0,711470	0,000627
	0,713138	0,000115
	0,711403	0,000267
	0,709155	0,000007
Outer Distal		
Repl dolomite	0,712604	0,000349
	0,708572	0,000301
	0,708758	0,000225
	0,708254	0,000188
Dolomite vein	0,71002	0,00015
	0,709821	0,000142
	0,708968	0,000142
	0,716308	0,000246
Dol septaria	0,708529	0,000131
Cc ophicalcite	0,709924	0,000536

ANNEX D - He isotopic values. PVL = Piz Val Lunga area; FCT = Fuorcla Cotcschna area; MP = Mal Pass area.

Sample	He	R/Ra	Ar	$^{40}Ar/^{36}Ar$	CO_2
	ccSTP/g		*ccSTP/g*		*ccSTP/g*
Central Distal - Vein Dolomite					
PVL 26	3,11E-06	0,044	0,00070	798,6	8,70E-04
FCT_1	3,96E-07	0,038	0,00048	434,6	2,88E-03
FCT_3	5,34E-08	0,047	0,00021	296,3	6,02E-05
FCT_8	1,46E-07	0,028	0,00015	368,9	1,17E-03
FCT_71	6,74E-09	0,100			4,86E-04
FCT_75	2,56E-07	0,027	0,00074	297,5	
Outer Distal - Vein Dolomite					
MP 8	3,77E-06	0,039	0,00099	296,6	4,90E-03
MP 18	1,14E-06	0,028	0,00043	379,9	8,25E-04
MP_23	2,44E-06	0,022	0,00034	296,3	7,94E-04
MP_19	1,19E-06	0,034	0,00027	295,5	1,04E-03
Central Distal - Dedolomite					
PVL_15	4,81E-07	0,034			4,09E-03
Outer Distal - Vein Quartz					
MP 18	1,26E-06	0,026	0,00152	334,5	7,45E-04

ANNEX E - U-Pb ages of the Alpine samples.

Sample	age (Ma)
Replac. Dolomite	
MO	198,9 ± 3,3
PA	206 ± 20
PVL	176,7 ± 4,7
	179 ± 11
	144 ± 24
	145 ± 12
	200,4 ± 6,4
FCT	176 ± 17
	192,5 ± 9
	202 ± 4,8
MP	202 ± 10
	207,8 ± 2,7
	202,9 ± 4

Sample	age (Ma)
Cem Calcite - Dedolomite	
PVL	118 ± 29
	231 ± 18
	198 ± 3,5
Dolomite vein	
PVL	45 ± 36
FCT	169 ± 11
	228 ± 64
	113 ± 36

ANNEX F - Main and trace elements geochemistry of the Alpine samples.

SAMPLE		SiO2	Al2O3	Fe2O3	CaO	MgO	Na2O
		%	%	%	%	%	%
REF HD	RE 13	0,05	0,02	0,06	31	21,5	0,01
	RE 30	0,34	0,18	0,07	30,6	21,2	0,01
HD	MO 1	1,12	0,49	0,37	31	20,8	0,03
	MO 2	0,39	0,19	0,18	30,6	20,7	0,02
	PA 1	14,4	6,96	3,39	22,9	14,8	0,05
	PA 1	1,83	0,7	0,35	31,2	20,5	0,05
	PVL 8	1,73	0,69	0,3	34,2	17,8	0,01
	PVL 22	4,88	0,45	0,17	51,5	1,03	0,01
	FCT 1	1,62	0,68	0,39	30,6	20,7	0,01
	FCT 3	18,25	0,34	0,66	25	16,65	0,03
	FCT 8	1,67	0,49	0,4	31,1	20,9	0,01
	FCT 65	39	0,19	0,35	19,05	13,3	0,01
	MP 21	1,39	0,24	0,31	31,1	21,4	0,03
	MP 23	5,43	1,07	0,61	28,9	19,7	0,03
HD GOUGE	PVL 1	14,95	1,49	1,52	31,9	10,8	0,01
	PVL 2	9,4	1,25	1,46	34,4	12,6	0,01
	FCT 7	4,25	0,41	0,86	30,4	19,75	0,01
HD CAT	PVL 12	2,58	1,27	0,38	37,1	13,95	0,01
	PVL 54	25,4	0,03	1,18	23,4	15,65	0,03
DEDOL	PA 10	1,76	0,58	0,28	51,3	2,3	0,02
	PVL 15	1,77	0,58	0,35	52	1,45	0,02
	PVL 59	1,83	0,22	0,23	51,1	1,58	0
	PVL 60	2,75	0,92	0,45	49,5	2,84	0,01
	PVL 61	5,83	0,12	0,38	34,1	16,8	0,03
SILIC	PVL 58	78,7	0,44	0,56	10,45	0,52	0,02
	FCT 12	25,4	0,58	1,97	21,4	12,9	0,05
SEPT	MP 10	80	2,49	0,94	5,46	3,31	0,16
	FCT 11	88,1	0,28	4,17	1,53	0,87	<0.01
	FCT 71	97,9	0,09	1,32	0,34	0,12	0,14
	MP 4	78,3	2,04	1,15	7,9	2,22	0,08

K2O	Cr2O3	TiO2	MnO	P2O5	SrO	BaO	LOI	C
%	*%*	*%*	*%*	*%*	*%*	*%*	*%*	*%*
<0.01	<0.01	<0.01	0,01	<0.01	<0.01	<0.01	45,8	12,95
0,02	<0.01	0,01	0,01	0,02	<0.01	<0.01	45,6	12,75
0,17	<0.01	0,02	0,01	0,02	<0.01	<0.01	46,3	12,1
0,07	<0.01	0,01	0,01	0,01	<0.01	<0.01	45,9	12,7
2,58	0,01	0,33	0,04	0,27	<0.01	0,01	34,3	8,85
0,18	<0.01	0,03	0,02	0,02	<0.01	<0.01	44,8	12,5
0,23	<0.01	0,04	0,03	<0.01	0,01	<0.01	46,3	12,4
0,14	<0.01	0,02	0,02	0,03	0,03	<0.01	43,1	11,35
0,22	<0.01	0,03	0,01	0,02	0,01	<0.01	47	12,5
0,08	<0.01	0,01	0,01	<0.01	0,01	<0.01	39	10,6
0,18	<0.01	0,03	0,03	0,01	0,01	<0.01	46,6	12,5
0,08	<0.01	0,01	0,01	<0.01	<0.01	<0.01	28,9	7,91
0,1	<0.01	0,01	0,07	0,01	<0.01	<0.01	45,1	12,65
0,34	<0.01	0,03	0,04	0,01	0,01	<0.01	43,7	11,65
0,28	<0.01	0,06	0,48	0,03	0,02	0,03	38,4	10,25
0,2	<0.01	0,05	0,38	0,02	0,02	0,01	41,3	11,05
0,11	<0.01	0,01	0,15	0,01	0,01	<0.01	45,6	12,4
0,37	<0.01	0,07	0,05	0,02	<0.01	<0.01	45,1	12
<0.01	<0.01	<0.01	0,02	0,01	<0.01	<0.01	34,9	9,46
0,18	<0.01	0,03	0,02	0,03	0,01	<0.01	43	11,4
0,19	<0.01	0,03	0,18	<0.01	0,01	0,03	43,7	11,75
0,05	<0.01	0,01	0,13	0,01	<0.01	0,05	43,1	11,6
0,33	<0.01	0,03	0,2	0,01	<0.01	0,03	42,1	11,3
0,04	<0.01	<0.01	0,07	0,01	<0.01	0,07	43,7	12
0,11	0,01	0,03	0,02	0,62	<0.01	<0.01	8,69	2,3
0,08	<0.01	0,03	2,74	0,01	0,01	<0.01	33,9	9,22
0,79	0,01	0,08	0,03	0,01	<0.01	<0.01	8,02	2,11
0,12	0,01	0,01	0,11	<0.01	<0.01	0,01	3,43	0,6
<0.01	<0.01	<0.01	0,01	<0.01	<0.01	<0.01	0,52	0,09
0,64	0,01	0,07	0,04	0,02	<0.01	<0.01	8,89	2,37

S	Ba	Cr	Cs	Ga	Ge	Hf	Nb	Rb
%	*ppm*	*ppm*	*ppm*	*ppm*	*ppm*	*ppm*	*ppm*	*ppm*
<0.01	1,8	<10	<0.01	<0.1	<5	<0.2	<0.2	0,3
<0.01	4,9	<10	0,21	0,3	<5	<0.2	0,2	2
0,01	10,6	10	0,66	0,7	<5	<0.2	0,5	6,3
<0.01	5	10	0,14	0,3	<5	<0.2	0,2	2,8
0,01	113,5	50	5,11	9	<5	1,8	7,8	90,2
0,01	13	<10	0,34	0,9	<5	<0.2	0,7	7,3
0,01	19,4	10	0,62	1	<5	0,2	0,9	10,7
0,01	13,1	20	0,43	0,6	<5	<0.2	0,4	6,1
<0.01	8,2	10	0,46	0,9	<5	0,2	0,4	8,3
<0.01	5,7	<10	0,31	0,2	<5	<0.2	<0.2	3,5
<0.01	10,1	10	0,35	0,4	<5	0,2	0,4	8,9
0,1	7	10	0,09	0,5	<5	<0.2	0,2	2,5
<0.01	6,4	10	0,06	0,5	<5	<0.2	0,2	2,9
<0.01	21,9	10	0,35	1,5	<5	0,2	0,7	12
0,06	293	20	0,95	2,4	<5	0,5	2,4	13,1
0,03	93,7	20	0,79	2,2	<5	0,3	1,6	9,9
<0.01	16,7	<10	0,21	0,3	<5	<0.2	<0.2	6
0,01	27,9	20	2,02	1,9	<5	0,6	1,4	18,6
0,01	4	10	<0.01	0,1	<5	<0.2	<0.2	0,3
0,01	12,5	10	0,47	0,8	<5	0,2	0,7	7,7
0,05	240	10	0,85	0,8	<5	<0.2	0,6	8,9
0,02	473	10	0,16	0,5	<5	<0.2	0,3	2,9
0,06	226	10	1,37	1,3	<5	0,2	0,8	15,7
0,01	538	10	0,04	0,4	<5	<0.2	0,2	2
0,01	15,7	50	0,34	0,7	<5	0,2	1,2	5,7
0,02	12,5	20	0,23	2,2	<5	0,4	0,4	4,6
0,02	38,5	30	1,22	3,1	<5	0,4	1,6	31
<0.01	45,7	30	0,24	0,7	<5	<0.2	<0.2	4,5
0,02	4,6	30	0,03	0,3	<5	<0.2	<0.2	0,2
0,01	46,6	30	1,26	2,8	<5	0,5	1,7	30,8

Sn	Sr	Ta	Th	U	V	W	Zr	As
ppm	*ppm*	*ppm*	*ppm*	*ppm*	*ppm*	*ppm*	*ppm*	*ppm*
1	85,7	0,1	<0.05	7,49	57	<1	2	0,4
<1	97,3	0,1	0,16	4,56	21	<1	3	0,8
1	108	0,1	0,42	5,92	140	<1	5	53,6
<1	108,5	0,1	0,23	5,87	63	1	3	11,8
2	89,8	0,5	5,72	1,93	54	1	67	4,9
1	93,9	0,1	0,55	0,56	10	<1	7	3,4
2	107,5	<0.1	0,51	2,42	23	<1	8	1,1
<1	320	<0.1	0,32	1,73	18	1	5	0,7
1	106,5	<0.1	0,39	0,59	24	<1	9	1,3
1	99,7	<0.1	0,18	0,39	14	<1	4	0,4
<1	89,7	<0.1	0,42	1,48	29	<1	8	1,6
1	54,2	0,1	0,13	2,38	9	<1	2	14
1	56,5	0,2	0,13	0,48	19	<1	3	0,4
1	235	0,2	1,01	1,12	13	<1	9	2,9
3	284	0,1	1,12	3,06	36	1	20	4,4
1	251	<0.1	0,83	1,79	16	1	11	50,3
1	125,5	<0.1	0,12	1,1	7	<1	2	1,1
1	104	0,1	1,02	2,85	72	1	20	1,6
1	57	0,1	<0.05	3,28	19	<1	0	4,5
1	273	0,1	0,53	1,03	13	<1	8	1,3
<1	129	<0.1	0,5	3,59	22	1	7	6,6
1	113	0,1	0,3	1,6	14	<1	2	4,1
1	133	0,2	0,83	2,98	13	<1	7	7,3
1	145	0,1	0,11	2,29	14	<1	2	3,6
1	53,1	0,2	1,83	1,35	18	<1	9	4,8
<1	193	<0.1	0,63	2,72	20	1	12	2,6
1	41	0,3	1,35	1,43	27	1	16	1,4
<1	23,2	<0.1	0,11	0,37	75	6	2	2,4
1	3,8	0,1	<0.05	0,11	7	2	<2	3,8
1	86,6	0,2	1,34	0,42	20	1	19	1,9

Bi	Hg	In	Re	Sb	Se	Te	Tl	Ag
ppm	*ppm*	*ppm*	*ppm*	*ppm*	*ppm*	*ppm*	*ppm*	*ppm*
0,02	0,008	<0.005	0,001	0,16	0,2	<0.01	<0.02	<0.5
0,02	0,009	<0.005	0,001	0,17	<0.2	0,01	0,03	<0.5
0,1	0,02	0,006	0,013	1,64	0,3	0,01	0,14	<0.5
0,06	0,02	<0.005	0,008	0,85	0,3	<0.01	0,08	<0.5
0,15	0,019	0,02	<0.001	0,35	0,8	0,57	0,05	<0.5
0,12	0,036	0,009	<0.001	0,42	0,4	0,08	0,03	<0.5
0,03	0,013	<0.005	0,003	0,13	0,4	0,01	0,02	<0.5
0,01	0,019	<0.005	0,001	0,06	0,2	0,01	0,02	<0.5
0,01	0,044	<0.005	<0.001	0,18	0,2	<0.01	0,02	<0.5
<0.01	0,026	<0.005	<0.001	0,08	0,2	<0.01	<0.02	<0.5
0,01	0,011	<0.005	0,001	0,06	0,2	0,01	0,02	<0.5
0,62	0,205	0,022	0,001	2,04	0,3	0,01	0,17	<0.5
0,02	0,012	<0.005	<0.001	0,19	0,2	<0.01	<0.02	<0.5
0,07	0,023	0,007	<0.001	0,24	0,4	0,01	0,03	<0.5
0,07	0,029	0,011	0,002	0,12	0,8	<0.01	0,12	<0.5
0,05	0,016	0,008	0,001	0,14	0,7	<0.01	0,03	<0.5
<0.01	0,014	<0.005	0,001	0,1	0,3	<0.01	0,02	<0.5
0,02	0,035	0,006	0,001	0,19	0,4	<0.01	0,04	<0.5
0,12	0,034	0,005	0,002	0,55	0,2	0,01	0,03	<0.5
0,06	0,008	<0.005	<0.001	0,23	0,3	0,02	<0.02	<0.5
0,01	0,027	<0.005	0,06	0,46	0,8	<0.01	0,18	<0.5
0,02	0,016	<0.005	0,015	0,3	0,4	0,01	0,1	<0.5
0,05	0,023	0,005	0,003	0,51	0,7	<0.01	0,12	<0.5
0,03	0,03	<0.005	0,01	0,26	0,2	0,01	0,03	<0.5
0,1	0,029	0,01	<0.001	0,39	1	0,01	0,04	<0.5
0,02	0,025	<0.005	0,001	0,07	0,4	<0.01	<0.02	<0.5
0,26	0,023	0,011	<0.001	0,41	0,2	0,03	0,04	<0.5
0,06	<0.005	<0.005	<0.001	0,68	<0.2	0,14	<0.02	0,5
0,17	0,043	<0.005	<0.001	0,51	0,2	0,01	0,03	<0.5
0,2	0,035	0,01	<0.001	0,44	0,4	0,05	0,04	<0.5

Cd	Co	Cu	Li	Mo	Ni	Pb	Sc	Zn
ppm	*ppm*	*ppm*	*ppm*	*ppm*	*ppm*	*ppm*	*ppm*	*ppm*
<0.5	1	2	<10	1	1	3	<1	4
<0.5	2	3	<10	1	2	6	<1	6
<0.5	4	10	<10	12	6	10	1	15
<0.5	3	6	<10	6	2	9	<1	13
<0.5	9	6	20	1	31	4	7	41
<0.5	2	11	<10	<1	5	10	1	18
0,6	2	6	<10	1	1	<2	1	12
0,6	2	<1	<10	<1	<1	<2	<1	2
0,5	4	1	<10	1	1	<2	1	8
0,5	2	1	<10	1	1	<2	<1	9
<0.5	3	<1	<10	<1	<1	<2	1	5
<0.5	1	60	<10	2	2	52	<1	34
<0.5	2	4	<10	2	2	<2	<1	11
<0.5	2	4	<10	1	2	10	1	22
0,7	5	24	10	1	3	77	1	79
0,5	3	3	10	<1	1	100	1	50
0,7	2	1	<10	1	<1	5	<1	9
0,5	2	4	<10	<1	3	5	1	14
<0.5	<1	11	<10	1	1	10	<1	12
<0.5	1	6	<10	<1	6	4	1	12
0,5	2	2	<10	37	2	10	1	4
<0.5	1	2	<10	7	4	3	<1	16
<0.5	3	6	<10	6	3	13	1	9
<0.5	1	3	<10	6	3	7	<1	13
<0.5	1	11	<10	1	4	3	2	15
0,7	6	2	<10	1	2	8	1	7
<0.5	3	14	<10	1	8	20	3	20
0,7	2	41	<10	1	4	<2	<1	7
<0.5	2	24	<10	3	5	13	<1	11
<0.5	3	25	<10	2	5	12	1	18

SAMPLE		SiO2	Al2O3	Fe2O3	CaO	MgO	Na2O
		%	%	%	%	%	%
DOL VEINS	PVL 26	8,22	1,19	1,19	33,2	14,1	0,03
	FCT 8	1,59	0,4	0,5	30,8	21,5	0,01
	MP 8	10	0,76	1,05	29,4	18	0,01
	MP 18	38	0,12	0,27	19,45	13,45	0,01
	MP 19	0,69	0,22	0,5	30,7	21	0,03
	MP 20	0,24	0,06	0,18	32	22,1	0,04
	MP 21	20,4	0,09	0,38	25,9	17,45	0,02
Fe-Mn	PVL 11	9,77	1,6	1,9	29,7	16,5	0,04
	FCT 12	24,2	0,56	1,7	22,5	14,15	0,05
OPH	MP 24	9,41	0,7	1,91	44,8	7,71	0,01

K2O	Cr2O3	TiO2	MnO	P2O5	SrO	BaO	LOI	C
%	%	%	%	%	%	%	%	%
0,38	0,01	0,07	0,05	0,02	0,01	<0.01	42,5	11,45
0,14	<0.01	0,02	0,06	0,01	0,01	<0.01	46,4	12,5
0,27	<0.01	0,03	0,15	0,01	0,01	<0.01	41,7	11,2
0,05	<0.01	<0.01	0,04	<0.01	<0.01	0,01	28,7	8,04
0,08	<0.01	0,01	0,05	<0.01	<0.01	<0.01	45,1	12,6
0,04	<0.01	<0.01	0,05	<0.01	<0.01	<0.01	45,3	12,8
0,05	<0.01	<0.01	0,05	<0.01	<0.01	<0.01	36,4	8,41
0,4	<0.01	0,07	0,05	0,03	<0.01	<0.01	41,4	10,95
0,07	<0.01	0,03	2,42	<0.01	0,02	<0.01	34,7	9,37
<0.01	0,07	0,03	0,15	0,03	0,01	<0.01	36,6	8,93

S	Ba	Cr	Cs	Ga	Ge	Hf	Nb	Rb
%	*ppm*	*ppm*	*ppm*	*ppm*	*ppm*	*ppm*	*ppm*	*ppm*
0,05	21	60	1,32	1,4	<5	0,6	1,3	16,4
<0.01	13,1	10	0,31	0,5	<5	<0.2	0,2	7,4
<0.01	13,8	10	0,38	1,2	<5	<0.2	0,5	10,6
0,01	81,2	10	0,16	0,1	<5	<0.2	<0.2	1,9
<0.01	5,6	10	0,13	0,4	<5	<0.2	0,2	2,4
<0.01	4,2	10	0,08	0,1	<5	<0.2	<0.2	0,7
<0.01	5,5	10	0,03	0,2	<5	<0.2	<0.2	1,2
0,02	32,6	20	1,4	2,5	<5	0,5	1,9	18,3
0,01	12,1	10	0,18	2,5	<5	0,2	0,2	3,9
<0.01	8,9	470	0,16	0,9	<5	<0.2	<0.2	0,5

Sn	Sr	Ta	Th	U	V	W	Zr	As
ppm	*ppm*	*ppm*	*ppm*	*ppm*	*ppm*	*ppm*	*ppm*	*ppm*
2	172,5	<0.1	1,11	2,16	19	1	22	2,6
<1	130,5	<0.1	0,22	1,32	26	<1	6	0,6
1	173,5	0,1	0,56	0,65	15	<1	8	0,8
1	114	0,1	0,29	0,33	8	<1	2	10,5
1	177	0,1	0,13	0,19	14	<1	2	1,8
1	160,5	0,1	0,05	0,06	18	2	0	0,6
1	124	0,1	0,08	0,09	14	<1	<2	<0.1
1	96,9	0,1	1,32	1,98	32	1	16	2,3
<1	190,5	<0.1	0,43	2,39	17	<1	7	3,8
1	149	0,1	<0.05	0,08	10	<1	2	2,4

Bi	Hg	In	Re	Sb	Se	Te	Tl	Ag
ppm	*ppm*	*ppm*	*ppm*	*ppm*	*ppm*	*ppm*	*ppm*	*ppm*
0,03	0,036	0,006	0,014	0,26	0,7	<0.01	0,07	<0.5
0,01	0,015	<0.005	0,001	0,06	0,2	0,01	<0.02	<0.5
0,03	0,036	0,008	<0.001	0,14	0,4	<0.01	0,02	<0.5
0,28	0,033	0,011	<0.001	1,16	0,5	0,01	0,03	<0.5
0,04	0,023	0,014	<0.001	0,27	0,5	<0.01	<0.02	<0.5
0,02	0,01	0,008	<0.001	0,1	0,2	<0.01	<0.02	<0.5
0,02	0,012	0,011	<0.001	0,17	0,3	<0.01	<0.02	<0.5
0,05	0,156	0,009	<0.001	0,33	0,6	0,1	0,05	<0.5
0,02	0,016	<0.005	0,003	0,12	0,3	0,01	0,02	<0.5
0,02	0,011	<0.005	<0.001	0,12	0,2	0,01	<0.02	<0.5

Cd	Co	Cu	Li	Mo	Ni	Pb	Sc	Zn
ppm	*ppm*	*ppm*	*ppm*	*ppm*	*ppm*	*ppm*	*ppm*	*ppm*
0,8	5	3	<10	1	1	3	1	11
0,5	2	<1	<10	<1	<1	<2	<1	10
<0.5	2	5	<10	1	6	4	1	17
<0.5	1	2	<10	1	1	379	<1	52
<0.5	1	4	<10	1	5	4	2	16
<0.5	<1	2	<10	1	2	4	1	14
<0.5	2	3	<10	1	<1	<2	1	11
0,6	4	17	10	2	4	8	2	36
<0.5	5	2	<10	2	1	11	1	7
<0.5	30	11	<10	1	382	2	3	13

ANNEX G - Rare earth elements analyses performed on the Alpine samples.

SAMPLE		La	Ce	Pr	Nd	Sm	Eu
		ppm	*ppm*	*ppm*	*ppm*	*ppm*	*ppm*
REF HD	**RE 13**	0,6	0,5	0,05	0,2	0,03	<0.03
	RE 30	1	1,3	0,15	0,5	0,12	<0.03
	cond	3,4086	1,492	1,1223	0,7737	0,5099	0
HD	**MO 1**	1,8	3,1	0,37	1,3	0,29	0,06
	MO 2	1,5	1,9	0,22	0,8	0,2	0,03
	cond	7,0303	4,1446	3,3109	2,321	1,6655	0,8036
	PA 1	3	5,8	0,61	2,4	0,41	0,11
	cond	12,782	9,6154	6,8462	5,305	2,7872	1,9643
	PA 1	18,2	50,9	4,21	15,8	2,88	0,62
	cond	77,546	84,383	47,25	34,925	19,579	11,071
	PVL 8	1,8	3	0,35	1,4	0,24	0,06
	PVL 22	2	3,1	0,33	1,3	0,29	0,05
	FCT 1	2,7	4,8	0,58	2,5	0,57	0,1
	FCT 3	2,6	5,3	0,59	2,3	0,4	0,11
	FCT 8	2,5	4,2	0,43	1,8	0,39	0,1
	FCT 65	1,1	1,4	0,17	0,5	0,06	<0.03
	cond	9,0186	6,0234	4,5829	3,6104	2,2094	1,25
	MP 21	1,8	2,8	0,38	1,4	0,28	0,06
	MP 23	5,3	10,2	1,16	4,3	0,83	0,26
	cond	15,126	10,776	8,642	6,2997	3,7729	2,8571
HD GOUGE	**PVL 1**	8,8	13,9	1,85	7,9	2,39	0,9
	PVL 2	10,2	17,3	2,11	8,4	2,63	1,36
	FCT 7	2,1	3,6	0,42	1,7	0,31	0,43
	cond	29,967	19,231	16,386	13,263	12,078	16,012
HD CAT	**PVL 12**	3	5,4	0,65	2,4	0,41	0,09
	PVL 54	0,7	0,8	0,07	0,3	0,04	<0.03
	cond	7,8824	5,1393	4,0404	2,9841	1,5296	0,8036
DEDOL	**PA 10**	4	4,9	0,75	3,1	0,61	0,14
	cond	17,043	8,1233	8,4175	6,8523	4,1468	2,5
	PVL 15	9,1	13,8	1,55	6,8	1,69	0,63
	PVL 59	2,3	3	0,33	1,3	0,18	0,05
	PVL 60	9,2	16,8	2,13	8	2,11	0,48
	PVL 61	1,4	1,8	0,22	0,8	0,18	0,03
	cond	23,434	14,672	11,869	9,3391	7,07	5,3125

Gd	Tb	Dy	Y	Ho	Er	Tm	Yb	Lu
ppm	*ppm*	*ppm*	*ppm*	*ppm*	*ppm*	*ppm*	*ppm*	*ppm*
<0.05	<0.01	<0.05	<0.5	<0.01	<0.03	0,01	<0.03	<0.01
0,11	<0.01	0,06	<0.5	<0.01	0,03	0	0,03	0,01
0,2798	0	0,1236	0	0	0,0944	0,2066	0,0923	0,2058
0,24	0,03	0,22	1,1	0,04	0,08	0,01	0,12	0,02
0,14	0,02	0,1	0,7	0,01	0,08	0,01	0,04	0,01
0,9664	0,6887	0,6593	0,5769	0,4496	0,5035	0,4132	0,4923	0,6173
0,48	0,08	0,4	3,1	0,08	0,26	0,03	0,23	0,03
2,4415	2,2039	1,6481	1,9872	1,4388	1,6362	1,2397	1,4154	1,2346
2,98	0,41	2,23	14,6	0,51	1,36	0,17	1,13	0,18
15,158	11,295	9,1883	9,359	9,1727	8,5588	7,0248	6,9538	7,4074
0,26	0,05	0,35	1,5	0,06	0,18	0,01	0,19	0,02
0,23	0,04	0,24	1,3	0,04	0,12	<0.01	0,12	0,01
0,5	0,07	0,35	2,1	0,07	0,18	0,02	0,16	0,02
0,48	0,06	0,34	2,1	0,07	0,14	0,01	0,14	0,02
0,36	0,05	0,26	1,6	0,05	0,15	0,01	0,15	0,02
0,08	0,01	0,05	<0.5	<0.01	0,04	0,01	<0.03	<0.01
1,6192	1,2856	1,0919	0,9188	0,8693	0,8496	0,4132	0,7795	0,6173
0,3	0,05	0,24	1,9	0,03	0,16	0,02	0,11	0,02
0,89	0,14	0,75	4,9	0,15	0,43	0,05	0,36	0,04
3,0264	2,6171	2,0396	2,1795	1,6187	1,8565	1,4463	1,4462	1,2346
2,96	0,53	3,17	19,7	0,6	1,81	0,23	1,47	0,2
3,28	0,5	3,31	19,4	0,55	1,57	0,19	1,13	0,14
0,41	0,04	0,28	1,9	0,04	0,16	<0.01	0,1	0,01
11,275	9,8255	9,2844	8,7607	7,1343	7,4261	5,7851	5,5385	4,8011
0,45	0,07	0,31	2,2	0,1	0,26	0,03	0,29	0,03
0,05	0,01	<0.05	<0.5	0,01	<0.03	<0.01	0,03	<0.01
1,2716	1,1019	0,6386	0,7051	0,9892	0,8181	0,6198	0,9846	0,6173
0,63	0,1	0,48	4,3	0,12	0,28	0,04	0,27	0,05
3,2045	2,7548	1,9778	2,7564	2,1583	1,7621	1,6529	1,6615	2,0576
2,29	0,34	2,51	15,7	0,53	1,67	0,18	1,45	0,19
0,26	0,04	0,29	2,7	0,05	0,19	0,03	0,13	0,02
2,54	0,41	2,36	15,3	0,43	1,26	0,17	0,81	0,13
0,14	0,02	0,09	0,6	0,01	0,07	0,01	0,03	<0.01
6,6506	5,5785	5,4079	5,4968	4,5863	5,0189	4,0289	3,7231	3,4979

ΣREE	Y/Ho	La/Yb	Ce/Ce*	Eu/Eu*
ppm				
1,39				
3,31				
	0	36,927	0	0,7628
8,78				
5,76				
	36	14,28	0,6334	0,8591
17,02				
	38,75	9,031	0,753	1,0279
116,18				
	28,627	11,151	0,6427	1,394
9,47				
9,17				
14,72				
14,66				
12,07				
3,42				
	29,655	11,57	0,6609	0,9369
9,55				
29,76				
	37,778	10,459	0,8455	0,9425
66,41				
72,07				
11,5				
	34,454	5,4108	1,3721	0,8678
15,69				
2,01				
	20	8,0056	0,5762	0,9107
19,77				
	35,833	10,257	0,6858	0,6782
58,43				
10,87				
62,13				
5,4				
	33,627	6,2943	0,7747	0,8797

SAMPLE		La	Ce	Pr	Nd	Sm	Eu
		ppm	*ppm*	*ppm*	*ppm*	*ppm*	*ppm*
SILIC	**PVL 58**	28,1	16,9	6,39	26	4,66	0,99
	FCT 12	2,5	4,5	0,47	1,9	0,41	0,11
	cond	65,19	17,739	38,496	30,836	17,233	9,8214
SEPT	**MP 10**	5,3	10,6	1,17	4,1	0,81	0,17
	FCT 11	1,4	12	0,25	0,9	0,32	0,03
	FCT 71	0,7	0,7	0,06	0,3	0,05	<0.03
	MP 4	5,8	15,2	1,71	5,8	1,15	0,24
	cond	14,061	15,957	8,9506	6,134	3,9599	1,9643
DOL VEINS	**PVL 26**	4,9	8,3	0,96	4,2	0,63	0,18
	FCT 8	2,7	4,5	0,5	2,1	0,37	0,08
	cond	16,191	10,61	8,193	6,9629	3,399	2,3214
	MP 8	7,2	14,4	1,83	6,9	1,33	0,35
	MP 18	2,2	4,2	0,54	1,8	0,49	0,06
	MP 19	2,9	6,3	0,82	3	0,56	0,12
	MP 20	2,7	5,6	0,75	2,7	0,54	0,11
	MP 21	2,6	5,3	0,71	2,9	0,65	0,1
	cond	14,998	11,87	10,438	7,6481	4,8538	2,6429
Fe-Mn	**PVL 11**	6,2	10,9	1,33	5,4	1,23	0,3
	FCT 12	2,2	3,6	0,4	1,6	0,39	0,07
	cond	17,895	12,019	9,7082	7,7365	5,5065	3,3036
OPH	**MP 24**	1,2	0,5	0,13	0,7	0,18	0,09
	cond	5,1129	0,8289	1,459	1,5473	1,2237	1,6071

Gd	Tb	Dy	Y	Ho	Er	Tm	Yb	Lu
ppm	*ppm*	*ppm*	*ppm*	*ppm*	*ppm*	*ppm*	*ppm*	*ppm*
5,15	0,66	3,74	31,6	0,81	2,14	0,25	1,25	0,18
0,45	0,08	0,47	3	0,1	0,29	0,05	0,31	0,05
14,242	10,193	8,6733	11,09	8,1835	7,6463	6,1983	4,8	4,7325
0,83	0,11	0,72	4,9	0,16	0,38	0,07	0,34	0,06
0,25	0,05	0,24	1,2	0,04	0,13	<0.01	0,17	0,02
<0.05	<0.01	<0.05	<0.5	<0.01	<0.03	<0.01	<0.03	<0.01
1,08	0,17	0,99	6,6	0,18	0,53	0,07	0,46	0,05
2,7467	2,2727	2,0087	2,0353	1,7086	1,6362	1,4463	1,4923	1,3374
0,73	0,09	0,63	3,4	0,11	0,38	0,04	0,24	0,03
0,32	0,05	0,31	2,2	0,07	0,18	0,01	0,15	0,01
2,6704	1,9284	1,9365	1,7949	1,6187	1,7621	1,0331	1,2	0,823
1,39	0,19	0,96	6,7	0,17	0,48	0,06	0,31	0,04
0,34	0,05	0,21	1,3	0,03	0,14	0,02	0,11	0,02
0,51	0,1	0,49	3	0,09	0,27	0,02	0,31	0,04
0,6	0,08	0,47	2,4	0,08	0,27	0,03	0,2	0,04
0,48	0,06	0,37	2,7	0,07	0,26	0,04	0,25	0,04
3,3774	2,6446	2,0602	2,0641	1,5827	1,7873	1,405	1,4523	1,4815
1,14	0,17	1,14	6	0,22	0,67	0,07	0,5	0,07
0,35	0,05	0,35	2,2	0,07	0,24	0,02	0,21	0,03
3,7894	3,0303	3,0696	2,6282	2,6079	2,8634	1,8595	2,1846	2,0576
0,21	0,04	0,24	2,2	0,04	0,13	0,02	0,16	0,03
1,0682	1,1019	0,9889	1,4103	0,7194	0,8181	0,8264	0,9846	1,2346

ΣREE	Y/Ho	La/Yb	Ce/Ce*	Eu/Eu*
ppm				
128,82				
14,69				
	38,022	13,581	0,6269	0,3541
29,72				
17				
1,81				
40,03				
	33,421	9,422	0,5956	1,4224
24,82				
13,55				
	31,111	13,492	0,7705	0,9212
42,31				
11,51				
18,53				
16,57				
16,53				
	36,591	10,327	0,6527	0,9487
35,34				
11,78				
	28,276	8,1915	0,7232	0,9119
5,87				
	55	5,1928	1,4057	0,3035

ANNEX H - O and C isotopic values of Pyrenean samples and homogenization temperatures (T_h) of fluid inclusions.

Unit	$\delta^{13}C$	$\delta^{18}O$
BDU - Host	***% VPDB***	***% VPDB***
MAR 23	3,29	-6,77
MAR 8	2,62	-4,52
MAR 33	2,27	-3,84
MAR 39	2,61	-7,79
MAR 30	2,67	-10,78
RI 9	3,05	-6,51
MB 2	2,95	-3,37
BDU - Cement		
MAR 8	1,61	-9,25
MAR 39	1,38	-8,60
MAR 33	2,16	-9,32
MB 2	1,81	-12,10
BLU - Host		
RI 1	1,19	-1,26
RI 1	1,17	-1,79
RI 5	0,82	-1,09
MAR 43	2,58	-7,37
MAR 2	2,39	-5,29
MAR 10	2,57	-7,37
BLU - Cement		
MAR 10	0,97	-7,66
RI 11	1,61	-6,54
MB 2	-1,97	-13,62
Mylon-Marb		
MAR 37	2,06	-6,87
MAR 38	1,67	-1,11
MAR 5	3,09	-6,71
MAR 3	1,11	-7,86

Unit	T_h	
BLU - Cement	***°C (±0,1)***	
Cc breccia type 1		
	227,9	
	240,7	
	240,2	
	249,2	
	249,3	
	228,9	
	232,8	
	244,7	
Dol breccia type 3		
	156,6	162,7
	157,7	177,3
	152,2	173
	158,9	185,8
	155	180,2
	163,3	175,7
	181,3	190,2
	184,6	191,4
	187,4	179,4
	203,1	186
	163,3	189,9
	164	195,9
	166,1	194,8
	172,8	181,2
	172,9	185,3
	171,2	181,8
	179,9	182
	184,7	